STRUCTURE AND MECHANICAL PROPERTIES OF FAT CRYSTAL NETWORKS

A Thesis

Presented to

The Faculty of Graduate Studies

of

The University of Guelph

by

SURESH S NARINE

In partial fulfilment of requirements

for the degree of

Doctor of Philosophy

March, 2000

ABSTRACT

STRUCTURE AND MECHANICAL PROPERTIES OF FAT CRYSTAL NETWORKS

Suresh S. Narine
University of Guelph, 2000

Advisor:
Professor Alejandro G. Marangoni

This thesis provides a review of the continuing endeavour to define the structure of fat crystal networks, and to relate this structure to the observed mechanical properties of the network. The quantification and characterisation of microstructure in fat crystal networks is studied using the relationship of the shear elastic modulus (G') to the solid fat content (Φ_{SFC}) via the mass fractal dimension (D) of the network. Results from application of a scaling theory (weak link theory), developed for colloidal gels, to the microstructure of fat crystal networks are presented and discussed. A method to measure mass fractal dimensions from *in situ* polarised light microscope (PLM) images of the microstructural network of fat crystals is developed and applied to the fat systems studied. Fractal dimensions measured from *in situ* PLM images of the various fat systems are in good agreement with fractal dimensions measured using rheological measurements and the weak link theory.

A mechanical model is developed which allows G'of the system to be correlated with forces acting within the network. The fractal arrangement of the network at certain length scales is taken into consideration. The final expression for G' agrees with the experimentally-verified scaling behaviour of fat crystal networks, and is given by:

$$G' \sim m\left(\frac{\rho_t}{\rho_{ME}}\right)^{\frac{1}{3-D}} \frac{A}{6c\pi\sigma\xi d_o^3} \Phi_{SFC}^{\frac{1}{3-D}} \qquad (1)$$

where m is the number of pairs of microstructural elements at the interface between two microstructures, ρ_t is the density of the entire network, ρ_{ME} is the solids density within the microstructural elements, A is the Hamaker's constant of the network, σ is the size of the microstructural elements, ξ is the size of the microstructures, d_o is the distance between neighboring microstructures, c is a constant defined during the calculation of fractal dimensions from polarized light microscope images, and G', Φ_{SFC}, and D are as defined earlier.

The physical implications of the fractal dimension of fat crystal networks are developed, and related to density, packing order, and crystallisation conditions. Suggestions are made to vary the G'of fat networks by varying processing conditions under which the network is formed. Experimental evidence is provided which demonstrate that by varying the processing conditions of milkfat, G' can be altered in a manner predicted by Eqn. (1).

To

Rekha
(and the Strawberries)

ACKNOWLEDGEMENTS

I am painfully aware that this acknowledgement is small recompense for the essential ways in which so many helped make this thesis a success. It however gives me no small amount of pleasure to express my gratitude to those without whom this work would still be floundering in the corners of my mind.

If there is anyone who deserves this doctorate more than I do, it is my wife Rekha. She has been a life-spring of motivation to me throughout my academic career, even during those periods when I have been at my lowest points. It is true to say that without her, none of this would have been remotely possible. She has also contributed to this thesis in a more pragmatic manner: she laboriously proof-read the manuscript, and many of the publications arising out of this work would have been flawed had she not caught my many mistakes. Rekha, I thank you.

I would also like to thank my academic adviser, Dr. Alejandro Marangoni. His enthusiasm and boundless energy creates a heady environment within which to work. He displayed amazing confidence in my abilities, to the point of allowing me to pursue directions that seemed dubious at the time. I could not have asked for a better person to introduce me to the world of Food Science. Without him, none of this work would have been possible. I owe many thanks as well to Dr. Rob Lencki for the many stimulating discussions on science, but also on the perhaps more important discussions on the nature of the world around us. I also express my gratitude to Dr. John Dutcher for his many helpful comments on the first draft of the thesis, and to Dr. Micha Peleg, my external examiner, for the many helpful comments he made.

I must also express my thanks to my fellow graduate students in the lab, who have all helped to make my stay here a pleasant one. In particular, I would like to thank Derick Rousseau, a former Ph.D. student in this laboratory, for allowing me to use so much of his experimental data. Dr. Richard Hartel, Dr. Lidia Herrera, Stephan Jampen, Wendy Willis, Amanda Wright, Sara McGauley, Rob Blenkinsop, Leslie Copp, Dulce Abascal, Rodrigo Campos, Claire McCague, Joy Munro, Dr. Peter Norton, Dr. Allen Blaurock, Dr. Mick Smart, Dr. Massimo Marcone, Dr. Rickey Yada, and many others too numerous to mention have helped in large and small ways to make this work possible. My thanks.

To my mom, Phulmat Bowdnaraine; my sisters, Yvonne, Anita and Gaitri; my nieces Marsha, Michelle and Chandini; and my brother-in-laws, thank you very much for all the support you have given me throughout my academic career. In particular, I would like to mention my nieces Candace and Maria, both of whom were an integral part of my life during the writing of this thesis. My in-laws have been and continue to be, more like parents to me. Their unwavering support throughout my academic career was something I always counted on. In particular, I would like to thank my father-in-law, Roy Singh, and my sister-in-law, Radha Arjune. Constant sources of motivation and encouragement, Roy and Radha have both in many ways made my academic career possible. I would also like to mention Roy Nian Singh, my nephew who has brought so much life and joy with him.

To those whom I have neglected to mention, a thousand pardons. You know who you are, and you know how much I appreciate your contributions.

Table of Contents

List of Tables

List of Figures

Chapter 5 (Where Lies the Fractality in Fat Crystal Networks?)

Chapter 1

Introduction

Lipids form a group of compounds that are generally soluble in organic solvents and slightly soluble or insoluble in water. This definition of lipids includes a group of compounds that is very diverse and composed of a vast collection of organic substances. However, as is usually the case with natural materials, there is an underlying order to the structure of these compounds, which makes this definition easier to work with in reality. This underlying order or underlying logic to the structural organization of complex natural materials will be a repetitive theme in this thesis. For example, ninety-nine percent of the lipids of plant and animal origin are made up of glycerol esters of fatty

acids. These materials have traditionally been called fats and/or oils, fats being used to describe solid oils. However, the two terms are used interchangeably.

Lipids used as food are either in the form of constituents in foods such as milk, cheese, spreads, etc. or in the form of "visible" fats such as butter, lard, ghee, etc. Dietary lipids assume an important role in human nutrition. They can supply a number of essential functions, such as providing calories and essential fatty acids and acting as vitamin carriers. Additionally, fats increase the palatability of foods. It is important to note that fats have also been implicated in the controversy over a number of adverse food-related health issues, such as obesity, cancer and cardiovascular disease. Lipids in foods also provide essential characteristics of texture and functionality, due to their unique physical and chemical properties, which include their composition, crystalline structure, melting and solidification behavior, association with water and non-lipid molecules, and rheological behavior.

The macroscopic rheological properties of networks formed by lipids are of extreme importance in food products that contain significant amounts of fats. Such products include butter, margarine, chocolate, peanut butter, many spreads such as cream cheese, and ice cream. Many of the sensory attributes such as spreadability, mouthfeel, snap and texture are dependent on the mechanical strength of the underlying fat crystal network. However, it must not be inferred from this that knowledge of the mechanical properties of the fat network provides complete knowledge of the food product within which it is formed. In addition to this obvious industrial importance, fat crystal networks form a particular class of soft materials, which demonstrate a yield stress and viscoelastic

properties, rendering these materials plastic. From a materials sciences point of view, the rheological behavior of these materials is also extremely important.

This thesis provides a review of the development of techniques and models which attempt to relate the structural organization of fat crystal networks to their mechanical properties. In addition, the thesis provides a chronicle of the author's own attempts at the problem, focussing mainly on the effects of the microstructural level of structure on the macroscopic elastic moduli of fat crystal networks, and the quantification of this level of structure utilizing fractal geometrical analysis techniques.

Fat crystal networks, like many other materials, demonstrate distinct hierarchies of structural organization, the identification and quantification of which provides insight into the relationship of composition, processing, structure, and mechanical properties of the networks formed by these materials. As such, the macroscopic properties of the network are influenced by the different levels of structure as well as the processing conditions under which the network is formed. Figure 1.1 depicts the structural hierarchy defined during the crystallization of a typical fat crystal network.

Efforts to model the mechanical strength (Kamphuis and Jongschaap, 1985; Kamphuis *et al.*, 1984; Nederveen, 1963; Papenhuijzen, 1971; Papenhuijzen, 1972; Payne, 1964; Van den Tempel, 1961; Van den Tempel, 1979) of these networks have met with more failure than success over the past 50 years, mainly due to the lack of a comprehensive model to relate *all* structural network characteristics and solid/liquid

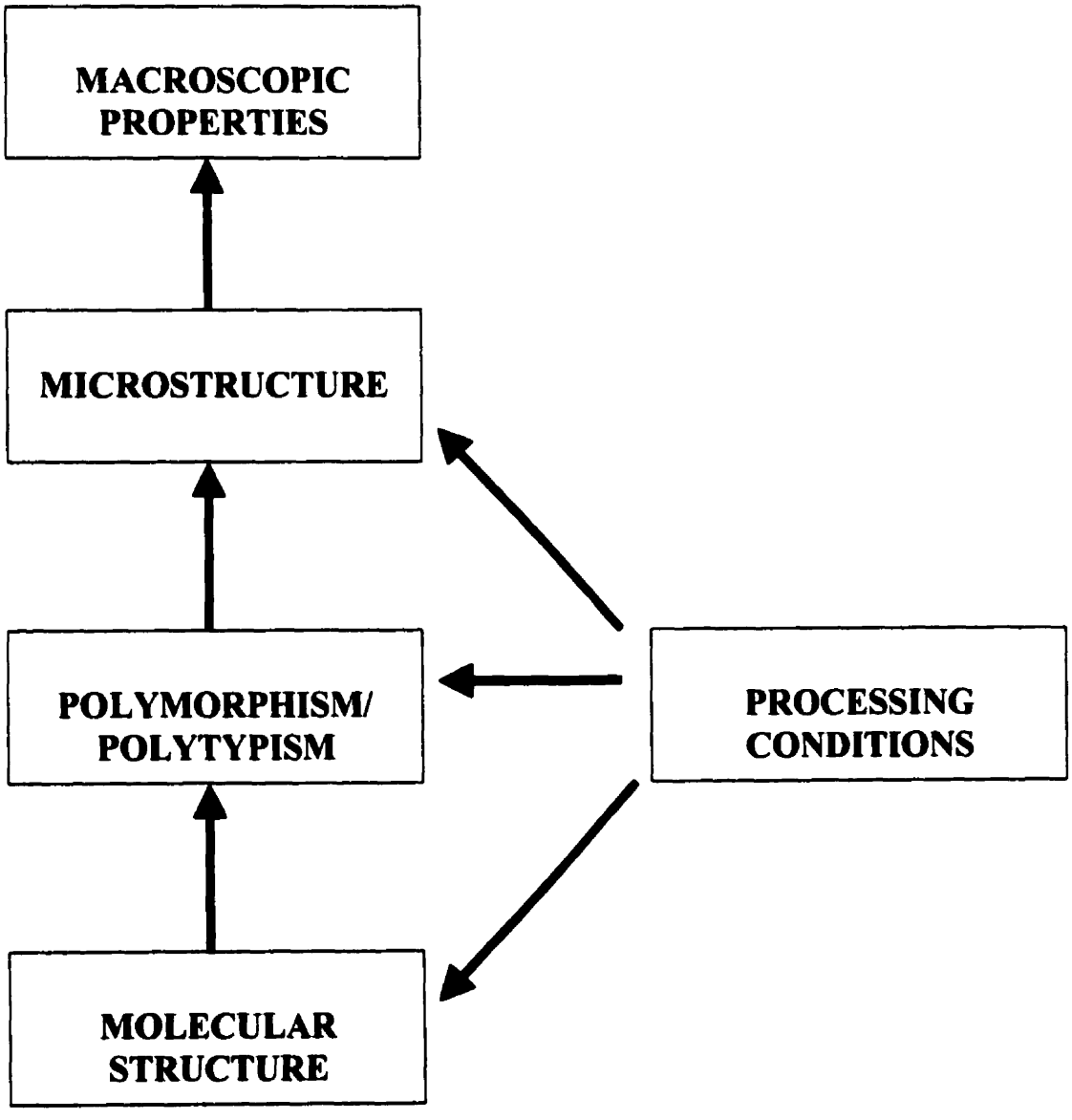

Figure 1.1: Schematic showing the structural hierarchy defined during the formation of a fat crystal network.

ratios of lipid networks to their mechanical strength. This lack stemmed partly from the fact that many scientists in this area concentrated only on the lipid composition and the polymorphism of the networks, in large part ignoring the *in situ* microstructure of the network. Lately, much work has been done in analysis of the microstructural level of the network, leading to encouraging results, which suggests that consideration of this level of structure (together with the other levels previously studied) is absolutely essential in assessing the mechanical strength of the fat network.

This thesis details work by the author and coworkers which has resulted in the ability to quantify microstructure with the application of fractal mathematics to the geometry of the microstructure. Over a period of seven years, this area of microstructural quantification using fractal geometry has seen an explosive burst of success, reviewed in chapter 2 of this thesis. In addition, microstructural analysis via fractal methods is also applicable to other food areas as well, for example in characterizing structures of whey protein gels (Hagiwara *et al.*, 1997; Marangoni *et al.*, 1999; Stading *et al.*, 1993; Vreeker *et al.*, 1992a).

The importance of the microstructural level of structural organization becomes apparent when one examines the different levels of structure in a fat network in the context of how these levels of structure are responsible for the values of macroscopic physical measurements performed on the network. An introduction to the various levels of structure, and the analysis techniques used to quantify them is provided in chapter 2. Additionally, the implication of the various levels of structure in determining the values

of measurable indicators of mechanical strength or sensory attributes is discussed in chapter 2. In this thesis, it is the main intention to concentrate on the analysis of the microstructural level and the illustration of the importance of this level in predicting the elastic properties of the network. However, the importance of the microstructural level in predicting macroscopic rheological properties of fat networks can only be placed in context when the other levels of structure are discussed in terms of their analysis and the knowledge of the mechanical strength of the network that may be inferred from the quantification of these levels of structure.

Motivation for this study stemmed from a series of rheological analysis performed in our laboratory previous to this work (to be detailed in chapter 2), where fits to fractal theory existing for colloidal gels yielded encouraging results.

In order to place the work to be detailed in this thesis in context of the larger effort to predict the sensory impressions of a fat-containing food product, the reader is referred to figures 1.2 and 1.3. Referring to figure 1.2, the sensory impressions of a fat containing product such as chocolate will be determined by the physical and chemical properties of the fat crystal network, in conjunction with the properties of any composite network that is formed with fat and other ingredients. Additionally, the properties of any other non-fat networks (and non-fat ingredients present in a random fashion) will also affect the sensory impressions of the product. One of the many factors determining the physical properties of the fat network is the hardness of the network. Referring to figure 1.3, the shear elastic modulus is only one of the rheological properties of the network that

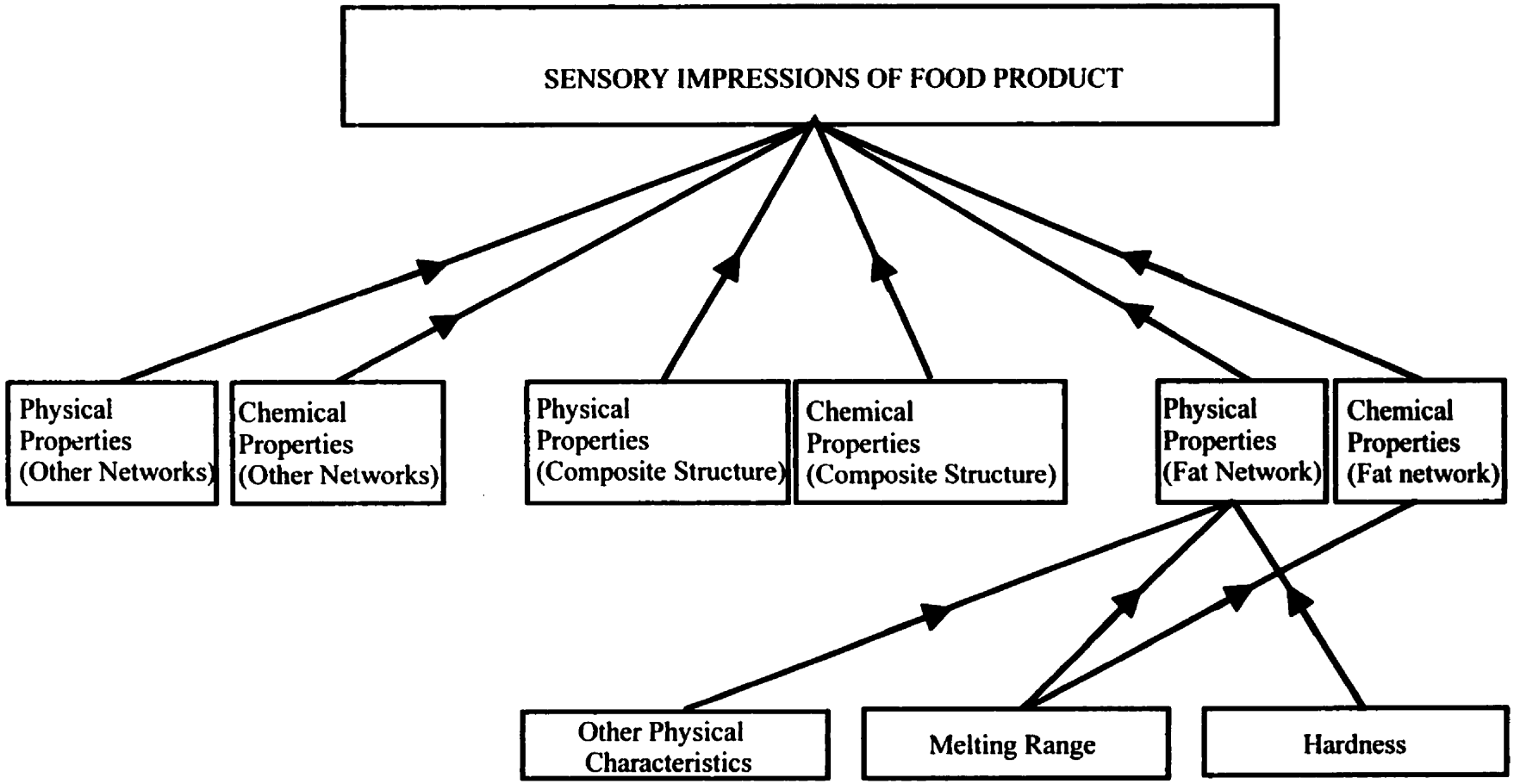

Figure 1.2: Schematic showing origins of sensory impressions of a fat-containing food product.

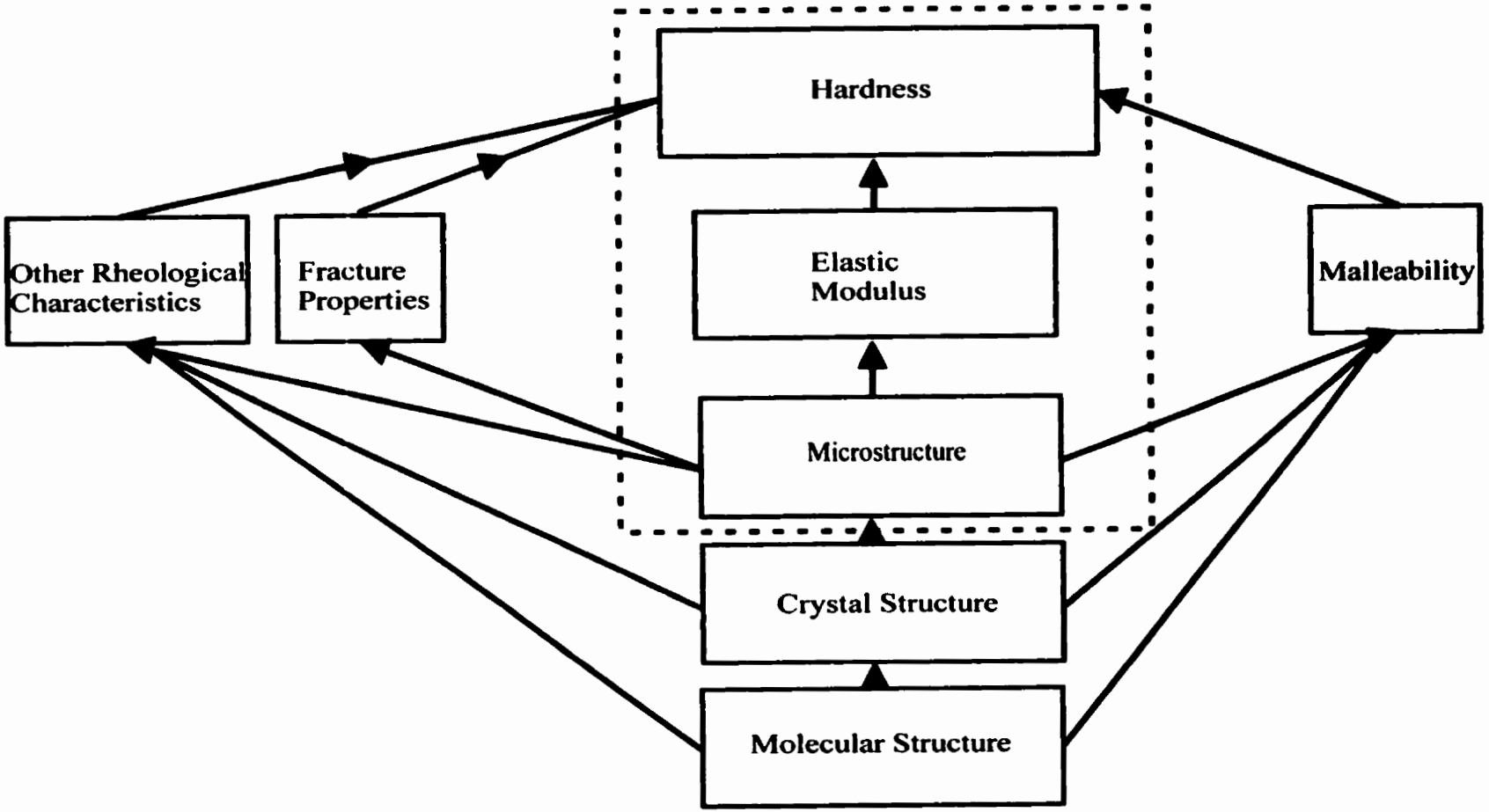

Figure 1.3: Schematic of the relationship between thestructural hierarchy, rheological properties, and hardness of fat crystal networks. The region bounded by the dotted line represents the area of focus of this thesis.

determines the hardness. This thesis is concerned primarily with the relationship between microstructure and the elastic modulus of the network.

It is perhaps pertinent to discuss two important points concerning nomenclature at this early stage. Throughout this thesis, the phrase elastic modulus is used. Some researchers prefer to describe this parameter as the *storage modulus.* Please be advised that *elastic modulus* as used in this thesis is the same as the *storage modulus.*

Fractal dimension is a parameter that is central to the theories developed in this thesis. However, because of the limited length range over which fats behave in a fractal-like manner, some researchers prefer to refer to fractal dimension as an *apparent fractal dimension.* Another term that may be used equivalently with fractal dimension in the thesis is *scaling factor.* Suffice it to say that when fractal dimension is used in this thesis, it refers to the dimensionality characterizing the fractal-like behavior of fat crystal networks between length scales bounded by the size of one microstructural element and the size of one microstructure. Microstructure and microstructural elements are defined in Chapter 5 of this thesis.

Chapter 2

Literature Review

This chapter provides a review of scientific developments pertaining to the study of the different levels of structure of fat crystal networks and to the relationship of structure to macroscopic mechanical properties. Each level of structure identified in Chapter 1 is discussed, with respect to methods used for quantification, as well as the information that particular levels of structure provide on the macroscopic physical properties of the system. Since the solid fat content of fat crystal networks has long been known to play a role in the determination of the macroscopic hardness of the network, a brief discussion of solid fat content is also provided. Additionally, this section also includes an introduction to fractal geometry and fractal analysis of colloidal gels as mass fractals. The application of fractal scaling relationships developed for colloidal gels to

the study of fat crystal networks is also reviewed. A review of the models proposed by other researchers to relate structure to mechanical properties is also made. At the end of this chapter, a set of objectives for this thesis are identified, based on an identification of the areas requiring further development of the relationship between structure and the macroscopic hardness of fat crystal networks.

2.1 Solid Fat Content

The ratio of solids to total mass in a plastic fat expressed as a percentage is referred to as the solid fat content (Φ_{SFC}). The solid fat content is one of the major factors affecting the macroscopic rheological properties of plastic fats (de Man and Beers, 1987). A number of methods exist for the determination of the solid content of plastic fats, the oldest being dilatometric methods (AOCS Official Method Cd 10-57, 1980), which produces a result referred to as the solid fat index(SFI). However, determinations of SFI are cumbersome and difficult. Differential scanning calorimetry has also been used as a method of determining solid content in plastic fats (de Man and Beers, 1987), but again, this method has inherent limitations and is not widely utilized. The most widely used method to determine solid contents of plastic fats is pulsed nuclear magnetic resonance (NMR). Methods of wide line and pulsed NMR have been described by Haighton *et al.* (1971), Madison and Hill (1978), Waddington (1980), van Boekel (1981) and Mills and van der Voort (1981). Correlations between NMR and dilatometry and differential scanning calorimetry measurements have also been made (van den Enden *et al.*, 1978, van Duynhoven *et al.*, 1999).

Most of the early investigations into the influence of solid fat content on the macroscopic rheological properties of plastic fats have been done on the effect of solid fat content on the penetration hardness (Bailey, 1950; de Man, 1962, Haighton, 1976). It was found that the yield value (the definition and implications of this parameter will be discussed in Chapter 3, however, it can be viewed loosely as a measure of macroscopic hardness) was inversely proportional to the second power of the solid fat content. Other researchers have discovered that the elastic modulus of fat networks is proportional to the solid fat content raised to a power, as will be described in the sections to follow this.

2.2 Triglyceride composition and structure

The smallest scale of structure present in fat crystal networks, the triglyceride molecules (also called triacylglycerols or TAGs) are three-fold esters of glycerol and fatty acids. The general organization of a triglyceride molecule is shown in Figure 2.1. The acyl chains may be saturated, unsaturated with either *cis*- or *trans*-double bonds, branched or straight, short or long, contain even or odd number carbon-numbered fatty acids, etc (Small, 1986; 1984; Yano, 1998). The physical properties of the triglyceride molecule is dependent on the acyl chain composition. Some TAGs contain identical acyl chains, and these are called mono-acid TAGs. Those with more than one type of acyl chain are called mixed-acid TAGs, and in general have more complicated physical properties than the mono-acid TAGs (Bailey, 1950; Lutton *et al*, 1972).

Methods to determine triglyceride and fatty acid composition in fat crystal networks are well established and well reviewed in the book by Christie(Christie, 1982).

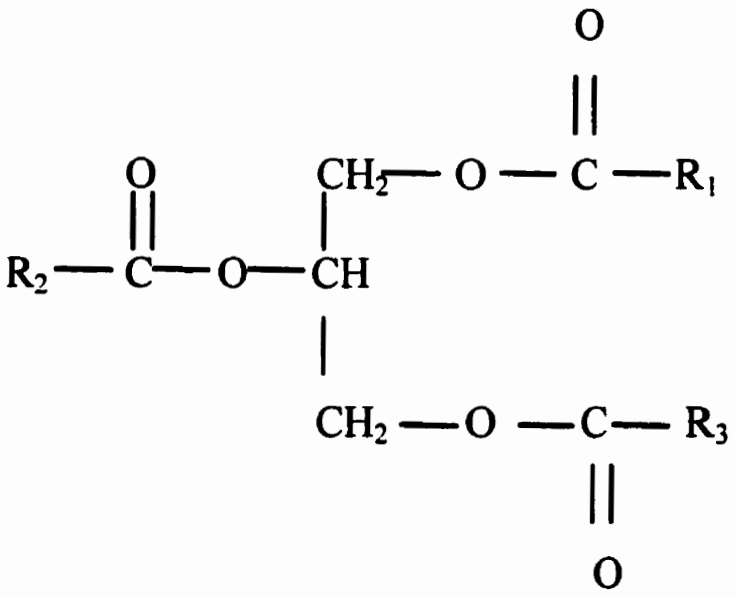

Figure 2.1: General organization of a triglyceride molecule.

In addition, methods to determine the fatty acid positional distribution within a triglyceride have been established by two separate groups(Brockerhoff, 1965; Lands *et al.*, 1966). Triglycerides are well-known organic molecules, and therefore the bond angles and bond lengths of the various atoms within each triglyceride molecule are easily established on the basis of standard structural organic chemistry. What is non-trivial is the prediction of a particular crystal structure formed by an ensemble of triglyceride molecules of known stereospecific orientation. The complexity and flexibility of the triglyceride molecules also allows different crystalline packing of the same ensemble of molecules, leading of course, to the existence of different polymorphs. At this point, there is no theory which links triglyceride composition to the macroscopic mechanical strength of the network, at least in any clear and direct manner. Molecular modeling has been used to some extent to explain the packing of triglyceride molecules into known polymorphs (Applegate and Glomset, 1991a; Applegate and Glomset, 1991b; de Jong and van Soest, 1978; de Jong *et al.*, 1991; Hagemann and Rothfus, 1992; van Soest *et al.*, 1990; Yan *et al.*, 1994), but to this date there has been no predictive use of such methods. It is conceivable that triglyceride composition can be linked to macroscopic mechanical strength via models relating the polymorphism of the resulting network to the triglyceride composition and of course, the polymorphism to the mechanical properties. Since the triglyceride composition of the network directly influences the polymorphism of the network, the melting profiles of the fat crystal network are directly related to the triglyceride composition (Narine and Marangoni, 1999c), but unfortunately currently there exists no predictive method to relate triglyceride composition to melting profiles.

Whilst the structure of fat crystal networks was represented in Chapter 1 as being composed of three hierarchical levels of structure, it should also be mentioned that the smallest level of structure is not limited to only triglycerides. The presence of mono- and diglycerides will also affect the structure of the network, as well other such minor components as phospholipids and other polar and non-polar compounds present in minute amounts. The role of these compounds in the structure of the network seems to be primarily be at the nucleation stage of crystallisation (Wright *et al.*, 2000). The effects of these "minor components" on nucleation and growth of the fat crystal network is a current subject of intense interest, and active research is being undertaken in this area by a number of groups, ours among them. The effects of minor components on crystallisation is a not an unknown phenomenon (Wright *et al*, 2000; Cebula and Smith, 1992; Gordon and Rahman, 1991; Loncin, 1958; Niiya *et al.*, 1973; Reddy and Prabhakar, 1987; Sambuc *et al.*, 1980; Siew and Ng, 1996; van den Tempel, 1968), but this area can now benefit from new analysis techniques that were not previously available, such as fractal analysis.

Therefore, certainly the ensemble of molecules that are present will determine the macroscopic mechanical properties of the network, but currently we lack the tools to make this relationship a quantitatively predictive one. It must be stated unequivocally, however, that this level of structure is of paramount importance to the macroscopic properties of the final network and therefore the forging of links from this level, through the other levels of structure, to the macroscopic mechanical properties is of fundamental importance.

2.3 Polymorphism and polytypism

The polymorphism of triglycerides was and in many ways still is the most important advancement in the academic pursuit of an understanding of the structure of fat crystal networks. As such, it is important to provide a brief chronology of the discovery of fat polymorphism. The existence of two or more distinct crystalline forms of the same substance, or polymorphism, has been known since 1820. The polymorphic states of a particular substance have different physical properties but on melting yield identical liquids, since the polymorphic states are merely due to differences in packing of the constituent molecules upon crystallization. The physical and chemical properties of glycerides have been studied for more than a century. One of the indicators of different polymorphic forms of triglycerides and acylglycerides in general has been a multiple melting behavior, noted as early as 1849. As summarized by Chapman(Chapman, 1962) and by Hagemann(Hagemann, 1989), numerous early observations of variation in melting points of the same glyceride compound was made, which in the mid-19th century was thought to be due to a form of isomerism.

Malkin and co-workers were the first to utilize powder X-ray diffraction to demonstrate conclusively that the variable melting points (m.p.) of identical glyceride solids were due to polymorphism(Clarkson and Malkin, 1934). This work resulted in the identification of four solid forms for tristearin. The lowest melting form of tristearin was designated gamma, γ which showed a diffuse X-ray Bragg spacing at 0.415 nm – this form was considered a non-crystalline vitreous solid and melted at 54°C. The next polymorph (increasing m.p.) was designated alpha, α, and melted at 65°C (Bragg

spacing 0.415 nm), with the next polymorph being designated beta prime, β', melting at 70°C (Bragg spacings 0.38 nm and 0.42 nm). The final form was designated beta, β, and melted at 72°C with Bragg spacing 0.46 nm.

Later work by other researchers (Filer *et al.*, 1946; Lutton, 1945) brought into question Malkin's work in terms of association of the different melting points with X-ray spacings. As will be explained below, this controversy ended with the view of Lutton and others being accepted over Malkin's group, but it is important to note that Malkin's group was the first to demonstrate conclusively that the existence of multiple melting points for tristearin was due to a detectable, by X-ray diffraction, difference in crystalline packing.

Lutton and Malkin most energetically contested the controversy over the assignation of XRD spacings to the different polymorphic forms. Lutton denied the existence of the vitreous or γ form, ascertaining that there were only three distinct crystalline forms. Lutton claimed that the lowest melting point polymorph was the α form with a Bragg spacing at 0.415 nm, which transformed into the β' form (corresponding to Malkin's α form) which transformed to the highest-melting β form. In 1955, Chapman(Chapman, 1955) used infrared spectroscopy to confirm the claims of Lutton. The correlation of infrared and X-ray data led to the classification of basic polymorphs, designated α, β' and β according to the cross-sectional packing mode of the hydrocarbon chain, called "subcell structure." The α form has a hexagonal subcell packing and a Bragg spacing of 0.42 nm, the β' form has orthorhombic perpendicular

subcell packing with Bragg spacings of 0.42 – 0.43 nm and 0.37 – 0.40 nm, and the β form has a triclinic parallel subcell with Bragg spacing of 0.46 nm. The crystal structure has only been determined for the stable β polymorph of three mono-acid triglycerides; tricaprin (Jensen and Mabis, 1966); trilaurin (Larsson, 1964); and the triglyceride of 11-bromoundecanoic acid (Larsson, 1963) and one mixed acid triglyceride; 1,2-dipalmitoyl-3-acetyl-*sn*-glycerol (Goto *et al.*, 1992). Depending on the acyl chain composition, other metastable polymorphs called the γ and δ forms and plural β' and β forms have been observed in mixed acid triglycerides (Padley, 1996).

Nomenclature of the different polymorphic forms has been covered by a number of authors, for example Yano(Yano, 1998). However, the main structural factors used to characterize the different polymorphic forms are the subcell structure and the layered structure. The subcell structure deals with the packing mode of the hydrocarbon chains, whilst the layered structure arises out of the repetitive sequence of the acyl chains which forms a unit lamella along the hydrocarbon chain axis (see Figure 2.2(a) and (B)). The subcell and layered structures give rise to the short and long Bragg spacings often referred to in X-ray diffraction studies of fat polymorphism. This information is the extent of our knowledge of the crystalline structure of the systems: except for the mono-acid triglyceride β forms, our knowledge is limited to the subcell and layered structures – no other information at the molecular level is available as to the packing of the triglyceride molecules. Therefore for the structures of the metastable polymorphic forms such as the α and particularly the β' forms, the molecular packing of the triglycerides still remains to be determined. Furthermore, the structures of saturated-unsaturated

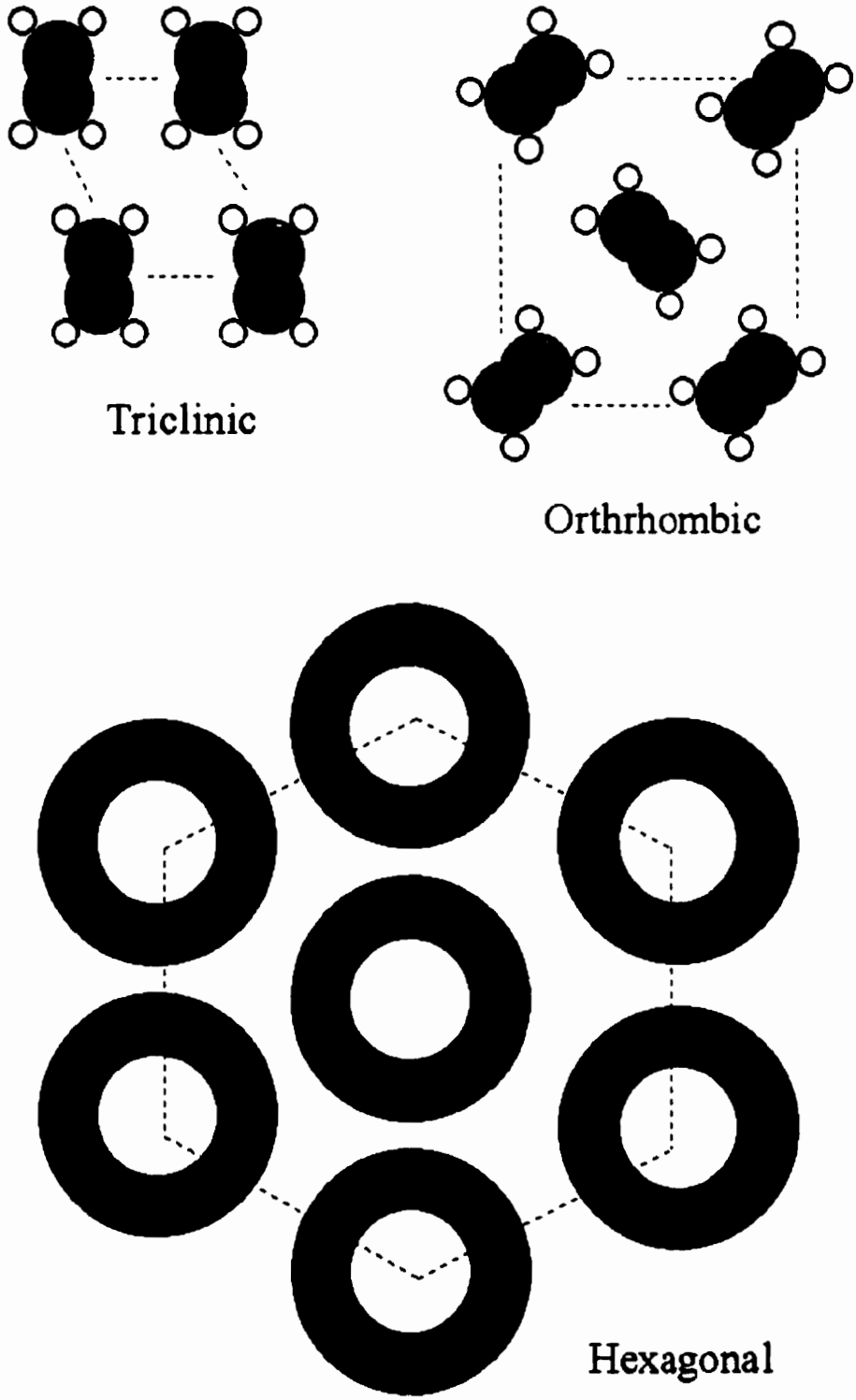

Figure 2.2(A): Schematic of various subcell structures found in fat crystal networks.

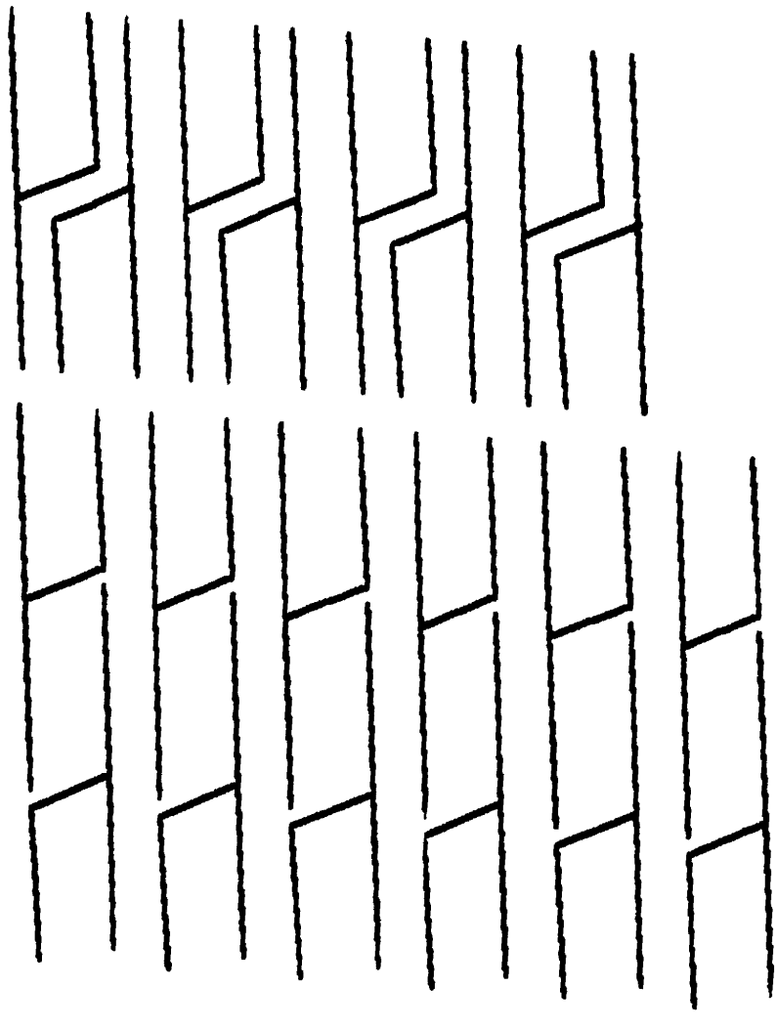

Figure 2.2 (B): Shematic of triglyceride molecules packed in the layered formation – repetitive sequences of acyl chains.

mixed acid triglycerides and the structures of mixtures of different triglycerides such as is to be found in natural systems like cocoa butter are still to be determined as well.

The investigation of mixed-acid triglycerides have occupied many researchers (Arishima *et al.*, 1991; Engstrom, 1992; Filer *et al.*, 1946; Gibon *et al.*, 1986; Kodali *et al.*, 1987; Landman *et al.*, 1960; Larsson, 1972; Lovegren *et al.*, 1971; Lutton and Jackson, 1950; Sato *et al.*, 1989, Yano and Sato, 1999). However, no fundamental set of rules for constructing molecular structures has been determined; in fact beyond the subcell and layering lattice parameters, little is known of the structure of mixed-acid triglycerides. Due to the studies cited above, however, much is known of the thermodynamic behavior of these systems. Rossel (Rossel, 1967) reported molecular compound formation (mixed-crystals) for some specific sets of mixed acid triglycerides. The phase behavior, kinetic behavior and X-ray diffraction studies have been used to support mixed crystal formation of different triglycerides as well as to investigate the resultant polymorphism of a mixture of triglycerides (de Man, 1963; Engstrom, 1992; Knoester *et al.*, 1972; Lambelet and Raemy, 1983; Marangoni and Lencki, 1998; Minato *et al.*, 1997a; Minato *et al.*, 1997b; Mulder, 1953; Oyano *et al.*, 1992; Timms, 1980; Timms, 1984). However, the same problem exists as for the structure of mixed-acid triglycerides; beyond the kinetic and phase behavior and the lattice parameters of layering, there is no conclusive evidence of the fundamental molecular structures, and no acclaimed method for the construction of such structures.

In addition to X-ray diffraction, a number of other techniques are employed in the identification of the different polymorphic forms; as mentioned before, infrared vibrational spectroscopy has been used (Amey and Chapman, 1984; Chapman, 1960a; Chapman, 1964; Freeman, 1968; O'Connor *et al.*, 1955; Yano, 1998; Yano *et al.*, 1997a; Yano *et al.*, 1997b). Nuclear magnetic resonance (NMR) measurements have also been used to study the molecular mobility in polymorphs (Arishima *et al.*, 1996; Boceik *et al.*, 1985; Calaghan and Jolly, 1977; Chapman, 1960b; Eads *et al.*, 1992; Gibon *et al.*, 1986; Hagemann and Rothfus, 1983; Norton *et al.*, 1985). Atomic force microscopy has recently also been used to study the crystal structure of triglycerides (Birker and Blonk, 1993).

The type of polymorph(s) present in the network decidedly affects the macroscopic mechanical properties of the fat crystal network. Certainly, the type of polymorph present will dictate the melting point of the network. The shape and sizes of the crystals and crystal aggregates found in the network is affected by the polymorphic form of the crystals, but to varying extents in different fats (Hoerr, 1960; Hoerr and Waugh, 1955; Berger *et al.*, 1979; Kellens *et al.*, 1992). The shape and sizes of crystals and aggregates of crystals (microstructural elements) do affect the macroscopic elastic constant of the network. However, the measurements needed to establish the different polymorphic types as explained above do not yield additional information about the nature of the molecular structure. Therefore, the understanding of the link between polymorphism and morphology and size of crystals is still phenomenological in nature. Additionally, in a model created by Narine and Marangoni (Narine and Marangoni,

1999d), to be detailed in Chapter 6 of this thesis, the macroscopic elastic constant of the network is dependent on the Hamaker's constant (a constant depending on the polarizabilities of the triglyceride molecules) of the microstructural elements within the network, which in turn depends on the molecular packing in the crystals, but again, this is not yet a quantifiable link. There have been observations that show changes in macroscopic viscoelastic properties due to a polymorphic transformation in fat products, for example by Cornily and leMeste (Cornily and leMeste, 1985). The β' -type polymorph is usually the most functional in fat products, due to its small crystal size (~1 μm) and thin needle-shaped morphology. Typical X-ray diffraction patterns showing long and short spacings are shown in Figure 2.3; these were taken with the help of Dr. Allen Blaurock of Kraft Foods.

Therefore, the nature of the crystalline level of structure is of great importance to the macroscopic mechanical properties of the network, and in some cases, such as margarine, a change in the polymorphic state of the network is accompanied by very predictable changes in macroscopic hardness. However, this level of structure in isolation does not provide complete information about the mechanical properties of the network, and unfortunately there has been no quantitative link made between polymorphism of the network and the mechanical properties of the network.

2.4 Microstructure

The microstructural level of the fat crystal network may be defined as those structures in the length range between 1 μm and 200 μm. This level of structure has an

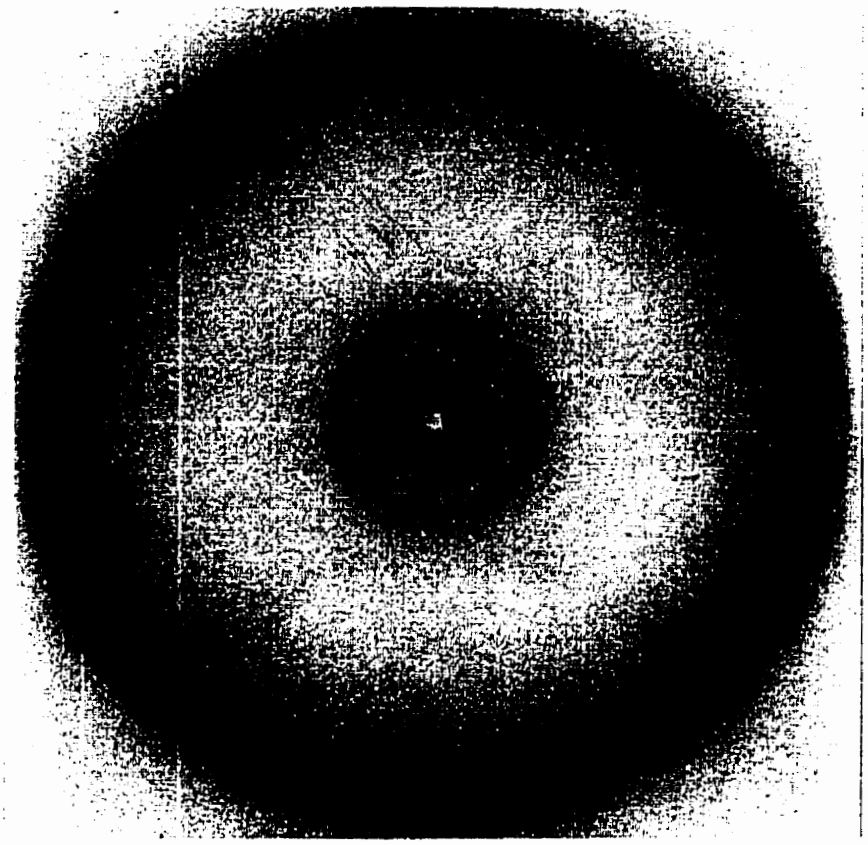

Figure 2.3: Typical X-ray Diffraction pattern, showing long and short spacings.

enormous influence on the macroscopic rheological properties of the network, noted as early as 1987 by deMan and Beers (1987). Other researchers have also noted the importance of the microstructural level on the rheological properties of the network, and the fact that the microstructure is easily changed with processing conditions of crystallization (Heertje *et al.*, 1987a; Heertje *et al.*, 1988; Shukla and Rizvi, 1996), as well as with interesterification (Marangoni and Rousseau, 1996).

With the advent of confocal laser scanning fluorescence microscopy (CLSFM) (Heertje *et al.*, 1987b) and multiple photon microscopy (MPM) (Marangoni and Hartel, 1998; Xu *et al.*, 1996), two new tools have been added to the standard tools of light microscopy (LM) (Flint, 1984; Flint, 1991; Inoe, 1987; Yiu, 1985) and electron microscopy(EM) (Brooker, 1990; Buchheim, 1982; de Man, 1982; Heertje *et al.*, 1987a; Kalab, 1983; Sargeant, 1988) that was most widely used in the past to study the microstructure of fats and foods in general. Heertje's work (1993; 1987a; 1987b; 1988) on the visualization of the microstructure in fats remains one of the most important contributions to the field. In his method, a cold solvent mixture (butanol-methanol) was used to remove the liquid oil from the solid fat in a sample mounted on a special holder. After removal of the liquid oil, the structure of the solid fat network could be visualized.

Interest in the microstructure of fat crystal networks in our laboratory arose during studies of factors affecting the hardness and spreadability of chemically interesterified (CIE) and enzymatically interesterified (EIE) milkfat, and chemically interesterified (CIE) palm oil and lard (Rousseau *et al.* 1996a; 1996b; 1996c; Marangoni and Rousseau,

1996; Rousseau and Marangoni, 1998a; Rousseau and Marangoni, 1998b; Rousseau *et al.*, 1998, Marangoni and Rousseau, 1998a, Marangoni and Rousseau, 1998b). The hardness index and elastic moduli of CIE milkfat at equivalent solid fat contents was lower than their noninteresterified (NIE) counterparts. The traditional indicators of macroscopic hardness such as dropping points, solid fat content and polymorphism of the chemically interesterified and non-interesterified milkfat samples were investigated, in an attempt to explain the observed changes in G' and hardness index. Figure 2.4 (adapted from Rousseau *et al.* , 1996c) shows the dropping points of CIE and NIE milkfat-canola oil blends (here, the canola is used strictly as a diluent to vary the solid fat content), Figure 2.5 (created from data published by Rousseau *et al.* , 1996a) shows the solid fat contents of CIE and NIE milkfat at different temperatures, and Figure 2.6 (data collected by Rousseau) shows the film from X-ray diffraction studies of CIE and NIE milkfat. As is evidenced by these figures, there was little or negligible change in dropping points of NIE and CIE milkfat at w/w percentages of milkfat between 60% and 90%. There was little or negligible change in solid fat content of NIE and CIE milkfat between 25% and 50% solid fat contents, and crystalline packing due to chemical interesterification was similar to that observed for non-interesterified milkfat (the polymorphism, as was defined earlier are the same). Figure 2.7(A) and (B) (adapted from Rousseau *et al.*, 1996 c) shows the hardness, as measured by the hardness index, of CIE and NIE milkfat-canola oil blends at different solid fat contents and w/w percentages respectively. As is evident, the NIE milkfat is consistently harder than the CIE milkfat at solid fat contents above 38%, and w/w percentages of milkfat-canola oil above 70%. Figure 2.8 (A) and (B) (created from data published by Rousseau *et al.*, 1996c) shows the

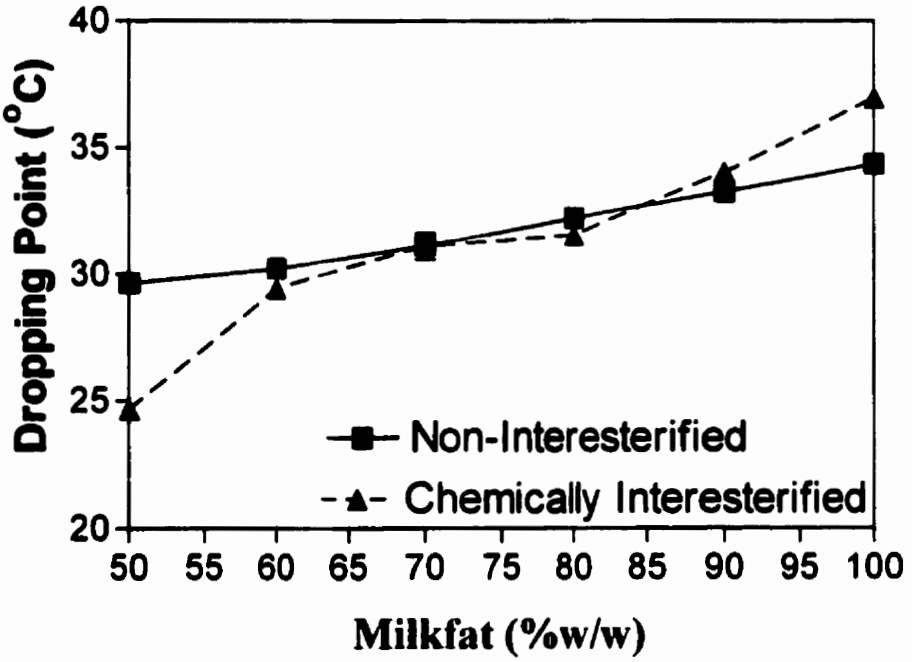

Figure 2.4: Dropping points of chemically and non-interesterified milkfat-canola oil blends.

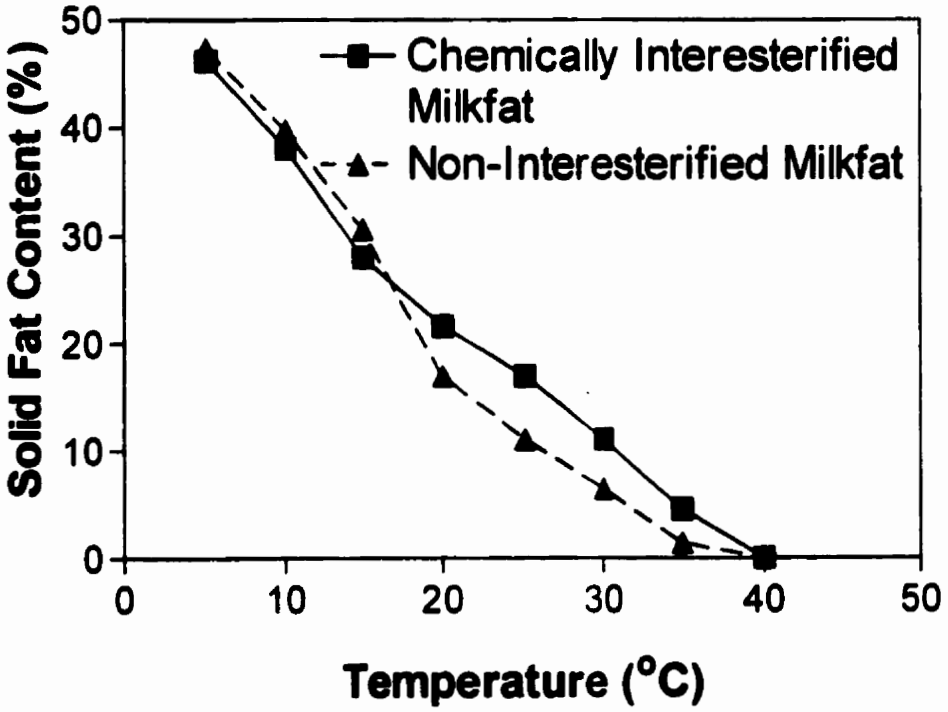

Figure 2.5: Solid fat content of chemically and non-interesterified milkfat at different temperatures.

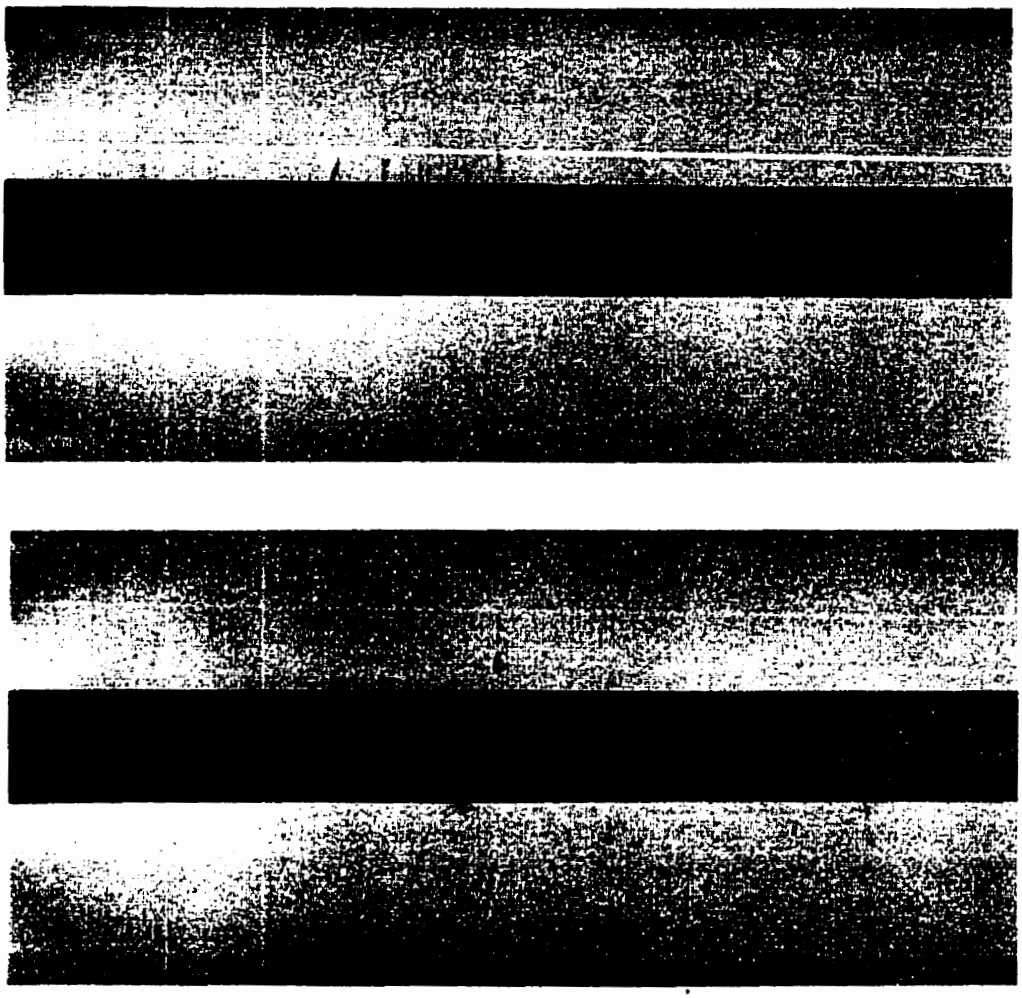

Figure 2.6: X-ray diffraction film of (a) Non-Interesterified milkfat, and (b) Chemically interesterified milkfat.

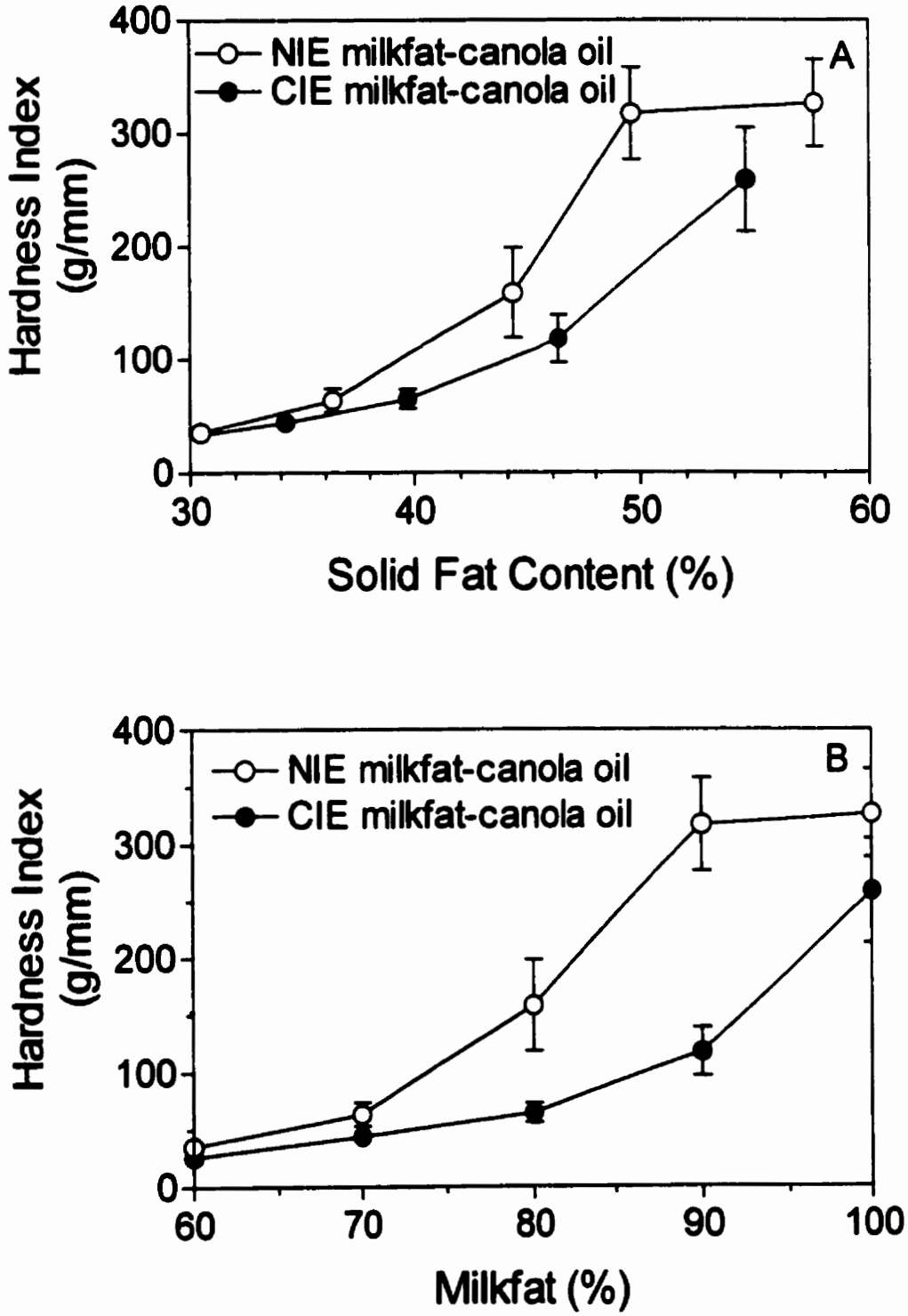

Figure 2.7: (A) Hardness index vs. solid fat content, and (B) Hardness index vs. weight percent of milkfat/canola oil, of chemically and non-interesterified milkfat.

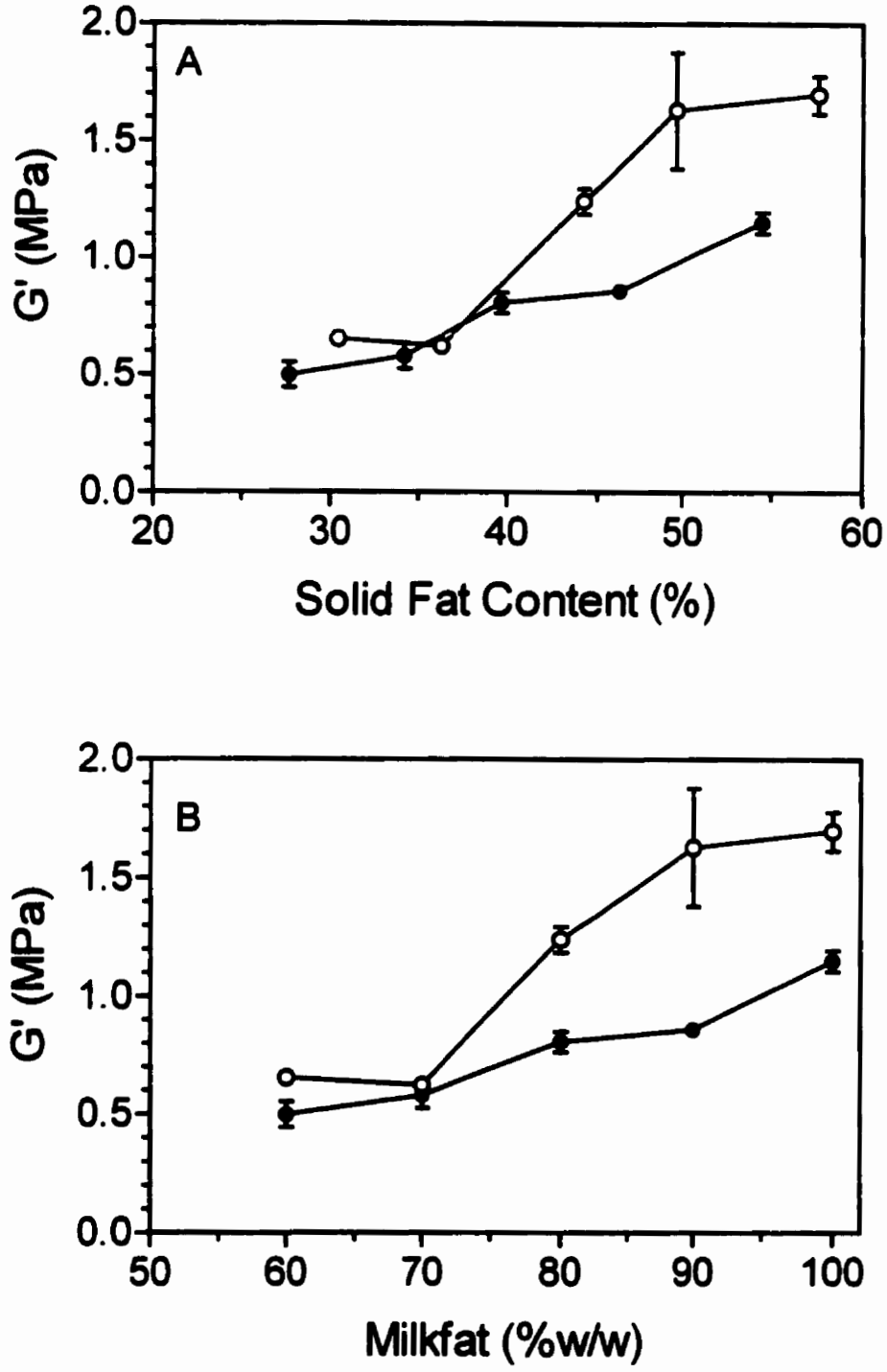

Figure 2.8: Shear elastic modulus of chemically and non-interesterified milkfat vs. (A) Solid fat content and (B) Weight percentage of milkfat-canola oil.

shear elastic moduli of CIE and NIE milkfat-canola oil blends at different solid fat contents and w/w percentages respectively. The elastic moduli of the NIE milkfat-canola oil blends at solid fat contents above 40% are consistently higher than the shear elastic moduli of the CIE milkfat-canola oil blends. This trend is also true for w/w percentages of milkfat-canola oil above 70%. Therefore, it was obvious that the traditional indicators of macroscopic hardness were insensitive to the changes in the structure of the milkfat on chemical interesterification, which caused the resulting changes in elastic moduli and hardness index. It must be mentioned here, in order to avoid mis-interpretation, that the above phenomena was observed for chemically interesterified and non-interesterified milkfat, but that this does not imply that traditional indicators such as dropping points, polymorphism, and solid fat content are *always* insensitive to changes in macroscopic mechanical properties. What this case study proved was that is was possible for these indicators to prove insensitive in some cases, therefore suggesting that perhaps there existed other structural indicators that must also be taken into consideration. It was interesting, however, that polarized light microscopy and confocal laser scanning microscopy demonstrated that the structure of the fat network at the microstructural level (i.e. at the level of structure that is visible by light microscopy) upon chemical interesterification was significantly altered (Rousseau *et al.* 1996b). This provided motivation to search for new "structural indicators" of the mechanical strength of fat crystal networks, that were somehow related to the next logical structural level; the microstructural level of structure of the network. A rheological approach was adopted by Rousseau and Marangoni (Marangoni and Rousseau, 1996; 1998b; Rousseau and Marangoni, 1998b), the motivation for which stemmed from work done on the fractal

nature of colloidal gels and adapted to fat crystal networks (Vreeker *et al.*, 1992b). In order to introduce the reader to the developments made in the rheological analysis of fat crystal networks utilizing the progress in the colloidal field, we provide an introduction first to fractal theory, and then to the application of fractal theory to colloidal gels.

2.5 Fractals

Classical or Euclidean geometry is based upon the use of regular shapes to describe objects. The reader will be familiar with the use of straight lines, circles, conic sections, polygons, spheres, quadratic surfaces, etc. and combinations of these elements to describe objects around us. However, many patterns in nature defy description by these regular shapes. The geometry of coastlines, mountains, trees and vegetables, for instance, cannot always be defined adequately by spheres, cubes, or cones. Fractal geometry was born out of this lack of geometrical tools. Benoit Mandelbrot is credited with having developed the field of fractal geometry to describe many of these natural shapes (Mandelbrot, 1982). According to Mandelbrot (1982), "...I conceived and developed a new geometry of nature and implemented its use in a number of diverse fields. It describes many of the irregular and fragmented patterns around us, and leads to full-fledged theories, by identifying a family of shapes I call fractals."

The unifying concept underlying fractals is the concept of self-similarity. Self-similarity essentially means invariance against changes in scale or size, and is demonstrated in many of the laws of nature. Self-similarity is one of a vast number of symmetries that exist in nature. Symmetry is usually taken to mean invariance against

some change – i.e. some aspect of an object stays the same regardless of changes in the state of the observer. For example, there is symmetry in regular bodies such that they may be operated upon by a number of operations, and yet after the operation is carried out, every point of the body in its original state is co-incident with an equivalent point in its altered state. We have been able to take advantage of underlying symmetries in nature – notably in the previous example in the application of group theory to the symmetry operations which render groups of molecules invariant against sets of operations consisting of reflections, rotations, translations, inversions, and combinations of these operations (Cotton, 1971). Equally useful and more popular symmetries in nature include the exploitation of invariance against uniform motion, which has spawned the theory of special relativity, and the equivalence of acceleration and gravity which is the basis of Einstein's general theory of relativity. Even classical physics is built along the lines of symmetry in nature – the electrostatic or gravitational attraction or repulsion between two bodies demonstrates mirror symmetry – there is no partiality shown to left or right. Suffice it to say, therefore, that symmetry in nature has aided us tremendously in understanding and quantifying our world. As will be demonstrated, the symmetry of self-similarity at different length scales is equally as useful as those mentioned above. To quote Schroeder (1991), "Yet, among all these symmetries flowering in the Garden of Invariance, there sprouts one that, until recently, has not been sufficiently cherished: the ubiquitous invariance against changes in size, called self-similarity."

The word fractal stems from the fact that fractal objects demonstrate fractional dimensions, rather than the integer dimensions for objects encountered in Euclidean

geometry. The connection between fractional and self-similarity is that the easiest way to construct a set that has fractional dimension is through self-similarity (Crownover, 1995). In classical Euclidean geometry, objects have integer dimensions: the reader would be familiar with the reasoning that a line is a 1-dimensional object, a plane a 2-dimensional object and a volume a 3-dimensional object. In this way, Euclidean geometry is suited for quantifying objects that are ideal, man-made, or regular.

One may imagine that if enough kinks are placed in a line or a plane, the result is to have an object that may be classified as being an intermediate between a line and a plane or a plane and a cube. The dimension of such an object is fractional (i.e. between 1 and 2 or between 2 and 3) and the object may be classified as a fractal object; from the fact that instead of having an Euclidean dimension (integer) it has a fractional dimension. One of the most important features of fractal objects is that they are self-similar; i.e. there is a repetition of patterns in the object at many different scales. For natural objects such as trees, clouds, coastlines, etc., Euclidean geometry fails to provide an adequate quantification, but many of these natural objects are self-similar at different scales. For example a tree has branches, these branches have smaller branches and so on, and if one changes the scale of observation of the tree, the same pattern is observed, at least in a statistical sense if not in a deterministic sense. Therefore, fractal geometry provides a good measure of such objects with non-integral dimensions.

The concept of fractional dimension was introduced by Hausdorf (1919). As early as 300 years ago, Leibniz (1721) used the scaling invariance of the infinitely long

straight line for its definition. However, as self-similar entities with fractional dimensions started appearing in the mathematical literature, they were met with distaste. Charles Hermite, the famous mathematician, for example, labeled such entities monsters. However, largely due to the efforts of Benoit Mandelbrot (1982), fractal geometry is now an accepted and extremely useful method of describing and quantifying entities that demonstrate scale invariance and fractional dimensions.

The reviews by Jullien and Botet (1987), Meakin (1988) and Lin *et al.* (1989) on the subject of fractal aggregation are recommended.

For a disordered distribution of mass, such as in a clustering of stars in the Milky Way or the clustering of particles in a colloid, fractal geometry is also useful. A short example is useful. For a solid 2-dimensional disk, the relationship of mass to the radius of the disk is given by:

$$M(r) \sim R^2 \qquad (1)$$

so that in this case, the dimension is an integer and the object is an Euclidean object. However, for a disordered distribution of mass, if at different scales of observation the patterns are statistically self-similar, then the relationship of radius to mass may be given by (Mandelbrot, 1982; Jullien and Botet, 1987; Uriev and Ladyzhinsky, 1996; Vreeker *et al.*, 1992b):

$$M(r) \sim R^D \qquad (2)$$

where D is a fractional or *fractal dimension,* know as the mass fractal dimension. Here, the symbol ~ is taken to mean "approximately proportional to."

2.6 Scaling Theory as applied to Colloidal Gels

The irreversible aggregation of small particles to form clusters is a common natural phenomenon; for example this is seen in colloids (Medalia, 1971), coagulated aerosols (Friedlander, 1977), chemical species precipitating from a supersaturated matrix and crystals growing from a supercooled melt (Mullins and Sekerka, 1963). The final structure of such aggregates is important not only because it potentially can yield information about the mechanical strength of the resulting structures, but can also suggest methods to alter the structure kinetically. In many cases, the rate limiting step of the formation of these aggregates is the diffusion of species towards a growing surface (mass-limited transfer), or the transfer of heat away from the growing surface, or a combination of these factors, depending on the stage of growth.

As early as 1979, Forrest and Witten (1979) demonstrated a class of aggregates that were shown to have density correlations of a power-law form. These aggregates were formed when a metal vapor produced by heating a plated filament was quench condensed, causing metal particles of the order of 40Å radius to drift down onto a microscope slide. The particles were found to arrange in aggregates of the order of 10^5 particles per aggregate. In 1981, Witten and Sander (1981) constructed a computer simulation model for random aggregation which is diffusion limited, and demonstrated that the density correlations within the model aggregates fall off with distance with a fractional power-law, like those of the metal aggregates. Following their earlier work, Witten and Sander (1983) showed that by constructing diffusion limited aggregation

models, the objects so formed are scale-invariant whose fractional dimensionality (Hausdorf dimension) is independent of short-range details. Additionally, they showed that diffusion-limited aggregation has no upper critical dimension. This study made the point that the properties associated with scale invariance are long-range and universal, and that such long-range properties do not arise from long range forces – rather, these long-range correlations are built up by short-range forces. In 1983, cluster-cluster aggregation models which are diffusion-limited were introduced by Meakin (1983) and Kolb *et al.* (1983, 1984), serving to fuel the flurry of interest in analyzing the structural properties of aggregated colloids using fractal theories generated by the work of Witten and Sanders. Meakin's and Kolb *et al.*'s simulation studies suggested that the colloidal aggregates behave as stochastic mass-fractals on a scale that is large compared to the primary particle size. Subsequent experimental studies by Weitz *et al* (1984, 1985) on aqueous gold colloids and Schaefer *et al* (1984) on colloidal aggregates of small silica particles, confirmed the behavior suggested by the simulations. Following this, in 1985, Brown and Ball produced a computer model, which simulated chemically limited aggregation, and suggested that the structures so formed should also behave as mass fractals. Much experimental work in this area ensued in the following years, with Aubert and Cannell performing further work on colloidal silica aggregates (Aubert and Cannell, 1986), Schaefer and Keefer (1986), Courtens *et al* (1987) and Vacher *et al* (1988) on silica aerogels, Rojanski *et al* (1986) on mesoporous silica gels, Dimon *et al* (1986) on gold colloids, Bolle *et al* (1987) on polystyrene lattices, and in a Nature paper, Lin *et al* (1989) investigated three different colloids – colloidal gold, colloidal silica, and polystyrene latex. In all the experimental work detailed above, the fractal nature of the

colloidal aggregates was well demonstrated. Additionaly, colloidal-like gels such as casein gels (e.g. Bremer *et al.*, 1989) have been shown to be composed of homogenous clusters of particles, with the structure within the particles being fractal in nature.

For a particulate system that is composed of a number of aggregate clusters which are fractal, the number of particles, assumed identical, making up the fractal aggregate may then be given by (following Equation (2)):

$$N_p(\xi) \sim \left(\frac{\xi}{\sigma}\right)^D \qquad (3)$$

where $N_p(\xi)$ is the number of particles in a fractal aggregate of size ξ containing particles of size σ, and the system is assumed to be fractal within the range bounded by the size of one primary particle and the size of the entire structure. The particle volume fraction of the object may be expressed in terms of the size of the aggregate and the fractal dimensionality, if one assumes a model such as is described below, originally developed by de Gennes (1979) for polymer gels, independently by Brown (1987) for a network of fractal clusters, and shown experimentally to be applicable to colloidal gels by Dietler *et al.* (1986). The treatment below is loosely adapted from Bremer *et al.* (1989), since these researchers provide an elegant development of the model originally developed by de Gennes and Brown.

One may imagine that a regular square lattice is laid over the fractal object, where each lattice site is occupied by a primary particle, or by a volume element of solution. If the particles are arranged in a fractal manner, the number of lattice sites occupied by

particles in an aggregate is given by equation (3). It is important to note that each particle does not completely fill each lattice site; we do not often encounter square particles in nature. The total number of lattice sites taken up by an aggregate, either with solution, or as particles, is given by:

$$N_a = \left(\frac{\xi}{\sigma}\right)^3 \qquad (4a).$$

Again, this assumes a completely square aggregate, which is not usually the case, so that Eqn. (4a) is more correctly written as:

$$N_a \sim \left(\frac{\xi}{\sigma}\right)^3 \qquad (4b)$$

Therefore, the volume fraction of particles within an aggregate is given by:

$$\Phi_a = \frac{N_p}{N_a} \sim \frac{(\xi/\sigma)^D}{(\xi/\sigma)^3} = \left(\frac{\xi}{\sigma}\right)^{D-3} \qquad (5)$$

According to the models for cluster-cluster diffusion-limited aggregation which were verified experimentally as discussed above, the aggregates grow until they become space filling, thus forming a gel. Therefore, the fractal dimensionality within each gel is maintained, whilst at length scales above the characteristic length of one aggregate, the colloid scales in a Euclidean manner. The sum of all the lattice sites occupied by all the aggregates is equal to the number of lattice sites occupied by the gel, N_t (both by solution and particles):

$$N_t = \sum_{i=1}^{n} N_{a,i} \sim \sum_{i=1}^{n} \left(\frac{\xi}{\sigma}\right)_i^3 \qquad (6)$$

where n is the total number of aggregates. Therefore, the overall volume fraction of particles, Φ_t, is given by the total number of sites filled by particles, divided by the total number of sites in the gel:

$$\Phi_t = \frac{\sum_{i=1}^{n} \Phi_{a,i} N_{a,i}}{N_t} \sim \frac{N_t \sum \left(\frac{\xi}{\sigma}\right)^{D-3}}{N_t} = \left(\frac{\xi}{\sigma}\right)^{D-3} \qquad (7)$$

From Eqn. (7):

$$\xi \sim (\Phi_t)^{\frac{1}{D-3}} \qquad (8).$$

Therefore, the characteristic diameter of an aggregate is related to the overall volume fraction of particles via the mass fractal dimension of the aggregates. As will be discussed in Chapter 5, this relationship suggests that the two factors influencing this relationship is the degree of occupancy of the regular lattice by particles, and the degree of order of the packing of the lattice sites by particles.

2.6.1 Elastic Properties of Colloidal Gels: exploiting the fractal nature of the aggregates

Colloidal gels respond to small amplitude deformations as elastic solids. In 1986, Sonntag and Russel (1986) showed that the elastic modulus of a volume-filling network formed by Brownian flocculation of aqueous polystyrene lattices scaled with the volume fraction of particles in a power-law manner, given by:

$$G' \sim \Phi^{u} \qquad (9).$$

Sonntag and Russel were not the first to experimentally demonstrate this behavior for aggregated systems, for example, other researchers such as Nederveen (1963) and Van

den Tempel (1979) showed that elastic modulus of dispersed systems of microcrystals formed from oils vary with the particle concentraion in a power law manner, and Payne (1964) showed that the elastic modulus of systems formed from aggregates of carbon-black particles in mineral oil demonstrated a power law relationship with particle concentration. Buscall (1982) demonstrated a similar relationship with systems of polystyrene lattices in water. However, Sonntag and Russel were among the first researchers to suggest that scaling arguments put forward by other researchers such as Kantor and Webman (1984), on the elastic properties of random percolating systems, and computer simulations of random lattices by Feng *et al* (1984(a), 1984(b)) may support the relationship that they observed experimentally. At this point, however, the scaling theory had not been developed sufficiently to totally explain the experimental behavior observed by Sonntag and Russel.

Brown (1987) soon after addressed the elasticity of a network of clusters. His method consisted of calculating the elasticity of an individual fractal cluster, and then supposing that in an overcrowded system, fractal behavior survived on a scale related to the overall volume fraction by:

$$\xi \sim \Phi^{\frac{1}{D-3}} \qquad (10)$$

which is the same relationship arrived at in the treatment above (Eqn. 8). Brown predicted that the elastic modulus should scale in the following manner:

$$G \sim \Phi^{u} \qquad (11),$$

which is consistent with that seen by Sonntag and Russel and a number of other researchers, cited above. Additionally, Brown suggested that the exponent u is given by:

$$u = \frac{3 + d_{chem}}{3 - D} \qquad (12)$$

where d_{chem} is the so-called chemical length exponent, introduced earlier in simulation studies by Brown and Ball (1985). Soon after the model of Brown, Buscal *et al* (1988) published experimental evidence supporting this model, for a system of silica particles. Later work by Ball (1989) on the elasticity of aggregates explains higher fractal dimensions (than was originally suggested by Kolb *et al* (1983) and Meakin (1983)) that had been reported by Courtens (1987) and Vacher (1988), by considering that there may be consolidation beyond a critical size of the clusters. Soon after, Edwards and Oakeshott (1989) outlined broad guidelines for the treatment of the transmission of stress in an aggregate, without really achieving more than stating the complexity involved. However, this work is worth mentioning here, since it does point out that the model by Brown (1987) assumes that stress is transmitted in one-dimensional paths, which are branched and are characterized by a fractal dimension, whilst in some cases the situation is more complicated, since the stress has to be spread amongst several neighbours in order to maintain stability of the aggregate.

Following Brown and Ball, Bremer *et al* (1989, 1990) suggested elastic models for colloidal protein networks. These researchers envisioned the networks to be composed of strands of elastic material, where deformation causes a stretching of the strands of the network. The elastic modulus is then a function of the number of stress-carrying strands per unit area, the geometry of the network, and the character of the bonds within the strands. Bremer *et al.* formulated two different scaling relationships for

the elastic modulus to the particle volume fraction, depending on the geometry of the strands. For straight stress-carrying strands, the relationship is:

$$G' \sim \Phi^{\frac{2}{3-D}} \qquad (13)$$

and for curved stress-carrying strands the relationship is:

$$G' \sim \Phi^{\frac{3}{3-D}} \qquad (14).$$

In 1990, Shih *et al* (1990) developed a scaling theory to explain the elastic properties of colloidal gels well above the gelation threshold. The model of a colloidal gel visualized by Shih *et al* corresponds well with the model of a colloidal gel described above: i.e. they define a colloidal gel above the gelation threshold to be a collection of flocs or clusters, which are fractal in nature. These researchers defined two regimes based on the relative value of the elastic constant of the inter-floc links to that of the flocs themselves, and claim that the scaling in these types of gels is affected mainly by the structure of the individual flocs as opposed to percolation-type scaling.

An in-depth development of the model created by Shih *et al* (1990) is provided below, since this model is used extensively in other parts of this thesis. In large part ignoring the progress made in describing the scaling relationship of the characteristic length of the cluster/floc size with particle volume fraction for colloidal gels described earlier, Shih *et al.* uses this identical relationship (given by Eqns. (8) and (10)), but justifies its use because of the fact that it was found to be true for polymeric gels by de Gennes (1979). They defend the use of this relationship for colloidal gels because colloidal gels are similar to polymeric gels by the fact that both are viscoelastic materials,

and that both are formed by aggregation processes; polymeric gels by polymerization and/or crosslinking, and colloidal gels by particle aggregation. However, Shih *et al.* does quote the experimental evidence of Dietler *et al.* (1986) for the validity of this relationship for colloidal gels. It is important to mention that there is indeed sound theoretical reason why this relationship may be used for colloidal gels as well, as was developed above (after Brown (1987), and Bremer (1989)).

According to Shih *et al*, the elastic properties of a floc/cluster is dominated by its effective backbone (connected path of particles responsible for transmission of stress), the size of which is ξ, same as the size of the floc/cluster. This backbone may be assumed to be a linear chain of springs, with each spring representing the bond between particles forming the backbone; a justifiable assumption, since the formation of aggregates via cluster-cluster aggregation which is either reaction limited or diffusion limited have very few loops. The point made by Edwards and Oakeshott(1989), as discussed above, concerning the limitations of an effective backbone argument must also be reiterated at this point – it is not entirely clear to the author whether this is a valid assumption, for the reasons given by Edwards and Oakeshott. An earlier publication by Kantor and Webman (1984) formulated the elastic constant of a linear chain of springs as:

$$K_s = \frac{G}{N_{bb} S^2} \qquad (15)$$

where G is the bending elastic energy, N_{bb} is the number of springs in the chain and S is the radius of gyration of the projection of the nodes of the chain in the **F X Z** direction, **F** being the applied force and **Z** being the normal of the plane within which the chain lies.

Equation (15) ignores the stretching elastic energy of the chain, since it has been shown by Kantor and Webman (1984) to be negligible for long chains, and is only important for comparatively straight chains stretched along their long dimension. Therefore, when the chain in question is the effective backbone of a floc/cluster, the elastic constant of the floc is given by:

$$K_\xi = \frac{G}{N_{bb}\xi^2} \qquad (16)$$

where the radius of gyration has now been replaced by the size of the effective backbone (or the size for the floc), since these two quantities would be the same. Now, the backbone of the flocs themselves are fractal objects, for which a fractal dimension between 1 and 2 can be defined, since instead of a straight chain, the backbone would have a certain tortuosity. In keeping with the fractal concept, where a line is kinked enough so that its dimension is raised to a fractional index between 1 and 2, the number of particles, and therefore the number of springs, in the backbone is given by:

$$N_{bb} \sim \xi^x \qquad (17)$$

where x is the fractal dimension of the effective backbone, or the tortuosity of the effective backbone, and $x \geq 1$ in order to provide a connected path through the floc/cluster. Now, combining Eqns. (16) and (17), one may represent the elastic constant of the floc by:

$$K_\xi \sim \frac{G}{\xi^x \xi^2} = \frac{G}{\xi^{2+x}} \qquad (18).$$

Now, if the elastic energy G is not a function of concentration, then the elastic constant of the flocs should decrease rapidly with increasing floc size. This point strikes the author as being suspect, since it is inconceivable that the elastic energy of a bent chain is

not dependent on the density of the springs which comprises the chain. It is conceivable that the density of the particles (density of springs) never really changes with concentration, since the length of the effective backbone (length of the chain) also changes with concentration (via Eqn. (8)). If the change in particle volume concentration of the entire system is compensated for in terms of an increased effective backbone length, resulting in no change of the density of particles in the effective backbone, then the bending elastic energy, G, may be considered independent of particle volume concentration. Therefore, if the flocs are allowed to grow larger, they behave as weaker springs. Now, the macroscopic elastic constant of the system of flocs may be expressed either as a function of the elastic constant of the flocs, K_ξ, or the elastic constant of the links between flocs, K_l, depending on the relative strength of K_ξ and K_l. Since from Eqns. (8) and (10) the characteristic length of the flocs/clusters, ξ, is related to the particle volume concentration, and since the elastic constant of the flocs will decrease with increasing ξ to a power of $2 + x\,(>3)$, then the relative strengths of K_ξ and K_l will be affected by the particle concentration of the system. To illustrate this, one may express the elastic constant of the flocs in terms of the particle volume concentration, by substituting for ξ in Eqn. (18):

$$K_\xi \sim \frac{G}{\xi^{2+x}} \sim \frac{G}{\left(\Phi^{\frac{1}{D-3}}\right)^{2+x}} = \frac{G}{\Phi^{\frac{2+x}{D-3}}} = G\Phi^{\frac{2+x}{3-D}} \qquad (19).$$

Therefore, the elastic constant of the flocs will get larger with increasing particle volume concentration. Obviously, as the particle volume concentration increases, there will be a cross-over point at which the elastic constant of the flocs is greater than the elastic links

between the flocs, resulting in the elastic constant of the entire system being determined by the nature of the links between clusters (this is called the weak-link regime). The converse, where the particle volume fraction decreases beyond the cross-over point, is also true, and in this case the elastic constant of the flocs grow weaker than the elastic constant of the links between flocs, leading to the elastic constant of the system being determined by the nature of the elastic constant of the flocs (this is called the strong link regime).

Therefore, for the strong link regime, the macroscopic elastic constant of the system is given by:

$$K \sim \left[\frac{L}{\xi}\right] K_\xi \qquad (20),$$

where L is the macroscopic size of the system. Therefore, for a constant macroscopic size of the system, combining Eqn. (20) with Eqn. (19), and again substituting for ξ from Eqn. (8):

$$K \sim \xi^{-1} G \Phi^{\frac{2+x}{3-D}} \sim \Phi^{\frac{1}{3-D}} \Phi^{\frac{2+x}{3-D}} = \Phi^{\frac{3+x}{3-D}} \qquad (21),$$

assuming that the elastic energy of the effective backbone does not change with concentration. Therefore, the macroscopic elastic constant of a colloidal gel at comparatively low concentrations is given by (the strong link relationship):

$$K \sim \Phi^{\frac{3+x}{3-D}} \qquad (22).$$

As is evident from Eqn. (22) and (12), the strong-link formulation of Shih *et al* is consistent with that developed by Brown (1987), if one assumes that the tortuosity, x, is

the same as the chemical length exponent, a concept which is does not deviate from the explanation offered by Brown. Shih *et al*(1990) also studied two types of boehmite alumina gels, Catapal and Dispal powders, rheologically. The elastic behavior of both gels confirmed the strong link relationship given by Eqn. (22). Fractal dimensions calculated from the rheological measurements agreed well with those calculated from static light-scattering measurements.

For the weak link regime, the macroscopic elastic constant of the system is given by:

$$K \sim \left[\frac{L}{\xi}\right] K_l \qquad (23).$$

Substituting for ξ from Eqn. (8):

$$K \sim \Phi^{\frac{1}{3-D}} \sim G' \qquad (24).$$

where G' is the shear elastic modulus of the system. Here, Eqn. (24) assumes that the links between flocs/clusters are of constant strength. It is important to note that the elastic constant of the links between flocs is not expressed in terms of the geometry of the network. However, Eqn. (24) does provide a scaling relationship of the elastic constant of colloidal gels at high concentrations, with the particle volume fraction.

After the development by Shih *et al.* (1990), Chen and Russel (1991) studied the elastic behavior of a synthesized model system consisting of submicrometer silica spheres coated with octadecyl chains suspended in hexadecane. This study demonstrated

that the elastic modulus of the colloidal system increased with particle volume concentration in a power law manner, and that the power law exponent increased with increasing temperature, indicating a structural change in the network. It was obvious that the power law exponent was sensitive to the packing of the particles (disturbed when the temperature is increased) – suggesting that the power was dependent on the fractal dimension. This work further served to lend credibility to the scaling models outlined by Brown (1987), Bremer (1989, 1990) and Shih *et al.* (1990).

Vreeker *et al.*(1992a) showed that colloidal-like aggregates of whey proteins gels are fractal in nature, utilizing dynamic light scattering measurements. Additionally, they analyzed the protein gels rheologically, showing that the elastic moduli and yield stresses varied with protein concentration according to a power law. They related the power law exponent to the equivalent models by Brown(1987) and (strong link model) by Shih *et al.*(1990), and to the models by Bremer (1989, 1990). By the value of the exponent measured experimentally, they were able to calculate fractal dimensions according to the various models. The fractal dimensions so calculated were all in reasonable agreement with those measured by the dynamic light scattering experiments. Therefore, these researchers concluded that there was no basis for the validity of one model versus another, based on their experiments. This partly stemmed from their inability to measure the chemical length exponent or tortuosity. In this work, they assumed x had a value which varied between 1.0 and 1.3 (suggested by Shih *et al.* (1990) based on conductivity measurements).

Hagiwara *et al.* (1997, 1998) have analyzed a number of different types of protein gels using both rheological measurements to study the elasticity of the gels, and analysis of confocal laser scanning microscopy images of the gels, to study the structure of the gels. These researchers found that for the gels they studied, the weak link regime of Shih *et al.* (1990) was valid. The gels demonstrated a power-law dependence on particle volume concentration, and the fractal dimensions calculated from the power law exponent, using the weak link formulation, agreed very well with fractal dimensions calculated from image-analysis of the confocal laser scanning micrographs of the gels. Therefore, both the strong link formulation and the weak link formulation of Shih *et al.* (1990) have been demonstrated experimentally. The weak link has been demonstrated more convincingly, since with the strong link regime, experimentalists have had to assume a value for the tortuosity of the backbone, and therefore the theory could not be tested well against those of Bremer (1989, 1990).

2.7 Application of scaling theory developed for colloidal gels to fat crystal networks

In 1992, Vreeker *et al.* (1992b) presented an interpretation of rheological data for aggregate fat networks in the framework of scaling theories developed for colloidal gels. These authors showed that the elastic modulus of the network (G') varied with solid fat content (Φ_{SFC}), according to a power law, similar to that predicted by models for the elasticity of colloidal gels. I have used the symbol Φ_{SFC} for the solid fat content of the fat network to distinguish it from the particle volume concentration Φ, since these two parameters are not equivalent, but in the Vreeker *et al.* (1992b) paper and in many such publications following, these two parameters have been used as being equivalent. As will

be demonstrated in Chapter 5 of this thesis, Φ_{SFC} and Φ are directly proportional to each other, however. The article by Vreeker *et al.* provides an interpretation of rheological data for low Φ_{SFC} fats in terms of the strong link model of Shih *et al.* (1990), developed, as is detailed above, for colloidal gels at low particle concentrations. From this rheological investigation of the fat network, a fractal dimension could be calculated, using the strong link formulation given by Eqn. (22), and assuming that the tortuosity of the system, x, had a value between 1 and 1.3. This article also details the measurement of a fractal dimension of the network via light scattering methods, which agreed well with that calculated from the strong link formulation. However, no attempt was made in this article to show that the structure of a fat crystal network at such low solid fat contents (low Φ_{SFC}) is organized in a similar manner to the way a colloidal gel is organized, in order to warrant the use of the strong link formulation. It was unclear as well, in this article, what the primary particles of the gel constituted, and at what length scales the network was fractal (although the fact that light scattering methods were used to calculate the fractal dimension suggests that perhaps the length scales of importance lay in the microstructure region i.e., at a length scale greater than the crystalline level of structure). Therefore, this article served to demonstrate solely that the elastic constant of the network varied in a power law manner, reminiscent of that demonstrated by colloidal gels. No justification for using the strong link model was made from a structural perspective, mainly because these authors did not adequately define the structure of the network. However, this article remains one of the most important developments in the field, for it demonstrated conclusively that the elastic modulus of low Φ_{SFC} fat crystal networks scale in a power law fashion with the solid fat content. The physical and structural

implications of the calculated fractal dimension using the strong link formulation of Shih *et al.* (1990) was at this point unclear.

The analysis of Vreeker *et al.* was interesting enough for Marangoni and Rousseau (1996) to apply the model developed by Shih *et al.* (1990) for high concentration colloidal gels (weak-link theory described above) to fat crystal networks of high solid fat concentration. As is explained above, the weak link model offers the ability to relate small deformation rheological measurements (shear elastic modulus) to the fractal dimension of the network. As was the case with the work by Vreeker *et al.* (1992b), Marangoni and Rousseau had no structural basis upon which to justify the application of the weak link theory, developed for a particular geometry of colloidal aggregates, to fat crystal networks. The main reason for applying this type of analysis was the fact that the analysis by Vreeker *et al.* (1992b) produced a power-law relationship for low solid fat content fats. Additionally, as described before, the only variation of structure that accompanied the decrease in hardness index and elastic moduli of milkfat upon chemical interesterification, was a change in the microscopically-observed microstructure. Marangoni and Rousseau (1996) attributed the weak link model with a quantification of the microstructure of the network, but offered no explanation as to why the fractal dimension calculated from the application of the weak link theory was a quantification of microstructure. However, the rheological application of the weak link theory of Shih *et al.* (1990) to NIE and CIE milkfat blends demonstrated a power law relationship between the shear elastic moduli of the networks and the solid fat content of the networks, given by $G' \sim \Phi^{n}$. Fractal dimensions calculated using the weak link

theory produced fractal dimensions of 2.46 and 2.15 for the NIE milkfat and CIE milkfat, respectively. Given that there was a qualitative change in microstructure upon chemical interesterification, and that there was a large change in the fractal dimension of these gels upon application of the weak link theory, it did indeed seem possible that the fractal dimension was a measure of microstructure, in some undefined manner. At any rate, Marangoni and Rouseau (1996) attributed the change in structure indicated by a change in fractal dimension to the change in hardness of the milkfat upon chemical interesterification, a reasonable conclusion. In defense of the claim by Marangoni and Rousseau(1996) that the fractal dimension was in some manner a quantification of microstructure, it must be recalled that Vreeker *et al.* (1996) utilized dynamic light scattering measurements to calculate a fractal dimension that agreed well with their rheological analysis, therefore suggesting that the structures that were indeed fractal are in the microstructural range.

Following their 1996 work, Rousseau and Marangoni (1998b) utilized the weak link model to analyze the rheological behavior of non-interesterified (NIE) milkfat and enzymatically interesterified milkfat (EIE). The fractal dimension of milkfat changed from 2.59 to 2.50 upon interesterification. However, there was also a large decrease in solid fat content upon enzymatic interesterification, so that the drop in hardness index and shear elastic moduli observed by these authors was not entirely due to the decrease in fractal dimension. However, here again, the rheological scaling behavior was observed, and fractal dimensions could be calculated from the weak link formulation. One is reminded by the results of this study that indicators of macroscopic mechanical properties

such as solid fat content are indeed valid and necessary for a comprehensive description of the mechanical properties of the network, although as in the case of the CIE and NIE milkfat samples detailed earlier, such variables are not always direct indicators of changes in mechanical properties.

Marangoni and Rousseau (1998b) also studied the rheological scaling behavior of non-interesterified (NIE) and chemically interesterified (CIE) lard-canola oil blends and palm oil-soyabean oil blends. The power law relationship of elastic modulus to solid fat content was again observed, and fractal dimensions could be calculated for all the systems, by using the weak link formulation. No change was observed in hardness index or elastic modulus of the palm oil-soyabean oil blends upon chemical interesterification, and neither were there any changes in the fractal dimension upon chemical interesterification. Solid fat content did not change upon chemical interesterification either. Therefore, it seems that indeed the fractal dimension was an indicator of macroscopic hardness: whether this was true because it was an indicator of the microstructure could not reasonably be extrapolated from the evidence presented by Marangoni and Rousseau (1998b). The hardness index and elastic moduli of lard increased upon chemical interesterification, but the fractal dimension did not change, neither did the solid fat content. It therefore seems at first glance that not only is the solid fat content an insensitive indicator of macroscopic hardness, but so is the fractal dimension. Here again, one is reminded that there are many structural indicators of macroscopic mechanical properties, and one must consider them all in concert. However, are there other indicators of hardness that can be accessed through the rheological

analysis? At this point, it is perhaps important to briefly examine the method of rheological analysis used by these authors. The weak link theory of Shih *et al.* was tested by plotting $\ln(G')$ as a function of $\ln(\Phi_{SFC})$ for various fat systems. According to the weak link theory of Shih et al. (Eqn. 24) the slope of such a plot should yield (1/3-D). What about the intercept of the graph? Marangoni and Rousseau(1998b) wrote Eqn. 24 as:

$$G' = \gamma \Phi^{\frac{1}{3-D}} \qquad (25),$$

and defined γ as a constant which is related to the particles which make up the network. In this, Marangoni and Rousseau were influenced by Bremer *et al.* (1990), who in their publication, formulated a similar law, where the pre-exponential factor was a constant depending on the nature of the particles and the links between them. Equation (25) bears further scrutiny at this point – it should be evident that Eqn. (24) may be written as:

$$G' \sim \Phi^{\frac{1}{3-D}} K_l \qquad (26),$$

where, as the reader would recall, K_l is the elastic constant of the links between aggregates. Certainly, therefore, K_l would depend on the nature of the particles and the links between them, and would contribute to the value of γ. Although Marangoni and Rousseau (1998b) did not offer this justification for their description of the constant γ, it however seems to be appropriate. At any rate, the intercept of the $\ln(G')$ vs. $\ln(\Phi_{SFC})$ graph should yield $\ln(\gamma)$ as the intercept, allowing a value of γ to be calculated. Therefore, if the fractal dimension offered a quantification of the spatial distribution of the microstructure (as yet undefined how), then the constant γ contained information on the influence of the particles and the links between them on the elastic constant of the

network. Now, on chemical interesterification, there was a four-fold increase in the value of the constant γ for the lard-canola oil system, which according to Eqn. (25), should have been accompanied by an increase in the elastic modulus, as was observed experimentally by Marangoni and Rousseau. As for the palm oil-soyabean oil system, there was comparatively no change in the value of γ. Therefore, the scaling behaviour of the fat crystal network, if the weak link is utilised, seems to suggest that there are three important indicators of macroscopic hardness: solid fat content, the fractal dimension, and the constant γ. It must be stated at this point that this does not mean that other indicators such as the crystalline nature of the network and the molecular ensemble of the network is being ignored by identifying D, Φ, and γ as the three important indicators. Since γ has been suggested to depend on the nature of the particles and the links between them, it almost certainly is dependent on the polymorphism of the network, which in turn is dependent on the molecular composition of the network.

2.8 Network Models

As presented above, phenomenological investigations have been made on the rheology of fat crystal networks, the results of which have been interpreted by models developed for colloidal gels. Not only has this not been structurally justified, but this analysis excluded any structural and mechanical model of the fat network. In large part, the authors working in the field (mainly Marangoni and Rousseau, *et al.* and Vreeker *et al.*, detailed above) could not include a structural and mechanical model of the network, since there existed at the time no mechanical and structural model that predicted that the

structure of the fat crystal network at any length-scale was fractal in nature. It must also be mentioned that the scaling behavior demonstrated experimentally by these authors were not adequately explained by the existing network models. Presented below is a brief introduction to the network models that existed in the literature before the work to be detailed in this thesis.

Early work on a network model was performed by van den Tempel (1961). In his 1961 publication, he suggested modeling the network as a collection of particles held together by van der Waals-London forces. The structural model that was assumed by van den Tempel was that the network is made up of straight chains oriented in three mutually perpendicular directions, each chain consisting of a linear array of particles. The bonds between particles were formed from van der Waals-London forces. The relationship of the elastic modulus to the solid fat content of the network arrived at by van den Tempel is:

$$G' = \frac{5AD^{0.5}\Phi_{SFC}}{24\pi H_o^{3.5}} \qquad (13)$$

where A is the Hamaker's constant, D is the diameter of the particles, H_o is the equilibrium distance between particles, and Φ_{SFC} is the solid fat content.

The relationship of G' to Φ_{SFC} is a non-linear, power-law type of relationship, as was experimentally verified by the researchers detailed in 2.7 above. The work by van den Tempel failed to correctly predict this experimentally observed power law relationship of G' to Φ_{SFC} because, according to Vreeker *et al.* (1992b), it did not take

into consideration the fractal arrangement of the network at certain length scales. Furthermore, van den Tempel only considered the attractive forces in his treatment, choosing to ignore whatever repulsive forces were present.

In 1963 Nederveen (1963) used the same structural model as van den Tempel, but incorporated the repulsive forces acting between particles (he considered the Lennard-Jones potential between two particles). Nederveen found the following formula for the modulus of elasticity:

$$E = \left(\frac{A\Phi_{SFC}}{2\pi d_o} \right) \left(1 - \frac{11R\varepsilon}{d_o^2} \right) \qquad (14)$$

where R is the particle radius, ε is the strain of the deformation, d_o is the equilibrium distance between two particles, and A and Φ_{SFC} are as defined earlier. Again, Nederveen's formulation failed to show the non-linear dependence on Φ_{SFC}, due perhaps to an unrealistic structural model of the network which did not involve the fractal geometry claimed by the authors detailed in section 2.7 above.

In 1964, Payne (1964) tried to apply the linear chain concept of van den Tempel to carbon black networks in oil, but found that the shear modulus was inversely proportional to some power of the particle diameter, not in agreement with van den Tempel's or Nederveen's equation. This study may however be inconclusive about the

validity of these equations, since the discrepancy may have been due to the non-homogenous distribution of the carbon black spheres.

In 1968, Sherman (1968) proposed a different model for flocculated o/w emulsions involving chain-like configurations which form coils with cross-linkages, resulting in interlinked spherical structures. In his model, localized regions of densely packed particles are joined to less densely packed regions, consequently the degree of interlinking is not the same throughout the entire flocculate. The formulation of G' for this model is:

$$G' = \Phi_{SFC}(1 + 1.828v)\frac{A}{36\pi D^3 H_o^3} \qquad (15)$$

where v is the total volume of the continuous phase held in voids between the particles, D is the diameter of the particles, H_o is the minimum equilibrium distance between particle surfaces and A is called the interaction constant (Hamaker's constant) and Φ_{SFC} is as defined above. Whilst Sherman's equation agreed with Payne's observations in terms of particle diameter, it also shows a linear relationship with Φ_{SFC}, contrary to what has been demonstrated experimentally.

In 1979, van den Tempel (1979) revised his structural model of fat crystal networks; he suggested that clusters (microstructures) of particles make up the chains, rather than particles. Additionally, he suggested that the forces holding the clusters together were due to common "chains" of particles between clusters. He used this argument to modify his original equation, but again did not take into consideration any

fractal arrangement of the network. Various other researcher have tried to modify van den Tempel's work, in varying degrees of complexity (Kamphuis and Jongschaap, 1985; Kamphuis *et al.*, 1984; Papenhuijzen, 1971; Papenhuijzen, 1972). However, none of these models took into consideration a fractal arrangement of the network, and none demonstrated a power-law dependence of G' on Φ_{SFC} as is observed experimentally.

2.9 Objectives

The progress made in the ability to predict the macroscopic rheological properties of fat crystal networks from a consideration of the structure of the network has been summarized in sections 2.1 – 2.8. Now that the reader has been made aware of the development of the field, it is pertinent to introduce the objectives of this thesis. These are:

1) Firstly, because the over-arching goal of the field is concerned with being able to predict the macroscopic hardness of fat crystal networks from a structural perspective, a suitable rheological indicator of macroscopic hardness will be investigated. The hardness index is not suitable since its measurement requires the destruction of the network. An indicator of hardness which allows one to predict hardness whilst maintaining the structural integrity of the network is therefore needed. The elastic modulus of the network will be investigated for its suitability as such an indicator.

2) Two confectionary fats of interest to the fats and oils industry will be investigated

utilizing the rheological analysis established by Vreeker *et al.* and Marangoni and Rousseau, detailed above. The weak link theory will be used to analyze the rheological behavior, since high solid fat content samples of these fats are important to the industry, and we have seen (as detailed above) that the weak link is appropriate at these concentrations. The microstructure of these fats will also be studied microscopically, with an aim to unravel the reason for the applicability of the weak link theory to fat crystal networks.

3) Imaging techniques will be utilized in order to visualize the microstructure of fat crystal networks, so that a clear and concise summary of the different hierarchies of structural organization within fat crystal networks is available.

4) The structure, especially the microstructure, of fat crystal networks will be investigated microscopically, in order to determine whether the structure is fractal in nature, and to establish the length scales that bind the fractality of the system. The kinetics of formation of the network will also be investigated, in order to relate the nature of formation of the network to similar growth modes demonstrated by colloidal gels. Effort will be made to calculate the fractal dimension of the network from image analysis of representative micrographs of the network, since light scattering experiments are not applicable to the high solid fat contents. Attempts will be made to answer the question: is it possible to construct a model similar to the Shih *et al.* weak link model for fat crystal networks?

5) Attempts will be made to construct a mechanical model for the deformation of the fat crystal network at such levels of deformation that the network is within its linear viscoelastic range. The intent of this model will be to express the elastic link between the fractal flocs of the network (if indeed one can relate the structure of the fat crystal network to that of a colloidal gel) in terms of the structural characteristics of the network. The motivation is the expression of the constant γ in terms of the structural attributes of the network.

6) If the above objectives can be met, the effectiveness of the weak link theory in predicting changes in elastic modulus due to changes in environmental conditions under which the network is formed will be investigated. Specifically, it will be investigated whether observed changes in structure of the network may be used to predict changes in those parameters prescribed by the weak link theory to affect elastic properties of the network. The physical implications of the fractal dimension and the constant γ in terms of structure and processing conditions will therefore be investigated, with the purpose of assessing the manipulation of these parameters via processing conditions in order to achieve desired mechanical properties for a particular fat network.

Chapter 3

Elasticity and Hardness

The food engineer is concerned, among other things, with the parameters that affect the sensory impressions of the food product. Those engineers who work on foods containing significant amounts of fat are ultimately concerned with predicting and influencing the sensory attributes of the food itself, which may not be necessarily related in a direct manner to the sensory impressions contributed by the fat crystal network formed within the food. It is however generally accepted in the fats and oils field that the sensory impressions of a food product containing significant amounts of fat is

significantly influenced by the sensory impressions contributed by the fat crystal network formed within the food. Hardness is but one macroscopic parameter that contribute to the sensory impression of a fat crystal network. However, even hardness is difficult to relate to structure, as is discussed below. It has been previously established that the hardness of a fat crystal network, as determined by large-scale rheological analyses such as cone penetrometry, is directly correlated to hardness determined by sensory analyses (Haighton, 1959; Dixon and Parekh, 1979; Hayakawa and de Man, 1982, Lefebre, 1983; Rousseau and Marangoni, 1999). The determination of hardness by large deformation measurements such as cone penetrometry, however, destroys the structure of the network. It is therefore uncertain what role the undisturbed network plays in the contribution to the hardness properties observed by sensory analyses, when large-scale rheological analyses are performed. The structure of the undisturbed network must certainly affect the hardness of the network, and one can only trace the effect of processing conditions to the observed hardness through the formation of a particular structure of the undisturbed network. Certainly, the way in which the undisturbed networks breaks under large scale rheological analyses is of paramount importance, but the nature of the undisturbed network will play a large role in the manner in which the network is broken under such analyses. It is therefore important to identify a rheological indicator of the undisturbed network, and its relationship to large scale rheological measurements, so that the influence of the undisturbed structure of the network on hardness may be followed. The elastic modulus of the network is a rheological indicator the measurement of which does not destroy the structure of the network, since this small-deformation measurement is done within the linear viscoelastic range of the network. Since the use of elastic modulus

as an indicator of the mechanical strength of the fat crystal network will be used throughout this thesis, this chapter outlines the definition of the elastic modulus, as well as yield values obtained from large-scale rheological analyses. Details of experiments performed to relate measurements of elastic modulus to hardness index measurements (or yield values) performed by cone penetrometry are provided, along with the results from such experiments. In many ways, taking this approach to the problem reduces even further the complexity of the situation, but at the same time, using the elastic constant of the system as an indicator of hardness certainly also results in reduced ability to predict macroscopic hardness. However, one begins building the picture by first simplifying and then hopefully adding levels of complexity as the understanding of the area progresses.

3.1 Theory and Review: Elastic Modulus

In most solids, atoms and molecules are arranged in some order. How rigidly these atoms and molecules are held about their equilibrium positions depends on the relative strength of the short-range forces between them. In the classical picture of a regular material such as a metal, the extension of say a metal wire is due to a displacement of the molecules within the wire from their mean positions. If the displacement is small enough, the restoring force towards the mean positions of the molecules is proportional to the displacement. To understand this statement, one may consider the variation of potential energy, U, between two molecules at a distance r apart. Depending on the separation distance, the potential energy is either negative or positive. The general form of the potential energy function, therefore, is given by:

$$U(r) = \frac{a}{r^p} - \frac{b}{r^q} \qquad (3.1)$$

where p and q are powers of r and a and b are constants. Since the force F between the two molecules is given by:

$$F = -\frac{dU}{dr} \qquad (3.2),$$

the positive term with the constant a in Eqn. (3.1) indicates a repulsive force and the negative term with the constant b represents an attractive force. It is difficult to formulate the exact mathematical form of the potential energy curve that describes the interaction of molecules, partly because there are different types of bonds or forces between atoms and molecules in solids, depending on the nature of the solid. A much-used general expression for the potential energy relationship for non-polar molecules is given by the expression attributable to the English chemist J. E. Lennard-Jones:

$$U(r) = \left[\left(\frac{\mu}{r}\right)^{12} - \left(\frac{\lambda}{r}\right)^{6}\right] \qquad (3.3)$$

where λ and μ are adjustable parameters. In an ionic solid, for example sodium chloride, the potential energy relationship is given by:

$$U(r) = \frac{a}{r^9} - \frac{b}{r} \qquad (3.4).$$

If one considers the Lennard-Jones form of the potential energy function, as is depicted in Figure 3.1, it can be seen that there is a value of r which corresponds to a potential energy minimum; this value of r, r_o, is the equilibrium spacing between the molecules. Figure 3.1 also shows the force as a function of r, given by Eqn. (3.2). At a distance r_o, the repulsive and attractive forces balance, i.e. $F = 0$. If the separation r between the molecules is slightly increased from r_o, the attractive force between them will restore the molecules to their equilibrium position after the external force is

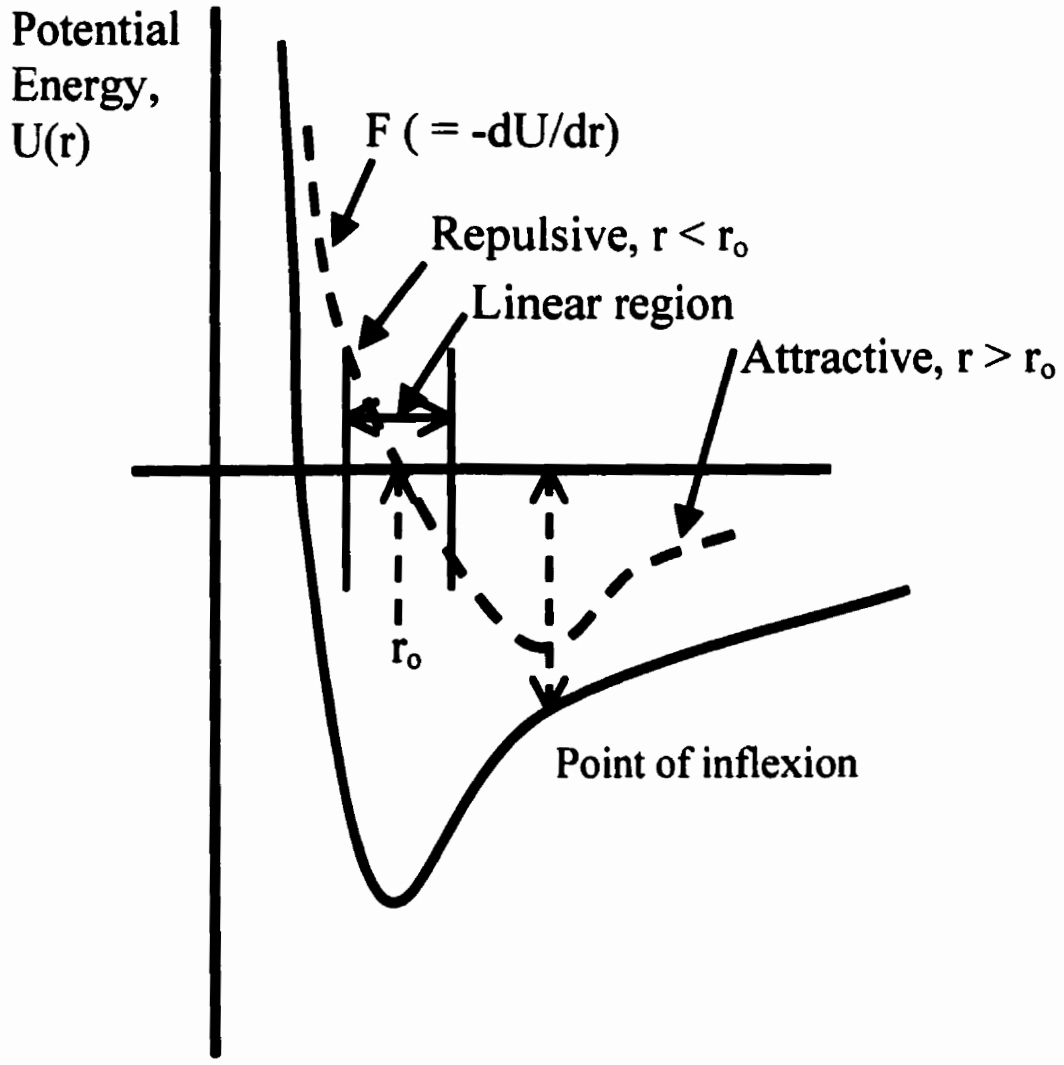

Figure 3.1: Schematic Lennard-Jones potential energy curve

removed. If the separation is decreased from r_o, the repulsive force will restore the molecules to their equilibrium position after the external force is removed. Therefore, the molecules of a solid oscillate about their equilibrium or mean position. Now, if one examines Figure 3.1 closely, the graph of F vs. r is approximately linear at small distances from the equilibrium position r_o. This means that the extension of the bond is proportional to the applied force, when the displacement is small distances away from the equilibrium position of the molecules. The force constant, k between the molecules is given by:

$$F = -k(r - r_o) \tag{3.5}$$

where r is slightly greater than r_o. Therefore,

$$k = -\frac{dF}{dr} \tag{3.6}$$

or the force constant is given by the negative of the gradient of the tangent to the force-distance curve at $r = r_o$. In a macroscopic sense, this behavior of the molecules leads to Hooke's law (discovered by Robert Hooke, founder of the Royal Society, in 1676), which states: " the extension is proportional to the force or tension in a material if the proportional limit is not reached." So the extension of the wire is due to the displacement of its molecules from their equilibrium positions. The molecules are therefore undergoing simple harmonic motion, vibrating about their equilibrium position, and up to the proportional limit, the energy gained or stored by the stretched wire is molecular potential energy, which is recovered when the external force is removed. Therefore, for systems such as a wire or a large sodium chloride crystal, where the arrangement of the molecules are such that the macroscopic structure is built up by the constant repetition of

the molecular lattice, or unit cell, the elastic properties, characterized by an elastic constant k, may be inferred from a molecular argument.

The Hooke's law behavior is, however, also observed for materials where one cannot easily explain the elasticity from molecular considerations. Such materials include colloidal gels, fat crystal networks, composite materials such as concrete, and ceramics, etc. In such materials, there are distinct hierarchies of structure, and the stressing or elongation of the macrostructure does not necessarily relate to a stressing of the molecular level. In such materials, the limit of elasticity is encountered at levels of structure which are super-molecular. Therefore, the structural entities which are stressed when the macrostructure is stressed may be aggregates of molecules, aggregates of crystals, single crystal entities, polymer strands, etc. However, the molecular picture does provide an important analogy in the pursuit of an understanding of the elasticity of such materials. It is not an unreasonable assumption that at some level of structure that is being stressed, the applied force varies with the change in distance between the structural entities of importance in a linear manner, which translates to the macroscale. It is never a trivial matter to attribute responsibility for the elasticity of a material to a particular structural level. Therefore, although it is implicitly understood that the material is composed of a large number of discrete structural entities that are responsible for its elasticity, it is advantageous to regard the system as a continuous distribution of matter.

To therefore develop an understanding of physical quantities of a material such as its elastic modulus, we consider the material as a deformable continuum. When external

forces are applied to such a system, a distortion results because of the displacement of the "relevant structural entities" from their equilibrium positions, and the body is said to be in a state of stress. After the external force is removed, the body returns to the equilibrium position, providing the applied force was not too great. Therefore, the elasticity of a material is defined as the ability of a body of this material to return to its equilibrium shape after the application of an applied force. To reach a quantitative definition of elasticity, one must first understand the concepts of stress and strain.

If we consider that a body is acted upon by an external force $\Delta\bar{F}$, which is neither tangential or normal to the surface upon which it acts, as is depicted in Figure 3.2, then the average stress on the surface with area ΔA is defined as the force per unit area:

$$\bar{S} = \frac{\Delta\bar{F}}{\Delta A} \qquad (3.7).$$

Therefore at some infinitesimal point p on the surface, the stress is given by:

$$\bar{S} = \lim_{\Delta A \to 0} \frac{\Delta\bar{F}}{\Delta A} = \frac{d\bar{F}}{dA} \qquad (3.8).$$

If we consider that the external force $\Delta\bar{F}$ acting may be resolved in two components – one that is tangential to the surface, and one which is normal to the surface at the point p, then the stress $\bar{S}$ may also be resolved into tangential and normal stress. The tangential component of the stress is referred to as the shear stress, and the normal component is referred to simply as normal stress. The normal stress may either be in compression or tension, depending on whether the applied force is a push or pull, respectively. Referring to Figure 3.2, the normal stress, s, at point p is given by:

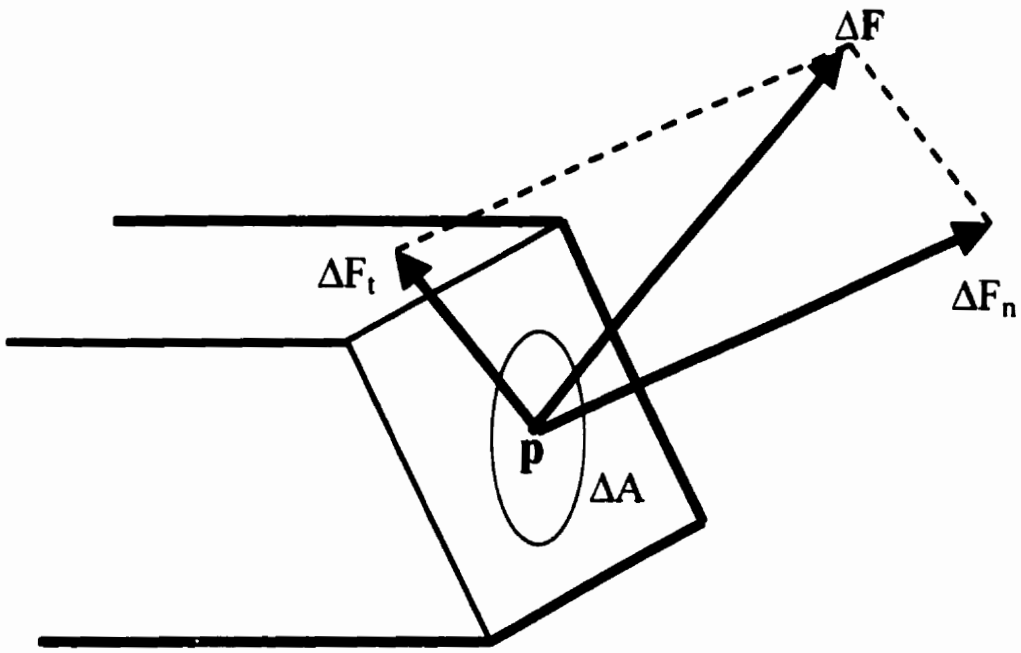

Figure 3.2: Schematic of a body being acted upon by an external force.

$$s = \frac{dF_n}{dA} \qquad (3.9)$$

and the shear stress, τ, at the point p is given by:

$$\tau = \frac{dF_t}{dA} \qquad (3.10)$$

Now, the effect of an applied stress on a body is to cause a change in size and shape of the body. Strain is the quantity that measures the relative change in size or shape of the body when under the applied stress.

If one considers a rectangular rod, with a cross-sectional area A, which is subject to a normal force, F, then the application of the force will induce a change in length of the rod. If the initial length of the rod is L_o and the increased length of the rod is L, then the change in length is given by $\Delta L = L - L_o$. Recall that the normal stress is given by:

$$s = \frac{F_n}{A} \qquad (3.11)$$

and the strain ε induced by this stress, called the longitudinal or tensile strain, is given by:

$$\varepsilon = \frac{L - L_o}{L_o} = \frac{\Delta L}{L_o} \qquad (3.12).$$

Within the elastic region of the material, the ratio of stress to strain is called the elastic modulus and is constant, and in the case of a normal stress and a tensile strain, the ratio of stress to strain is called the Young's modulus or tensile modulus. The Young's modulus, E, is given by:

$$E = \frac{s}{\varepsilon} = \frac{F_n / A}{\Delta L / L_o} \qquad (3.13)$$

The dimensions of the Young's modulus are the same as those of stress, since strain is a dimensionless quantity. These dimensions are N/m^2 or Pa. Now, within the region where stress/strain is constant, the material is obeying Hooke's Law:

$$F_n = k\Delta L \qquad (3.14)$$

where k is the stiffness of the material, sometimes referred to as the spring constant of the material. One may then relate the stiffness of the material to its Young's modulus by considering Eqns. (3.14) and (3.13):

$$k = \frac{E A}{L_o} \qquad (3.15).$$

Therefore, for a given material, within the elastic region, the Young's modulus and stiffness constant are important parameters that yield information about the deformability of the material, and therefore about the sensory impact of the material when one deforms it in the mouth.

The proportionality relationship between s and ε holds only if stress is less than a certain maximum value. This point at which maximum value is reached is referred to as the proportional limit or yield point or yield value. Beyond the yield point, the material begins to undergo a plastic deformation and a small increase of stress causes the material to not regain its original shape and length upon removal of the applied force, but rather, induces the material to begin flowing.

The shear elastic modulus, which is the ratio of the shear stress to the shear strain, may be derived in like manner to the Young's modulus as above. Figure 3.3 shows a schematic of a material deformed under the action of a pair of equal and opposite forces

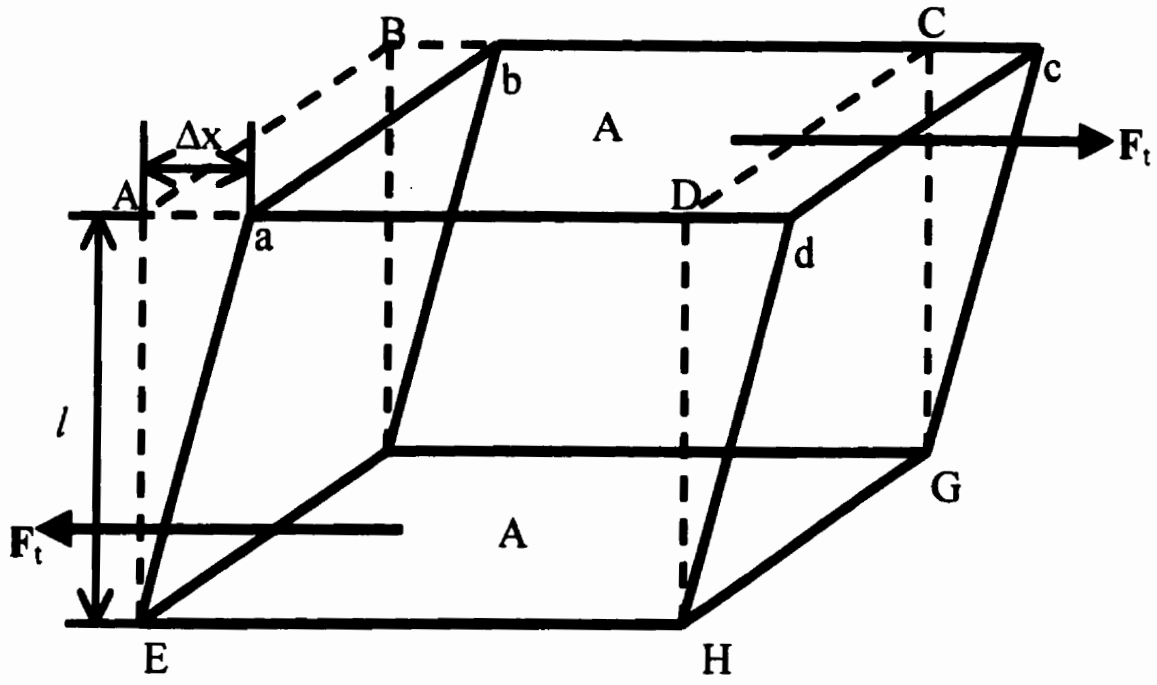

Figure 3.3: Schematic of a material deformed under the action of a pair of equal and opposite forces.

not acting along the same line of action. The resulting shear stress produces a change in the shape of the body (but no change in length) and therefore induces a strain, called the shear strain. The points ABCD under the action of the shear stress have moved to the points abcd, whilst the points EFGH are not displaced. The shear stress is therefore given by:

$$\tau = \frac{F_t}{A} \qquad (3.16)$$

and the shear strain, ν, is defined as the ratio of the displacement, Δx and the length l as shown in Figure 3.3. Therefore, the shear elastic modulus G' (also called the modulus of rigidity or torsion modulus) is given by:

$$G' = \frac{\tau}{\nu} = \frac{F_t / A}{\Delta x / l} \qquad (3.17).$$

The shear elastic modulus therefore also have units of N/m^2 or Pa. In general, the tensile modulus or Young's modulus, E, is related to the shear elastic modulus or rigidity modulus by (e.g. Kamphuis and Jongschaap, 1985):

$$G' = \frac{E}{3} \qquad (3.18).$$

Fat crystal networks demonstrate a tensile modulus as well as a shear elastic modulus. It is one of the objectives of this thesis to determine the level of structure stressed during a measurement of the elastic properties of the network. Figure 3.4 shows an example of the shear elastic modulus of cocoa butter. For visco-elastic materials like fat crystal networks, both a viscous modulus or loss modulus, G'' (related to the liquid portion of the network) and an elastic modulus, G' (related to the solid network) can be

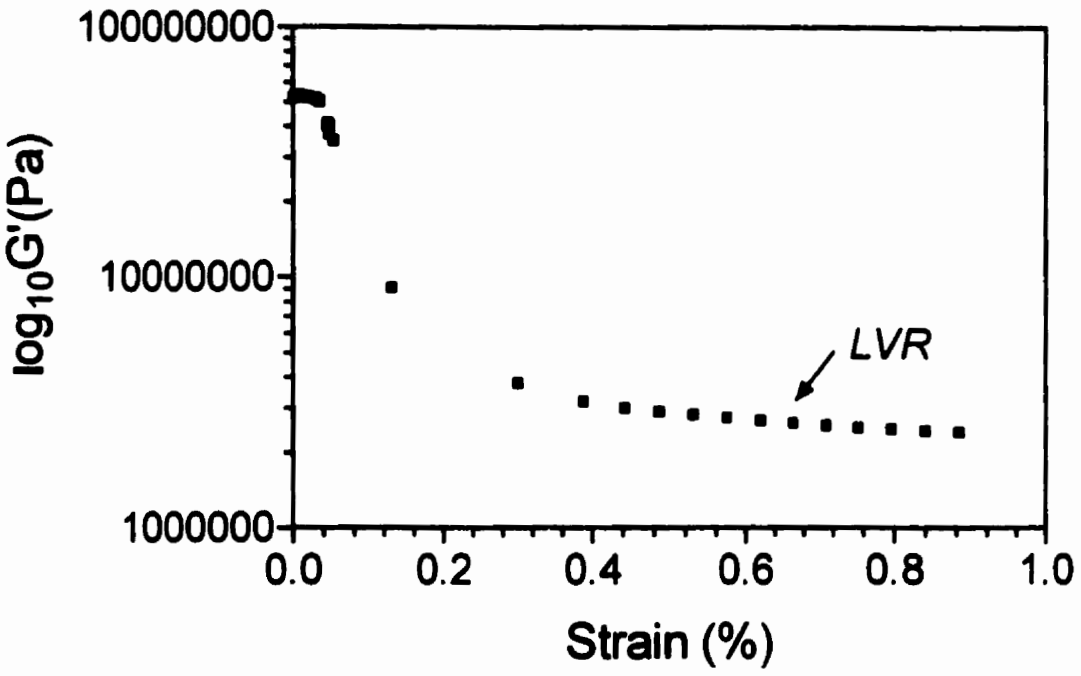

Figure 3.4: Shear elastic modulus of cocoa butter demonstrating a linear elastic region.

measured. The range of stress/strain within which the elastic modulus is constant is called the linear elastic range. As is demonstrated by Figure 3.4, this range for fat crystal networks is very small. Therefore, the system is elastic only for very small stress values. Figure 3.5 shows the behavior of a typical elastic system: up to point A, the system is perfectly elastic, then between point A and point B, stress is not proportional to strain, but if the stress is removed, the body should return to its original shape. If the applied stress is beyond point C, then permanent deformation occurs in the body and leads to breakage of different levels of structure. Point A is usually taken as the yield point. Since the shear elastic modulus is the slope of the plot of stress vs. strain, it is obvious that changes in elastic modulus will be produced by changes in the yield point. In a classical material such as a metal wire, at stresses beyond the yield point, the elongation of the material is caused by the movement of crystal planes, called slip, and the origin of slip lies in crystal dislocations, which correspond to a lack of symmetry in the crystalline nature of the material. In a way, these dislocations may be thought of as fault lines or planes, along which the material flows under external forces large enough to stress the material beyond its elastic point. However, since the yield point is influenced by the ability of the material to flow beyond its elastic limit, it is not immediately evident that the magnitude of changes in the yield point of a material will be related in a straightforward manner to magnitudes of changes in elastic modulus for materials such as fat crystal networks. Even in classical materials such as a crystal of sodium chloride, the yield point would be affected by the amount of dislocations in the crystal, which is a function of the purity of the material and of the environmental conditions under which the crystal was formed. The relationship of elastic modulus to yield value would therefore depend on the levels of

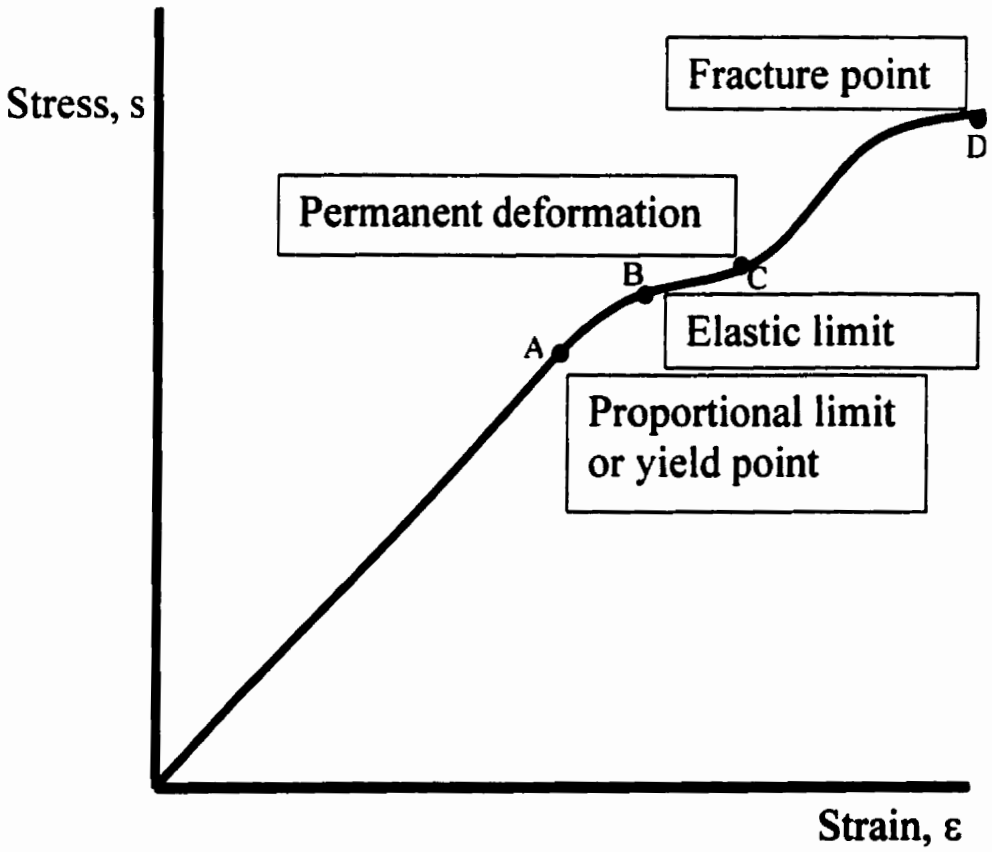

Figure 3.5: Stress-strain behaviour of a typical elastic system.

structure that are affected in the network during elastic measurements and measurements of the yield value, and the relative strength of these levels of structure. At any rate, the establishment of a theoretical link between elastic modulus and yield value is a non-trivial challenge, and one which would need to be supported well by experimental evidence of structural changes during deformation of the material. This link has not been made for fat crystal networks, but in this chapter it is shown experimentally that there is a proportional relationship between elastic modulus and yield value of a particular fat crystal network.

3.2 Theory and Review: Yield Value from Cone Penetrometry Measurements

The cone penetrometer is widely used in the fats and oils industry for the measurement of the consistency of plastic fats (American Oil Chemists Society, AOCS method Cc 16-60). This method involves the penetration of the fat network by a metal cone of known mass and geometry. By monitoring the depth reached by the cone and the time it takes to achieve that depth, a parameter referred to as the yield value of the network may be calculated. As explained above, yield values are determined to be the point at which the stress on the network is such that the network is just at its elastic limit. If one considers a typical plastic material, at stresses below the yield point, the material will behave as a perfectly elastic solid i.e., the strains are proportional to the applied stress. However, from the yield point onwards, this proportional relationship is lost, and the material begins to flow, i.e. some level of structure has been broken. The relation of cone penetrometer measurements to the yield value of the network has been formulated by a series of investigators in the fats and oils field, but unfortunately, many of these

formulations did not totally agree. However, it is important to provide a brief review of these developments, as is done below.

Rebinder and Semenko (1949) formulated the yield value as calculated from cone penetrometry measurements to be given by:

$$Y = \frac{Mg\cos^2(\alpha)}{p^2 \tan(\alpha)} \qquad (3.19)$$

where M is the mass of the penetrating cone, α is the half-angle of the cone, p is the penetration depth of the cone in a prescribed amount of time (5 seconds), and g is the acceleration due to gravity. Later, Haighton (1959) proposed the following formulation:

$$Y = \frac{K M g}{p^{1.6}} \qquad (3.20)$$

where K is a constant depending on the cone angle, and the other parameters are as defined earlier. Following the work of Haighton, Mottram(1961) proposed the following formula:

$$Y = \frac{K M g^2}{p^n} \qquad (3.21)$$

where K is a constant, and n is an exponent which is close to 2, but allowed to vary with the nature of the network. Following this work, Vasic and de Man (1968) proposed to define hardness as force divided by area of penetration (so, essentially defining hardness as a pressure, which has been done before). They related this hardness to penetration values by the following equation:

$$H = \frac{Mg.10^{-3}}{\left[p\pi \frac{\tan(\alpha)}{\cos(\alpha)}\left(p + \frac{2r}{\tan(\alpha)}\right) + r^2\pi\right]10^{-4}} \qquad (3.22)$$

where H is the hardness and r is the radius of the flat tip of the cone, and all other symbols are as defined earlier. Dixon and Parekh (1979) related hardness of butter from sensory investigations with a measure of hardness from cone penetrometer measurements, which they called the cone stress index (C_v), and found that C_v correlated very well with sensory impressions of hardness. They formulated the cone stress index as:

$$C_v = \frac{MA^{-1.65}}{p^2} \tag{3.23}$$

where A is the angle of the cone, and all other symbols are as defined earlier.

As noted by Hayakawa and de Man (1982), Eqns. (3.19) – (3.23) all suggest that the yield value used as a measure of hardness, or hardness expressed as some relationship to the yield value, follows a general form of dependence on the mass of the cone, the geometry of the cone, and the penetration depth, given by:

$$H = C \frac{M}{p^n} \tag{3.24}$$

where H is hardness or yield value, C is a constant depending on the geometry of the cone, and other symbols are as defined earlier. Hayakawa and de Man (1982) also noted that if a cone of 20° angle is used as is specified in the AOCS method, then Eq. (3.24) may be reduced to:

$$HI = \frac{M}{p^n} \tag{3.25},$$

where HI is the hardness index of the material.

Hayakawa and de Man (1982) presented experimental proof from their own experiments, and summarized the experiments of others to support that the hardness index of a plastic fat is best represented by Eqn. (3.25) when n is equal to 1. However, this relationship does not hold unless the penetration depth is between 15 and 150 units. Penetration depth is measured in units of 0.1 mm, therefore the actual range for the penetration depth for Eqn (3.25) to be valid when n=1, is 1.5mm to 15 mm.

3.3 Experimental

The cone penetrometer (AOCS Method Cc 16-60) was used to determine the hardness index of blends of butterfat-canola oil (BFCO), chemically interesterified butterfat - canola oil (CIE BFCO), enzymatically interesterified butterfat - canola oil (EIE BFCO), palm oil - soya bean oil (POSO), chemically interesterified palm oil - soya bean oil (CIE POSO), lard - canola oil (LCO) and chemically interesterified lard - canola oil (CIE LCO). The interesterified systems were prepared by Derick Rousseau during his Ph.D. work in our laboratory (Rousseau *et al.* 1996a, Marangoni and Rousseau, 1998a). As well, the data for the cone penetrometry measurements and elastic constant measurements were collected by Derick Rousseau (Rousseau *et al.* 1996c, Rousseau and Marangoni, 1998b, Marangoni and Rousseau, 1998b), although the importance of the relationship of G' to HI was not realised in these publications, and other than in Rousseau *et al.*, 1996c, the relationship between G' and HI was not investigated. Subsequently, during the preparation of this thesis, because of reasons outlined above, plots of G' vs. HI were prepared from data that was collected by Rousseau. His methods of analysis are reported here, for convenience.

For cone penetrometry measurements, on all of the systems involving butterfat, a 92.5 g cone was used, with an angle of 20°. For the systems involving palm oil, a 45 g cone with a 10° angle was used, and for the systems involving lard, a 57.7 g cone with a 30° angle was used. Liquefied blends of the samples were placed in cylindrical polypropylene containers (inner diameter of 16 mm, height of 23 mm), and allowed to crystallize statically at 5°C for 24 h, except for the samples including lard – these were crystallized at 5°C for 72 h. The blends of the fat systems used were in 10% w/w increments, for example, for the butterfat-canola oil systems, the samples analyzed were 100 % butterfat, 90% butterfat – 10% canola oil, 80% butterfat – 20% canola oil, 70% butterfat – 30% canola oil and 60% butterfat – 40% canola oil. The penetrating cone was placed just above the surface of the sample and released. The penetration depth in 0.1 mm increments was read on the dial after 5 s of contact. Analyses were performed in a refrigerator maintained at 5°C. Five replicates were performed for each sample, and penetration readings between 15 and 150 units were considered a suitable range for the penetration depth (after Hayakawa and de Man, 1982).

Measurements of G' were made using a CarriMed CSL^2 500 Rheometer (TA Instruments) with a 2-cm parallel plate attachment. One of the attachment plates is a Peltier plate, which allows the samples to be analysed at specific temperatures (5°C for all samples). The liquefied blends of the fat were poured into moulds in order to ensure uniform diameters and thickness for the samples. The diameter of the resulting samples is the same as the diameter of the attachment plates on the CarriMed machine. The

thickness of the sample is an important parameter, since too thick a sample makes it impossible to attain a uniform strain field through the sample, whilst too thin a sample results in interference due to particulates. A sample thickness of 3.2 mm was used. The fats were allowed to crystallise in the moulds at 5°C for 24 h, except for the samples involving palm oil, which were allowed to crystallise for 72 h. To prevent slippage between the sample surface and the surface of the sample-attachment of the CarriMed, 50 grit sandpaper was attached to both the sample attachment plate and the surface of the Peltier plate, with Krazy Glue™. The sample was then compressed to approximately 10% of its original thickness, utilising the software interface of the CarriMed, the compression force being applied in an exponentially increasing manner at a rate of 50 μm/s. The reason for this compression was to ensure that the sandpaper was thoroughly embedded into the sample, thereby preventing surface slippage.

After the sample was mounted in the manner described above, the rheometer was run through an oscillatory stress program, with applied stresses ranging from 1 to 31800 Pa at a frequency of 1Hz. This stress program was performed in order to determine the boundaries of the linear elastic region (LVR). One has to exercise caution in the determination of the LVR since it is absolutely imperative that the machine is being operated at strain levels that are above its minimum detection limit. For the CarriMed CSL^2 500, a strain of approximately 0.02% is the minimum detection limit. On establishing the LVR, frequency sweeps of the material can be carried out by applying either a constant stress or a constant strain. Generally, frequency sweeps were carried out over a frequency range of 0.1 to 10 Hz at a strain level of 0.2% to 0.5%. Apparent

storage and loss moduli (G' and G'') values were obtained from both the stress sweeps and the frequency data. Triplicates of all measurements were carried out.

3.4 Results and Discussion

The hardness index, *HI* of a fat is given by Eqn. (3.25), where $HI = M / p$. Therefore, for each of the systems studied, the shear elastic modulus of each blend was plotted against the reciprocal of the penetration depth, in units of 0.1 mm^{-1}. Figure 3.6 A shows such a plot for non interesterified butterfat(#1) – canola oil blends, 3.6 B for chemically interesterified butterfat – canola oil blends, 3.6 C for non interesterified butterfat(#2) – canola oil blends and 3.6 D for enzymatically interesterified – canola oil blends. Figure 3.7 A shows such a plot for non interesterified palm oil – soya bean oil blends, 3.7 B for chemically interesterified palm oil – soya bean oil blends, 3.7 C for non interesterified lard – canola oil blends and 3.7 D for chemically interesterified lard – canola oil blends. Since the blends within each system were all characterized for hardness with the same cone, within a particular system, the hardness index is represented well by the reciprocal of the penetration depth. As can be seen from Figures 3.6 and 3.7, the elastic modulus of all the systems varied in a proportional manner with the hardness index. It is important to note that the slope of the straight lines are all different, but this is to be expected, since the structure form one network to the next will vary, therefore varying the relationship between hardness and elastic modulus. However, the fact that for a particular system, the relationship of the elastic modulus to the hardness of the sample is a linear relationship is an important finding. One has to be careful when interpreting this result, however. It is enticing to conclude from this relationship that for

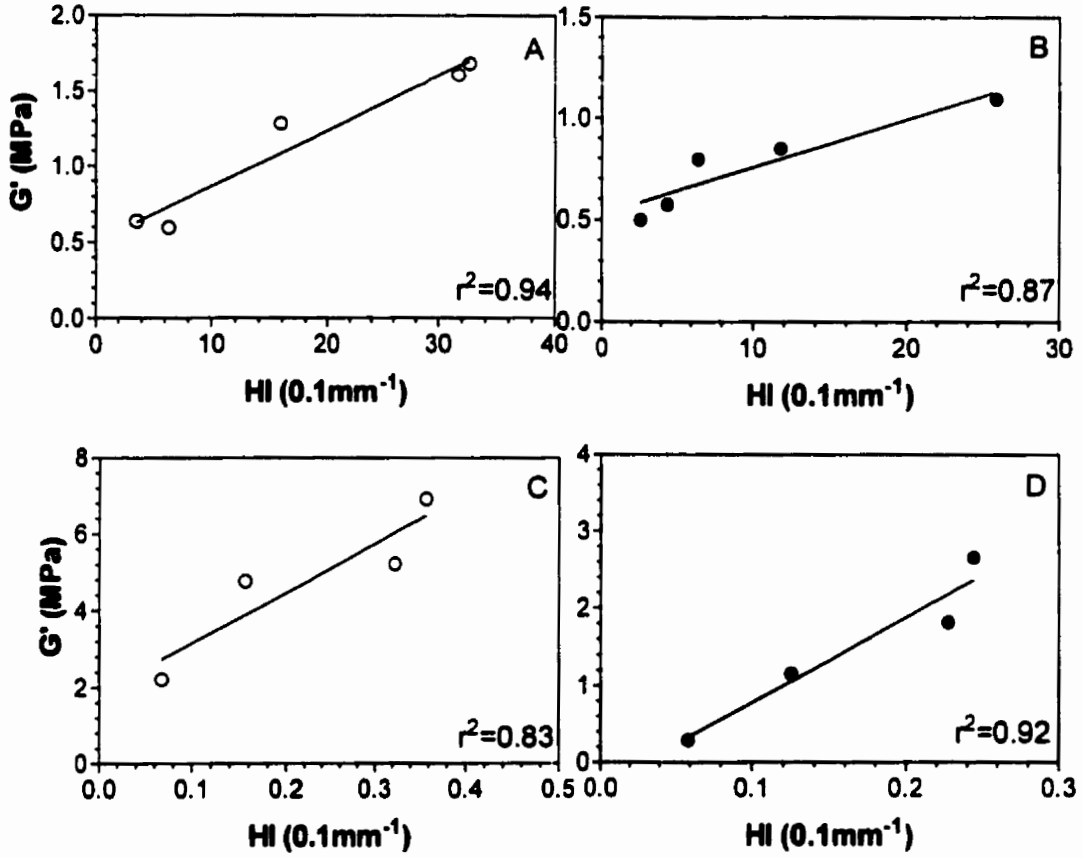

Figure 3.6: Plots of shear elastic modulus vs. reciprocal of penetration depth;
(A) Non-interesterified butterfat(#1)-canola oil blends,
(B) Chemically interesterified butterfat-canola oil blends,
(C) Non-interesterified butterfat(#2)-canola oil blends,
(D) Enzymatically interesterified butterfat-canola oil blends.

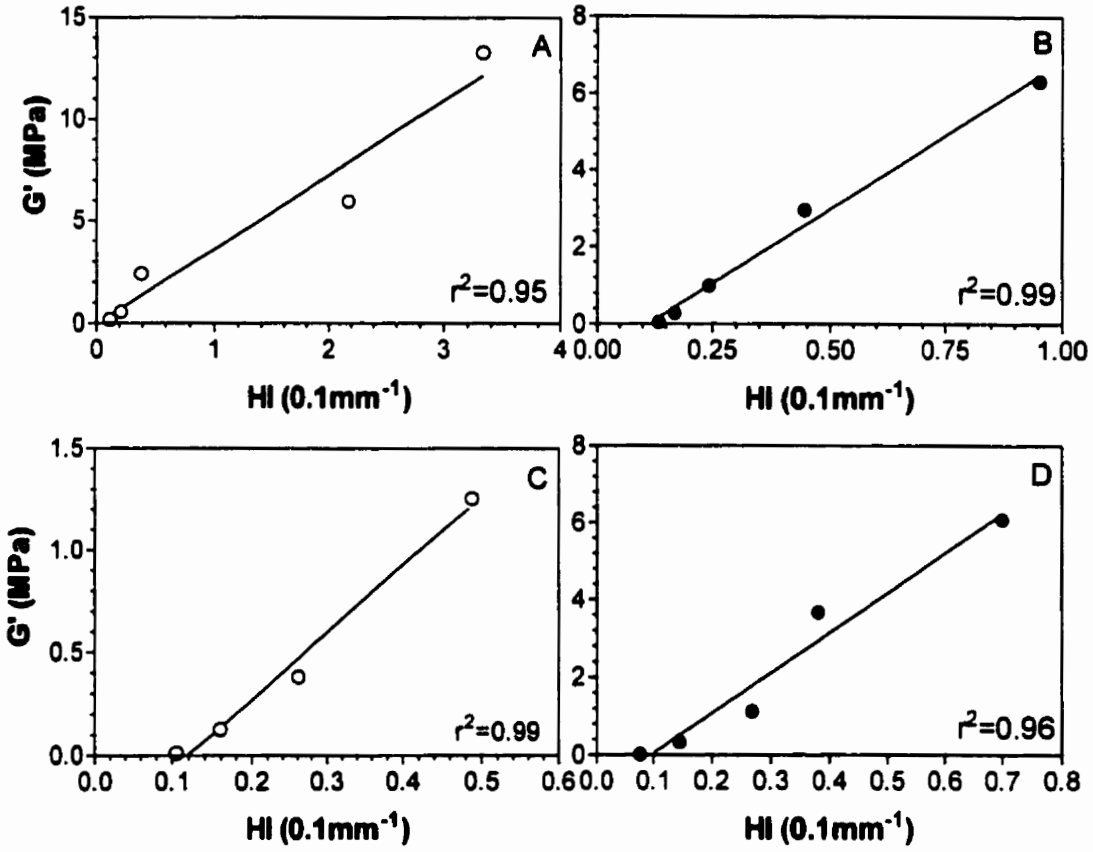

Figure 3.7: Plots of shear elastic modulus vs. reciprocal of penetration depth;
(A) Non-interesterified palm oil - soyabean oil blends,
(B) Chemically interesterified palm oil - soyabean oil blends,
(C) Non-interesterified lard - canola oil blends,
(D) Chemically interesterified lard - canola oil blends.

a particular fat crystal network, changes in hardness may be indicated by changes in elastic modulus. This may be true, but not in such a straightforward manner. The structure of the fat network at all levels definitely influences the nature of the relationship between hardness index and elastic modulus – therefore, if structural changes can be effected by processing conditions, the nature of that relationship will certainly change. One can then not expect the slope of the straight line when hardness index is plotted against elastic modulus to remain constant. This therefore suggests that if the elastic modulus of a fat is changed via processing conditions, that the changes in hardness would not necessarily be of a magnitude predicted from a previous relationship between hardness index and elastic constant. This said, the straight lines demonstrated in Figures 3.6 and 3.7 all have a positive slope. This suggests that the hardness indices of fat networks are always positively correlated to the elastic modulus. This implies that the changes in elastic constant of a network will be mirrored by changes in hardness, in terms of the direction of the change, if not the magnitude of the change. In other words, an increase in elastic modulus would certainly be followed by an increase in hardness, but the magnitude of the increase in hardness is not necessarily predicted by the change in elastic modulus. Therefore, the elastic modulus may be used as a rheological indicator, which not only implies changes in hardness measurements, but also as we have developed in the pages before, relate the intact structure of the network with hardness. In the rest of this thesis, the shear elastic modulus (and in some cases the tensile modulus) is used both as an (imperfect) indicator of macroscopic hardness and as an indicator of structure. In its own right, the elastic modulus is related to the sensory impression of the fat network, since it is the first level of structural resistance that is felt and overcome in

the mouth as the fat is consumed. So therefore, the problem of predicting the macroscopic sensory attributes of a food product has been simplified to determining the elastic modulus of the fat crystal network formed within such products. Certainly, taking this approach is fraught with problems: one is perhaps over-simplifying the problem. However, from an industrial perspective, the elastic modulus is related, however imperfectly, to the sensory impression of hardness of the product. Additionally, predicting the elastic modulus of fats from a materials sciences perspective is of fundamental importance.

It should be pointed out also that the seeming straight line relationship between hardness index and shear elastic modulus shown in the previous figures can only be assumed to apply at solid fat contents which allow the fat to be analyzed via cone penetrometry methods and by a CarriMed rheometer, as described in section 3.3. For instance, it is not possible to extrapolate this relationship beyond the range of values represented on the ordinate and abscissa axes.

Chapter 4

Case Study: Cocoa butter and Salatrim®

In this chapter, the importance of the microstructure of a fat crystal network as an indicator of macroscopic properties is re-visited. Two confectionary fats, cocoa butter and Salatrim® were studied using the rheological techniques established by the work of Rousseau *et al.* detailed in Chapters 2 and 3, in order to investigate the applicability of these methods to the study of two additional fat systems. Figure 4.1 demonstrates that the melting profiles of cocoa butter and Salatrim® (obtained from Cultor Food Science, Inc.) are quite similar up to approximately 20°C, however, their functionality is very different. To obtain the melting profiles of these two fats, they were first tempered using the AOCS official tempering method (AOCS Official Method Cd 16b, 1993). The melting profile shown here bears some additional discussion. Salatrim® is sold as a substitute for cocoa butter on the basis of the similarity of its melting profile to that of cocoa butter. However, at temperatures above 20°C, the melting profiles of the two fats shown in Figure 4.1 are not very similar. According to a personal conversation with Dr. Ralph Timms, however, when these two fats are tempered according to the IUPAC

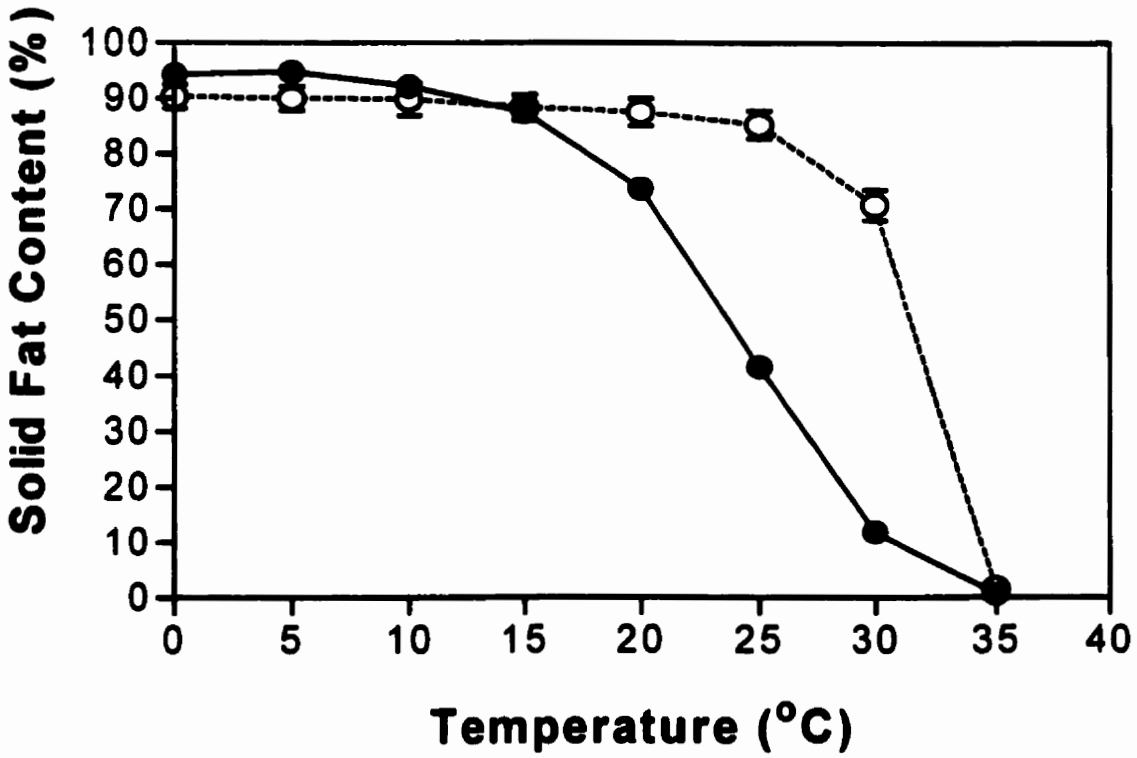

Figure 4.1: Melting profiles of cocoa butter (●) and Salatrim®.

method, rather than the AOCS method, the melting profiles of the fats are identical. As will be shown in this chapter, the melting profiles and solid fat contents (SFC) at different temperatures do not explain the difference in physical properties of these fats. It is proposed in this chapter that the microstructure of these two fats offer insight into the reasons for observed differences in mechanical properties.

The study of crystal polymorphism and morphology has increased our understanding of the properties of cocoa butter (Wille and Lutton, 1966; Manning and Dimick, 1985, Hicklin *et al.*, 1985; Koyano *et al.* 1990; van Malssen *et al.*, 1996). However, the *in situ* microstructure of the fat crystal network has never been visualized or quantified before the work to be detailed in this chapter and Chapter 5 of this thesis. Hicklin *et al.* (1985) have shown that crystal morphology cannot be easily predicted from knowledge of the polymorphic state of cocoa butter TAGs and Kellens *et al.* (1992) has shown that the same crystal polymorphic forms in tripalmitin can give rise to different microstructures. This points to the fact that the relationship that exists between polymorphism and macroscopic properties is at best of an indirect nature. The theoretical prediction of polymorphism from triglyceride composition remains a daunting task that has not been undertaken because of the variety of variables involved in a typical confectionary fat. Therefore, consideration of the microstructural level of structure in the determination of the macroscopic properties of fat crystal networks is of crucial importance. Obviously, the complete picture would necessarily be formed by considering all levels of structure, and their inter-dependence. The over-arching goal would be to quantitatively link triglyceride structure, polymorphism and microstructure. The melting profiles of fat crystal networks are related to triglyceride structure and polymorphism, since the melting of the network results in complete breakage of these levels of structure. However, rheological measurements performed on the fat crystal network, especially when one is working in the linear visco-elastic region of the network,

do not result in the breakage or sometimes even stressing of levels of structure below the level of the microstructure. Therefore, it is conceivable that fats with almost identical melting profiles can have very different rheological characteristics if their microstructures are sufficiently different.

In this chapter, differences in the microstructure of the fat crystal network between cocoa butter and Salatrim® are reported. It is proposed that differences in the macroscopic rheological properties between these two fats can be explained by the drastic differences in their fat crystal network microstructures. This has important implications in the manufacture of confections.

4.1 ***Experimental***

4.1.1 Materials and sample preparation.

Mixtures of cocoa butter and Salatrim® with canola oil were prepared in 5% (w/w) increments, from 100% to 75% (w/w) confectionery fat-canola oil. The confectionery fats were melted above 80°C to destroy any crystal memory, mixed with canola oil and stirred until thoroughly mixed.

4.1.2 Solid Fat Content determination.

Solid fat content was determined with a Bruker PC/20 series NMR Analyzer (Bruker, Milton, ON, Canada). The blends were introduced into NMR tubes, chilled in a refrigerator for 1 hour at 5°C and allowed to crystallize for 48 hours at room temperature (21-23°C). One determination on each of two replicate tubes was performed (n=2). The averages and standard deviations were calculated.

4.1.3 Polarized light microscopy.

A few drops of melted (80°C) samples of 85% (w/w) cocoa butter and Salatrim® in canola oil were placed on a microscope slide pre-heated to 80°C. A coverslip pre-heated to the same temperature was immediately placed on top of the sample. Care was taken to create an intermediate thickness film - thin enough to be able to observe the structure, but not too thin so as to create artifacts (Manning and Dimick, 1985), as well as to ensure that the plane of the coverslip was parallel to the plane of the slide, so that the thickness of the sample was uniform. The slides were chilled in a refrigerator for 1 hour at 5°C and allowed to crystallize for 48 hours at room temperature (21-23°C). Under polarization, the anisotropic solid phase of the network refracts light in a different manner than the isotropic liquid phase. The liquid phase appears black, whilst the solid phase is colored. Grayscale PLM photographs of cocoa butter-canola oil and Salatrim® - canola oil prepared as described above are shown in Figures 4.2(A) and 4.2(B). The solid phase appears as white or a shade of grey in these photographs. The entire solid mass of the thin samples is represented in the pictures, although some of the solid entities are out of focus due to the depth of the sample.

4.1.4 Dynamic rheological testing.

The rheological method used to measure G' and G'' values for the cocoa butter and Salatrim® samples was essentially the same as that described in Chapter 3, section 3.3. Only ways in which the analysis differed are therefore reported here. The lipid material was allowed to crystallize for 1 hr at 5°C, followed by 48 hr at 21-23°C. Samples were then removed from the molds, placed on a tray and stored at 18-20°C immediately prior to analysis.

For Salatrim®, to prevent slippage between the sample surface and the surface of the sample-attachment of the CarriMed, 50 grit sandpaper was attached to both the sample attachment plate and the surface of the Peltier plate, with Krazy Glue™. The

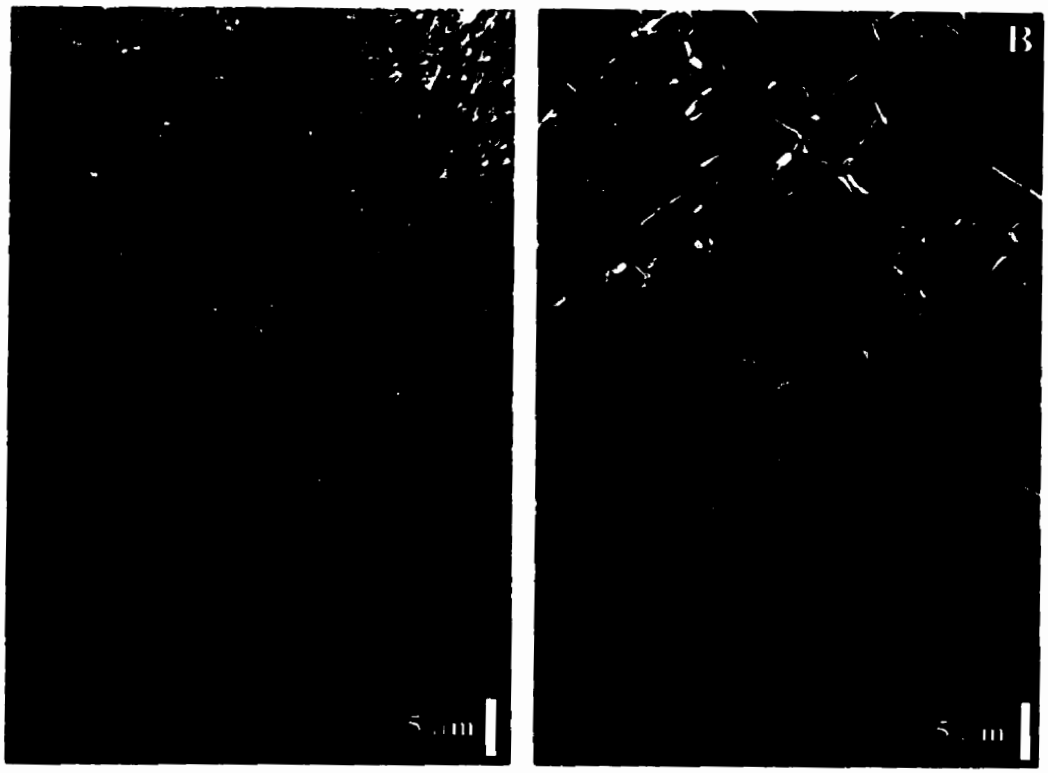

Figure 4.2: Polarised light microscope photographs of (A) cocoa butter and (B) Salatrim

sample was then compressed to approximately 10% of its original thickness, utilizing the software interface of the CarriMed, the compression force being applied in an increasing manner at a rate of 50 mm/s. The reason for this compression was to ensure that the sandpaper was thoroughly embedded into the sample, thereby preventing surface slippage.

For cocoa butter, each sample was glued directly onto the attachment plate and the Peltier plate with Krazy Glue™. This was done by removing the attachment plate from the machine, turning its flat surface upwards, applying a small amount of glue and carefully laying the sample onto it. Once the glue was cured, the attachment plate was reattached to the machine. A small amount of glue was then applied onto the Peltier plate after the instrument had set its *bias*. The ram was then quickly raised so that it just made contact with the sample. Since there was no compression of the sample, reproducibility was greatly increased. Unfortunately, Krazy Glue™ does not stick to Salatrim®, and therefore, sandpaper had to be used for this fat, as described above. On establishment of an LVR (as described in Chapter 3, section 3.3), frequency sweeps were carried out over a frequency range of 0.1 to 10Hz at a strain level of 0.2% for cocoa butter and a strain level of 0.5% for Salatrim®.

4.1.5 Data Analysis

Apparent storage G' and loss G" moduli values were obtained from both the stress sweeps and the frequency data. Two determinations on each of two replicate samples were performed (n=2). The averages and standard deviations are reported.

4.1.6 Fractal analysis.

Fractal dimension values were derived from the slopes (u) of the log-log plots of the storage modulus (G') against the solid fat content (Φ_{SFC}), as described in Chapter 2,

section 2.7. The weak link regime of Shih *et al.* (1990) was assumed for our high solid fat content (Φ_{SFC}) fats. The parameter γ was derived from the y-intercept of the log-log plot of G' *vs.* Φ_{SFC}. As explained in section 2.7 of Chapter 2, the parameter γ is a function of the nature of the particles in the fat network (as yet undefined) and the nature of the links between these particles.

4.2 Results and Discussion

The solid fat content of Salatrim® and Salatrim®-canola oil blends is about 9% higher than that of cocoa butter and cocoa butter-canola oil blends (Figure 4.3). Since the shear storage modulus of a plastic fat is essentially a measure of its elasticity, or solid-like character, from these results one would expect the shear storage modulus (G') to be higher in Salatrim® than in cocoa butter. Additionally, given that at equivalent temperatures above 20°C, the solid fat content of Salatrim® is higher than cocoa butter (Figure 4.1), one would expect again that at the temperatures this experiment was performed (21 – 23°C), the shear elastic modulus of Salatrim® to be higher than that of cocoa butter. However, as shown in Figure 4.4(A), the G' of cocoa butter is one order of magnitude higher than that of Salatrim® (Figure 4.4(B)). Although during the rheological analysis of Salatrim® sandpaper was utilized, whilst during the rheological analysis of cocoa butter it was not, it was found that in the case of cocoa butter, the rheological results are the same regardless if sandpaper is used. This would seem to indicate that the difference in the values of G' are not due to differences in the way the sample was analyzed, i.e. with or without sandpaper. As well, the ratio of the loss modulus to the storage modulus, or the ratio of the viscous to the elastic components, (G" /G'), in Salatrim® is twice that of cocoa butter (Figure 4.4 (C)). Cocoa butter can hold very high amounts of liquid oil within its structure (>50%). This characteristic may be described as a very high "oil trapping capacity". Salatrim® can barely hold 8% oil within its crystal network, and hence displayed a low "oil trapping capacity". One would expect that if the

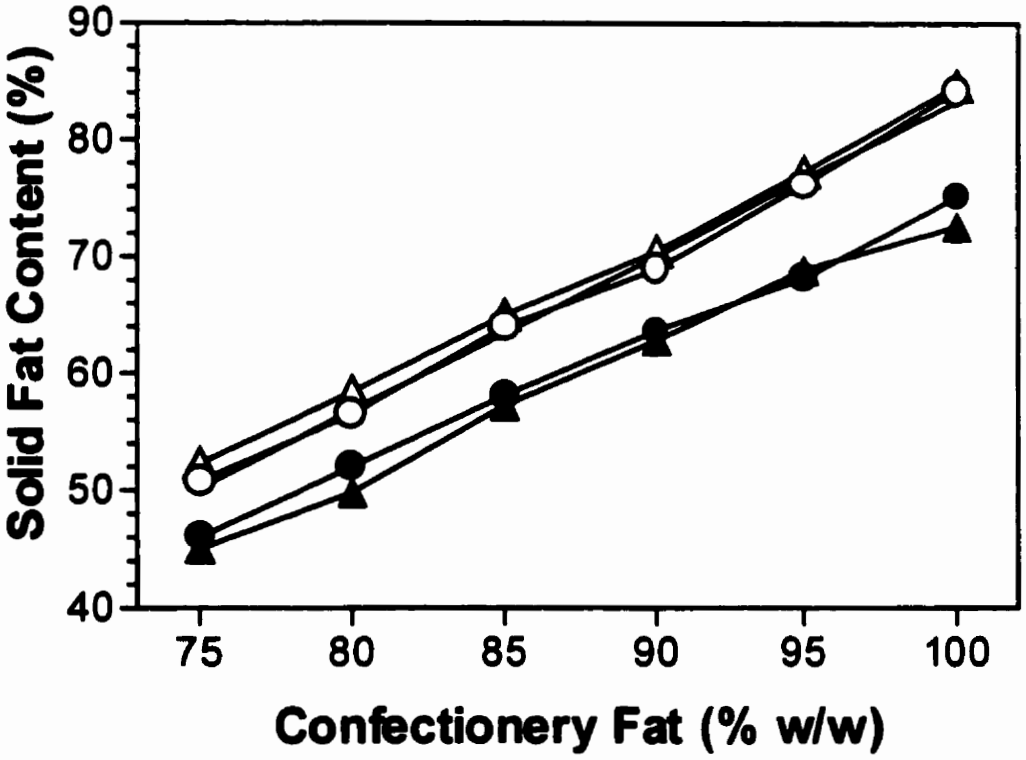

Figure 4.3: Solid fat content of cocoa butter and Salatrim blends with canola oil. Samples were crystallised statically at 5°C for 1 h, followed by incubation at 21 - 23°C for 24 or 48 h. (●) cocoa butter after 24 h, (○) Salatrim after 24 h, (▲) cocoa butter after 48h, (△) Salatrim after 48h.

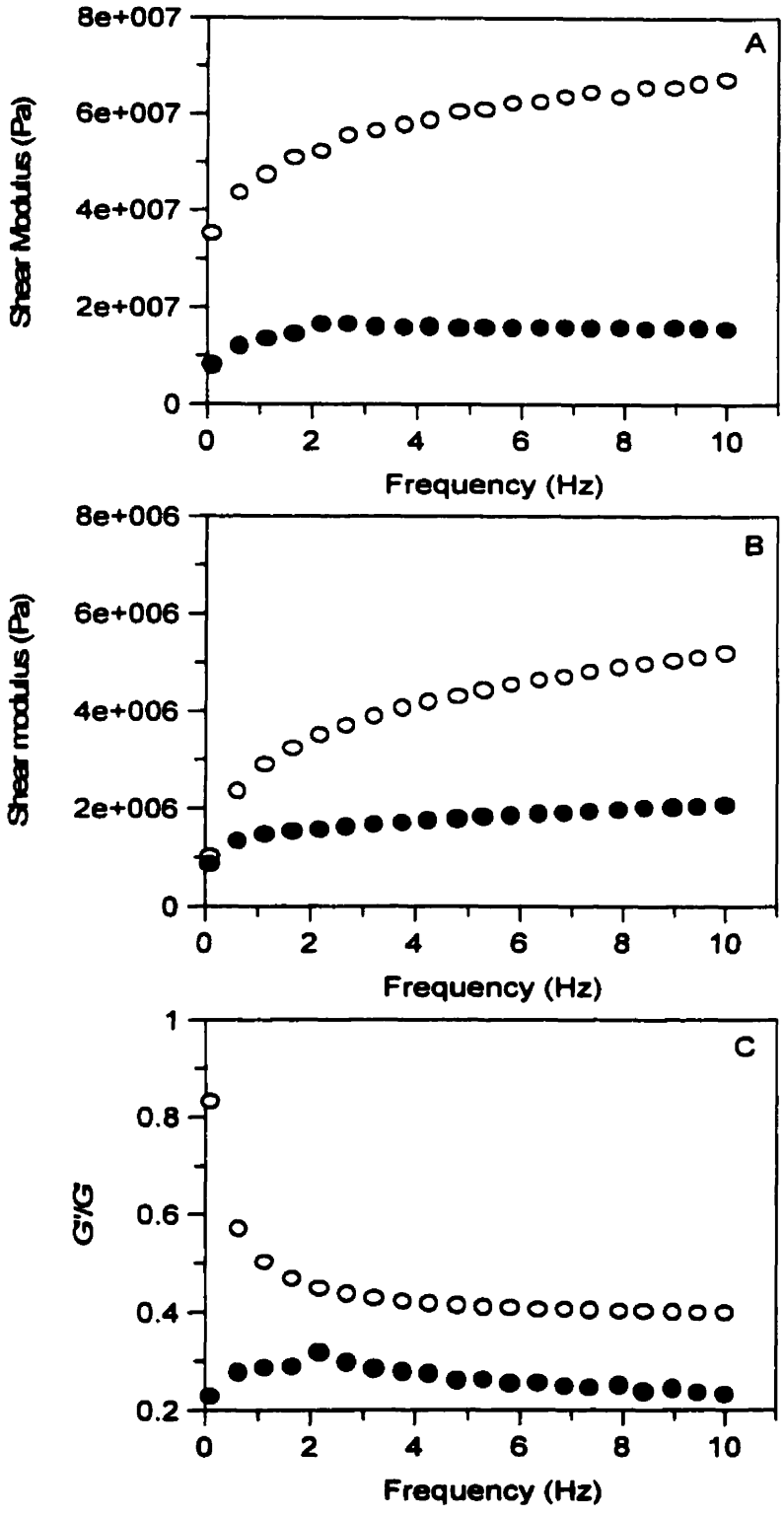

Figure 4.4: Dynamic oscillatory rheological analysis. Frequency dependence of G' and G'' of (A)cocoa butter at a 0.2 % strain level and (B) Salatrim at a 0.5% strain level. (●) – G', (○) - G''. (C) Frequency dependence of the tan δ, or ratio of viscous to elastic components, for cocoa butter (●) and Salatrim (○).

difference in the rheological measurements on Salatrim® and cocoa butter was due to differences in viscous drag, as opposed to differences in their solid network, that the observed ratios of G" /G' would be would be smaller for Salatrim®. Therefore, the differences in shear storage modulus may be attributed to the differences in the solid phase of the network. The similarity in melting profiles of these two fats up to 20°C have already been indicated and above 20°C, the differences in the melting would seem to indicate a mechanical behavior contrary to what is observed. Additionally the differences in solid fat content observed at different w/w percentages of the two fats with canola oil suggest differences in mechanical behavior contrary to that observed. Therefore, it is proposed that the differences are linked to the enormous differences in the structure of the microstructure of these fats.

Polarized light microscopy of Salatrim® and cocoa butter showed striking differences in crystal network characteristics (Figures 4.2(A) and 4.2(B)). At low magnification (100X) cocoa butter seems to be composed of large spherulitic aggregates of smaller solid entities, some as large as 120μm (Figure 4.5). A dense core is surrounded by less tightly packed crystalline material. This spherulitic morphology has been observed before (Manning and Dimick, 1985). Imaging under a PLM at high magnification (400X and 1000X) shows that these large spherulitic entities are made up of an aggregation of smaller crystalline microstructural units with an average diameter of 5μm. The addition of canola oil did not alter the morphology of cocoa butter or Salatrim®, for in the course of this work, different w/w percentages of confectionary fat - canola oil were imaged (not shown). The main effect of canola oil addition was to decrease the SFC of the network, thus improving image resolution. During the course of this work, nomenclature was assigned to the large aggregated entities and the smaller crystalline units seen in the polarized light micrographs of cocoa butter (Figures 4.2(A)

Figure 4.5: Polarised light micrograph of cocoa butter at low magnification. Horizontal bar represents 120 μm.

and 4.5). The details of this assignation will be discussed in Chapter 5. However, this nomenclature will be used in this chapter, from here onwards. The larger aggregated entities are called microstructures, and the smaller crystalline units are called microstructural elements.

The fat crystal network in Salatrim® is composed of small, randomly arranged, translucent platelets, about 10μm in diameter (Figure 4.2(B)). These striking differences in microstructure can be readily explained from a knowledge of triglyceride structure and polymorphic behavior. Salatrim® is a synthetic, random fat, containing short and long chain fatty acids. Due to the high asymmetry in the molecular structure of the triglycerides present in Salatrim®, packing into a crystalline structure is extremely difficult, and hence, no discrete crystalline polymorphic behavior has been observed, instead the fat remained in an alpha-like state upon crystallization(Hartel, 1999). There seems to be the formation of a solid phase characterized by weak interactions between mis-matched triglycerides. Salatrim®'s network seems to grow in one solid phase, with platelet growth discontinuing when the symmetry of the random triglycerides present is insufficient to form strong enough interactions to the platelet symmetry. The random spatial distribution of the platelets point to very weak links between them, since if the links were sufficiently strong a definite fractal or Euclidean inter-platelet distance would have been observed. Whenever strong inter-particulate forces are present in a 3-dimensional network, the 3-dimensionality of the system forces regular or pattern-forming inter-particulate distances. Therefore, the random nature of the triglycerides in Salatrim® results in the formation of a weak, random network. As is evidenced by the appearance of the microstructure shown in Figure 4.2(B), the effects of the levels of structure smaller than the microstructure have greatly affected the appearance of the microstructure.

On the other hand, cocoa butter triglycerides do form defined crystal lattices upon crystallization (Wille and Lutton, 1966), with a multitude of polymorphic forms. Therefore, the highly ordered nature of the triglycerides in cocoa butter results in the formation of a network with defined microstructural elements and a characteristic spatial distribution of solid mass.

It is possible to calculate a fractal dimension using scaling relationships between the storage modulus (G') and the solid fat content (Φ_{SFC}), as has been demonstrated before, and detailed in Chapter 2. As discussed before, this fractal dimension has been claimed by some authors to be a parameter that quantifies the microstructure of the network. From this type of analysis, it is also possible to determine a parameter, γ, dependent on the size of the primary particles and on the interactions between them, if the theory that was developed for colloidal gels is applicable to this type of analysis on fat crystal networks, and if there indeed exists a scaling relationship between G' and Φ_{SFC}. Figure 4.6 shows the results of a rheological determination of the fractal dimension so calculated, of the fat crystal networks in cocoa butter and Salatrim®. It must be mentioned here, however, that fractal dimensions calculated rheologically in this manner are physically significant only if the physical structure of the network is fractal in nature, and furthermore, that the structure of the network is organized in a fashion similar to a colloidal gel, as described in Chapter 2. Although extremely useful, one must be careful of the fact that unless the network itself is fractal, any apparent scaling relationship must be viewed with caution. It is often difficult to discern whether a straight line from a Log-Log plot is straight due to physical implications of scaling behavior (or a power-law relationship) or due to the fact that almost any Log-Log plot appears faintly linear. Without knowing the answers to the questions raised above as to the legitimacy of the use of fractal dimensions to quantify microstructure, the fractal analysis yielded fractal dimensions of 2.37 and 2.90 for cocoa butter and Salatrim®, respectively. Therefore, the

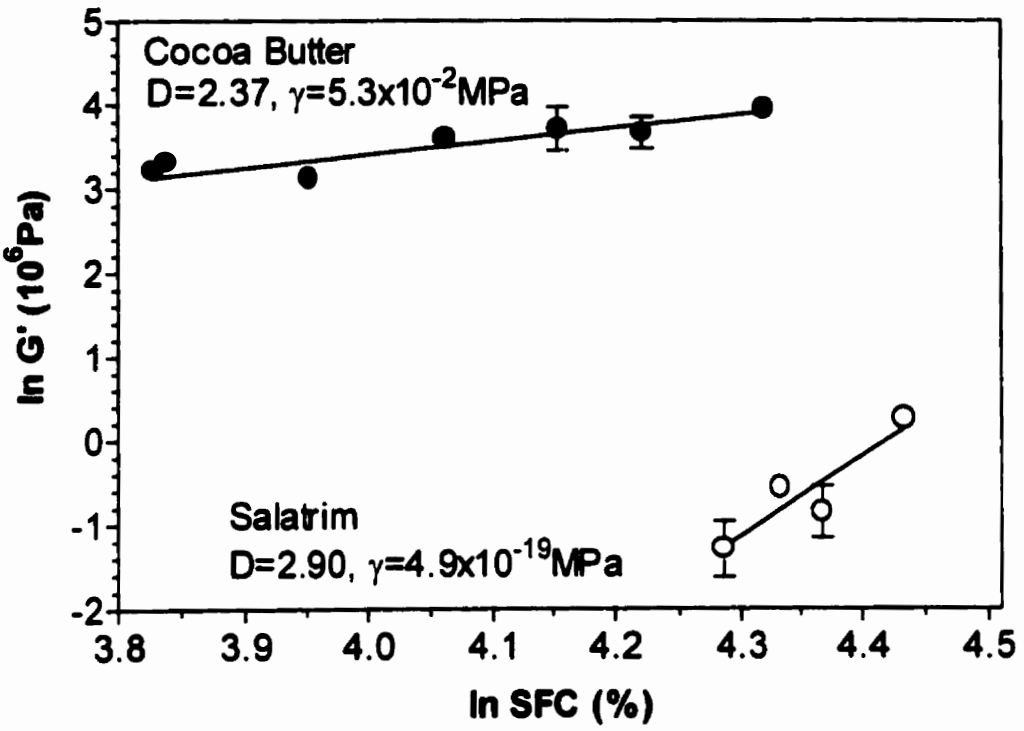

Figure 4.6: Scaling relationship between the storage modulus and the solid fat content for cocoa butter and Salatrim/canola oil blends.

difference in the fractal dimension calculated for these two materials is very large. Certainly, if the fractal dimension does constitute a measure of the microstructural level, one would expect to see large differences in the values for these materials, given the stark differences in the polarized light micrographs of cocoa butter and Salatrim®. Beyond this observation, nothing more can be said about this analysis. This topic will be developed and discussed fully in Chapter 5.

There are therefore fundamental differences in the structure of Salatrim® and cocoa butter at microstructural length scales. From the description of the differences in structure, it seems that small-deformation rheological measurements on Salatrim® stresses the platelets that make up the network and the weak links between the platelets. As described above, these links must be very weak, since they represent the boundary to the growth of the platelets, which it was proposed, may be due to the asymmetry of the triglycerides present, and the subsequent inability of the mis-matched triglycerides to form strong-enough interactions to continue the growth of the platelet. On the other hand, cocoa butter forms a comparatively well-defined network, with the distance between solid entities at the microstructural level statistically similar. This suggests that the interactions between these microstructural elements are quite strong and defined, thereby leading to a three-dimensional arrangement with the solid entities being similar distances apart. As mentioned before, the shear elastic modulus of Salatrim®'s network is one order of magnitude lower than that of cocoa butter at different SFC's. The explanation that the structure (links between the large aggregates or microstructures) being stressed during the measurement of the macroscopic shear elastic modulus in cocoa butter are stronger (higher elastic constant) than those being stressed in the Salatrim® network (links between platelets) is therefore a very probable cause of this difference, bearing in mind that the melting profiles and SFC's of these two confectionary fats do not explain these differences. An additional consideration is the fact that the small 5 μm

microstructural units themselves in cocoa butter are hard, crystalline particles, whereas the crystallinity of the platelets in Salatrim® are at best loosely-packed, rendering these relatively soft particles. In the event of the small-deformation measurements actually causing stress on the solid entities themselves, therefore, the cocoa butter network would be harder. Again referring to the fractal-type rheological analysis, the values of the constant γ are 5.3×10^{-2} MPa and 4.9×10^{-19} MPa for cocoa butter and Salatrim® respectively. If indeed this analysis is valid for fat crystal networks, the relative values of this constant would make sense, in that the links that are stressed when the cocoa butter network is stressed are stronger than those stressed in Salatrim®.

From the results demonstrated in Chapter 3, it has been made obvious that the elastic constant of a fat is indicative of the macroscopic sensory hardness. Therefore, from our measurements, cocoa butter is a much harder fat than Salatrim®. It would therefore seem that a highly organized, crystal network structure with a high G'/G" ratio is required to achieve proper "hardness" and immobilization of non-triglyceride components. Additionally, such a structure would be very efficient in trapping oil, or non-triglyceride components, since cocoa butter can store much more oil than Salatrim® as described above. One can imagine exogenous components being trapped within the network and between the solid entities at the microstructural level upon crystallization, since there is much more space within the microstructural network. A space-filling random structure such as the one present in Salatrim® does not have the ability to trap much exogenous material.

Apart from offering an explanation for the differences between cocoa butter and Salatrim®, an examination of the microstructural characteristics of these two networks also offers interesting insights into preferred microstructural characteristics of confectionary fats. Cocoa butter is a much-utilized confectionary fat, and can be thought

of as a good candidate for the representation of a perfect confectionary fat, whilst Salatrim® fails in many instances to justify its use as a confectionary fat. Therefore, the differences between these two fats outline the preferred characteristics of a good confectionary fat.

The very important "snap" characteristic of a good chocolate product is most probably related to the mechanical failure of the network along a microstructural fracture plane, i.e. a fracture plane defined by the boundaries of the large aggregates shown in Figure 4.5. With a network such as Salatrim®, the "snap" would not be achieved, since the random nature of the spatial arrangement of the platelets does not allow fracture planes to be defined along the links between the platelets, instead the network would bend due to the bending of the platelets themselves (as anyone who has worked a piece of solid Salatrim® in their hands would attest to). Therefore, the formation of a well-defined microstructural network seems to produce harder, brittle fats.

Contraction is another important property of confectionery fats. Without it, demolding would not be possible. The contraction zones we observed in low magnification PLM images of cocoa butter would not be possible if the network was not composed of an aggregate of hard solid entities separated by finite distances. Without the packing of crystals into these highly organized aggregates, contraction probably would not occur. In fact, one of the most problematic characteristics of Salatrim® is the difficulty it presents in demolding.

Therefore, although there are striking differences in the tryglyceride composition and crystalline nature of cocoa butter and Salatrim®, the traditional indicators of these properties failed to demonstrate these differences – i.e. melting profiles and solid fat contents are not indicative of the disparity between these materials at the triglyceride and

crystalline level. However, these differences are reflected well in the microstructure of both materials. It is also possible to arrive at a qualitative explanation for the differences in elastic constants of these two materials, based on an observation of the microstructure of these materials. The fact that the as yet nebulous fractal dimension is seemingly sensitive to the observed differences in microstructure is also promising, as it may provide a quantitative method of determining differences in microstructure. However, what is indeed certain is the fact that a consideration of the microstructural level is of immense importance in the pursuit of an understanding of the factors that affect the hardness of fat crystal networks. It therefore lends motivation for the characterization of microstructure and the quantification of microstructure, the subject of Chapter 5.

Chapter 5

Where Lies the Fractality in Fat Crystal Networks?

In this chapter, the structure of fat crystal networks at the microstructural level will be investigated and discussed. It has been detailed in previous chapters that other authors have attributed some amount of importance to the microstructure of fats. Particularly, the microstructure will be investigated so as to determine whether there is a structural organisation present which warrants the application of the weak link theory developed for colloidal gels to fat crystal networks. Furthermore, since the microstructure of fat networks have been rather loosely characterised before this work, effort will be made to utilise a number of different imaging techniques to attempt to provide a description of the network at the microstructural level that is supported by various types of microscopical evidence.

5.1 Microscopy

Experimental details of the various types of microscopy is provided below.

5.1.1 Experimental

Four different methods of imaging the network at the microstructural level was utilised. Scanning Electron Microscopy (SEM), Confocal Laser Scanning Microscopy (CLSM), Atomic Force Microscopy (AFM), and Polarized Light Microscopy (PLM) were used.

(a) Scanning Electron Microscopy

The SEM micrographs presented here are a result of the work of Derick Rousseau, a former student in our laboratory. The method by which these micrographs were taken is presented here in its entirety, and is also provided by Rousseau in a previous publication (Rousseau *et al.*, 1996b), although the micrographs shown here have not been published.

SEM micrographs of fat crystal networks were prepared from fat samples that had the liquid oil present. Small amounts of anhydrous milkfat-canola oil blends (80:20 w/w) (figure 5.1) and CIE milkfat-canola oil (80:20 w/w) (figures 5.2 and 5.3) were used in the preparation of the SEM samples. Small amounts of these fat blends were placed on brass blocks pre-cooled to 4°C. The brass blocks contained pre-cooled Tissue-Tek mounting medium. This was done immediately prior to transferring of the samples to a cryo-preparation unit. The blocks were plunged into liquid Nitrogen slush at –207°C. Subsequently, to obtain views of internal sample surfaces, the samples were freeze-fractured. Sublimation was performed at –80°C for 30 min. to remove any ice crystals that could obscure the fat microstructure. After sublimation, the samples were sputter-coated with 30 nm of gold. Cryo-fixation was used instead of osmium tetroxide fixation because this has been shown to aid in the definition of structure (Chawla *et al.*, 1990). Samples were viewed in a Hitachi (Tokyo, Japan) S-570 SEM maintained at –150 to –170°C. Accelerating voltages of 5 to 15 kV were used with magnifications ranging from 500 to 10, 000 X. An aperture of 50 mm was used with a condenser lens current setting

of 5. Photographs were taken on Ilford FP4-Plus film. The images shown in figures 5.1, 5.2, and 5.3 are typical for all samples examined.

(b) Confocal Laser Scanning Microscopy

Fluorescent Nile Blue dye was dispersed in a sample of liquefied milkfat at 60°C. This sample was then deposited onto a microscope slide as a thick film (approx. 1 mm) and covered with a glass coverslip. The sample was then allowed to crystallise at 18°C for 24 h. The Nile Blue partitions into the liquid phase of the network, negatively staining the solid fat crystals. A BIO-RAD MRC-600 Laser Scanning Confocal Microscope (Watford, Herts, England) with a krypton/argon mixed-gas laser, coupled with a Nikon Optiphot microscope (Tokyo, Japan) was used. This microscope is located at the National Biophotonics Resource at the University of Wisconsin-Madison, Wisconsin, U.S.A. Figures 5.7 and 5.8 show micrographs of milkfat from this analysis (courtesy of Alejandro Marangoni and Richard Hartel).

(c) Atomic Force Microscopy

Fat samples that are suitable to be imaged by atomic force microscopy must be mainly solid at the operating temperature of the microscope, therefore, the method is currently limited to fats which are mostly solid at room temperature. The microscopes used in this work, namely the Nanoscope IIIa (Digital Instruments) and the Dimension 3100 (Digital Instruments) were not equipped with temperature controllers, hence the

room-temperature limitation. However, there are environmental stages available for these microscopes, which would allow samples not solid at room temperature to be analyzed at lower temperatures at which they are solid. All the work done for this thesis have been at room temperature.

Samples imaged using the AFM were prepared in three different ways. Due to the limited vertical range of the scanning tip, a macroscopically smooth surface is required for problem-free imaging. One method of ensuring a macroscopically smooth surface (i.e. no visible craters, cracks, dust particles, etc.) is to spin-coat the sample onto a smooth surface. Samples of fat were melted at 80°C and then a small droplet was dropped onto a polished silicon (1 1 1) surface (pre-heated to 80°C), that was rotating at a speed of 4000 rpm. The droplet was thus spin-coated on the silicon for 90 s. The resulting thin coating of fat on the silicon wafer was then incubated at 20°C for 24 hours. The fat was still liquid after being spin-coated, therefore, this process is quite similar to using a Pasteur pipette to deposit a droplet of liquefied fat onto a glass slide and dropping a coverslip onto it. As will be seen when the method used to image fats using a polarized light microscope is discussed, these two sample preparation methods are quite similar. Figures 5.9, 5.10, 5.13, and 5.15 show samples of fat prepared by spin-coating in the manner described above. Figures 5.9 and 5.10 show the high melting fraction of milkfat (HMF) imaged at different positions on the same sample, figure 5.13 show 50:50 mixtures of the middle melting fraction of milkfat (MMF) and HMF, and figure 5.15 show a 70:30 mixture of HMF:MMF. Preparation of the milkfat fractions were

performed according to a method of solvent fractionation described in a publication by Marangoni and Lencki (1998).

Samples were also prepared in an identical manner to that described in Chapter 3 for the preparation of rheological samples for the CarriMed machine – the object here was to observe the general structural organization of the fat samples prepared for rheology. These samples were moulded at 80°C and incubated at 20°C for 24 hours. The moulded samples provided a macroscopically smooth surface, however, they also demonstrated local high spots, which were quite regularly shaped. It was assumed that these spots were due to dust particles on the surface of the sample. Figures 5.11(HMF) and 5.14 (50:50 HMF:MMF) show samples prepared in this manner.

The fat surfaces prepared using the above methods were then imaged using a Nanoscope IIIa atomic force microscope (Digital Instruments) operated in tapping mode with the cantilever being driven at 250 kHz. The cantilever used in this case had a force constant in the range 40-85 N/m.

Samples of cocoa butter on glass slides prepared using the *in-situ* polarized light microscope method detailed below were stored at 20°C for 1 year. One such sample was imaged using a Dimension 3100 atomic force microscope (Digital Instruments) operated in tapping mode with the cantilever being driven at 173 kHz. The cantilever had a force constant in the range 40-85 N/m. The samples were imaged on the

edge of the glass slide, i.e. the surface sandwiched between the glass slide and the coverslip, and one micrograph from this analysis is shown in Figure 5.16.

(d) Polarized Light Microscopy

As early as the 1960's, PLMs were used to analyse the birefringent solid structures of fat crystal networks (Hoerr, 1960). Under crossed polarisers, the anisotropic solid crystals of the network appear as white objects, whilst the isotropic liquid portion of the network remains black.

Two different methods of sample preparation were used for samples imaged using polarised light microscopy. In one method, the network was imaged by placing a small sample of fat, pre-crystallised under the desired conditions, on a microscope glass slide pre-chilled to the temperature of the fat and then immersing the solid fat with a small amount of similarly pre-chilled paraffin oil. A pre-chilled cover slip was then firmly pressed on the sample to remove air bubbles and excess liquid. This process breaks the network of the pre-crystallised fat, and the intent is that individual "particles" within the network would separate and therefore be discernible under a polarised light microscope with cross-polarisers. Figures 5.4, 5.5, and 5.6 show samples prepared in such a manner and imaged under a polarised light microscope (courtesy of Derick Rousseau and Alejandro Marangoni). Figure 5.4 shows samples of anhydrous milkfat, figure 5.5(A) shows a sample of non-interesterified (NIE) palm oil, figure 5.5(B) show a sample of

chemicaly interesterified (CIE) palm oil, figure 5.6(A) show a sample of NIE lard and figure 5.6(B) shows a sample of CIE lard. All samples were analysed at 5°C, and all the fat samples were first heated to 80°C, and then crystallised at 5°C – the anhydrous milkfat samples and the palm oil samples for 24 h, the lard samples for 72 h prior to analysis.

The method described above does not allow the imaging of the network *in-situ.* In a method designed to facilitate *in-situ* imaging, the samples were prepared by melting the prepared blends of the fat systems at 80°C and using a Pasteur pipette to deposit a small droplet of fat onto a glass slide pre-heated to the temperature of the melted fat. A similarly heated glass coverslip was then dropped onto the surface of the droplet, ensuring that the plane of the coverslip was parallel to the plane of the slide. This allowed the droplet to be smeared out into an extremely thin rectangular block of fat of uniform thickness. The samples were then allowed to crystallise in a refrigerator and/or at room temperature. A polarised light microscope (PLM) was then used to investigate the structure.

PLM images of anhydrous milkfat (figure 5.17(A)), palm oil (figure 5.19(A), lard (figure 5.19(B)) and tallow (figure 5.18(A)), were photographed at 5°C after being in the refrigerator at 5°C for 24 h, 24h, 72 h and 24 h respectively. Cocoa butter (figure 5.17(B)) and Salatrim™ (figure 4.2(B)) were photographed at room temperature after being refrigerated at 5°C for 1h and then allowed to sit at room temperature for 24 h. A blend of 50:50 HMF:MMF (figure 5.18(B)) and pure MMF (figure 5.20(A) and (B)) were photographed at 20°C after being crystallised at this temperature for 48 h. Use was made

extensively of 10X and 40X objective lenses on an Olympus BH polarised light microscope (Tokyo japan), mounted with a PM-6 35mm camera.

It has been shown by Heertje and co-workers (Heertje *et al.* 1987; Juriaanse and Heertje, 1988; Heertje, 1993) that fat crystal networks demonstrate a level of structural organisation which is arranged as clusters of smaller structural entities at the microstructural level. These clusters are of the order of 100 μm, and pack in a space-filling, orthodox manner to fill the space that the network occupies. The work by Heertje and co-workers was based on SEM images of fat crystal networks. These researchers utilised a method briefly described in Chapter 2, which is difficult to reproduce. They also showed that if the network is imaged after it has been subjected to stress, these large clusters were separated from each other, but maintained their shape and size. Therefore, in an attempt to identify similar structures, samples of cocoa butter, milkfat and tallow were heavily diluted with canola oil (50:50 w/w) and microscope slides prepared by first heating the samples to 80°C, then depositing a drop of the sample onto a slide pre-heated to 80°C. No coverslip was used. The samples were incubated at 20°C for 30 days, to allow the network to form. The intent was to allow the large structures seen by Heertje and co-workers to separate in the dilute solution, thus allowing them to be imaged. The *in-situ* network of fats or fats diluted with a small amount of canola oil does not allow discernment of the large clusters, since the boundaries of these clusters become indistinct due to the presence of other clusters in the depth of the sample. The large clusters of cocoa butter, milkfat, and tallow are shown in figures 5.21, 5.22 and 5.23 respectively.

Polarised light microscopy was also used to observe the formation of the fat crystal network from the melt. Since it had bearing on another project (Wright *et al.* 2000) in our laboratory which investigated the function of minor compounds in milkfat, we investigated the formation of networks of milkfat triacylglycerides (from which the minor compounds were removed) and networks of triacylglycerols of milkfat with 0.01% by mass of milkfat diacylglycerols added. In this study, the samples were prepared by dropping fat heated to 80°C onto a glass slide, and then placing a coverslip over the droplet – ensuring that the surface of the coverslip was parallel to the surface of the slide. The coverslip and slide were both pre-heated to 80°C. The sample was then placed on a polarised microscope stage at 22.5°C, and the crystallisation monitored. Images were captured with a CCD camera mounted on the microscope at 15 s intervals until there were no visible changes in the network. Figure 5.24 show images of the network formed by pure milkfat triacylglycerols at 5.5 min. (A), 7 min. (B), 8.5 min (C), 10 min (D), 11.5 min. (E), 13 min (F), 25 min (G), and 32.5 min. (H) after appearance of the first visible signs of crystallisation in the field of view. Figure 5.25 show images of the network formed by a mixture of pure milkfat triacylglycerols to which have been added 0.01% by mass of milkfat diacylglycerols at 7.5 min. (A), 12.5 min. (B), 17.5 min. (C), 22.5 min. (D), 27.5 min. (E), and 32.5 min. (F) after appearance of the first visible signs of crystallization in the field of view. The characteristics observed in the sequence of images shown in figures 5.24 and 5.25 were later observed to be similar to the formation of other fat networks such as lard, palm oil, cocoa butter, tallow and anhydrous milkfat. However, none of these sequences were captured and preserved, due to their similar nature.

5.1.2 Characterising Microstructure

Figures 5.1 (A) and (B) show SEM micrographs of anhydrous milkfat with the liquid oil not removed. The entire network, however, has been frozen and then sputter-coated. As is evidenced by the figures, it is difficult to tell which part of the structure is due to liquid oil and which to solid crystals. However, there does seem to be evidence of some type of repeating structure at the 30 μm range. Figure 5.2 shows a sample of chemically interesterified milkfat from which the liquid oil was not removed. Two structures are shown in this figure, which seem to be in the range of 50 μm – 60 μm, and since this surface image is a fracture surface, these structures seem to belong to spherical structural entities in the fat. It however cannot be ascertained whether the area around the two entities is frozen oil or also are of crystalline nature. The fracture plane being imaged here also does not necessarily pass through the equator of these entities. Therefore, these entities may actually be larger than represented. Figure 5.3 shows a micrograph from a sample of chemically interesterified milkfat, from which the liquid oil has not been removed. This micrograph shows a structural entity that is approximately 6 μm across, and which may be spherical-like. Not much else can be determined from this micrograph. Micrographs of SEM images of fat which were prepared according to the method outlined in the experimental section are very typical of the images shown here. In other words, nothing definitive can be said about the structure of the fat network from such images in most cases, due to the destructive sample preparation methods necessary for SEM imaging.

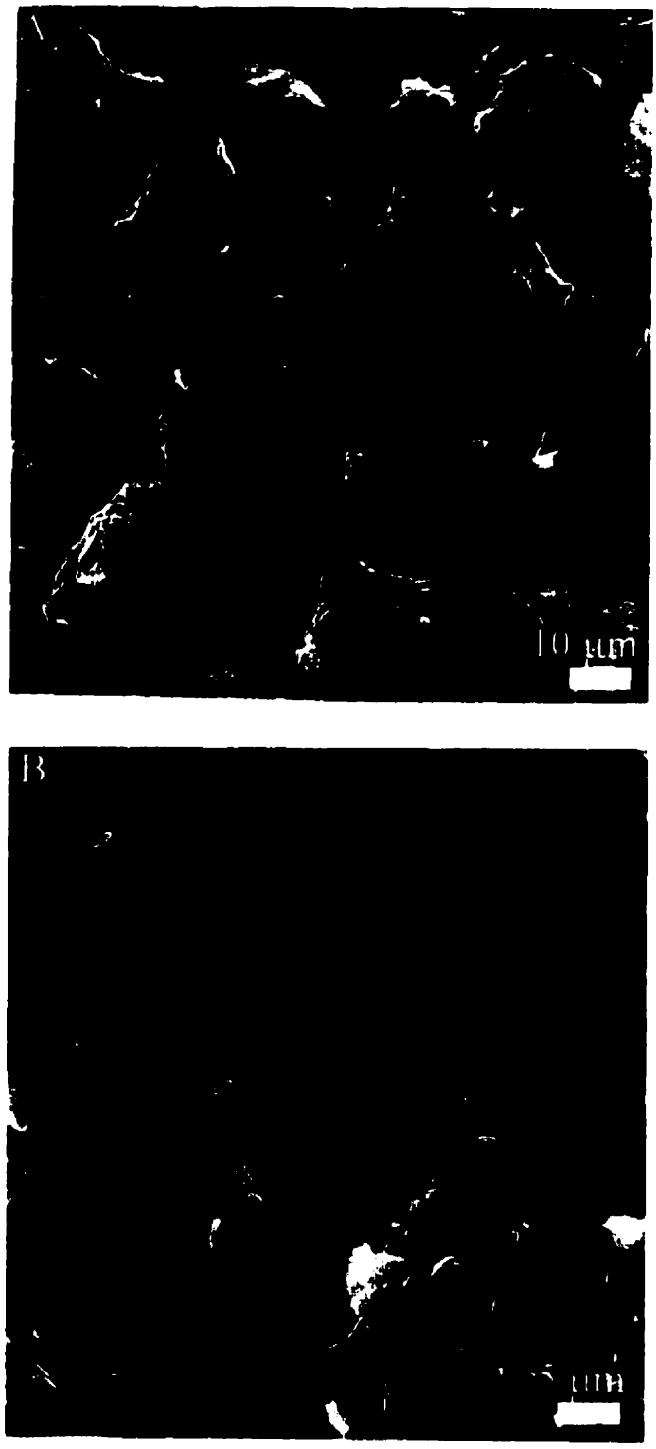

Figure 5.1: **Scanning electron microscope images of anhydrous milkfat, with the liquid oil in the samples not removed.**

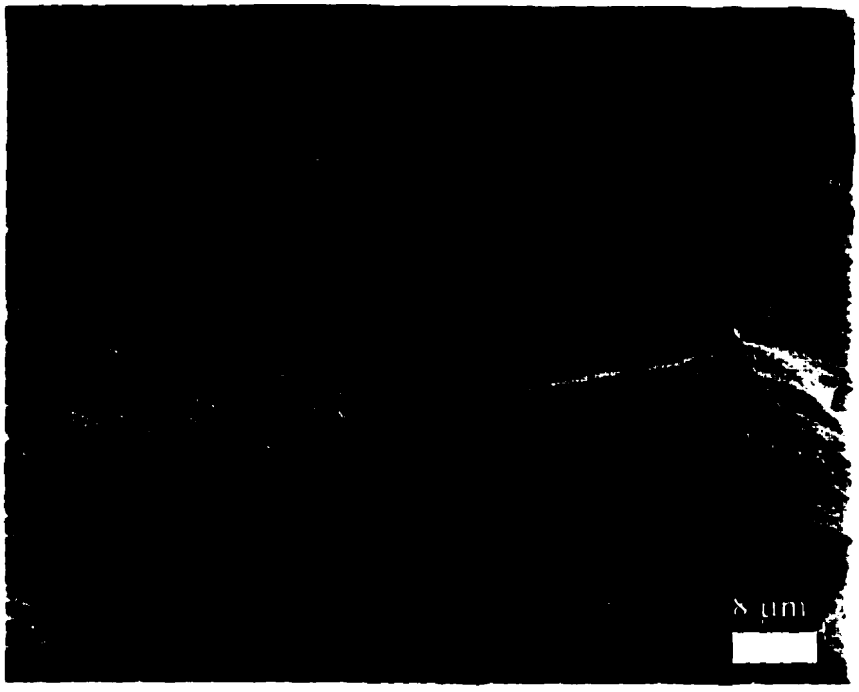

Figure 5.2: Scanning electron microscope image of chemically interesterified milkfat with the liquid oil not removed.

Figure 5.3: Scanning electron microscope image of chemically interesterified milkfat, with the liquid oil in the sample not removed.

Figure 5.4 shows polarised light micrographs of anhydrous milkfat, where the network has been broken and dispersed in paraffin oil. Figure 5.4 (A) demonstrates dense "particles" (which seems to be composed of smaller crystallites) and clusters of three or more of these particles which have been unbroken. The "particles" seem to be of the order of 3 μm to 4 μm. It seems likely that these particles once belonged to larger clusters, but the dispersing process allowed them to be separated. Figure 5.4(B) demonstrate the same characteristics of figure 5.4(A), with clusters of "particles" being more evident – it seems that the dispersing process did not succeed in breaking the network as well as it did for the case demonstrated by figure 5.4 (A). Additionally, figure 5.4 (B) indicates that the clusters themselves may have been a part of even larger clusters. Figures 5.5 (A) and (B) show similar images, of palm oil and interesterified palm oil respectively. The "particles" in the non-interesterified palm oil are approximately 2.5 – 3.0 μm, and there is also evidence of clustering. The "particles" of the chemically interesterified palm oil are also similar. The lard and chemically interesterified lard samples (shown in figures 5.6 (A) and (B) respectively) maintain this similarity. Therefore, although the network has been broken in an uncontrolled manner, there seems to be some amount of similarity in the structure demonstrated by the 5 different fats imaged by this method. At this stage, there seems to be clusters of smaller entities which I have referred to up till now as "particles" and these clusters themselves seems to belong to even larger clusters. Given the evidence provided by Herrtje and co-workers (Heertje *et al.* 1987; Juriaanse and Heertje, 1988; Heertje, 1993) which demonstrated that clusters as large as 100 μm are possible, this emerging picture of the network is at least plausible.

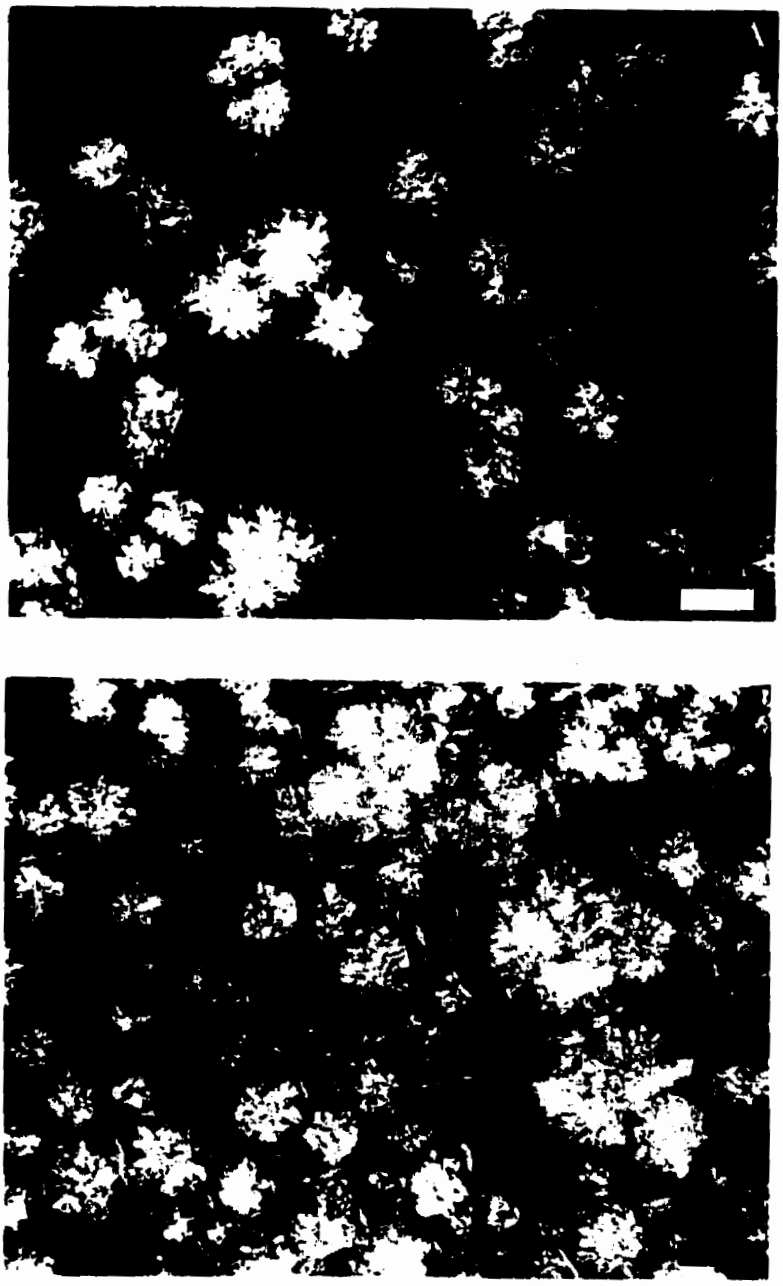

Figure 5.4: Polarised light microscope images of anhydrous milkfat. The network has been broken and dispersed in paraffin oil.

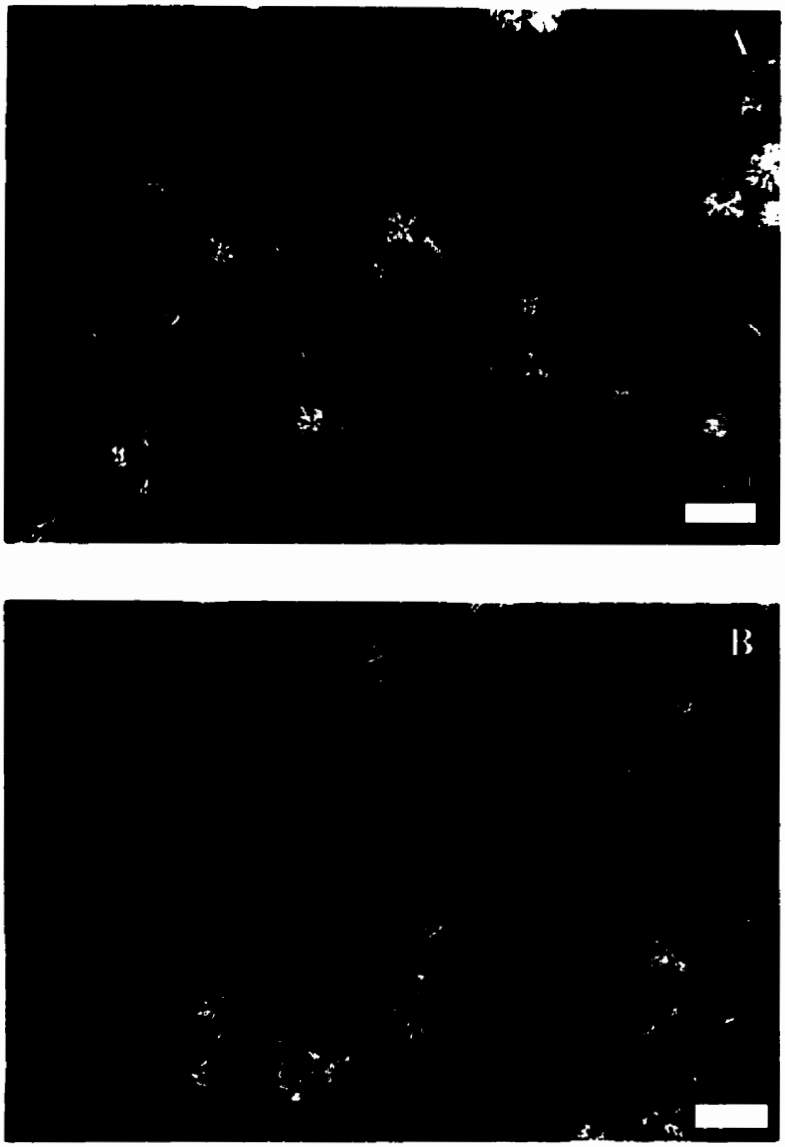

Figure 5.5: Polarised light microscope images of: (A) palm oil and (B) chemically interesterified palm oil. The network has been broken and dispersed in paraffin oil.

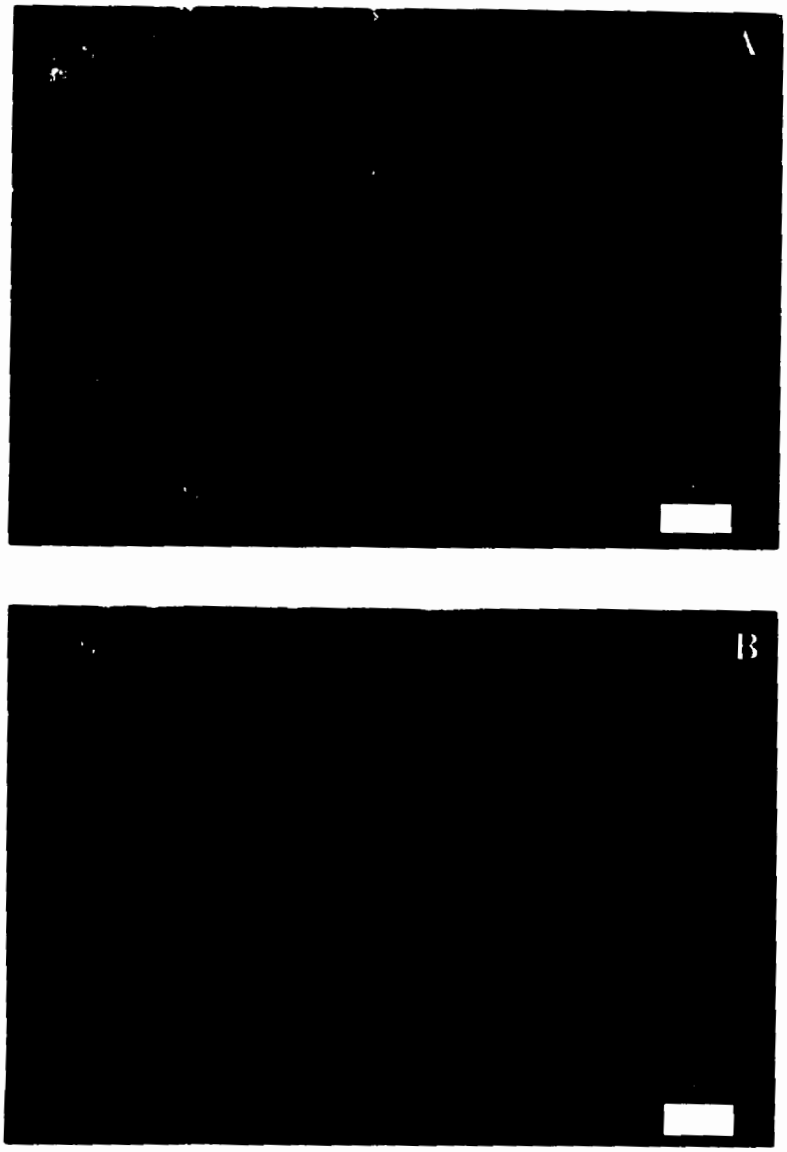

Figure 5.6: Polarised light microscope images of: (A) lard and (B) chemically interesterified lard. The network has been broken and dispersed in paraffin oil.

Figures 5.7 and 5.8 show confocal laser scanning micrographs of the crystal network of milkfat at 18°C. The samples were negatively stained with Nile Blue, causing the solid crystals to appear as darker entities in the micrographs. It must be mentioned here that it is uncertain how the presence of Nile Blue affects the formation of the network itself. Additionally the solid crystalline material may appear to have tendrils that are actually as a result of solid particles being covered by liquid oil stained by the Nile Blue. Figure 5.7 suggests that there are clusters present of the order of 30 μm. One must bear in mind that the individual "particles" are not present in this figure, since here the network is being observed at a lower magnification. Furthermore, it is seen that these clusters are part of an even larger cluster, of the order of 70 μm. Interestingly, the intermediate clusters seem to pack in the same manner as the "particles" did in the clusters shown in the PLM images of figures 5.4 – 5.6. Therefore, the network seems self-similar at these different length scales represented in figures 5.7 and 5.4 – 5.6. This is important, and will be developed later in this chapter. The evidence proposed by figure 5.7 also is in agreement with the observations of Heertje and co-workers, since they have reported cluster sizes of 100 μm in milkfat. Although the size of the large cluster in this micrograph is approximately 70 μm, this disparity in size compared to the work of Heertje and co-workers could be dependent on the focus depth of the confocal microscope. It must be remembered that a confocal image is a 2-dimensional slice of the network. Figures 5.8 (A) and 5.8 (B) serve to reinforce the arguments made above. Interestingly, the observations made above are also supported by the SEM images shown in figures 5.1, 5.2 and 5.3. The structural entities shown in figures 5.1 are almost

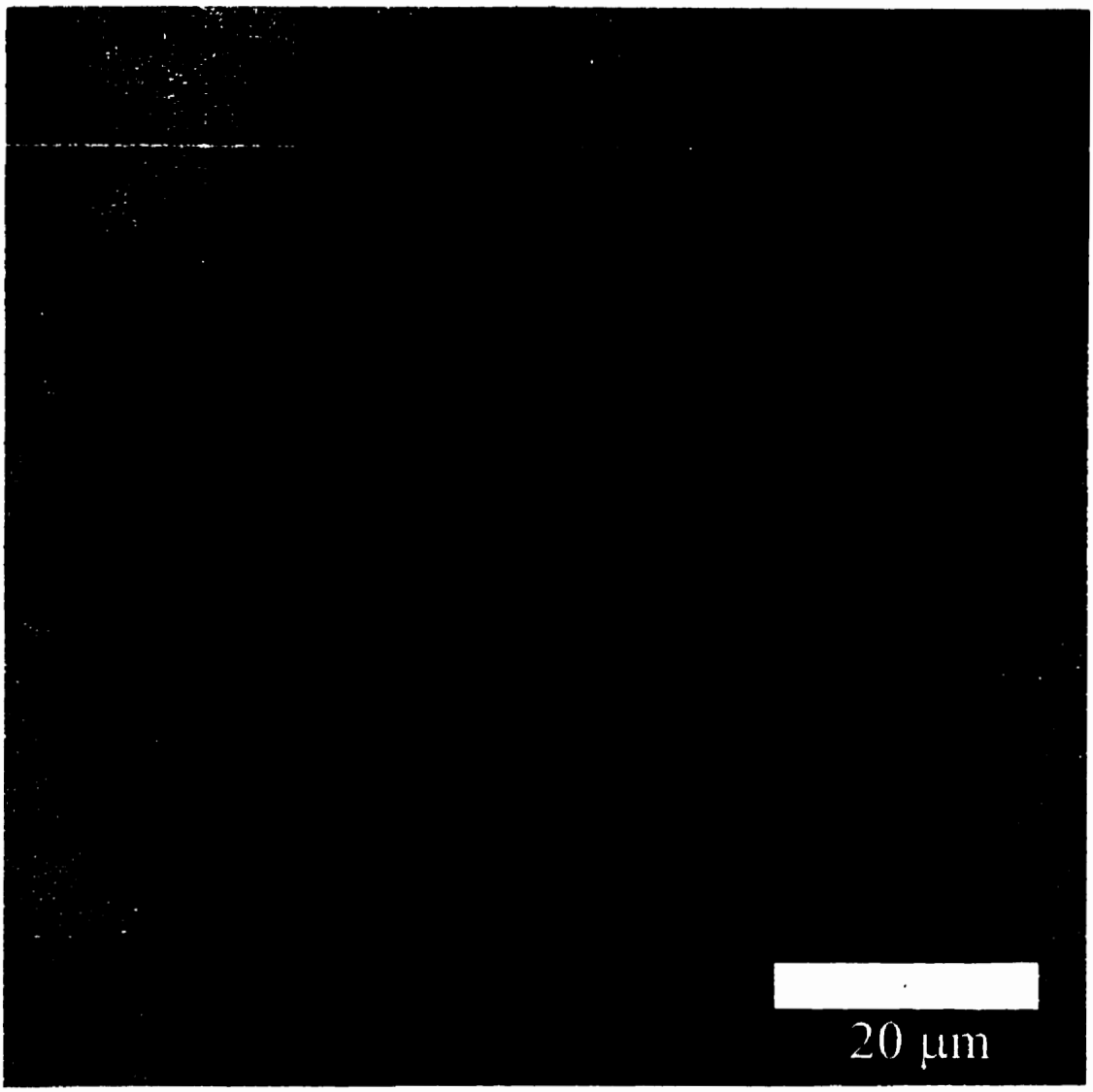

Figure 5.7: Confocal laser scanning microscopy images of milkfat stained with Nile Blue.

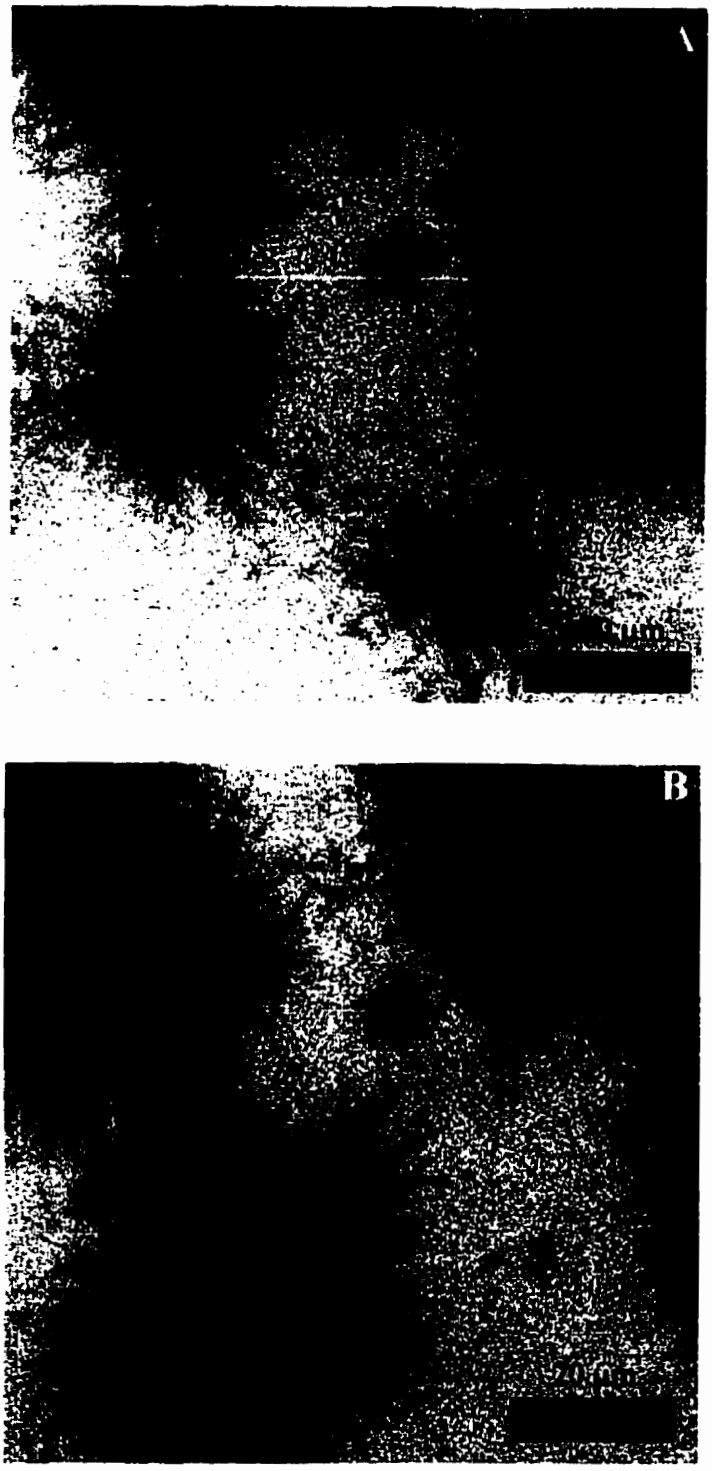

Figure 5.8: Confocal laser scanning microscopy images of milkfat stained with Nile Blue.

certainly clusters of intermediate size (recall they were of the order of 30 – 40 microns in size) and the larger structures shown in figure 5.2 are almost certainly the large clusters – i.e. clusters of clusters. The "particle" shown in figure 5.3 is also of a similar size to the particles seen in both the polarised light micrographs shown in figures 5.4 to 5.6. Therefore, the emerging picture of the structural arrangement of the fat crystal network at the microstructural scale has been consistent in the three different methods of imaging so far discussed.

Figure 5.9 shows a composite of atomic force microscopy images of a sample of the high melting fraction of milkfat that was spin coated onto a silicon substrate. Figure 5.9 (A) shows what appears to be a "particle" of the order of 4 – 5μm. The edges of this particle are not well defined, probably due to the nature of the atomic force microscope's method of imaging. It is difficult to effectively define the boundaries between closely spaced particles, since the vertical range of the atomic force microscope is limited – therefore, rather than define a definite boundary, the tip of the microscope will instead indicate a low point in the image, which may appear as an intermediate depth. Total darkness in these images represent the limit of the tip's vertical displacement, whilst the whitest colour in the image represents the highest point in the image. Figure 5.9 (B) identifies at least three neighbouring "particles" of the same average size. Figure 5.9 (C) and (D) show intermediately-sized clusters of particles, whilst figures 5.9 (E) shows what appears to be a section of a large cluster of the order of 90μm – 100μm. Figure 5.9 (F) shows what appears to be the boundary between two or three large clusters. All of these images were imaged on the same sample, with figure 5.9 (E) being taken over a spot

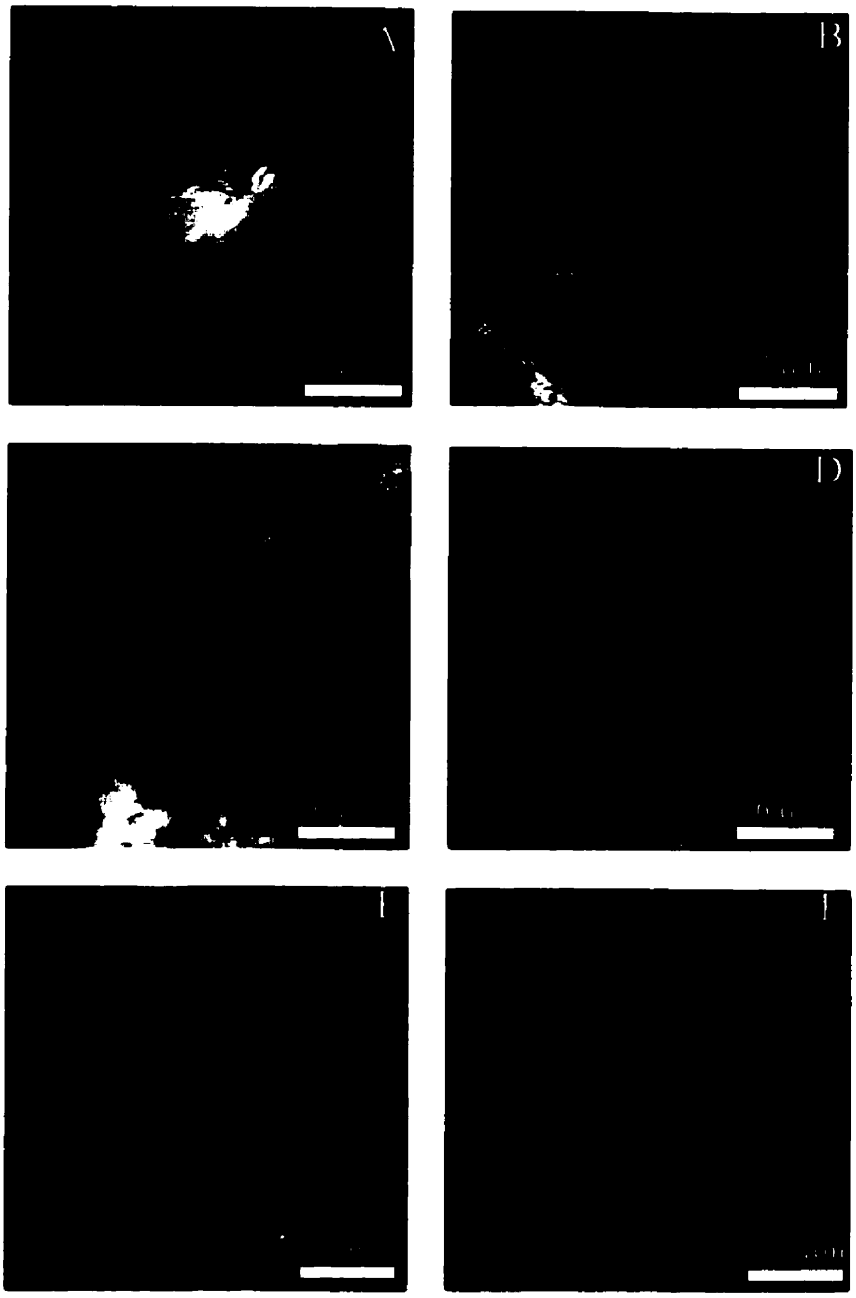

Figure 5.9: Atomic force microscopy images of the high melting fraction of milkfat. Sample was spin-coated onto a silicon substrate.

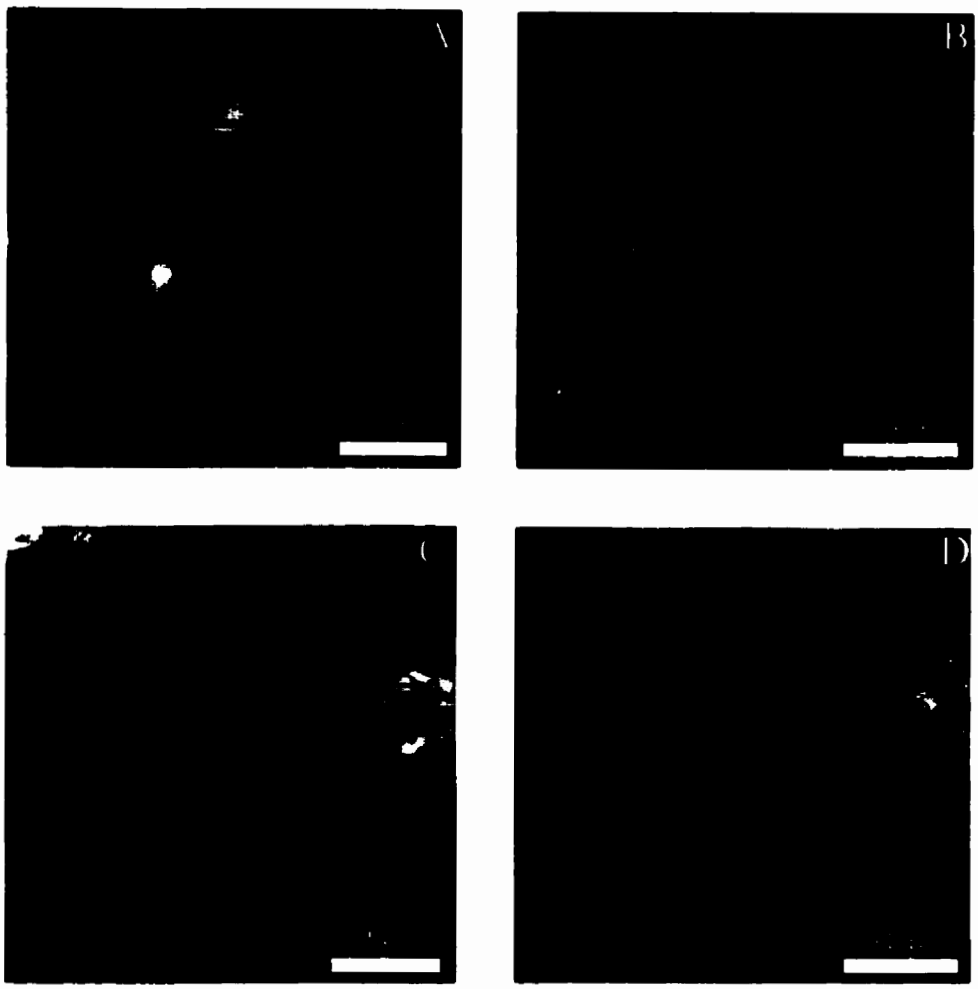

Figure 5.10: Atomic force microscopy images of the high melting fraction of milkfat. Sample was spin-coated onto a silicon substrate.

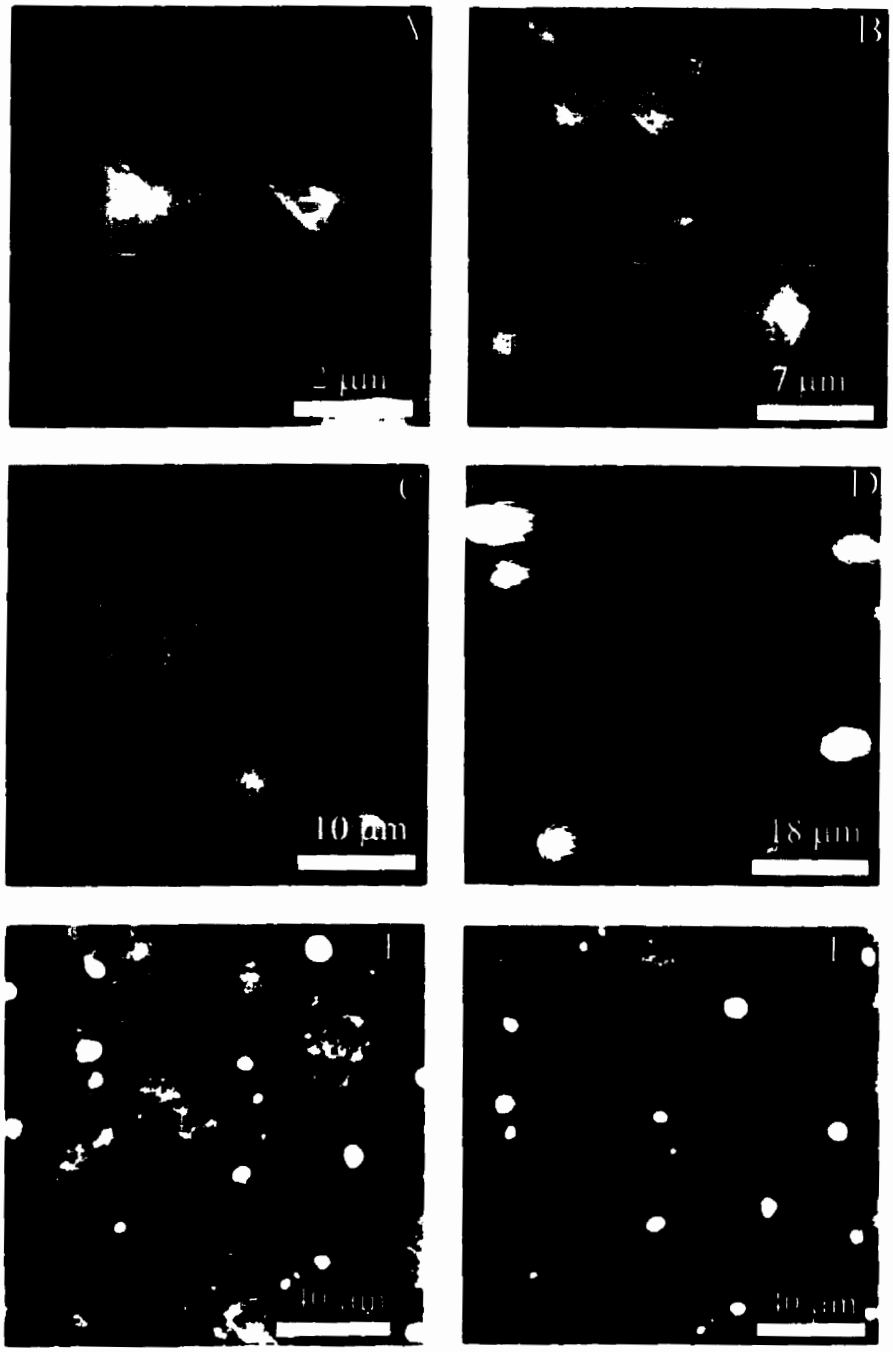

Figure 5.11: Atomic force microscopy images of the high melting fraction of milkfat. Sample was prepared in a rheological mould.

immediately adjacent to the spot over which figure 5.9 (F) was taken. Figures 5.9 (D), (C), (B), and (A) are all within the area shown in Figure 5.9 (E). Figure 5.10 shows a composite of images taken of the same sample as Figure 5.9, except that these images were taken over a different spot on the surface of the sample. As can be seen, similar types of structure as described above are observed. Figure 5.11 is of the high melting fraction of milkfat as well, only this sample was prepared in a rheological mould, as described in Chapter 3. As can be seen, this image is in agreement with Figures 5.9 and 5.10, except that at the low magnifications (i.e. for figures 5.11 (D), (E) and (F)) there are a series of very high, round spots. It is believed that these spots are due to dust particles found on the samples that were prepared in the rheological moulds (part of the process requires the sandwiching of the fat samples by Parfilm, which may have been contaminated with dust or wax crystals), since these types of spots were observed with all the samples prepared in the moulds. What is also important to note in Figures 5.9, 5.10 and 5.11, is that the structures at different magnifications, i.e. at different length scales, look quite similar. These structures seem to demonstrate some sort of statistical self-similarity at different length scales, bounded by the size of one "particle"and the size of one large cluster (since as we shall see from other images to be presented in this chapter and from Heertje's and co-workers publications, the large clusters pack in a regular space filling manner to form the network). Identification of self-similarity in natural structures is usually a rather qualitative process (due to the inexact nature of the self-similarity) such as the realisation that clouds and trees are self-similar. However, this process is usually the first physical clue that the object under scrutiny may be fractal in nature – for example, figure 5.12 shows the qualitative self-similarity of a cauliflower, which is a

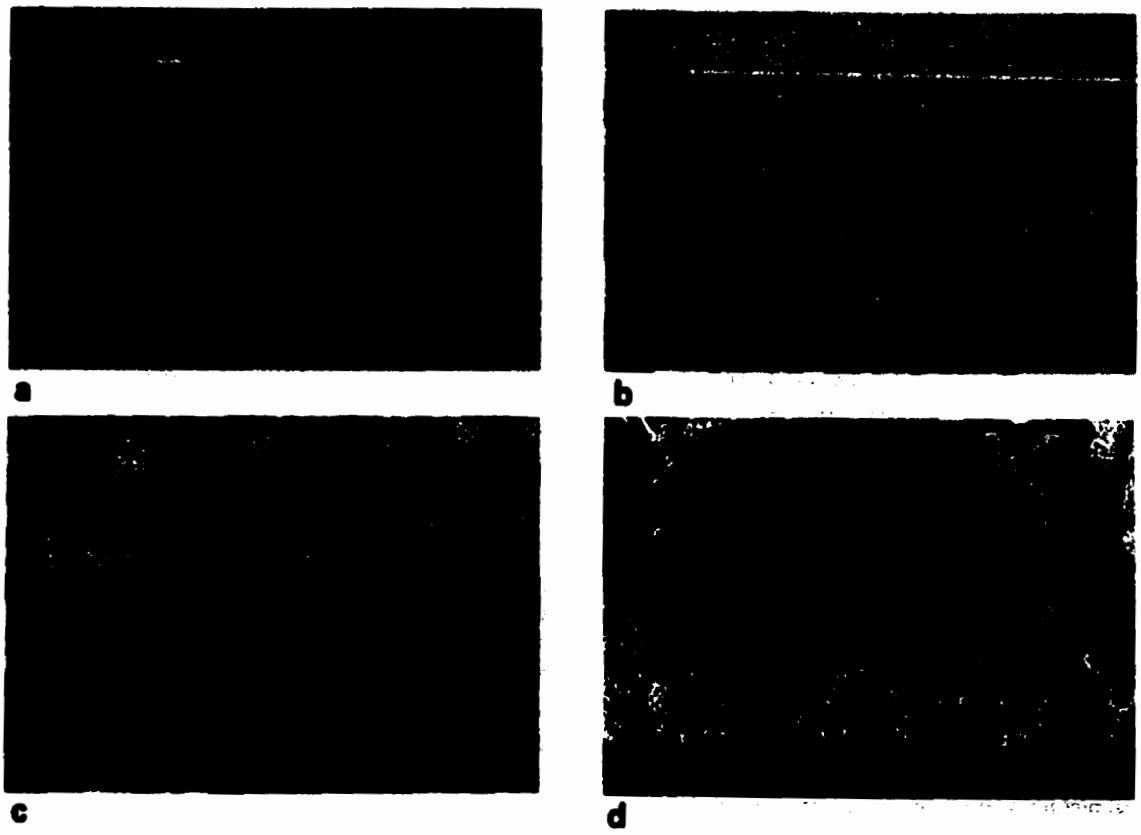

Figure 5.12: (a - c) Photographs of a Minaret cauliflower showing self-similarity at different length scales. (d) Electron micrograph (SEM) of Alverda cauliflower on sub-millimeter scale. (Adapted from Grey and Kjems, 1989)

typical natural fractal. Figure 5.13 show AFM images of a sample containing a 50:50 mixture of the high melting fraction of milkfat (HMF) and the medium melting fraction (MMF) of milkfat, spin coated onto a silicon substrate. Again, these structures are very similar to those of the high melting fraction – individual particles (not very defined, for reasons mentioned above) seem to be arranged in clusters, which are further arranged into one large cluster (of approximately 100 μm – 125 μm), shown in Figure 5.13 (D). As well, the self-similarity of the structure at the different magnifications shown is readily apparent. Figure 5.14 shows composites of a 50:50 mixture of HMF and MMF, but in this case the samples were prepared in rheological moulds. As is evident, the structures shown in figures 5.13 and 5.14 are quite similar, except for the appearance again of the suspected dust particles. As well, the self-similar nature of the structure at different magnifications is evident. Figure 5.15 show AFM images of a sample containing a 70:30 mixture of the high melting fraction of milkfat (HMF) and the medium melting fraction (MMF) of milkfat, spin coated onto a silicon substrate. The structures shown demonstrate the same general organisation as the other AFM images, and again the self-similar nature of the structures at all length scales within a large cluster (the smallest magnification, figure 5.15 (C) is still within an entire large cluster) is evident. Figure 5.16 shows AFM images of cocoa butter (details of samples preparation are provided in section 5.1 above). Figure 5.16 (A) is interesting in that it represents a level of magnification not shown previously in any of the AFM images. This level of magnification is showing structure that are within the "particles." The image suggests that the "particles" are composed of intertwined and sintered crystalline material, a picture which is reinforced by the polarised light micrographs shown in figures 5.4 to 5.6.

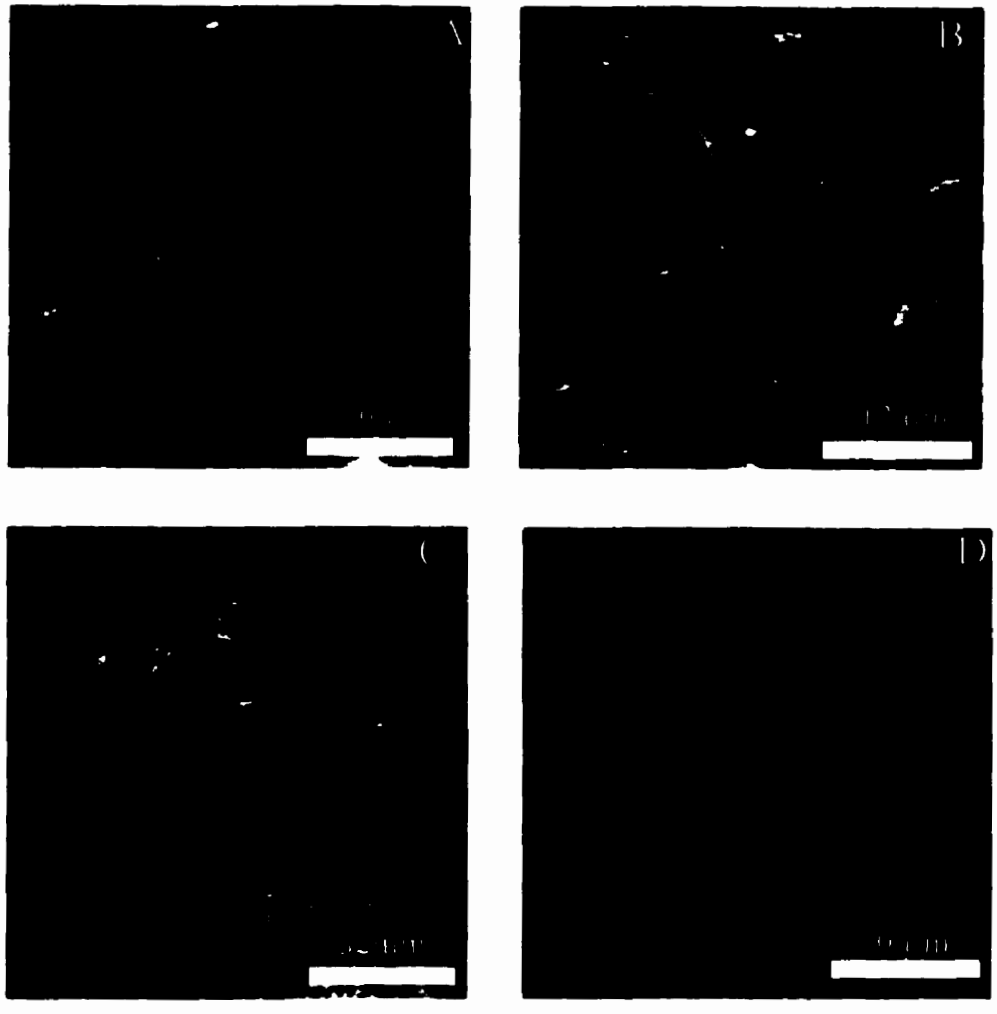

Figure 5.13: Atomic force microscopy images of a 50:50 w/w mixture of the high melting fraction of milkfat and the medium melting fraction of milkfat. Sample was spin-coated onto a silicon substrate.

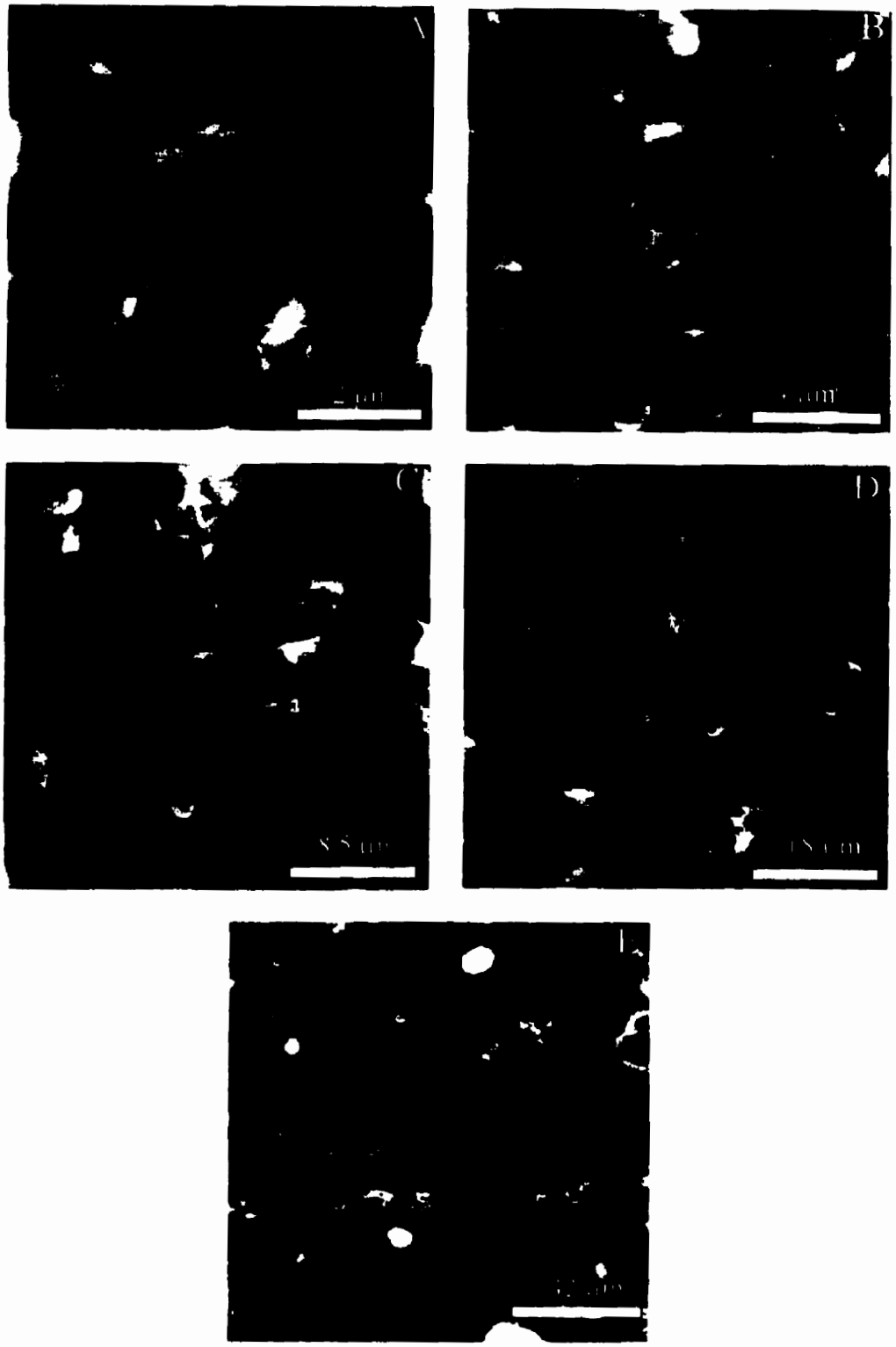

Figure 5.14: Atomic force microscopy images of a 50:50 w/w mixture of the high melting fraction of milkfat and the medium melting fraction of milkfat. Sample was prepared in a rheological mould.

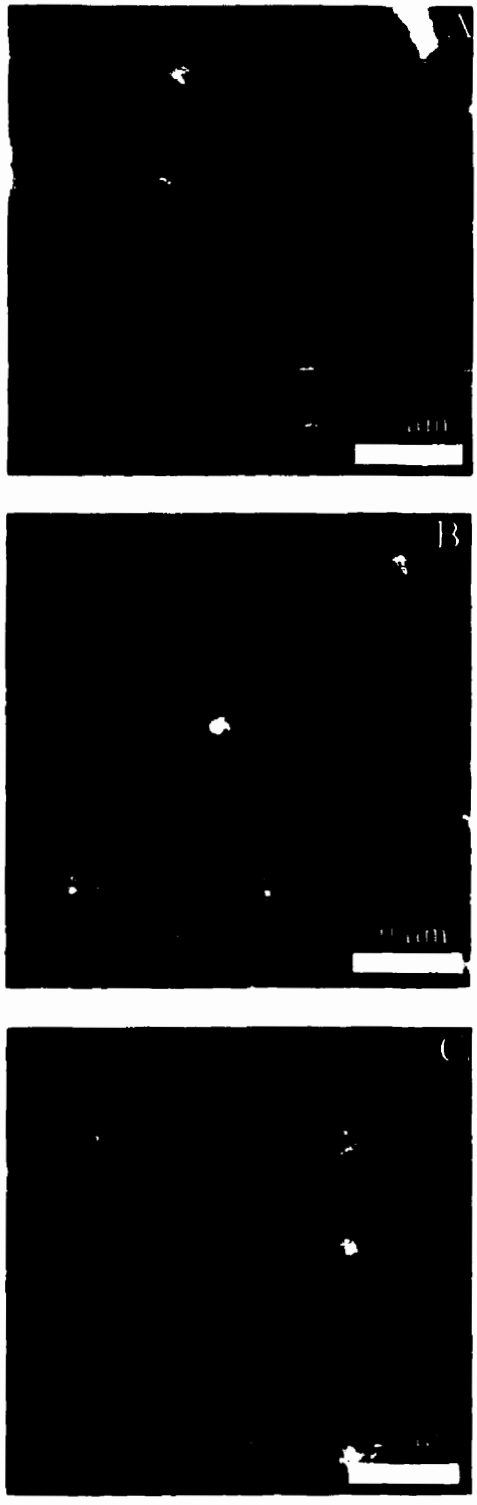

Figure 5.15: Atomic force microscopy images of a 70:30 w/w mixture of the high melting fraction of milkfat and the medium melting fraction of milkfat. Sample was spin-coated onto a silicon substrate.

Figure 5.16 (B) shows the familiar "particles" packed fairly close together, and again in this image, the appearance of the "particles" as being composed of intertwined crystallites is reinforced. Figure 5.16 (C) is a rather poor image at a lower magnification, which is however suggestive of the clustering of intermediately-sized clusters. It is unfortunate that current atomic force microscopes are not capable of a lateral range of scan much greater than 150μm. As a result, using this method, it is very difficult to image two or more of the large clusters reported by Heertje and co-workers and seen in the confocal images. However, some of the images do indicate the presence of these large clusters, although it is obviously not possible to assign to these structures a finite size, shape and regularity of packing. It is conceivable that one may be able to perform adjacent scans of a surface and then re-construct these images to represent the packing of a large area on the sample, but this procedure is not straight forward, due to the severe hysteresis found in the piezoelectric crystal drives of the atomic force microscope. However, the atomic force images presented here supports well the structural organisation suggested by the other forms of microscopy outlined so far.

Figures 5.17 to 5.20 show *in-situ* polarised light micrographs of seven different fat systems. It is important to discuss what these figures represent before we begin a discussion of the structures that are represented in them. Firstly, the maximum field of view represented in these images is approximately 65 μm – so therefore from all the evidence presented above, we are likely looking at an area which would be covered normally by two or three intermediate clusters. Secondly, these images are of the *in situ* network, and have a definite depth. Since the images have been deliberately made very

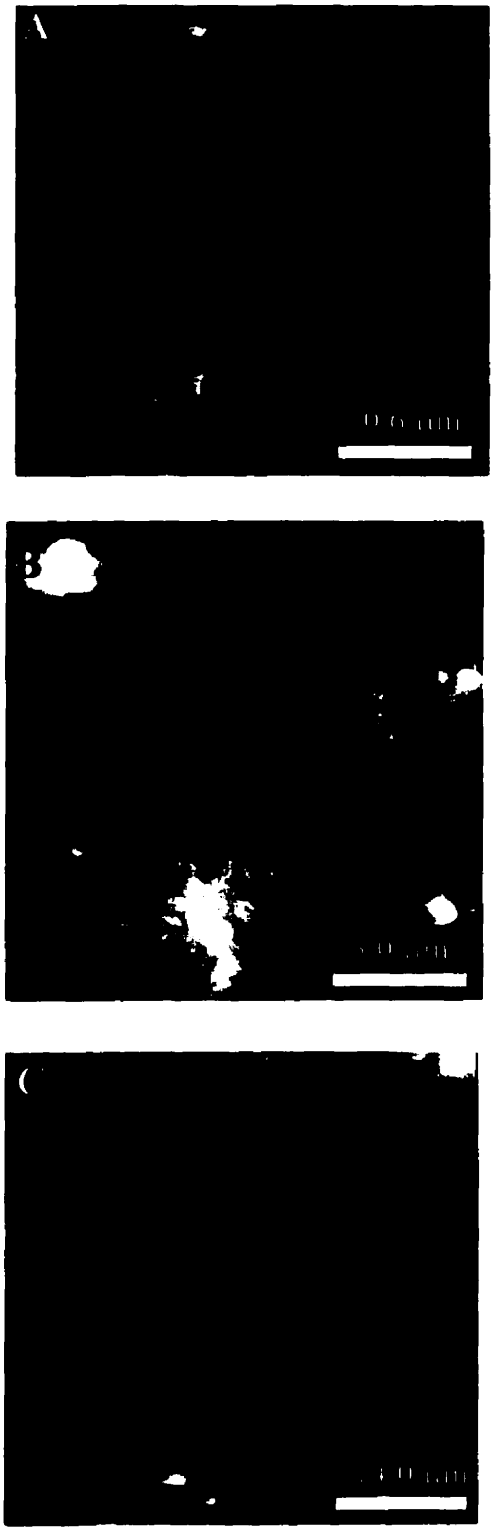

Figure 5.16: Atomic force microscopy images of cocoa butter. Sample was crystallised on a glass microscope slide; images are of the edge of the sample sandwiched between the slide and a coverslip.

thin, this depth is not significant enough to attenuate appreciable amounts of the light passing through, and therefore the image presented is not totally opaque, but gives a good representation of all the "particles" present – both in the depth of the sample as well as in the focal plane of the microscope. Care was taken to focus on those "particles" at the top of the sample, and those particles in the depth of the sample are therefore represented as out-of-focus entities that appear smaller than their actual size and as higher levels of gray than the in-focus particles which appear as higher levels of white. Since the depth of the samples are represented here, it is not possible to identify the boundaries of intermediate clusters that may be present – since if those were present, the boundaries would most likely be rendered indistinct due to the presence of particles belonging to other clusters in the depth of the sample, which are not at the same x-y cordinates of the clusters in focus. Therefore, the field of view is representative of *all* "particles" in the thin three-dimensional sample, except for those in direct geometrical shadow of "particles" in focus. Now, since the images are due to the refraction of polarised light through the anisotropic crystalline nature of the "particles" only part of a typical particle will be visible – however, by rotating the polariser by 45 degrees, it is possible to render those parts of the "particles" that were not visible, visible. This process of course renders the previously visible parts invisible. This process however serves to ensure that one can discern between neighbouring particles. The so-called Maltese Cross pattern is for instance due to a spherical-like "particle", but because of the orientation of the crystallites in the "particle" not all of them are visible when one looks at the particle under polarised light. Therefore, whilst it is possible to represent all of the "particles" present in the thin three dimensional sample in the polarised light microscope image, each particle will be missing

mass, some particles will appear larger than some, and some particles will appear more in-focus than some. However, the presence of all particles except those in direct geometrical shadow (negligible if the sample is sufficiently thin) may be noted, if the image is taken with some care. Figure 5.17 shows and *in-situ* image of milkfat at 5°C. The approximate diameter one of the "particles" in focus is between 2μm – 3μm, which are in agreement with the polarised light micrographs of milkfat at 5°C shown in figure 5.4. It should not be expected that the "particle" sizes agree exactly from the different methods of microscopy – for instance, the size of the "particles" (even the in-focus "particles") in the *in-situ* PLM images will be under-represented due to invisible mass. Figure 5.17 (A) therefore, given the above discussion, is in agreement with the other forms of microscopy discussed so far, with the added fact that it is an *in-situ* image of the network. Figure 5.17 (B) shows a similar micrograph of cocoa butter, taken at 20°C. This figure is very similar to the image shown in figure 5.17 (A). Figure 5.18 (A) shows a similar image of tallow, taken at 5°C. This image demonstrates "particles" of the order of 2 μm, and each particle appears as an image approximating a Maltese Cross pattern, suggesting that these "particles"may be spherical-like in shape. Figure 5.18 (B) shows a similar image (at higher magnification) of a 50:50 mixture of HMF and MMF, at 20°C. One can identify "particles" of the order of 5μm – 6μm, in good agreement with the AFM images shown before of the same fat. Figure 5.19 (A) shows "particles" in palm oil at 5°C and figure 5.19 (B) shows "particles" of lard at 5°C. These images are also quite similar to those of milkfat, tallow, and cocoa butter discussed before. One can easily identify that there are "particles" in the depth of the sample which are nevertheless represented in the image. Figures 5.20 (A) and (B) show "particles" of the middle

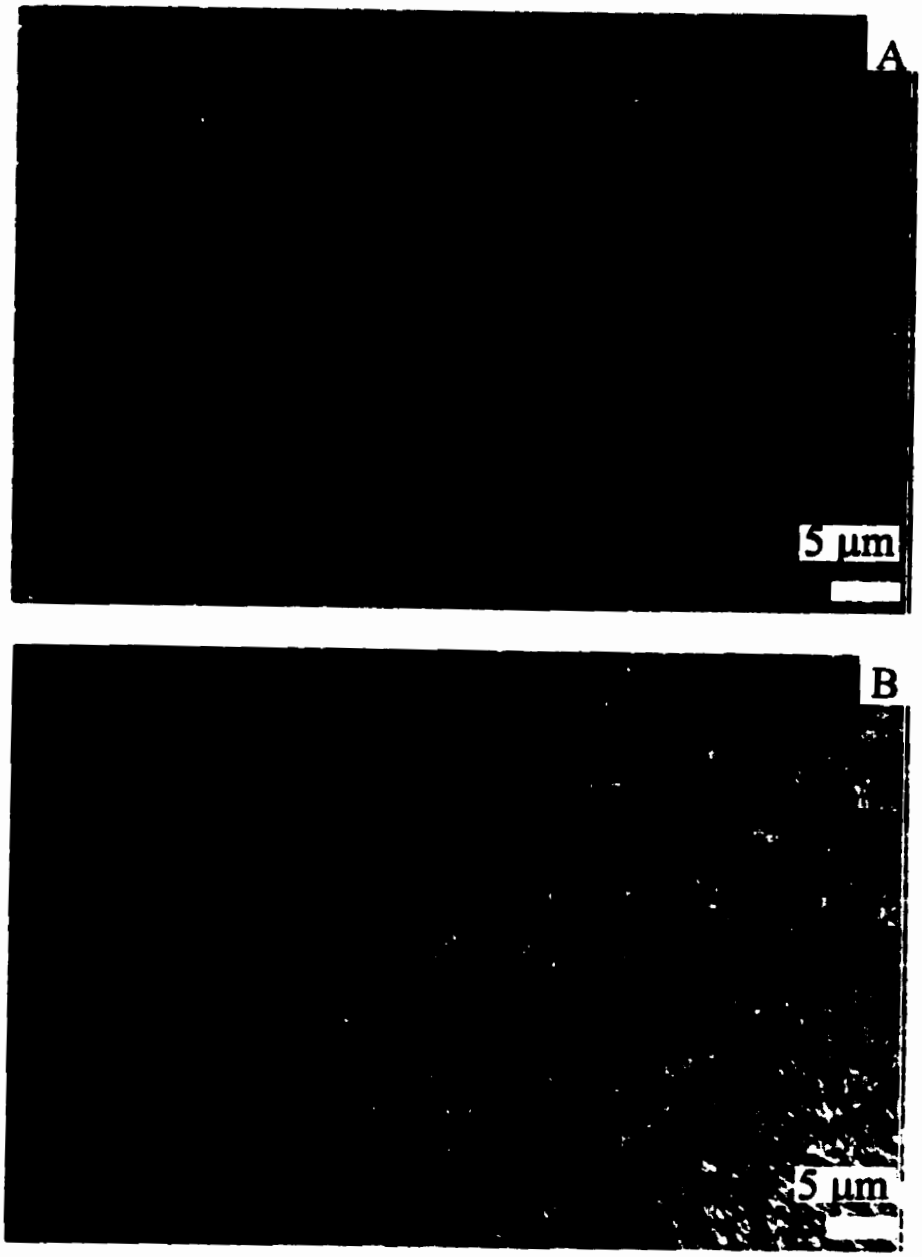

Figure 5.17: *In-situ* polarised light microscope images of (A) milkfat at 5°C and (B) cocoa butter at 5°C.

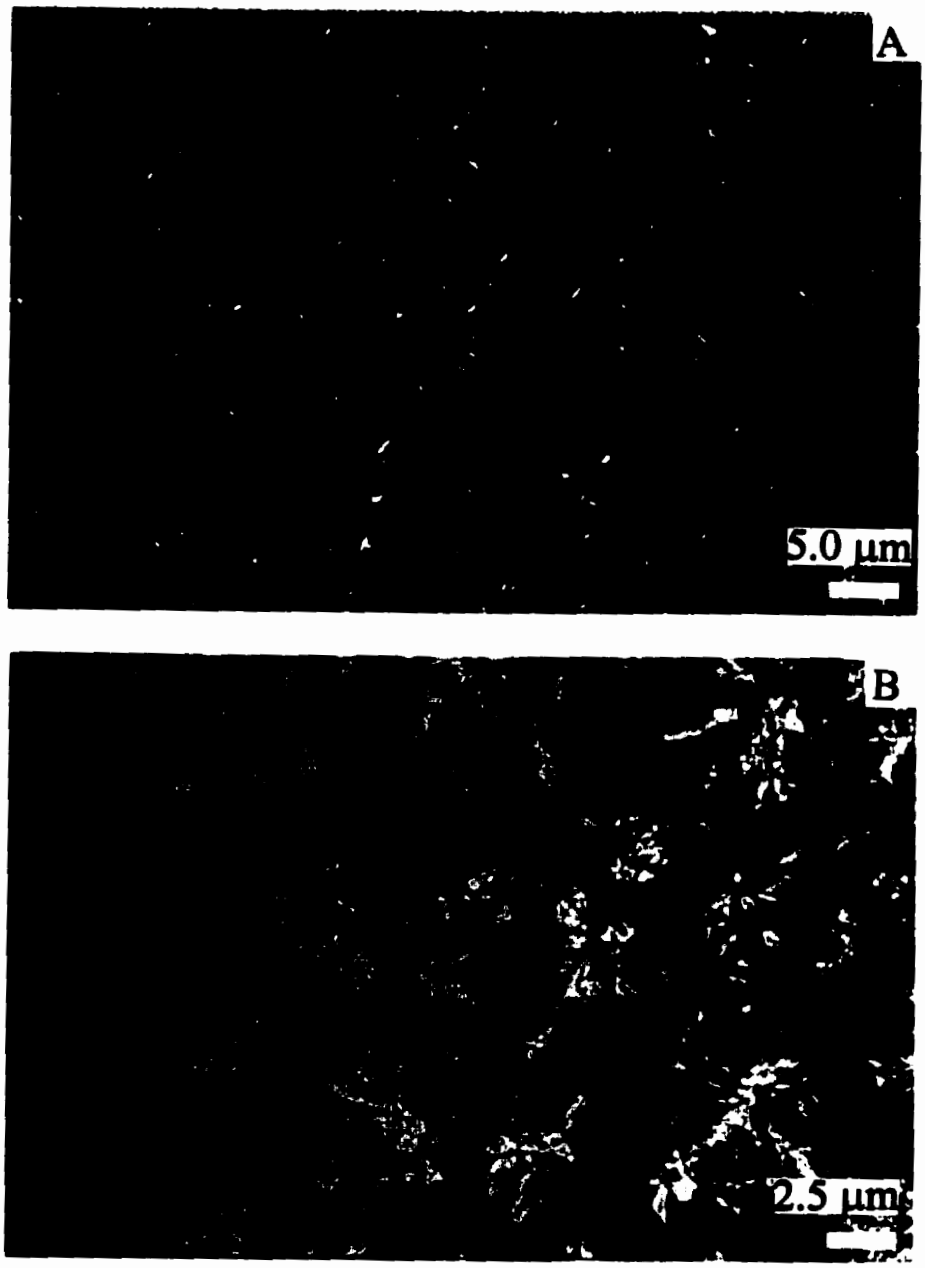

Figure 5.18: *In-situ* polarised light microscope images of (A) tallow at 5°C and (B) a 50/50 w/w mixture of the high melting fraction and the medium fraction of milkfat at 20°C.

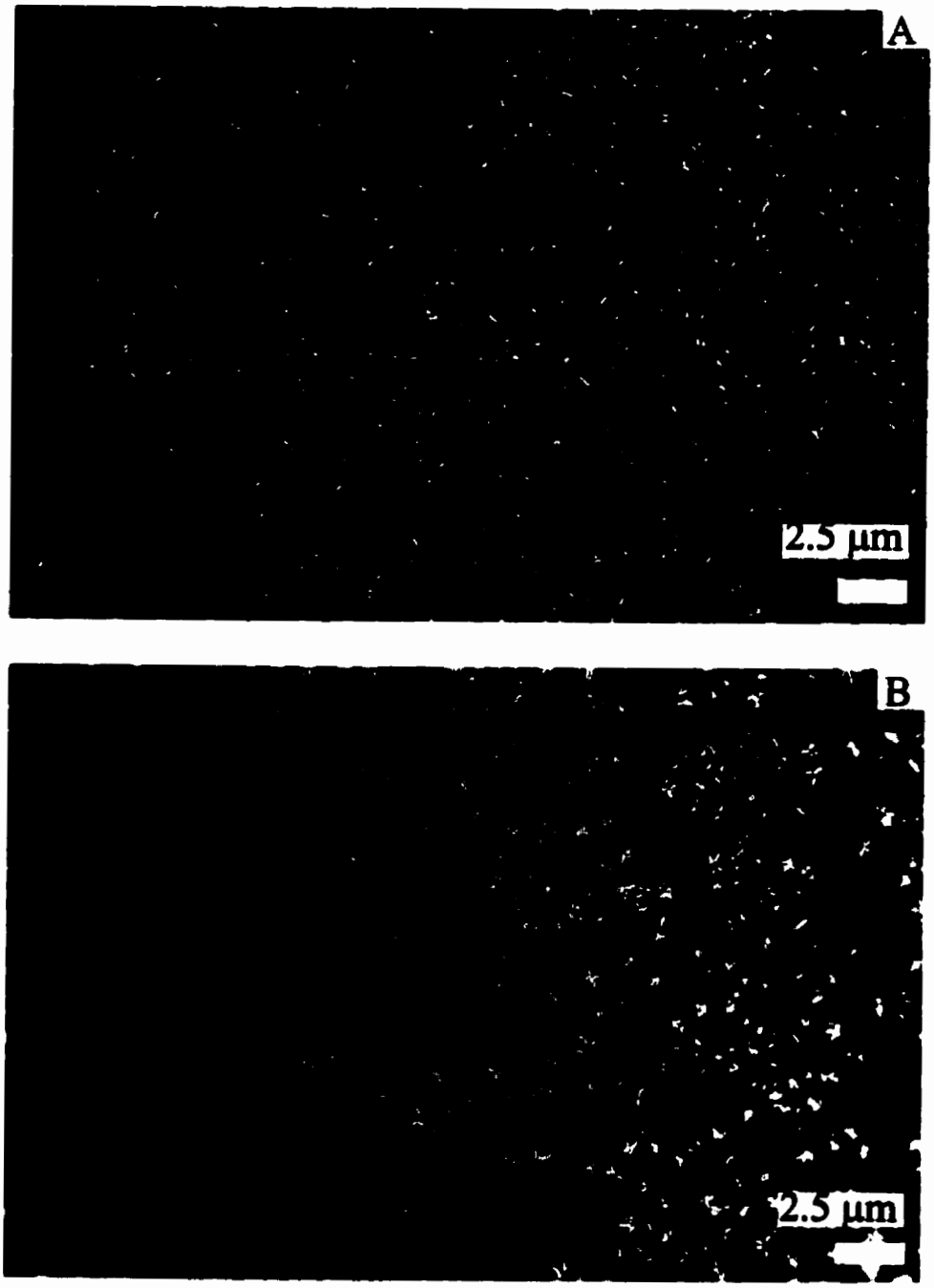

Figure 5.19: *In-situ* polarised light microscope images of (A) palm oil at 5°C and (B) lard at 5°C.

melting fraction (MMF) of milkfat at 20°C. One can see from these images that the "particles" here grow as large as those encountered in the 50:50 HMF:MMF mixture shown in Figure 5.18 (B) – of approximately 7μm to 8μm. Figure 5.20 (B) demonstrates that there are "particles" represented in the focal plane of the image, whilst those out of the focal plane, in the depth of the image, appear smaller and un-focussed. However, they can be identified and accounted for in this image. It is interesting to note that the "particles" in this image are very spherical (displaying well-defined Maltese Crosses), which may be due to the homogenous nature of the triglycerides making up the sample.

The evidence presented above by the different types of microscopy are all in agreement – the microstructure of fat crystal networks seems to be organised in hierarchical levels of structure: "particles" composed of intertwined crystallites, of the order of 1 μm – 8 μm are organized in intermediately-sized clusters, which are packed in a similar manner to the way the "particles" pack, into large clusters of the order of 100 μm – 150 μm. Not much evidence has yet been presented of the large clusters themselves, although the work of Heertje and co-workers has been quoted, which demonstrates that the large clusters in a fat network pack in an orthodox space filling manner to form the network. Figure 5.21 shows the large clusters present in cocoa butter. These are of the order of 120 μm, and they were imaged by diluting the network with 50% canola oil, thereby allowing the large clusters to separate and become discernable under a polarised light microscope. Figure 5.22 shows the large clusters present in milkfat, of the order of 100 μm, and Figure 5.23 shows the formation of the large clusters in tallow, of the order of 100 μm – 150 μm.

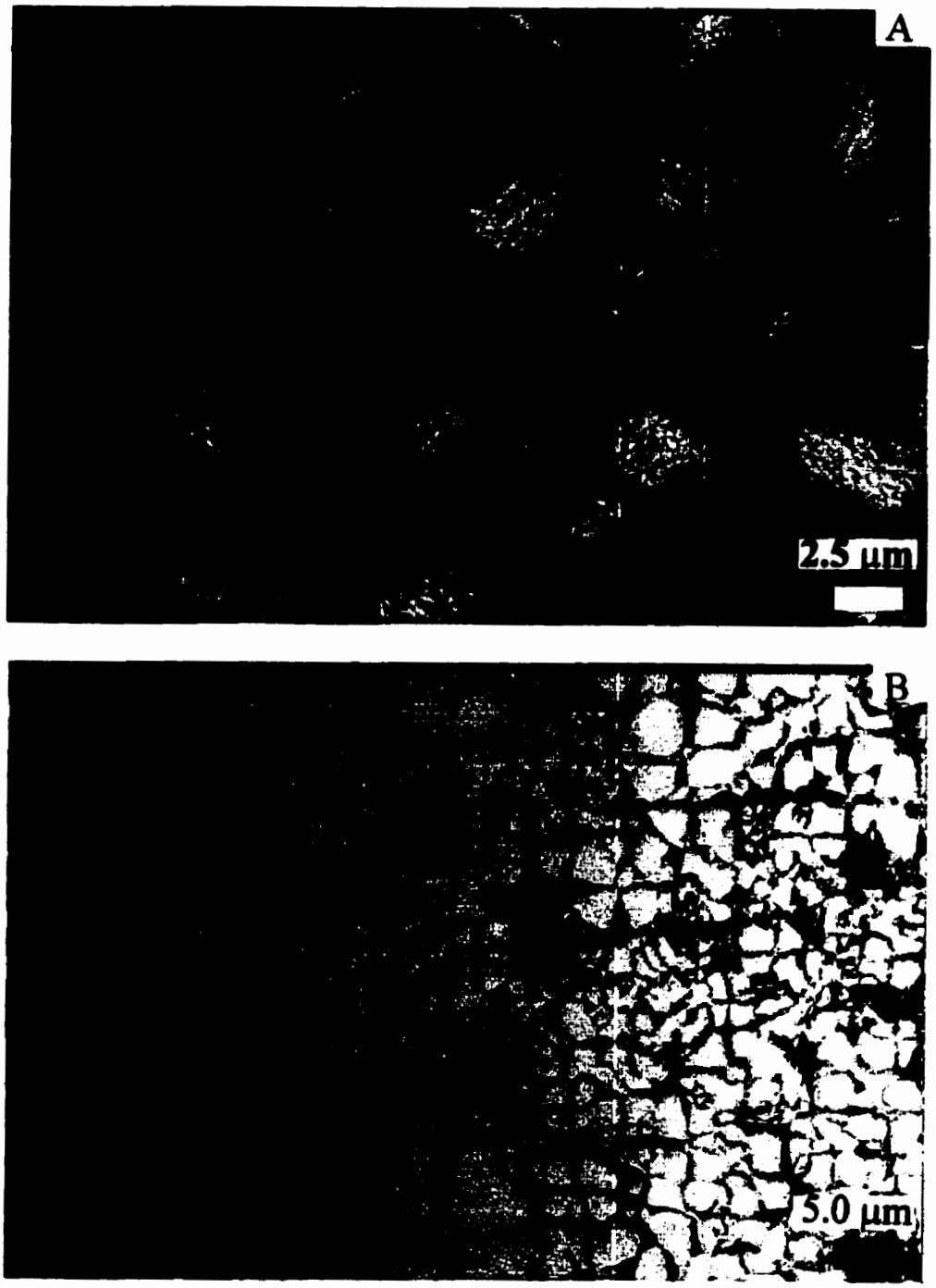

Figure 5.20: *In-situ* polarised light microscope images of the middle melting fraction of milkfat at 20°C.

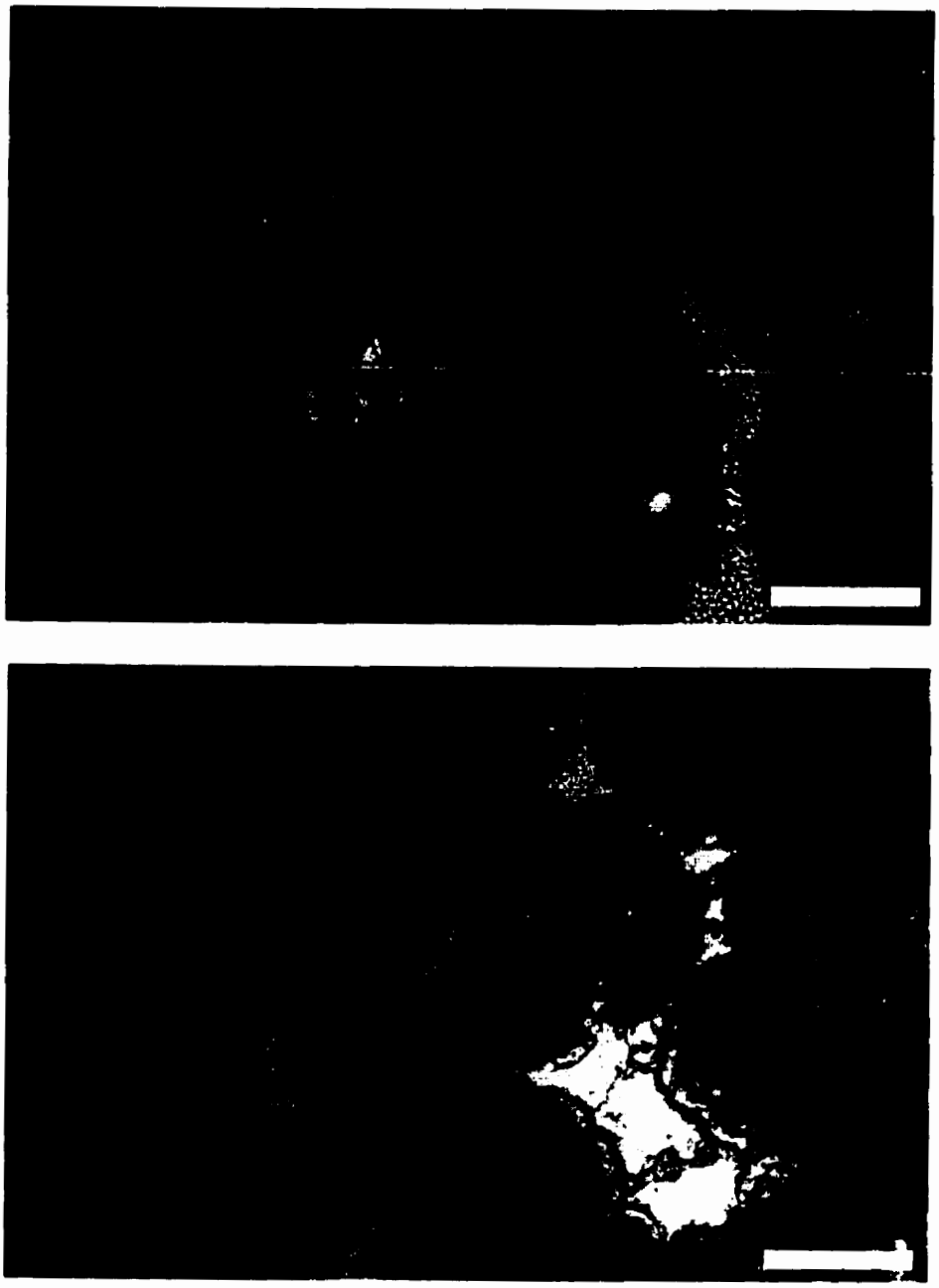

Figure 5.21: Polarised light microscope images showing large clusters of cocoa butter.

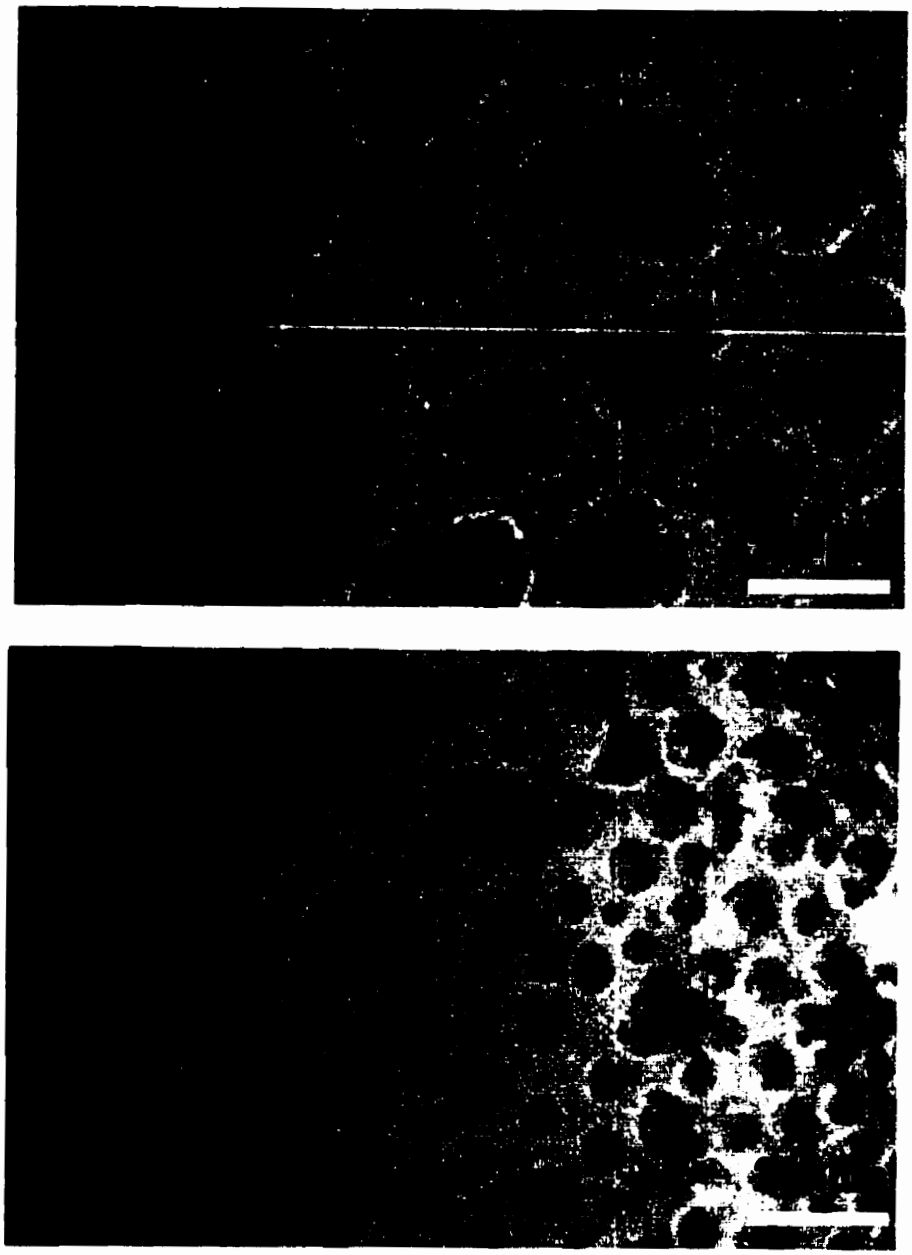

Figure 5.22: Polarised light microscope images showing large clusters of milkfat.

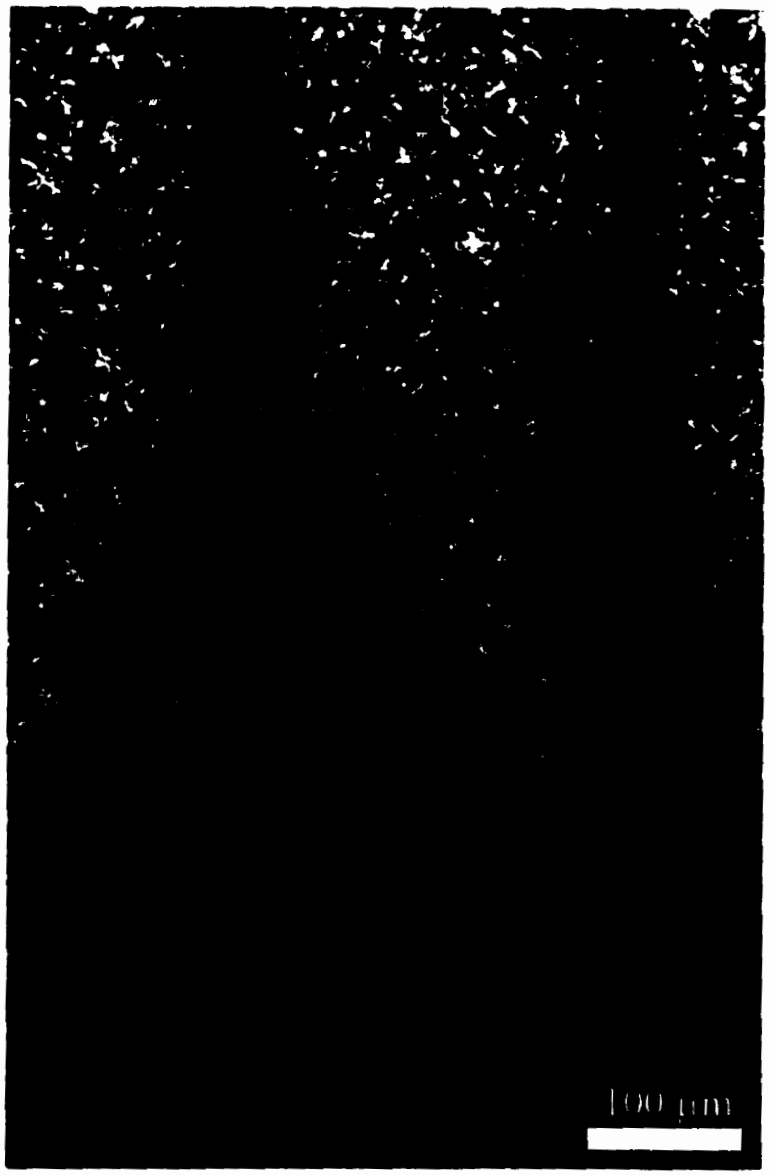

Figure 5.23: Polarised light microscope image showing large clusters of tallow.

In an effort to observe the formation of the fat crystal network from the melt, the kinetics of formation of the network was monitored by polarised light microscopy, as is described in section 5.1. Figure 5.24 show images of the network formed by pure milkfat triacylglycerols at 5.5 min. (A), 7 min. (B), 8.5 min (C), 10 min (D), 11.5 min. (E), 13 min (F), 25 min (G), and 32.5 min. (H) after appearance of the first visible signs of crystallisation in the field of view. Figure 5.25 show images of the network formed by a mixture of pure milkfat triglycerols to which have been added 0.01% by mass of milkfat diacylglycerols at 7.5 min. (A), 12.5 min. (B), 17.5 min. (C), 22.5 min. (D), 27.5 min. (E), and 32.5 min. (F) after appearance of the first visible signs of crystallization in the field of view. As is demonstrated by both figures, in the early stages of crystallisation, growth is concentrated around a few centres of nucleation. However, as the growth process continues, there is an aggregation process that takes place, since there are the appearance of many more centres of growth (with advanced growth having already taken place, therefore suggesting that these "new" centres of growth were not new nucleation events) than there were nuclei in the field of view. The process of growth of the centres of crystallisation continues until they reach a certain maximum size, whereupon the aggregation process continues slowly. After approximately ½ h, the aggregation process is no longer visibly evident, although quite often there is massive re-arrangement of the structure over 24 and sometimes even 48 and 72 h. It is unfortunate that this type of microscopy does not allow the definition of intermediately-size cluster boundaries, since it would be also interesting to observe the process of aggregation of these clusters themselves. One can begin to see cluster formation during the crystallisation/aggregation process demonstrated by both figures, for example, in figure 5.24 (C), one can begin to

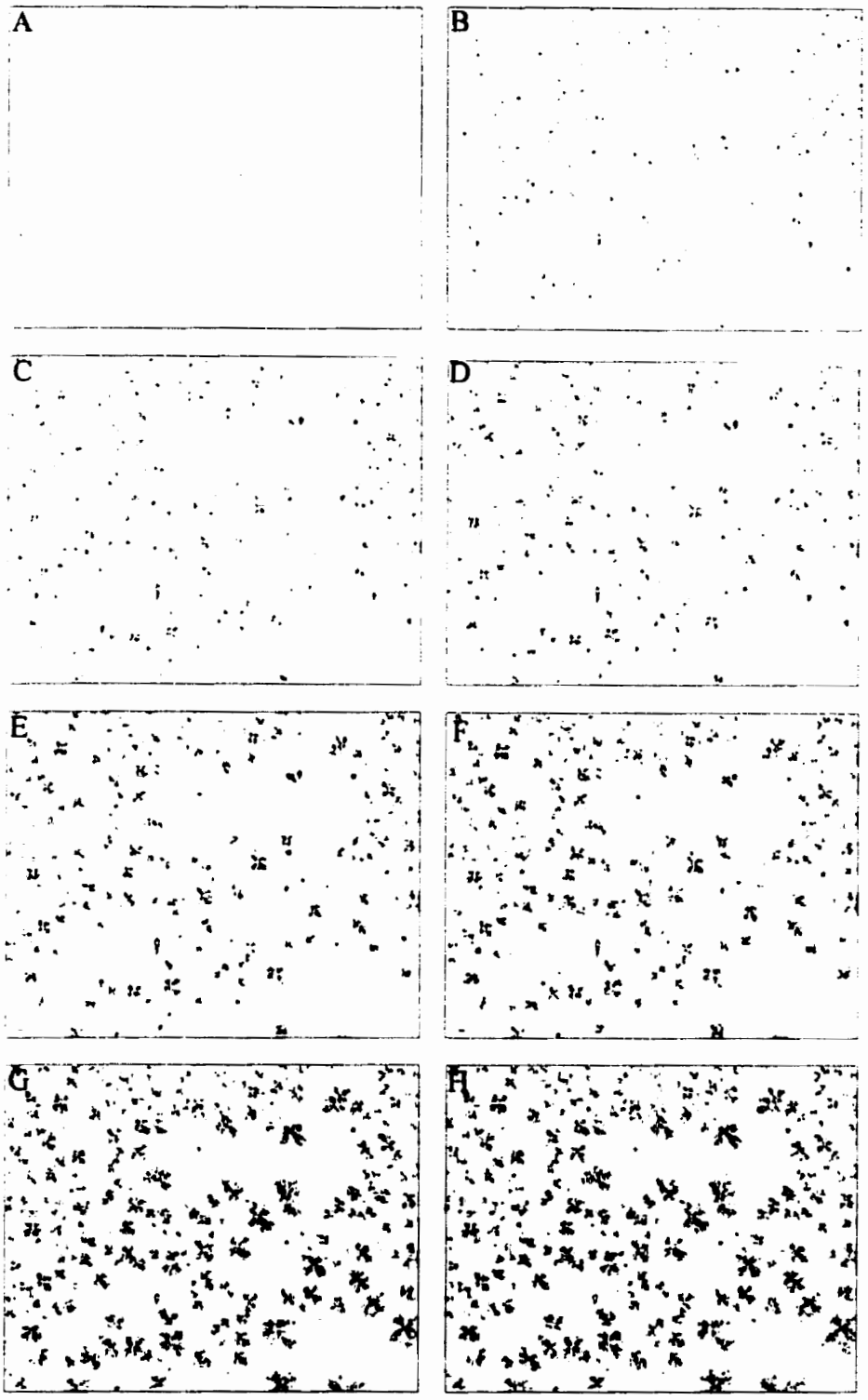

Figure 5.24: Polarised light microscope images of milkfat triacylglycerides at various times after appearance of first visible signs of crystallisation: (A) 5.5 mins, (B) 7 mins, (C)10 mins, (D)11.5mins, (E) 13 mins, (F) 25 mins, and (G) 32.5 mins.

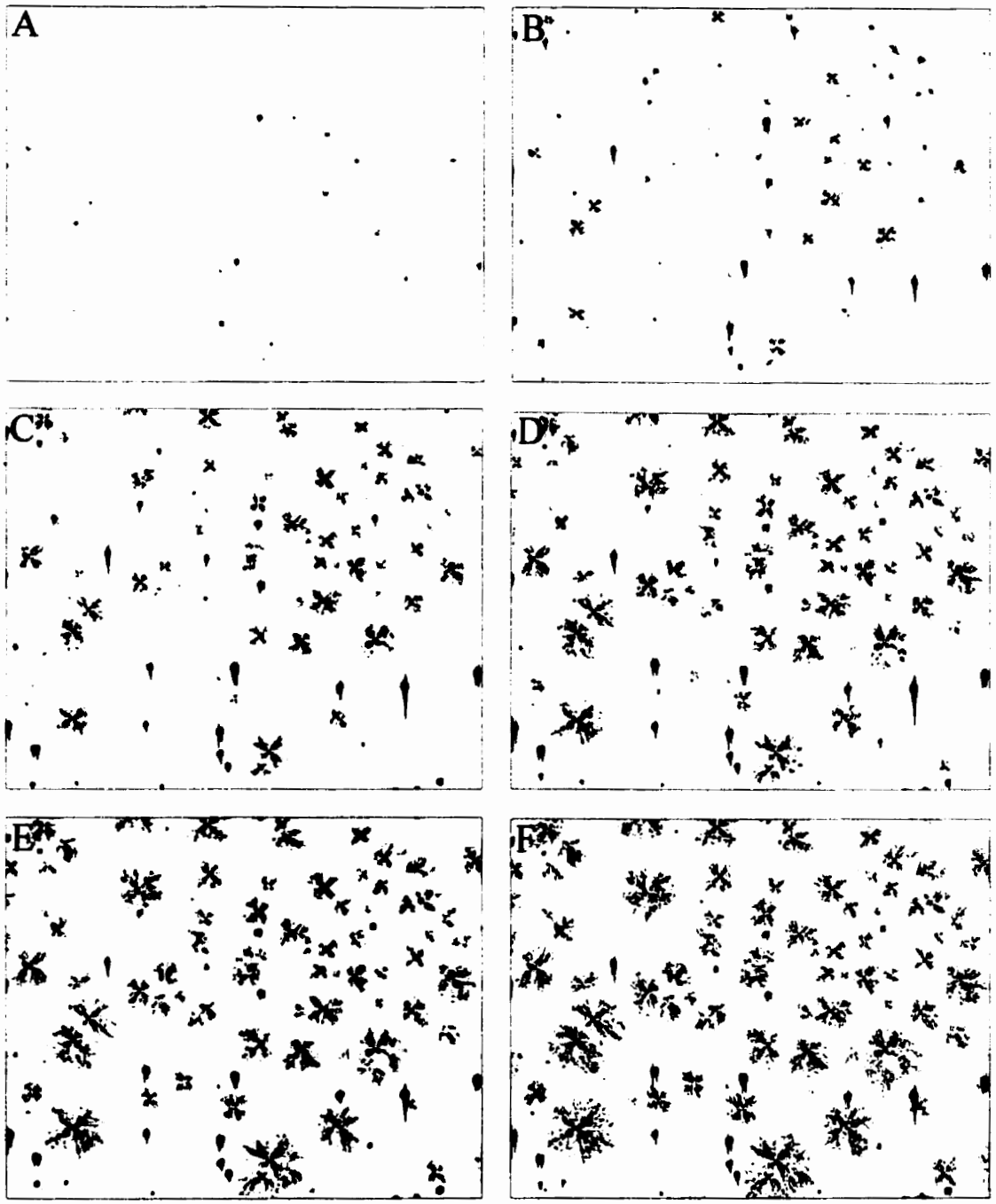

Figure 5.25: Polarised light microscope images of milkfat triacylglycerides and diacylglycerides at various times after appearance of first visible signs of crystallisation: (A) 7.5 mins, (B) 12.5 mins, (C)22.5 mins, (D)27.5 mins, and (E) 32.5 mins.

see the formation of the intermediately-sized clusters, and this process can be easily followed through figures 5.24(E) and 5.24(F), but by 5.24 (G) and 5.24(H), the field of view is sufficiently filled with "particles" that the cluster boundaries become indistinct. This is also the case in figure 5.25 – as early as 5.25(B), evidence of a cluster formation in the upper right hand corner of the image is evident, and this cluster grows through figures 5.25(C), 5.25(D), and 5.25(E). However, by 5.25(F), the cluster is no longer discernible from the rest of the network, due to the field of view being completely filled. One of the reasons the cluster boundaries are no longer visible, of course, is due to the aggregation of the clusters themselves - therefore blurring the boundaries. This type of growth/aggregation behaviour is demonstrated by all of the fats studied in this work – cocoa butter, tallow, lard, palm oil and milkfat all demonstrate these growth modes. It seems reasonable to assume that "particles" aggregate into intermediately sized clusters (whilst also growing to some optimum size) and then the intermediately sized clusters themselves aggregate into the large clusters. The aggregation processes for particles and intermediately sized clusters must be similar, given the similar manner in which they have been observed to pack, in the AFM and CSLCM images presented before. This is also true because the aggregation process continues after the clusters have been formed.

5.1.3 Structural Model of the Fat Crystal Network

The microscopic evidence presented above forms a composite picture of the structure of fat crystal networks. No one method of microscopy on its own reflects the composite picture, but by considering the various images from the different types of microscopy, one can build a structural model of fat crystal networks which is supported

by all the forms of microscopy. One of the needs in the fats and oils industry is the establishment of nomenclature that will unambiguously identify different levels of microstructure. Perhaps the best way to establish such nomenclature is to trace the development of the fat network as it forms from the melt. At the start of crystallisation, there is a process of nucleation followed by growth of these nuclei into crystallites. Molecular thermodynamics and kinetics most probably control this process. As we have seen, these crystallites associate in dense packets, several intertwined crystallites tending to form "particles" of the order of 1 μm – 8 μm. It is proposed that these "particles" be called **microstructural elements**, since they form the smallest repeating structure at a length scale visible under a light microscope. These microstructural elements then continue to grow larger through further crystallisation, but there is an aggregation process that takes place as well, leading to the formation of intermediately sized clusters, which further aggregate to form large clusters. This aggregation process is most probably controlled by mass and heat transfer limitations. The large clusters, which it is proposed be called **microstructures**, pack in an orthodox, space-filling manner to form the network, as has been shown by Heertje and co-workers. Additionally, evidence of the microstructures have been presented here, in CSLCM, AFM, and PLM images, and to a less certain extent, in SEM images. Figure 5.26 is a schematic two dimensional representation of the structural hierarchy of the microstructure of fat crystal networks. The microstructural elements, the intermediately-sized clusters and the microstructures have all been represented by circles, indicating that they are spherical. There is evidence from all of the methods of microscopy that these structures are spherical-like (which may be taken to mean stretched and distorted spheres as well). However, whether they are

smooth spheres is something that cannot be determined well, and this factor will most probably differ with the type of fat. Certainly, SEM and AFM micrographs of the microstructural elements suggest that these are not smooth spheres, and that the sphericity is not perfect. However, representing these structural entities as spheres is probably fairly representative, providing one keeps in mind that this is an imperfect approximation. The packing of the microstructural elements within the microstructures is quite disordered, as has been seen in the images presented before. However, it is important to recall that at length scales ranging from the diameter of the microstructural elements to the diameter of the microstructures, these structures appear to be statistically self-similar – i.e. the structure within this range of length scales, at different magnifications, appear to be similar. This of course is most strikingly obvious in the atomic force micrographs presented. Therefore, in an idealised attempt to demonstrate this self-similarity, figure 5.26 shows that the packing of the microstructural elements within clusters are similar to the packing of the clusters themselves into the microstructures. In order to easily achieve this effect, the microstructural elements and the clusters are arranged in an ordered manner, but in reality, these arrangements are quite disordered, as is evidenced by the microscopy images shown before. The fact that there appears to be statistical self-similarity in the length ranges between the size of the microstructural elements and the microstructures is not surprising, since the method of growth/aggregation between these two length ranges is limited by the same physical constraints. This is supported by the kinetic picture of the growth of the network offered by figures 5.24 and 5.25.

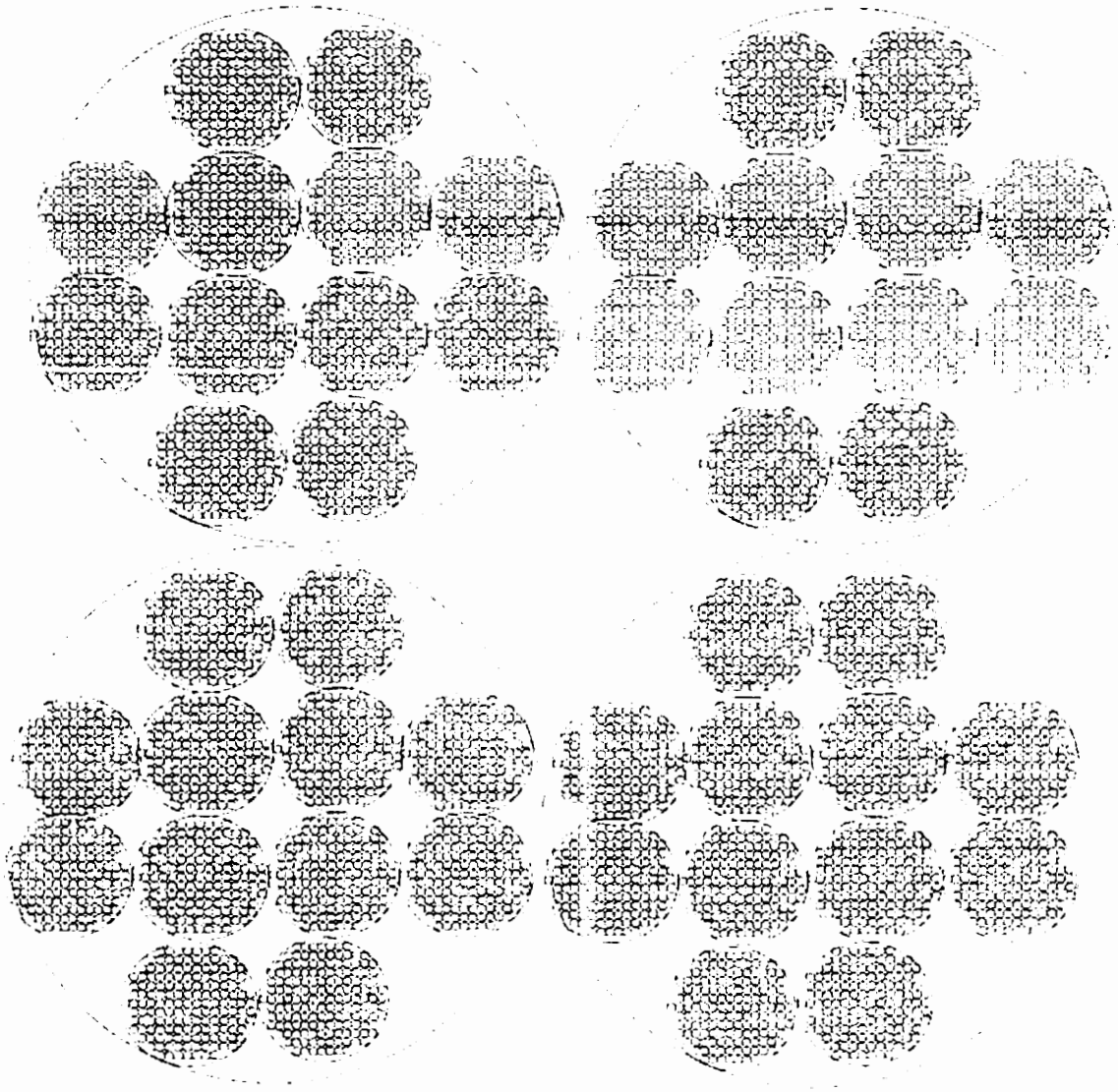

Figure 5.26: Idealised 2-dimensional schematic representation of the self-similar structural hierarchy of the microstructure of fat crystal networks.

5.2 Fractality

Now that the structural organisation of the microstructural level of a typical fat crystal network has been established, the next logical step is an attempt to quantify this level of structure. Apart from monitoring microstructural element size, cluster size, and microstructure size (not an easy task, because of the nature of the methods of microscopy), it seems important as well to ask the question: what is the spatial arrangement of the mass of the network at the microstructural level? Certainly, the size of the various hierarchical levels of structure will determine the way in which forces holding the network together will be affected, but equally as certain, the spatial arrangement of the various levels of structural entities will also affect the forces that hold the network together. Of course, additional factors such as the nature of the crystalline material (polymorphism) and the nature of the constituent molecules themselves are also important factors, but from a microstructural perspective, the parameters that can be determined are concerned with the size, shape, and spatial arrangement of the structural entities. Certainly, the density of this level of structure will yield some information about the spatial arrangement of the mass of the network, but does not give information about the actual packing – i.e. it is a rather macroscopic measurement, which does not yield structural information about the actual order of packing of the structural units of interest. Due to the extremely disordered nature of the packing of levels of structure below the size of the microstructures, it is difficult to assign lattice parameters to the positioning of the microstructural elements. Fractal analysis has in the past been used to characterise the spatial arrangement of such disordered structures that demonstrate self-similarity at different length scales. Additionally, based on the calculation of a fractal dimension from

rheological measurements on fats which were fitted to a fractal model developed for colloidal gels (Chapter 2), it seems fitting that one tries to apply fractal principles to the study of the microstructural level of structure in fats. Certainly, the self-similarity of the structure suggested by the AFM, CSLCM, SEM, and PLM images of the network encourages this endeavour. The issue then is to find a method of calculating fractal dimensions of images from one or more of the types of microscopy presented before. The challenge here is that each of the methods of microscopy that have been presented above demonstrate inherent artefacts, and none of them presents an unbiased, complete view of the network. What seems plausible is that the structure is self-similar at length ranges bounded by the size of the microstructural elements and the size of the microstructures.

5.2.1 Traditional Methods of Fractal Dimension Determination

To aid the reader unfamiliar with the topic, a brief description of the methods typically used to calculate fractal dimensions in the natural sciences is presented. This is not intended as an exhaustive review: for complete reviews, the work of Falconer (1990), Crownover (1995), and Mandelbrot (1982) are highly recommended. Additionally, a very concise historical description of the many types of different fractal dimensions that have been defined, and their uses, is given in an eloquent publication by H. E. Stanley (Stanley, 1984).

There are several different concepts of the fractal dimension of a geometrical configuration. The most widespread method of calculating fractal dimensions in the

natural sciences is the so-called box-counting dimension. Examples of other types of fractal dimension include the topological dimension and the Hausdorff dimension. It is worth mentioning here that the Hausdorf dimension was the dimension used by Mandelbrot to define a fractal in 1975, i.e. an object was defined to be fractal if it had a Hausdorf dimension strictly greater than its topological dimension – a line of reasoning that is in accordance with the brief description of fractals in Chapter 2 (if an object which is one or two dimensional is kinked and twisted sufficiently, its dimensionality is raised). The box-counting dimension is preferred for use in the natural sciences, since it is computationally easier to calculate, and is usually the same value as the more-difficult-to-compute Hausdorf dimension. This discussion is therefore limited to the calculation of box-counting fractal dimensions (variously called the Minkowski dimension, fractal dimension or similarity dimension).

Computer algorithms for the calculation of a box dimension are usually formulated by considering $N(r)$ as the least number of balls of radius r needed to cover the fractal object. Here, the fractal object is a either a mathematically generated fractal object, or the representation of a fractal object which has maintained the spatial integrity of the object. The box counting dimension, D, is then given by:

$$N(r) \approx \frac{C}{r^D} \qquad (5.1)$$

where $C > 0$. Taking logarithms on both sides of this equation yields:

$$\log N(r) \approx \log C - D \log r \qquad (5.2),$$

since $\log r \to -\infty$ as $r \to 0_+$, D satisfies:

$$D = -\lim_{r \to 0} \frac{\log N(r)}{\log r} \qquad (5.3).$$

The box dimension of the fractal object in question is therefore defined by Eqn. (5.2), with the condition that the limit expressed by Eqn. (5.3) exists. As have been mentioned before, various methods of calculating the box dimension exists, and for instance five of these are described succinctly by Falconer (1990).

In one method, square boxes are substituted for round balls in the actual computer algorithms used to calculate the box dimension. The value of $N(r)$ is taken as the least number of square boxes of side r needed to cover the fractal object. Then, values of $N(r)$ for several different values of r are recorded. A graph of $\log N(r)$ vs. $\log(r)$ then yields $-D$ as its slope, from Eqn. (5.2). It must be remembered that the values of $N(r)$ calculated are necessarily approximations, and therefore many values of r and corresponding values of $N(r)$ are usually used in this method. In the case of a planar fractal, one counts the number of squares, in the case of the fractal being a segment of a line, line intervals instead of squares are used, and in the case of the fractal object being a subset of three-dimensional space, the squares are replaced by contant-height volumes with a square base. In each of the cases, r corresponds to the side of the square, the line interval, or the side of the square base of the volume. For an exact object such as a Koch snowflake, shown in Figure 5.27, the method described above is well suited. This method, like all of the existing fractal methods, requires that the spatial integrity of the object be maintained in the image that is being analysed. Herein lies the problem with

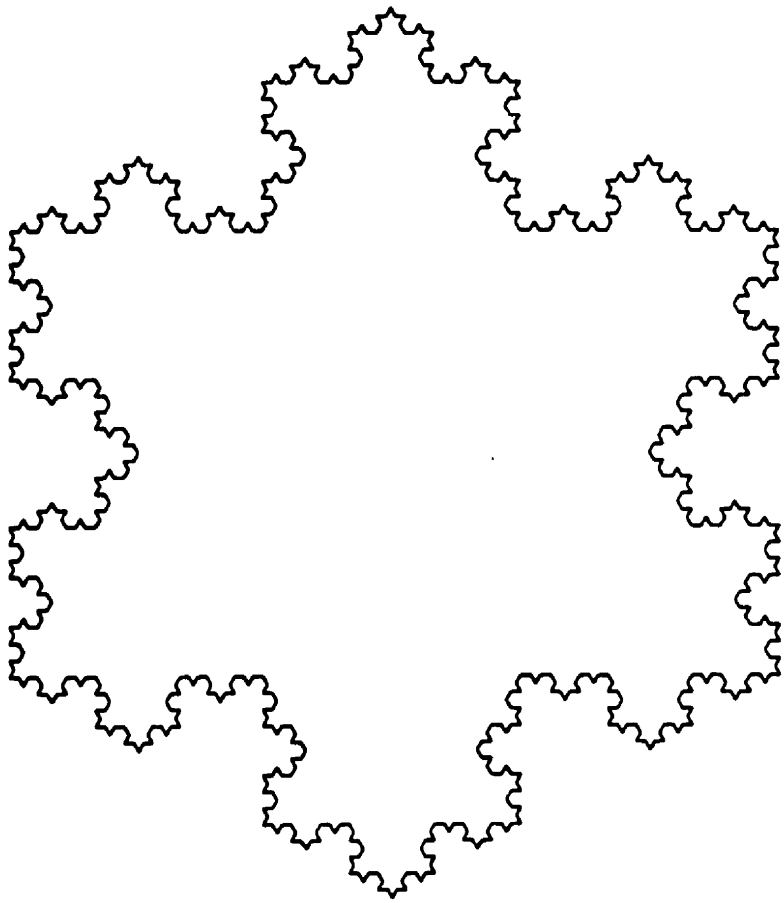

Figure 5.27: The Koch snowflake (a mathematical fractal made by Helge von Koch in 1904)

applying any of the existing traditional methods to calculate the fractal dimension of fat crystal networks at the microstructural level.

5.2.2 Particle Counting Method

None of the methods of microscopy that have been discussed so far provides images which would be necessary for any of the traditional methods of calculating fractal dimension to be useful. The SEM images are very unreliable – the samples are frozen, and additionally they only provide images of the surface of the samples. The AFM images as well only provide information on the surface of the sample, and additionally, do not provide definition of the boundaries of the microstructural elements well enough. The CLSM images are two-dimensional slices of the network – it is conceivable that if a series of slices is imaged, then the three-dimensional network can be reconstructed, and this would provide a spatially correct representation of the image. However, with this method, there are uncertainties with the behaviour of the dye, and from the tendrils that were demonstrated in the images shown from CLSM, it seems unlikely that the spatial integrity of the structure would be preserved. The PLM images with the broken networks of course are not useful, since the network is already broken. This leaves us with the *in-situ* PLM images, which bear additional scrutiny.

A thin sample of the fat network crystallised on the microscope slide provides an imperfect representation of the microstructural elements present in the entire three-dimensional sample, as has been discussed above. Those elements in the focal plane of the microscope appear sharp, larger, and well defined, whilst those in the depth of the

sample appear diffuse and smaller. Therefore, such an image is essentially representing all of the microstructural elements in the sample (excepting those in direct geometrical shadow, assumed negligible) projected unto the 2 dimensional focal plane of the microscope. Certainly, the exact spatial integrity of the image is not preserved, and therefore none of the traditional methods for the calculation of fractal dimensions are suitable for analysing this type of image.

If however, the images from the *in-situ* PLM method are rendered black and white by a thresholding method, one can ensure that each of the microstructural elements present in the original greyscale image are represented in the thresholded image. In this process, one may have to let those microstructural elements in focus appear larger, whilst those out of focus may only be represented by small points of white. However, *each* of the microstructural elements can be made to be represented in a thresholded image by a white spot. A grayscale image essentially is composed of 255 levels of grey – a thresholding process assigns a threshold grey level, so that any pixels which have a grey value above the threshold value is assigned the colour black, and any image below the threshold values is assigned the colour white. Figure 5.28 (A) shows a schematic of microstructural elements in a thin sample of fat, projected onto the focal plane of the microscope, and figure 5.28 (B) shows a schematic of this image thresholded to represent all of the microstructural elements within the sample.

How can the actual numbers of microstructural elements present aid in the calculation of the fractal dimension of the structure? The thresholded images are not

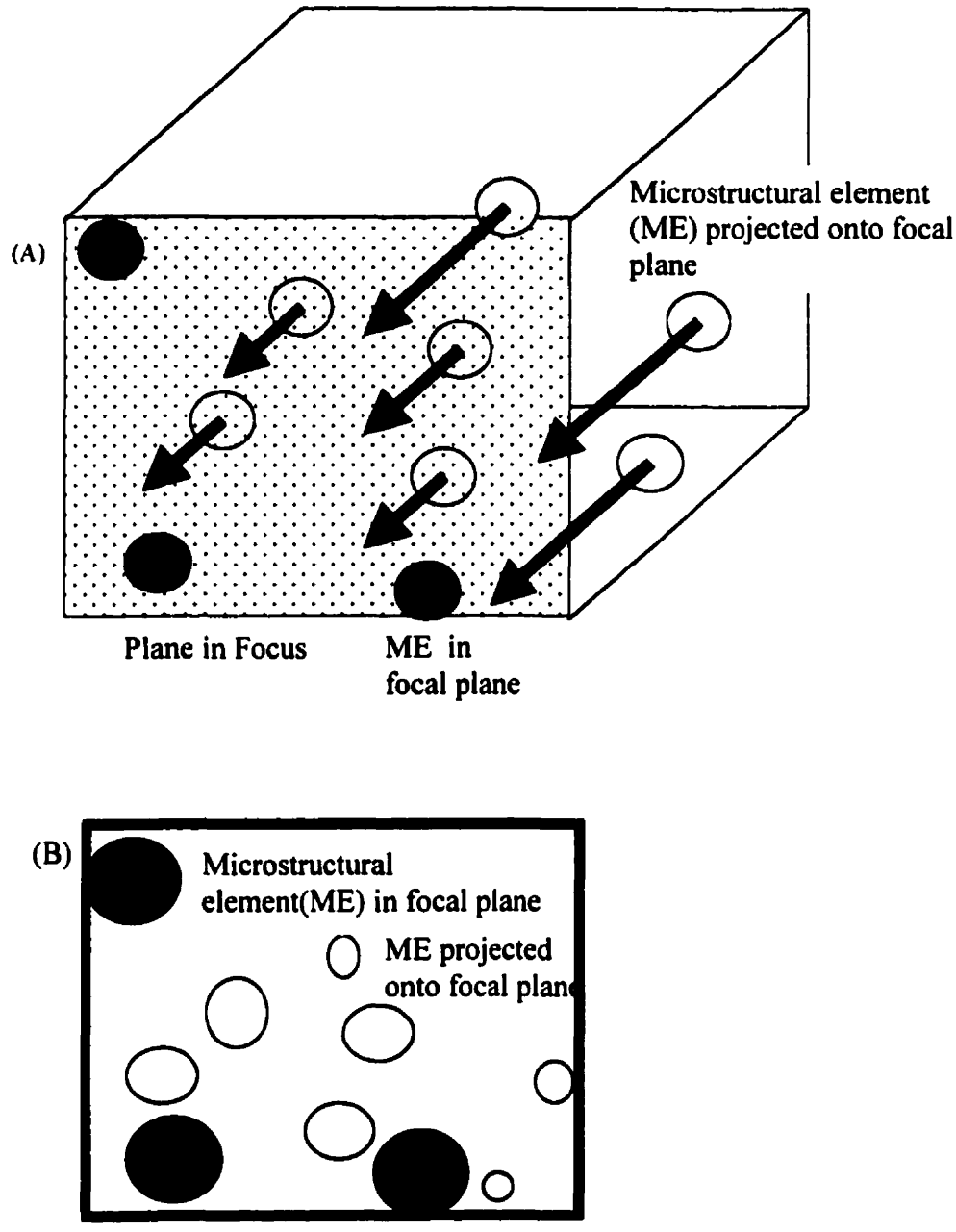

Figure 5.28: (A) Schematic of microstructural elements in a thin sample of fat, as seen under a polarised light microscope. (B) Example of how an image taken of the situation in (A) would appear when thresholded.

suitable to be analyzed by the traditional methods of fractal dimension determination. The reason is because these images are subsets of 2-dimensional space, but are representing a subset of a 3-dimensional network. Furthermore, because of the need to utilise thresholding methods to ensure the representation of all the microstructural elements within the 2-dimensional image, the sizes of the microstructural elements already in focus are increased, whilst those out of focus appears smaller than the magnification warranted. Therefore, the size of the individual microstructural elements are not representative of the size of the fractal, at whatever magnification the picture was taken. If we assume that the constituent particles (microstructural elements) of a particular fat network are of the same average diameter (not a bad assumption, from examining the microscopy images presented before), then for calculation of the mass fractal dimension, it is sufficient to just count the particles, regardless if some appeared larger when the image is thresholded. The number of particles present in a three-dimensional portion of the sample is counted by first representing all of the particles present in that portion of the sample in the plane of the image. Of course, those particles that did not appear in the picture due to geometrical shadowing are not counted, but the number of these can be rendered negligible by making the thickness of the sample very small. Use can then be made of Eqn. (2.3) in Chapter 2. This equation stems from one of the principal characteristics of a particle-aggregation fractal system, where the fractal dimension D relates the number of particles N_p to the linear size of the fractal R and the linear size of one particle (microstructural element) σ:

$$N \sim \left(\frac{R}{\sigma}\right)^{D}, \text{N>>1} \qquad (5.4)$$

Here, the fractal object is a mass fractal (a microstructure), and σ refers to the radius of the particles constituting the fractal (microstructural elements), whilst R corresponds to the radius of the entire fractal object. One can approximate R to be the length of a side of the square base of a constant-height volume that covers the fractal object if the fractal is in a d = 3 system, the length of an area for a d = 2 system and length of a line for a d = 1 system. Assuming a statistically constant particle size, or in our case, a statistically constant microstructural element size:

$$N \propto R^D \qquad (5.5)$$

Taking logarithms:

$$\log_{10} N(R) = \log_{10} c + D \log_{10} R \qquad (5.6),$$

where c is a constant, N(R) is the number of particles in the fractal of length R, and R is the length of the line segment, length of a side of an area, or length of the square base of a constant-height volume which envelopes the fractal. The lower limit of this relationship then becomes the size of one microstructural element, i.e. R = a, N(R) = 1 is the lower limit. Therefore, proceeding in like manner to the traditional form of box-counting, N(R) for various values of R >> a is counted, and $\log_{10}$(N(R)) plotted vs. $\log_{10}$(R), the resulting slope of the line being equal to D. D therefore represents the fractal dimension of the packing of the microstructural elements within a microstructure of the fat crystal network.

5.2.3 Experimental

The images of the *in-situ* fat systems captured under the PLM (Figures 5.17 to 5.20) were scanned into a Pentium 200 MHz IBM-compatible computer using a Hewlett

Packard 6100C scanner. In order to analyse the photographs of the polarised micrographs taken of the fat systems, the images were thresholded. In order to do this, a particular threshold value has to be utilised, which allows all of the microstructural elements to be seen as white, and all of the background to be reduced to black. This is an especially difficult and crucial task, since one has to take care to ensure that all of the solid particles are represented in the resulting thresholded image. Algorithms exist to calculate threshold values; one such method that was used in this study is the statistical correlation method (Parker, 1994).

The statistical correlation method was used to calculate threshold values for some of the images scanned into the computer, but since each time it was possible to better judge the threshold value visually, human judgement of the threshold value was used in all of the analysis. In some cases, this involved causing microstructural elements in focus to appear slightly larger than they were under the magnification used, in order to ensure that the microstructural elements out of focus were counted as particles. It was important to ensure that all the microstructural elements were represented, for once again, it is necessary to project all of the microstructural elements onto the plane of focus of the image, so that the resulting fractal dimension calculated would have been in a system with a Euclidean dimension of three.

In order to calculate the value of D (with Euclidean dimension, d = 3), the number of microstructural elements N(R) projected onto a square area of side of length R, drawn in the focal plane of the image, was counted. This count represents the number of

particles present in a volume of constant depth and of width R through the fractal. Values of $\log_{10}(N(R))$ were plotted against $\log_{10}(R)$ for varying values of R. The resulting slope of the line was taken as being equal to D. Figures 5.29 shows the greyscale and thresholded images of milkfat (A and B), tallow (C and D), palm oil (E and F) and lard (G and H). Figure 5.30 shows the plots of $\log_{10}(N(R))$ vs. $\log_{10}(R)$ for these fats (milkfat (A), tallow(B), palm oil (C), and lard (D)).

The images scanned into the computer were first opened with Corel PHOTO-PAINT-6, and the images inverted (black pixels made white and white pixels made black) – this was because the program used to do the actual particle-counting counts "black" particles . The image was then saved and two copies opened in SCION IMAGE Release Beta 3b (© 1998, Scion Corporation). One of the images was then thresholded, using the other image as a greyscale reference, to ensure that all of the microstructural elements in the image were being represented by a black dot. Much effort is taken with ensuring that all microstructural elements are represented – this is often an impossible task with the entire image, especially if the image represents a non-constant depth of sample. It is of maximum importance to ensure that the depth/thickness of the samples is kept constant. In such cases, sometimes the entire image must be discarded and new samples prepared, or sometimes it is obvious that only part of the image is at a constant depth – then the analysis is confined to that part of the image only. Additionally, the microstructural elements in some fats are just too densely packed to allow proper thresholding to represent individual microstructural elements with any degree of accuracy – in such cases, the fat cannot be analysed by this method. The important aspect of this analysis to bear in mind is that the person taking the image must be aware of what the

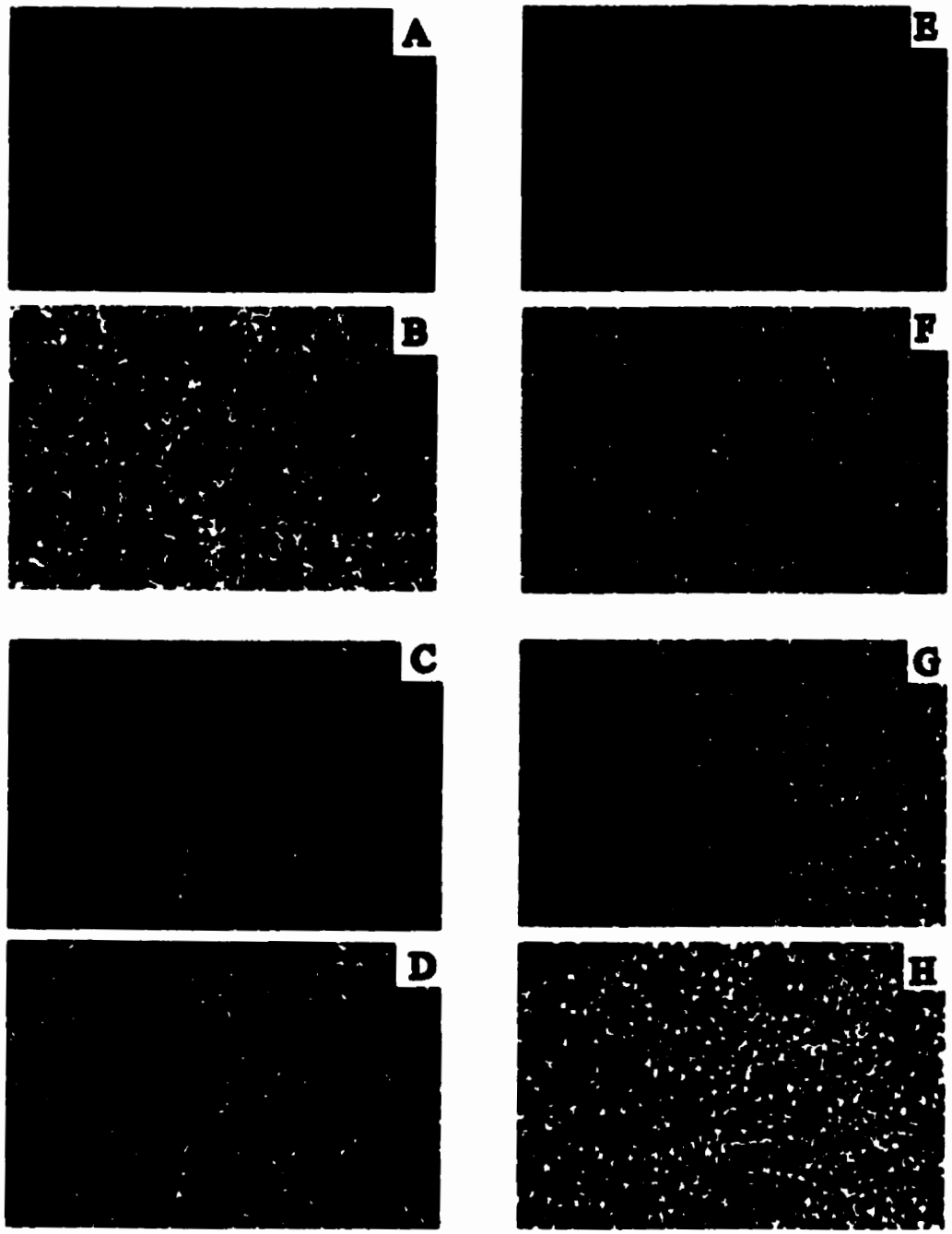

Figure 5.29: Greyscale *in situ* polarised light microscope images and corresponding thresholded images of milkfat (A and B), tallow (C and D), palm oil (E and F), and lard (G an H).

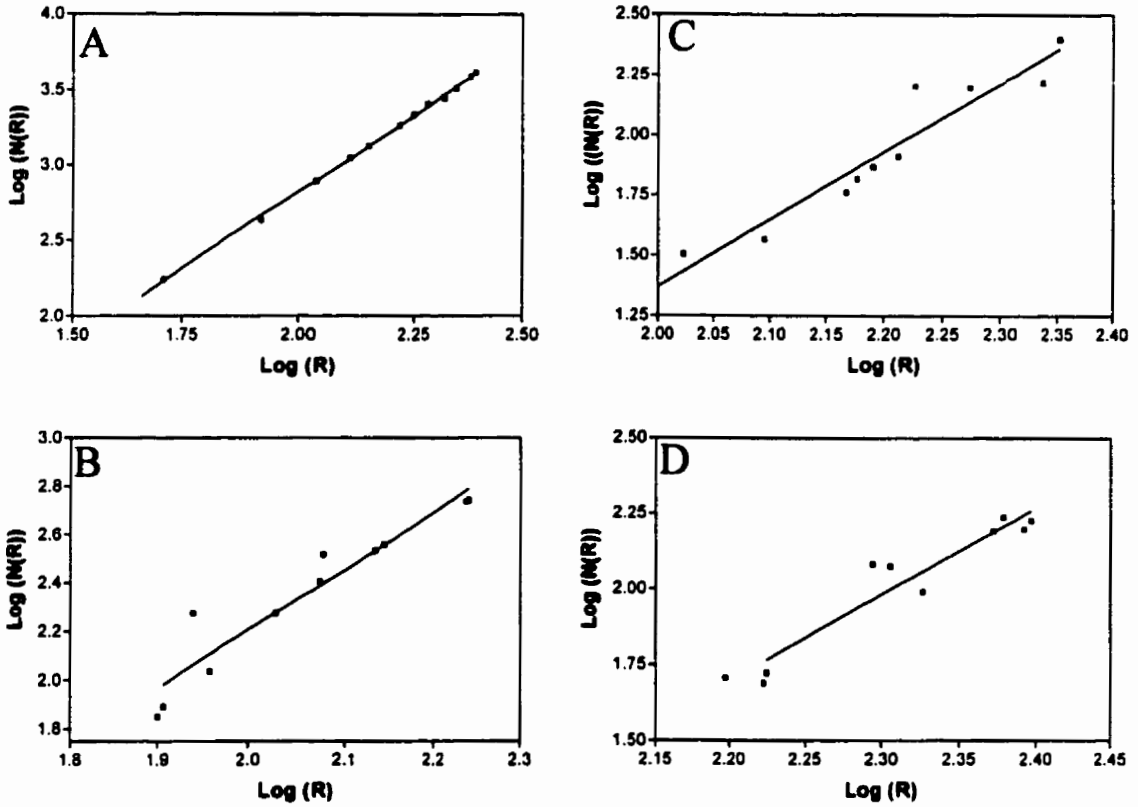

Figure 5.30: Plots of $\log_{10}(N(R))$ vs. $\text{Log}_{10}(R)$ for: (A) milkfat, (B) tallow, (C)palm oil, and (D) lard.

image represents – only someone that has taken the picture can be relied upon to decide at the thresholding stage which entities are microstructural elements. When the correct threshold has been achieved, SCION IMAGE allows one to select "boxes" of various sizes, drawn over the thresholded image, and to compute the area in pixels of each box, as well as the number of "particles" or thresholded microstructural elements, within each box. This facilitates the accumulation of values of N(R) and R.

To investigate the effect of changing threshold value on the fractal dimension calculated, two fats – tallow (crystallised at 5°C for 24h) and milkfat (crystallised at 20°C for 48h) were analysed. The "correct" threshold value was chosen visually, and the fractal dimension calculated. Then, threshold values greater and less than the "correct" value was chosen and the fractal dimension calculated. Values of fractal dimension were then plotted against values of threshold. Figure 5.31 shows these plots for the two fats – tallow (A) and milkfat (B).

5.2.4 The Fractal Nature of Fat Crystal networks

As is evidenced by figure 5.30, all of the fats analyzed (cocoa butter and milkfat at 20°C were also analyzed, but these plots are not shown) produced straight-line plots of $\log_{10}(N(R))$ vs. $\log_{10}(R)$. Additionally, all of the fractal dimensions calculated are between 2 and 3, as would be expected for fractal samples whose Euclidean dimension, d, is 3. Therefore, the level of structure bounded by the size of the microstructural elements and the size of the microstructures is fractal in nature. Furthermore, one can analyze PLM micrographs of this level of structure using the particle counting method, to yield a fractal dimension. This is not surprising, since the apparent self-similarity of this

level of structure hinted at this level of structure adhering to a fractal packing geometry. Now, it must also be pointed out here that the phrase fractal geometry as applied to natural objects has met with a lot of controversy. Over the past decades, the idea that fractal geometry is an appropriate geometry to describe nature has been proposed by many researchers. To a mathematician, for an object to be characterized as being fractal, it must demonstrate a quantitative power-law scaling of the parameters of the system at infinitely many orders of magnitude. Physicists and other scientists, however, have maintained that an object which demonstrate a power-law scaling of parameters between limited length ranges is no less a fractal. For example, the scaling of the number of microstructural elements as a power law function of the characteristic length of the system only spans a length scale between 1 – 8 μm and at most 100 – 120 μm. At any rate, the fractal-like scaling of natural objects, even within such narrow length ranges, can impart important scaling behavior to physical parameters of the system dependent upon structure. Indeed, because of this, whether the word "fractal" is justifiably used or not becomes dependent on ones definition of the word – whether as a mathematician or as a physicist. Whatever camp one belongs to, there is some amount of heuristic value in calling such natural objects fractal. In this thesis, it will be taken as understood that when the word fractal is used, it is used to describe the power-law scaling of the number of microstructural elements with length over a well-defined limited length scale: the length of the microstructural elements at the lower limit, and the length of the microstructures at the upper limit. Perhaps use of the phrase "spatial distribution of mass" is better suited than "fractal dimension," but realistically, when one calculates the fractal dimension as explained above, one is calculating a dimensionality of packing of the microstructural

elements within the microstructures. This dimensionality is indicative of the spatial distribution of mass, of course, but the debate then becomes one on semantics. As long as the parameters that we refer to are properly defined, it is my opinion that one can continue to refer to the dimension calculated as the fractal dimension.

The issue of thresholding is a contentious one with this analysis. As is evident from figure 5.29, however, the thresholded images hold true to the task of representing *all* of the microstructural elements within the image as white dots (obviously, these images do not show the inverted greyscale and thresholded images, but represents the greyscale images as they appear under the microscope, with the thresholded images making microstructural elements appear as white). In some of the images, for instance the milkfat image shown in figure 5.29 (A) and 5.29 (B), the upper right hand side of the image is obviously not at the same depth as the rest of the image (i.e. the sample was thicker at this end of the image) – in this image, only the left half of the image was used for the analysis. In some images, where the packing of the microstructural elements are very dense, it will be impossible to threshold the image to represent the individual microstructural images in the sample – such samples cannot be analysed using this method. Ultimately, the method is a subjective method – it depends on the ability of the person doing the analysis to recognise which entities are microstructural elements, and to threshold the image to represent those microstructural elements in the thresholded image so they can be counted. As mentioned before, it is helpful for the person analysing the images to also be the person who took the picture in the first instance. Additionally, details must be paid to such important things as making sure the sample is of uniform thickness, and that the image acquired is of the highest quality. However, even if the

threshold value is not the "correct" value – i.e. if the threshold value for a particular image was off by one or two threshold values (from 0 – 255), therefore leading to some microstructural elements being missed, or some being counted as more than one, the fact remains that this method has shown that the fat networks at this level is fractal in nature – i.e. even with a small amount of error, there is a scaling relationship between the number of microstructural elements and the length of the sample, bounded by the length of one microstructural element and the length of one microstructure. In fact, if the plots in figure 5.30 are examined, it will be seen that there is some amount of scatter in the points, which is probably indicative of an imperfect thresholding method. In fact using this method of microscopy, it is virtually impossible to have the "correct" thresholding value – there will always be an element of error, due to the nature of the microscopy itself.

Figure 5.31 is interesting in that it suggests some amount of objectivity to the thresholding method for a particular image; it shows plots of fractal dimension vs. threshold value for two different fat systems – tallow (A) and milkfat (B). The plots shown in figure 5.31 demonstrate a minima and a maxima at the visually "correct threshold value (these are most probably local minimas and local maximas, if one is to plot fractal dimension against the entire range of possible threshold values). Now, these figures were generated by choosing threshold values which were greater than and less than the chosen "correct" threshold value, selected visually. As is demonstrated, deviations from the "correct" threshold value lead in most cases to steep deviations from the fractal dimension at this threshold value.

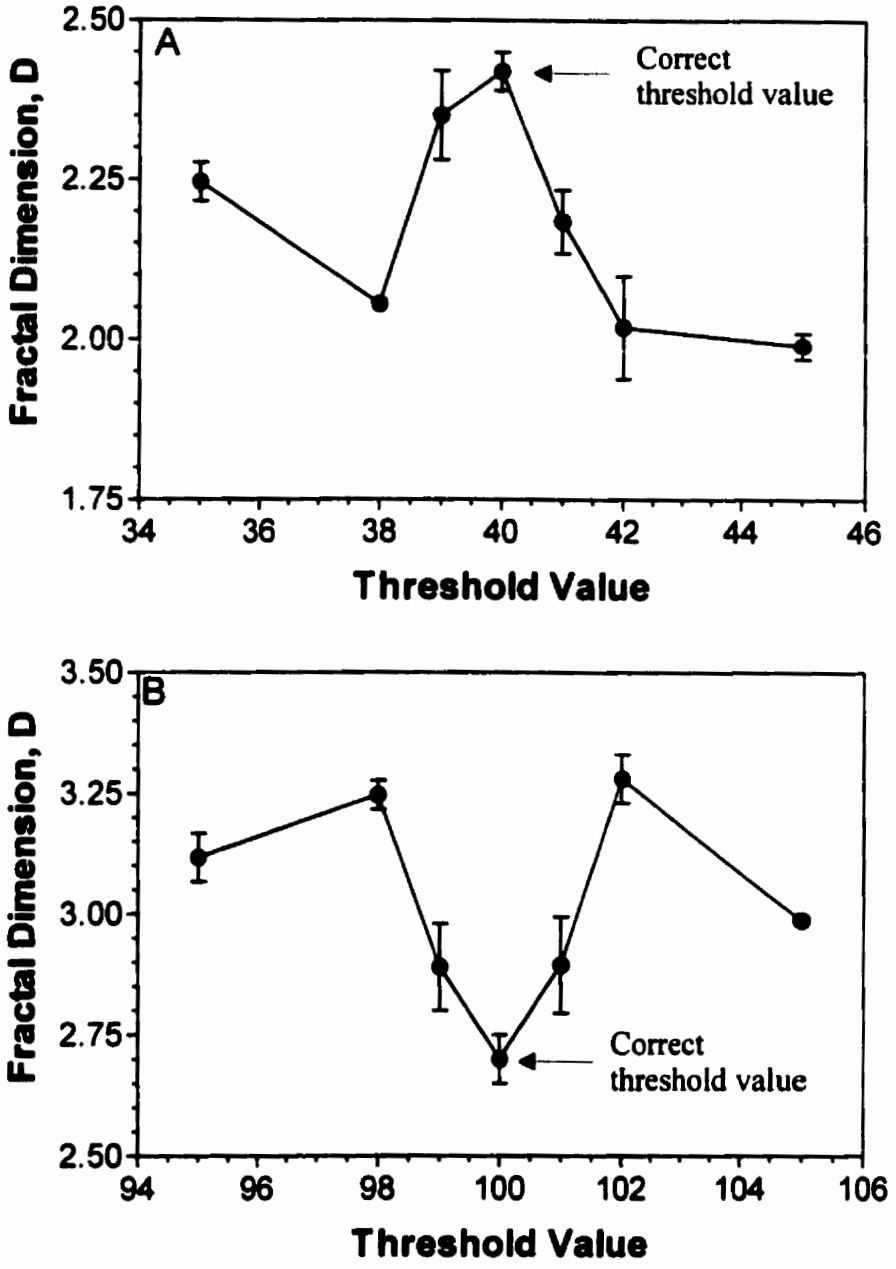

Figure 5.31: Plots of fractal dimension vs. threshold value for (A) Tallow at 5°C and (B) Milkfat at 20°C. A linear log-log plot was obtained for each data point shown. Error bars represent standard deviations from a mean fractal dimension (error in slope of log (N) vs log (R) plot).

If a threshold value is not the correct value, then the thresholded image either over-represents the number of microstructural elements present, or under-represents the number of microstructural elements present. For the purposes of this discussion, the images of the network will be regarded as having the microstructural elements represented as black objects (inverted images), so therefore on a scale of 255, 0 represents black and 255 represents white. Increasing the threshold value in such an image implies that more of the pixels in the image is being relegated to the white background, and decreasing the threshold value means that more of the pixels in the image are being made black. There are two reasons that can cause the number of microstructural elements in the image to be over-represented:

a) A threshold lower than the correct value may cause additional black spots that are not actual microstructural elements, but are background represented by a greyscale value, which because of the low threshold is rendered into a black object.

b) A threshold higher than the correct value may cause black spots originally representing individual microstructural elements to be represented by more than one black spots in the thresholded image. This of course happens when the threshold is made so high that a microstructural element represented by uneven levels of greyscale values can be split into two or more black spots in the thresholded image.

There are also two reasons that may cause the number of microstructural elements in the image to be under-represented.

c) A threshold lower than the correct value may cause two or more neighbouring microstructural elements to be represented as one black particle in the

thresholded image. This occurs of course because the threshold is low enough to cause the greyscale value of the background separating the microstructural elements to be rendered black in the thresholded image.

d) A threshold higher than the correct value may result in many of the microstructural elements not being represented in the thresholded image, since their greyscale values would be such that they are rendered as white in the thresholded image.

Equation 5.5 states that the number of microstructural elements are proportional to the characteristic length of the system raised to a power equal to the fractal dimension. An over-representation of the number of microstructural elements therefore, results in an over-representation of the fractal dimension value. Similarly, an under-representation of the number of microstructural elements in the sample results in an under-representation of the fractal dimension value. In other words, over-representation results in too-high values of D, and under-representation results in too-low values of D.

Now, suppose an image of a fat is thresholded to a value which is visually judged to be in the vicinity of the "correct" threshold value. Let us assume for the moment that this value is actually lower than the theoretical "correct" value. Now, this means that the number of microstructural elements will either be over-represented or under-represented. If the number of microstructural elements are over-represented (due to reason (a), from the foregoing discussion), then as one increases the threshold value, the number of microstructural elements will become less over-represented until one increases the threshold value to the correct value. Therefore, from the initial threshold value chosen,

the fractal dimension will decrease to the correct value. Increasing the threshold value beyond the correct value will result in either an over- or under-representation of the number of microstructural elements. If there is an over-representation (which would be due to reason (b) from the foregoing discussion), then the correct value will lie at a minima of the fractal dimension vs. threshold value plot. If there is an under-representation (which would be due to reason (d) from the foregoing discussion), then the correct threshold value would be at a point of inflexion in the plot of fractal dimension vs. threshold value. Similar arguments as above, starting with a threshold value which is lower than the correct value and which causes an under-representation makes it obvious that the correct value would lie either at a maxima or at a point of inflexion. Therefore, the correct threshold value should always correspond to a local minima, maxima, or point of inflexion in the fractal dimension vs. threshold value plot.

Therefore, the results shown in figure 5.31 are explained theoretically. What is surprising, however, is the fact that the "correct" value is only one value – one would expect there to be at least a few "correct" threshold values. However, this is a function of the images – images with microstructural elements packed in a low density conformation may have a few "correct" threshold values in a cluster, but those images which have been used in this thesis are quite dense, thereby perhaps explaining the steepness of the D vs. threshold value curves. With the dense images, it becomes obvious from examining the images that changing the threshold value by even one point may lead to the appearance/disappearance/merging of microstructural elements. The fact that the correct value of the threshold will lie in a local minimum or maximum point or point of inflexion

in the plot of D vs. threshold value, however, helps to make the thresholding process more objective – now, one can choose a reasonable threshold value (one which seems to be causing the representation of *all* the microstructural elements), and then do a series of analyses for fractal dimension with this threshold value and threshold values above and below this value. The resulting plot will yield either a local minima, local maxima or inflexion point and any of these should correspond to the correct threshold value. It must be expected, although it has not been my experience, that one may encounter images where the local minima, maxima, or inflexion point is actually due to two or three adjacent threshold values. This said, it is quite possible that a plot of fractal dimension vs. threshold value will continually yield local minima and maxima throughout the range of threshold values possible (0 – 255). One still would have to visually examine the image to ensure that the local minima, maxima or inflexion point chosen to be the correct value of the threshold was indeed adhering to the principles of the particle-counting method, and a valid representation of the greyscale image. In fact, because of this reason, thresholding still does remain a very subjective process. Therefore, whilst the foregoing discussion on threshold values is useful in explaining the results demonstrated in figure 5.31, it must not be misconstrued that this discussion somehow absolves the process of its subjective nature. It is quite possible to have two or more local turning points quite close to each other in a plot of fractal dimension vs. threshold value (as is demonstrated by figure 5.31). In these cases, it is absolutely essential for the operator to be able to discern the "correct" threshold. Additionally, it is of course required that a good first "guess" be made of the threshold, before even attempting the laborious analysis that is required to

produce a plot of fractal dimension vs. threshold value, which as discussed, is not entirely reliable unless one can visually verify the legitimacy of the "correct" threshold value.

It is important to mention that fractal dimensions calculated on samples of a particular fat diluted with varying amounts of canola oil (up to and including 80% w/w) were statistically the same. This seems to suggest that the fractal dimension of the network as a measure of the packing, is a fundamental physical constant, influenced by the nature of the forces involved at the microstructural level. The canola oil in each case was seen to act solely as a diluent (with cocoa butter, lard, milkfat, and tallow). The same effect was observed for palm oil diluted with soya bean oil.

Using the particle-counting method, a value for the chemical length exponent, or the tortuosity of the network may also be calculated, but since this value is not required for the application of the weak link theory, the details of this calculation are not presented here. For the interested reader, this method has been published by Narine and Marangoni (1999a).

5.3 The Weak Link Revisited

Now that the general structural arrangement of the microstructure of fat crystal networks has been established, it is relevant to examine how this structural organisation relates to the weak link theory. The model of the structure of fat crystal networks developed above identifies the microstructures as the largest structural building block of the network. It seems reasonable that any stress that is put upon the network will first be

felt by the microstructures. The question is, how do the microstructures behave under this stress? Heertje and co-workers (Heertje *et al.* 1987; Juriaanse and Heertje, 1988; Heertje, 1993) have demonstrated that the microstructures are separated when the network is stressed, whilst remaining intact (maintaining their shape and size). It therefore seems reasonable to expect that when the network is stressed, the first level of structure that is stressed are the links between microstructures. Figure 5.32 shows a theoretical schematic of the network under stress. From the discussion given in Chapter 3 on the elasticity of solids, it seems reasonable to expect that the stressing of the network within the elastic limit results in a stressing of the links between microstructures, which are a repeating, regularly packed structural unit. Referring to figure 5.32, if one were to express the force-constant of the links between microstructures as k, then the macroscopic elastic constant, K, (in 1 dimension) of the network could be written as (same as Eqn. 2.20):

$$K = \left[\frac{L}{\xi}\right]^{d-2} k \qquad (5.7)$$

where ξ is the diameter of one microstructure, L is the macroscopic size of the system, and d is the Euclidean dimension of the sample (=3). However, as have been shown above, the structure within the microstructures is fractal in nature. We can therefore relate the diameter of the microstructure (or aggregate) to the particle volume fraction of the entire network, according to the development made in Chapter 2. Therefore, using Eqn. 2.8:

$$\xi \sim (\Phi_t)^{\frac{1}{D-3}} \qquad (2.8),$$

and substituting this expression in Eqn. 5.7:

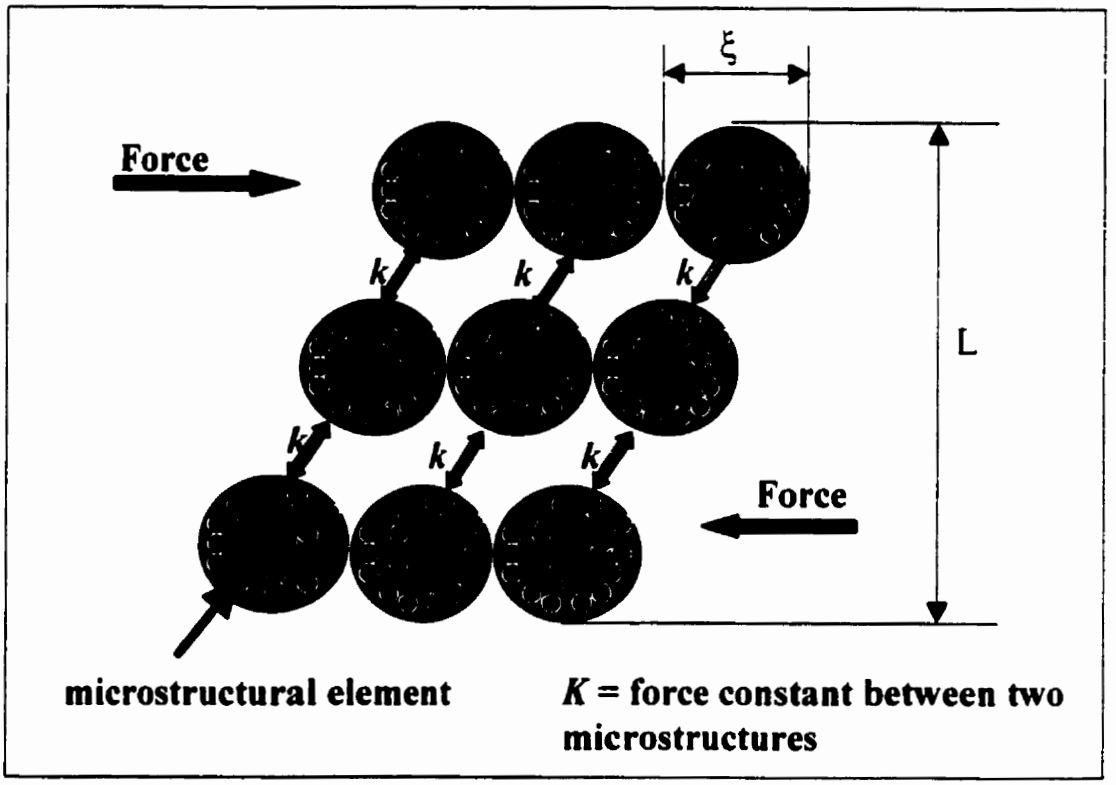

Figure 5.32: Theoretical schematic of the fat crystal network under a small stress which is insufficient to exceed the elastic limit of the network.

$$K \sim \left[\frac{L}{(\Phi)^{\frac{1}{D-3}}} \right] k \qquad (5.8).$$

Now, if the links between microstructures are constant, and the size of the system is a constant, we can write Eqn. 5.8 as:

$$K \sim (\Phi)^{\frac{1}{3-D}} \qquad (5.9).$$

Recognising that the shear elastic modulus of the network is related in a proportional manner to the tensile elastic constant (and the tensile elastic constant is proportional to the force constant of the material, according to Eqn. 3.15, Chapter 3), we can write Eqn. 5.9 as:

$$G' \sim \Phi^{\frac{1}{3-D}} \qquad (5.10).$$

The theory espoused by Eqn. 5.10 relates the shear elastic modulus to the particle volume fraction via the fractal dimension of the network. The particle volume fraction of the network is not easily measured (in fact, the author knows of no experimental method that yields this value). It must be stated clearly here that particle volume fraction is used to mean microstructural element volume fraction – it is obvious from the development above that the "particles" refers to the microstructural elements. It will be shown below that the solid fat content, Φ_{SFC}, is proportional to the particle volume fraction, Φ. Therefore, one may use Φ_{SFC} in the stead of Φ in Eqn. 5.10, bearing in mind that the nature of the proportionality constant is now changed. One can now replace the proportionality sign by the constant γ, bearing in mind that this constant would be dependent on the links between microstructures, and the relationship between ξ, Φ, and

D, as well as the nature of the proportionality between Φ_{SFC} and Φ, given the origin of the proportionality constant, as developed above:

$$G' = \gamma \Phi_{SFC}^{\frac{1}{3-D}} \quad (5.11).$$

Equation 5.11 is of course equivalent to the expression arrived at by Shih *et al.* (1990) for the weak link theory for colloidal gels. Therefore, from a structural perspective, it seems that use of this formulation for fat crystal networks is warranted. Not surprisingly, therefore, the work by Rousseau and Marangoni detailed in Chapter 2 showed that the weak link theory when applied to fats yielded plausible results. Additionally, these authors were not incorrect in assuming that the fractal dimensions that they calculated from this rheological treatment were related to the microstructure – as have been shown above, such a fractal dimension is related to the way in which the microstructural elements are distributed in the microstructures of the fat network. The obvious challenge is therefore to compare the fractal dimensions calculated by rheological methods to those calculated by image analysis methods. The most important issue here of course is the need to emulate the same processing conditions for the rheologically prepared samples and the samples prepared for microscopy on a glass slide.

5.3.1 Relating the particle volume fraction to the solid fat content

The solid fat content, Φ_{SFC}, of a fat network may be defined as:

$$\Phi_{SFC} = \frac{n_{ME} V_{ME} \rho_{ME}}{M_T} \qquad (5.12)$$

where n_{ME} is the number of microstructural elements, V_{ME} is the volume of one microstructural element, ρ_{ME} is the solids density of a microstructural element, and M_T is

the total mass of the network (solid mass + liquid mass). Equation 5.12 can be re-written as:

$$n_{ME} = \frac{\Phi_{SFC} M_T}{V_{ME} \rho_{ME}} \qquad (5.13).$$

Now, the total particle volume concentration, Φ_t of the network is given by:

$$\Phi_t = \frac{n_{ME} V_{ME}}{V_T} \qquad (5.14),$$

where V_T is the total volume of the network. Substituting for n_{ME} in Eqn. 5.13:

$$\Phi_t = \frac{\frac{\Phi_{SFC} M_T}{V_{ME} \rho_{ME}} V_{ME}}{V_T} \qquad (5.15).$$

This yields:

$$\Phi_t = \frac{\rho_t}{\rho_{ME}} \Phi_{SFC} \qquad (5.16),$$

where $\rho_t = \frac{M_T}{V_T}$, and is the density of the network itself. The solids density of the microstructural elements, ρ_{ME}, is higher than the density of the network, ρ_t, since the microstructural elements are very densely packed (recall the AFM image shown in figure 16 (A), which showed that the microstructural elements are made up of intertwined crystallites), whilst the network itself contains a lot of liquid oil and dispersed microstructural elements. However, as established by Eqn. 5.16, the particle volume fraction of the network is proportional to the solid fat content of the network. Therefore, although it is difficult to measure the particle volume fraction of the network, the solid fat content may be used in its stead, bearing in mind that these two entities are not equal, but are proportional.

5.3.2 Rheology

Samples of the fat systems studied microscopically were studied rheologically as well. Methods used to measure G' and Φ_{SFC} have been given in Chapter 3. Different solid fat contents of a particular fat was achieved by using small dilutions with canola oil – the resulting samples were then analysed for G' and Φ_{SFC} and plots made of G' vs. Φ_{SFC} (figure 5.33) and $\log_{10} G'$ vs. $\log_{10} \Phi_{SFC}$ (figure 5.34). The samples studied rheologically were tempered in an identical manner to those studied microscopically. However, it was uncertain that the temperature history of the rheologically prepared samples mirrored those of the microscopic samples, due to the large difference in thickness of these samples. Additionally, the rheological samples were tempered in plastic moulds, whilst the microscopic samples were tempered between a glass slide and a glass coverslip. In an effort to compare the structure of the microscopic and rheological samples, atomic force microscope images discussed above were taken from rheological samples and spin-coated samples (similar to samples prepared on a microscopic slide) which were tempered identically. Beyond the similarity of these images, no further proof of the equivalence of these structures are available, other than the comparison of the fractal dimension values calculated from rheological measurements, and those calculated from the particle-counting method, shown in Table 5.1.

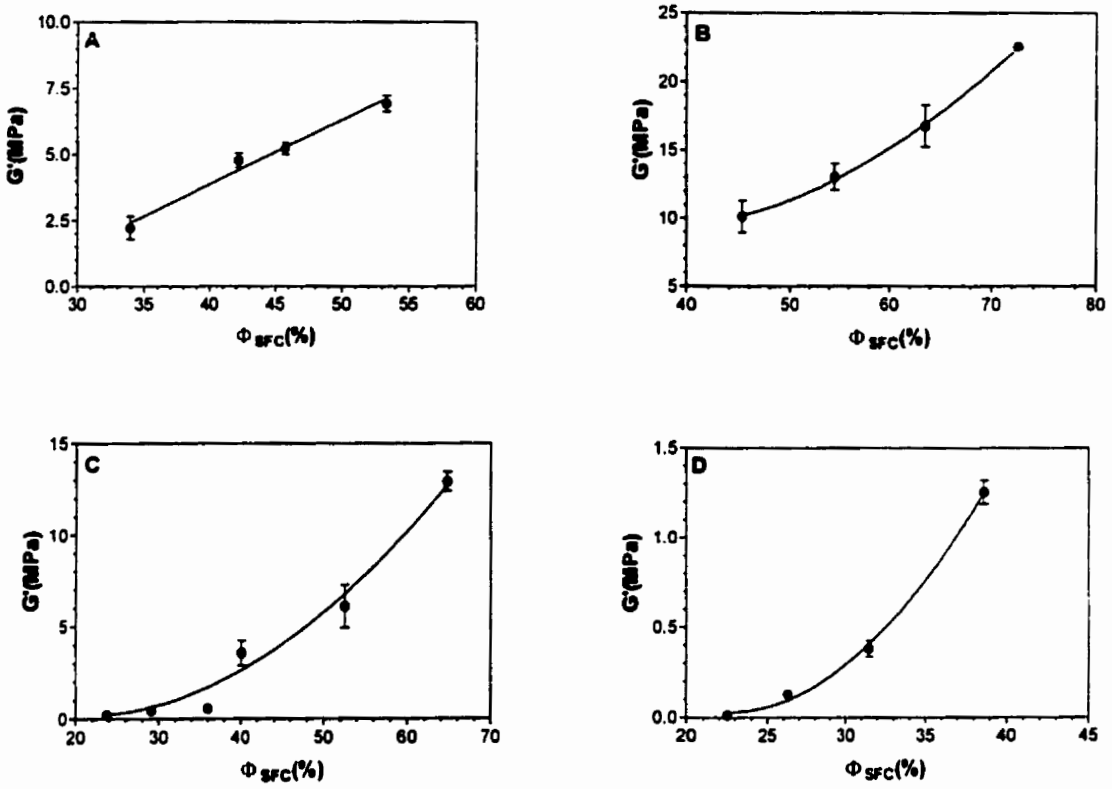

Figure 5.33: Plots of G'vs. $\Phi_{SFC}$for: (A) milkfat, (B) tallow, (C)palm oil, and (D) lard.

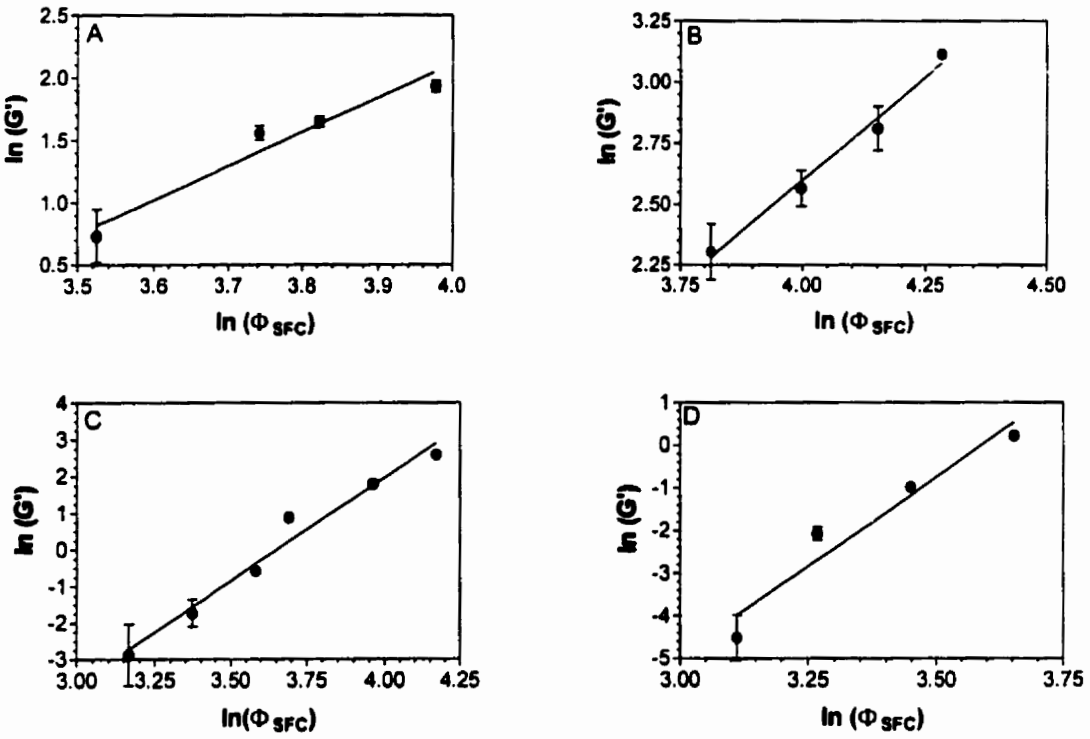

Figure 5.34: Plots of $\log_{10}G'$ vs. $\text{Log}_{10}\Phi_{SFC}$ for: (A) milkfat, (B) tallow, (C)palm oil, and (D) lard.

The plots of G' vs. Φ_{SFC} shown in figure 5.33 support the power-law dependence of G' on Φ_{SFC} suggested by Eqn. 5.10. Figure 5.33 (A) shows data for milkfat at 5°C. This is in the form of a straight line, which implies from Eqn. 5.10 that the fractal dimension must be equal to 2. The microscopically-calculated fractal dimension for milkfat at 5°C is 2.02 (as shown in figure 5.30 and table 5.1). Figure 5.33 (B) shows data for tallow at 5°C, 5.33 (C) shows data for palm oil at 5°C, and 5.33 (D) shows data for lard at 5°C. The strain levels used in the rheological analysis are 0.2%. All of figures 5.33 (B), (C), and (D) show a non-linear, power-law dependence of G' on Φ_{SFC}. As has been explained, a plot of $\log_{10} G'$ vs. $\log_{10} \Phi_{SFC}$ yields a straight line with slope equal to $1/3 - D$; such plots are shown in figure 5.34 for milkfat (A), tallow (B), palm oil (C) and lard (D). The fractal dimensions calculated in this manner are reported in Table 5.1, where they are compared to the fractal dimensions calculated microscopically for the same fats systems, crystallised in a similar fashion.

The values of fractal dimensions calculated from image analysis of polarised light microscopy images and those calculated from the rheological measurements agree very well, as is shown in table 5.1. This agreement has a few implications. Firstly, it suggests that the structure of the samples created for microscopy and those created for rheology was similar. Additionally, it suggests that the weak link approach is applicable to the study of fat crystal networks, and that fat crystal networks are indeed fractal at certain length ranges. Furthermore, it demonstrates that with careful thresholding efforts, image

Table 5.1. Fractal dimension calculated via image analysis compared to fractal dimension calculated via rheology using the weak link theory. Errors in D are standard errors of 3 replicates.

Fat System	Fractal Dimension from Image Analysis	Fractal Dimension from Rheology (weak link regime)	Percent Deviation	Fractal Backbone Dimension, x
Cocoa butter (20°C) #1	2.31 ± 1.7%	2.37 ± 4.0%	2.5	1.10
NIE milkfat #4 (5° (Analyzed using DMA)	2.02 ± 1.2%	2.01 ± 15.7%	1.5	1.00
Palm oil (5°C)	2.82 ± 0.6%	2.82 ± 0.6%	0.0	1.10
Lard (5°C)	2.86 ± 0.6%	2.88 ± 0.5%	1.0	1.15
Tallow (5°C)	2.42 ± 1.2%	2.41 ± 6.4%	0.4	1.10

analysis can provide very accurate numbers for the fractal dimension of the network.

5.4 Physical Significance of Fractal Dimension

The above discussion of experimental data shows that fat crystal networks are fractal within certain length ranges, and that the structural arrangement of the microstructure of fat crystal networks makes it possible to apply the weak link theory to analyse the mechanical properties of the networks. Central to this finding is the calculation of a fractal dimension. It is therefore relevant that we attach some physical significance to this quantity, if it is to be a useful parameter.

5.4.1 Elastic Constant and Fractal Dimension

Now that the weak link has been shown to be applicable to fat crystal networks, we can use Eqn. 5.11 to predict the effect changes in fractal dimension will have on the shear elastic modulus of the network. Now, the quantitative origins of the constant γ have not yet been addressed, and therefore any investigation of the effect of fractal dimension on the elastic modulus must be made with the effects of γ removed. Therefore, if the elastic moduli of a series of fat systems are normalised with respect to the constant γ, one would have a situation described by:

$$(G^{'} / \gamma) = \Phi_{SFC}^{\frac{1}{3-D}} \qquad (5.17).$$

Table 5.2 shows the values of fractal dimension and γ for some 14 different fat systems, from rheological analysis. Using Eqn. 5.17, a theoretical curve for $G^{'} / \gamma$ vs. D was created, for a constant Φ_{SFC} of 0.7; the solid line in Figure 5.35 represents this theoretical

Table 5.2. Summary of fat networks studied rheologically with corresponding fractal dimensions and values of γ.

FAT SYSTEM	FRACTAL DIMENSION, D	Pre-exponential factor, γ (MPa)
NIE Butterfat #1	2.45	1.0×10^{-3}
CIE Butterfat #1	2.16	9.5×10^{-3}
NIE Butterfat #2	2.59	4.6×10^{-4}
EIE Butterfat #2	2.50	9.9×10^{-4}
NIE Butterfat #3 (DMA Analysis)	1.96	2.6×10^{-1}
NIE Butterfat #4 (DMA Analysis)	2.01	2.2×10^{-1}
NIE Palm Oil	2.82	1.2×10^{-9}
CIE Palm Oil	2.82	2.0×10^{-9}
NIE Lard	2.88	9.2×10^{-14}
CIE Lard	2.84	6.7×10^{-10}
Cocoa butter #1	2.37	5.3×10^{-2}
Cocoa butter #2 (DMA Analysis)	2.40	2.1×10^{-2}
Salatrim™	2.90	4.9×10^{-19}
Tallow	2.41	1.5×10^{-2}

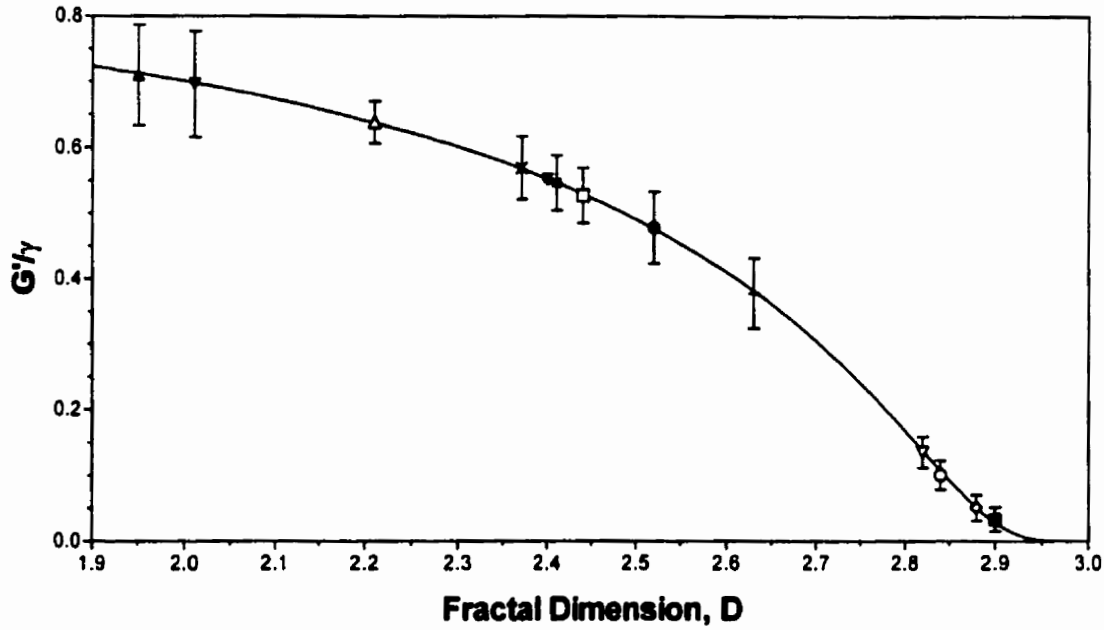

Figure 5.35: G'/γ as a function of D. The solid line represents Eqn. 5.17, symbols with error bars represent average values of rheological measurements (shown in table 5.2) and their standard errors.

curve. The points on the curve represent data from the fat systems represented in Table 5.2. All of the normalized elastic constants for the various fats were calculated for a 70% solid fat content value (i.e. $\Phi_{SFC} = 0.7$). As is evidenced by figure 5.35, the theoretical curve of Eqn. 5.17 predicts that the normalised elastic constant should decrease with increasing fractal dimension. The standard error bars represent the extent to which the fat systems studied rheologically deviate from this trend. As is evidenced by the figure, taking the error bars into consideration, the general trend of the theoretical curve is closely followed. A one way analysis of variance performed on this plot using GRAPHPAD (San Diego, Ca.) suggests that the normalised elastic constant strongly depend on the fractal dimension ($P < 0.0001$). The ramifications of this plot are important. It suggests that if one can influence the fractal dimension of a particular fat by altering processing conditions, one can manufacture model fats. In other words, alter processing conditions to make fats with smaller or larger elastic constants (which we have seen are related to hardness, although not in a direct manner), using fractal dimension as an indicator. One must realise here that this pre-supposes that the pre-exponential term γ remains constant when the processing conditions are changed, which as will be shown in Chapter 6, is not a good assumption. However, this development does tell us how fractal dimension in isolation affects the elastic constant of the network: it is now of course necessary to investigate those structural parameters which are indicators of the constant γ -- the subject of Chapter 6.

5.4.2 Order, density, and Fractal Dimension

The two methods presented to calculate fractal dimension are rather involved, and

in the case of the rheological method, requires specialised skill. Both methods take a fair amount of time, although the microscopic method is by far the easier and quicker method. However, it is useful to attempt to attach a visual index to the value of the fractal dimension.

Note that for a higher fractal dimension, the density of the packing of the microstructural elements must be higher – since the number of microstructural elements is proportional to the characteristic length raised to a power equal to the fractal dimension, according to Eqn. 5.5. Density of packing of the microstructural elements does not refer to the traditional definition of density of the network (total mass/total volume), nor does it refer to the density *within* a typical microstructural element (which has been used in Eqn. 5.16 as the symbol ρ_{ME}). The density of packing of the microstructural elements refers to the density of the microstructural elements *within* one microstructure. Therefore, if one is observing a particular fat after it has been processed differently, then the increase or decrease of the amount of microstructural elements within a certain characteristic length will signal the increase or decrease of the fractal dimension. However, given the nature of the PLM images, this is not a parameter that is easily ascertained without image analysis. Additionally, as is discussed below, the fractal dimension is not only dependent on the density of the packing of the microstructural elements, it is also dependent on the *order* in which they pack. Certainly, these two parameters are inter-related, since the order in which the elements pack also influences the density of the packing, and is itself influenced both by the nature of the inter-

microstructural element forces and the mass and heat transfer limitations during the formation of the network.

Figure 5.36 shows a composite of four of the fat networks shown earlier – milkfat(A), tallow(B), palm oil(C) and lard(D). These images are of the fats crystallised at 5°C for 24 h, except for lard, which was crystallised for 72h. As is evident from the figure, the order of packing of the microstructural elements increases from (A) through to (D). Additionally, the fractal dimension increases in the same way. It therefore seems that a higher fractal dimension implies a higher order of packing of the microstructural elements.

This result is not surprising. The fractal dimension is an index that is related to the order of the embedding space of the microstructural elements. If one can image that a plane is filled with close-packed microstructural elements taking up all the space, then that object is a 2-dimensional object. If one can imagine a cube filled with close-packed microstructural elements taking up all space, then that object is a 3-dimensional object. If one now takes the plane and starts putting kinks in it, the dimensionality of that space is raised to value between 2 and 3, as described before. The microstructural elements that were embedded in the fabric of the plane, now starts to look disordered – if the new positions of the microstructural elements are projected onto a plane, these positions will represent a disordered array. However, as the plane is kinked enough to start to approximate a cube, (i.e. with higher fractal dimensions), then when the positions of the microstructural elements embedded in the fabric of the kinked plane are projected onto a

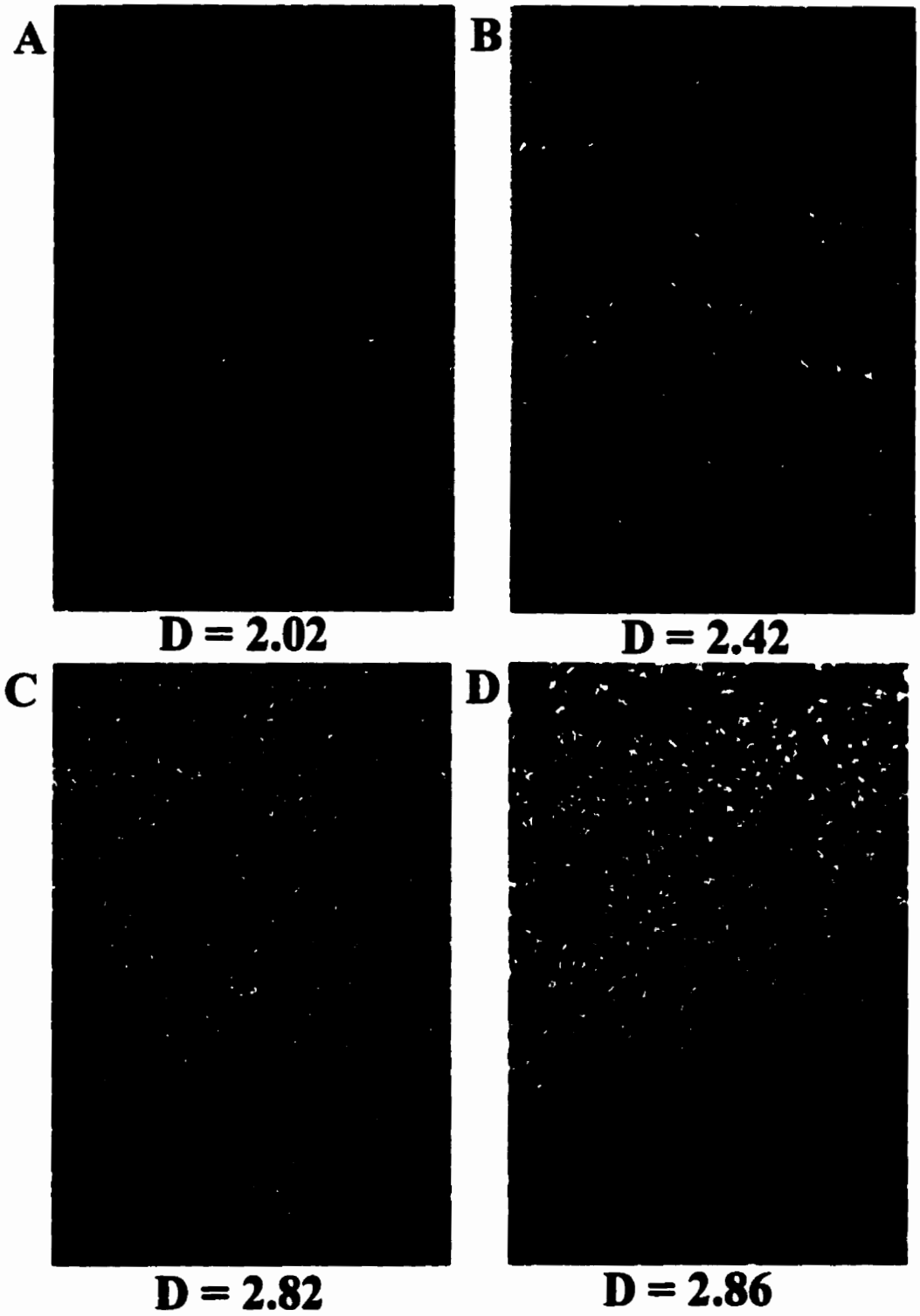

Figure 5.36: Increasing fractal dimension implies increasing order of packing: (A) Milkfat, (B)Tallow, (C) Palm Oil, (D) Lard.

plane, these positions starts to look more ordered. This is exactly the situation we have when we look at a PLM image of the *in-situ* fat network. This picture is difficult to represent in a schematic, but a shematic of this process built on the basis of a 1-dimensionl space being raised to a 2-dimensional space is useful in elucidating this concept.

If one considers a line, with microstructural elements placed at some equilibrium nearest-neighbour distance apart, then one has a picture represented by figure 5.37 (A). The projection of the positions of the microstructural elements onto a line represents an ordered array. Now, the line containing the microstructural elements represents a 1-dimensional object. If one starts to put kinks in this line, one starts to raise the dimension of the line to a value just above 1, and less than 2. This scenario is represented in figure 5.37 (B). Now, the microstructural elements must still be placed at a nearest-neighbour equilibrium distance from each other on this new "space", so therefore, the projection of the positions of the microstructural elements onto a line begins to look disordered, as shown in the figure. It is useful to have a working quantitative definition of order in this analogy. When one looks at the projection of positions, one may define high order as the positions all being a common average distance apart from each other. Therefore, the standard deviation of the various distances apart of nearest-neighbour projection positions is a good representation of the deviation from order (lower standard deviation implies higher order). Figure 5.37 (C) to (E) demonstrates situations in which more and more kinks are placed in the line containing the microstructural elements – therefore, the fractal dimension is increasing from (A) to (E). Table 5.3 shows the distance apart of nearest-neighbour projections of each situation (and lists an additional two situations following

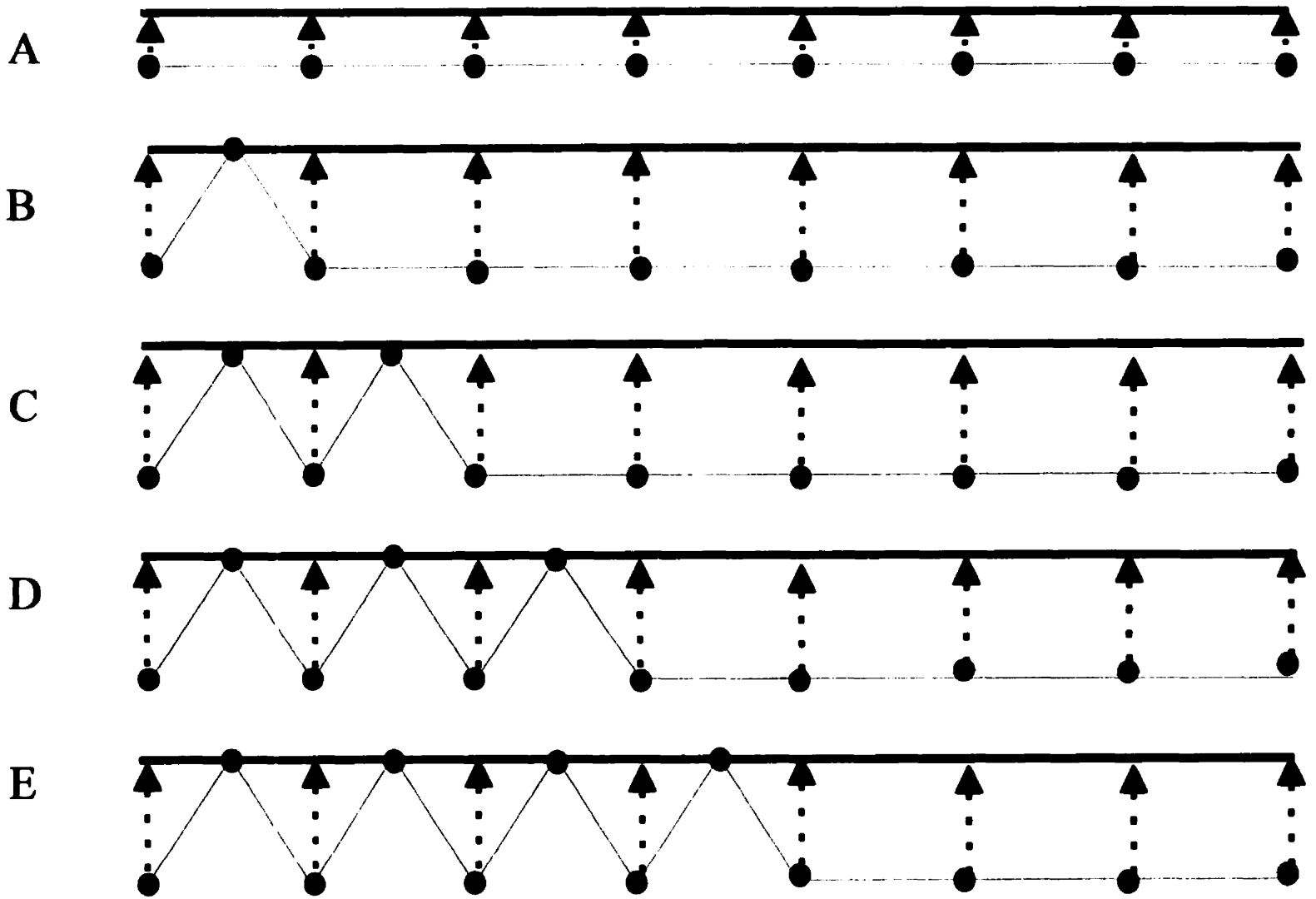

Figure 5.37: Schematic of microstructural elements placed on a line at equal distances apart. The dimensioality of the line increases from (A) to (E). Microstructural elements on the thin line are projected onto the thick line.

Table 5.3: Showing the decrease in standard deviation (after an initial increase) from an average distance between projected position of balls on a line, with increasing amounts of kinks in the line (fractal dimension is proportional to the number of kinks – less kinks, fractal dimension is closer to 1, more kinks, fractal dimension is closer to 2).

Projected Position	Distance between successive projected positions						
	0 kinks	1 kink	2 kinks	3 kinks	4 kinks	5 kinks	6 kinks
Figure 5.37⇨	A	B	C	D	E		
1	20	10	10	10	10	10	10
2	20	10	10	10	10	10	10
3	20	20	10	10	10	10	10
4	20	20	10	10	10	10	10
5	20	20	20	10	10	10	10
6	20	20	20	10	10	10	10
7	20	20	20	20	10	10	10
8		20	20	20	10	10	10
9			20	20	20	10	10
10				20	20	10	10
11					20	20	10
12						20	10
13							20
Packing Density (particles/cm)	**0.044**	**0.050**	**0.055**	**0.061**	**0.066**	**0.072**	**0.077**
Standard Deviation	**0**	**4.63**	**5.27**	**5.16**	**4.67**	**3.89**	**2.77**

the same trend of kinks, not shown in figure 5.37), and the standard deviation in these values for each situation. As can be seen, as the fractal dimension increases, the order initially (for a small amount of kinks in the line) decreases, and then order begins to increase as the fractal dimension gets larger and larger (i.e. closer and closer to 2). Of course, the fractal dimension referred to here is qualitatively getting larger (the actual dimension has not been computed), but it is generally accepted that more and more kinks in a line represents higher and higher fractal dimensions, since the line is closer approximating a plane. This situation is exactly what happens in the case where dimension is between 2 and 3. An interesting effect to note is also that as the fractal dimension and order increases, so does the density of packing of microstructural elements in the observed region. This is of course, in agreement with the foregoing discussion on density and order.

5.4.3 Order and heat limitations

Increasing density and order of packing of the microstructural elements are accompanied by increases in fractal dimension. Increasing fractal dimension suggests that the shear elastic modulus of the fat will decrease, although this does not take into consideration changes of the constant γ concomitant with changes in fractal dimension.

5.4.3.1 Theory

It is interesting to study the effect of crystallisation characteristics on the fractal dimension, since changing the environmental conditions under which the fat network is

formed will change the crystallisation characteristics, and therefore one may be able to relate changes in environmental conditions to changes in fractal dimension. It is expected that the crystallisation characteristics of the fat would be instrumental in determining the order of packing of the microstructural elements, due to the fact that the aggregation of the microstructural elements during formation of the network is through a process which is heat limited. This process is heat limited, since, as we saw in figures 24 and 25, there is growth of crystalline material (serving to increase the size of existing microstructural elements as well as the formation of new microstructural elements) during the aggregation process. This ongoing crystallisation will result in the release of the latent heat of fusion, and the network must be able to absorb and dissipate this heat, if the crystalline material is not to re-melt or cause melting of neighbouring crystalline entities. Consequently, the nature of packing of the microstructural elements will be dependent on the way the heat of crystallisation is released, which of course is also a function of the degree of supercooling of the material, as well as the rate of heat transfer from the material during formation of the network. For instance, if the nature of the crystallisation is such that all of the heat of crystallisation is released in a short length of time (of course, this is dependent on the environmental conditions), then the network will be forced to absorb and/or dissipate this large amount of heat in a very small amount of time. As the schematic in figure 5.38(A) shows, the most efficient way to achieve this dissipation of heat is to have the microstructural elements growing in ordered arrays, thereby allowing a maximum area of liquid oil (a good heat sink) around each centre of growth. However, if the heat of crystallisation is released over a long period of time (as in figure 5.38 (B)), then the heat limitation is removed and the network is allowed to aggregate in a fashion

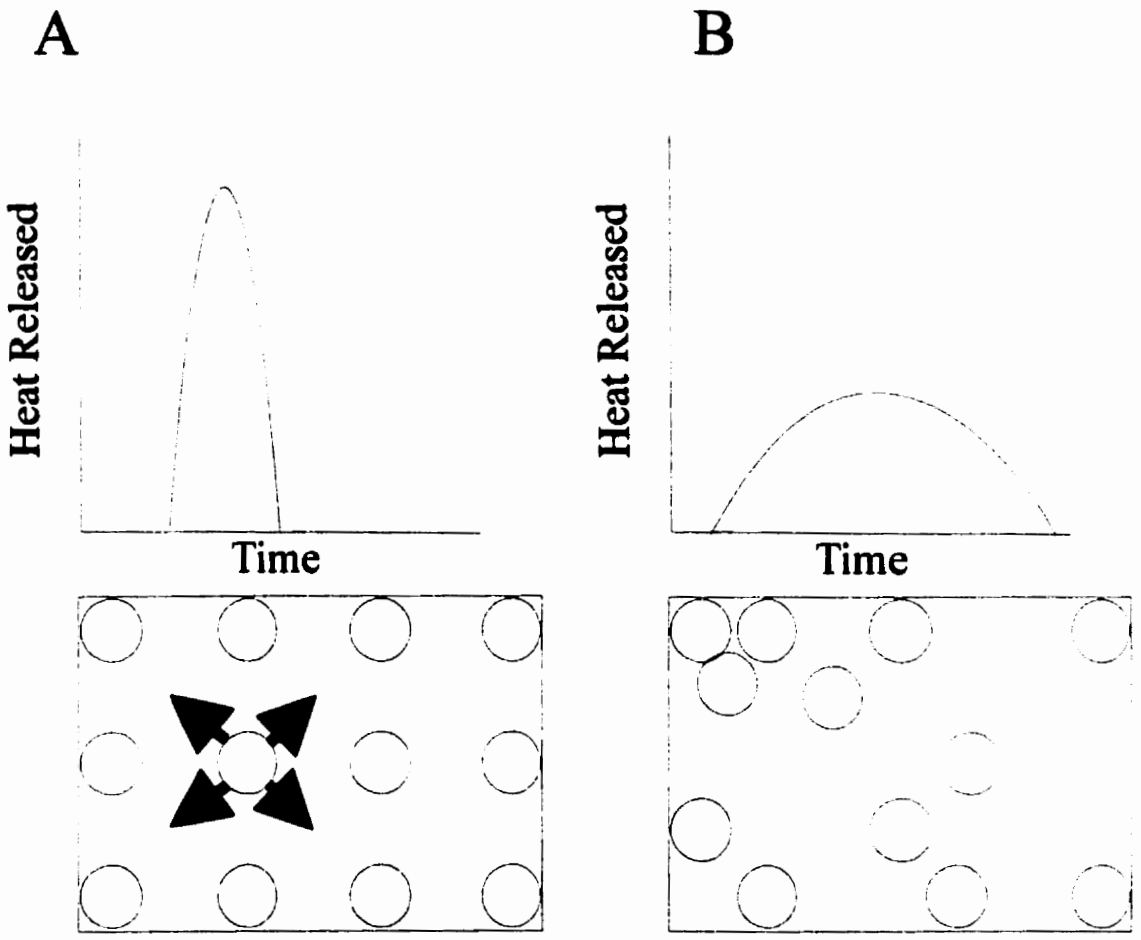

Figure 5.38: Schematics showing the ordering effect of heat limitations on the network. (A) Heat is released in a short time, the the network is forced to be ordered to dissipate the heat. (B) Heat is released over a longer period, and the network assume its preferred packing (represented here as disordered).

which allows it to resort to its thermodynamically preferred packing, or a state which is close to its thermodynamically preferred packing (most fat crystal networks will stay in thermodynamically unstable states for long periods). Of course, the manipulation of the environmental conditions to affect these changes is not trivial – such varied parameters as degree of supercooling, rate of heat transfer, presence of different melting fractions in the fat, etc. are dependent on how different environmental conditions will affect the crystallisation heat profile of the formation of a fat crystal network. However, one can monitor the crystallisation heat profile of a crystallising network using a differential scanning calorimeter (DSC), under different environmental conditions, and from this profile, one may be able to predict increases or decreases in order, and therefore, fractal dimension. If there are initial releases of heat which are in a short period of time, then one would expect these narrow "peaks" in the heat-released vs. time graphs to be order-setting steps, since subsequent crystallisation will occur as growth on the already-established microstructural elements. It must however be stated here also that heat profiles demonstrating a broad "peak" in the heat-released vs. time graph may also demonstrate an ordered packing, since this may be the thermodynamically preferred packing of that fat crystallised under those conditions. However, if one can succeed in changing the heat profile of a particular fat by changing the crystallisation conditions, any broadening or narrowing of initial peaks in the heat-released vs. time graphs should contribute to less order or more order, respectively. Some points to note here are that the crystallisation heat profile of a sample of the fat crystallising in a DSC pan will not necessarily represent the heat profile of a fat crystallised in bulk, and almost certainly will not represent the heat profile of a fat crystallised in a scraped-surface heat exchanger.

It is also uncertain that one can approximate the same environmental conditions on a microscope slide as in a DSC pan, or for a sample prepared for rheology. However, if for instance, increasing the rate of the cooling in the DSC for a particular fat results in a heat profile demonstrating a sharper or broader initial peak in the heat-released vs. time graph, then one should expect the packing of the microstructural elements for that fat to be more or less ordered when the rate of cooling is increased in any statically crystallised fat sample. However, the extent to which the peak in question was sharpened or broadened would not necessarily be matched for the fat crystallised statically in a bulk sample, due to the difference in heat transfer characteristics between the sample in a DSC pan and the sample which is prepared for rheology, for example. However, there would be some amount of sharpening or broadening of the peak for the bulk sample as well.

5.4.3.2 Experimental

In an effort to illustrate the ordering effect of sharp peaks in a heat-released vs. time graph of the crystallisation of fat networks, the DSC profiles of the four fats shown in figure 5.36 were monitored. Samples of milkfat, tallow, palm oil, and lard were melted to 80°C and immediately placed within aluminum pans that were then hermetically sealed. A Dupont Model 2090 differential scanning calorimeter was then used to monitor changes in heat flow of these samples during the crystallisation of the samples. Similar empty pans were used as standards. The machine was operated at a rate of 5°C per minute. The samples were cooled at this rate down to at least –20°C. Figure 5.39 shows heat-released vs. temperature plots for the 4 fats – milkfat(A), tallow (B),

palm oil(C) and lard(D). Since the samples were all cooled at an identical rate, the broadness or narrowness of peaks represents the relative time in which the heat was released.

Figure 5.40 (A) shows heat-released vs. temperature DSC plots for samples of milkfat cooled at different rates – 20°C/min (A), 12 °C/min (B), 5 °C/min (C) and 1 °C/min (D). The samples were prepared in a manner identical to what is described above, and the measurements were performed on the same calorimeter listed above. This was done in order to demonstrate the effectiveness of using changes in processing conditions to affect changes in order of packing of microstructural elements and therefore changes in fractal dimension for a particular fat.

Microscopy slides for *in-situ* polarised light microscopy were prepared as described before, with milkfat samples being prepared according to two tempering methods. In one method (slow cooling method), the sample was melted at 80°C for 30 min, then kept at 40°C for 30 min, then at 25°C for 60 min, then at 20°C for 60 min, then at 15 °C for 60 min, then at 10 °C for 60 min, then refrigerated at 5°C. The tempering steps listed above were performed using SANYO MIR1530 Cooled Incubator. In the other method (fast cooling method), samples were melted at 80°C for 30 min, then kept at 40°C for 30 min, and then refrigerated at 5°C. Figure 5.41 (A) shows a PLM micrograph of the milkfat sample cooled using the fast cooling method, and 5.41 (B) shows a micrograph of the sample cooled using the slow cooling method, after 10 days of both sets of samples being incubated at 5°C.

Rheological samples of 100% milkfat and various dilutions with canola oil (95% w/w, 90%w/w, 85% w/w, and 80% w/w milkfat-canola oil) were prepared for the Perkin Elmer DMA 7 rheometer. The rheometer had a 1-cm-diameter parallel-plate geometry. The milkfat and milkfat-canola oil samples were melted to 80°C and poured into moulds constructed of plastic material, each mould being cylindrical with a height of 0.5 cm and a diameter of 1 cm. Samples of the 100% milkfat and dilutions were also put into tubes suitable for measurement of solid fat content in a Bruker Minispec 120 pulsed-NMR machine. Two sets of samples for rheological and solid fat content measurements were prepared – one set were tempered according to the fast cooling method and one set according to the slow cooling method, described above. Each dilution analysed rheologically and for solid fat content was prepared in triplicate.

After incubation at 5°C for 10 days, the samples were transferred to the temperature-controlled DMA cell, set to 5°C. The upper plate was lowered manually until contact with the sample was established. All compression measurements were performed under a static force of 5 kPa to ensure proper mechanical contact. On top of the static stress, a dynamic stress wave was applied at a frequency of 1 Hz, increasing from 2.5 to 5 kPa at 1 kPa/min. A clear eastic region was observed in this stress range, and compressive storage, or Young's modulus (E) was recorded in triplicate. Strains were of the order of 0.01 %. Values of Φ_{SFC} were then measured (in triplicate) as described in Chapter 3. Plots of $\log E$ vs. $\log \Phi_{SFC}$ were made. Since $E / 3 = G'$ (chapter 3, Eqn. 3.18), then a plot of $\log E$ vs. $\log \Phi_{SFC}$ should yield as its

slope $1/(3-D)$. Values of fractal dimension were therefore calculated for the two sets of samples. For the samples cooled slowly, the fractal dimension was 2.65 and for the samples cooled quickly, the fractal dimension was 2.27.

5.4.3.3 Discussion

Figure 5.39 is somewhat limited in what it can suggest about the effects of processing conditions on crystallisation conditions, which may lead to order or disorder in the packing of microstructural elements. This is because the fats shown are all different, and therefore the appearance of a broad or narrow peak in one fat cannot strictly be compared to the appearance of a narrow or broad peak in another fat. The appearance of increased order or disorder due to the broadness of the peaks can only strictly be compared with samples of the same fat processed differently. This is because some fats will be inherently (thermodynamically) disordered, whilst others will be inherently ordered. Given this, if we compare figure 5.39 to the micrographs shown in figure 5.36, some useful conclusions can be drawn. The micrographs shown in figure 5.36 shows the same fats whose DSC profiles are represented in figure 5.39. However, the micrographs in figure 5.36 were all taken at 5°C. Therefore, any comparisons made must necessarily exclude those features in the DSC profiles which are below 5°C. As is evident from figure 5.39, all of the fats with a sharp initial peak above 5°C (tallow(B), palm oil(C), and lard(D)) demonstrate very ordered packing in the microstructural elements in figure 5.36. Milkfat (5.39 (A)) demonstrate a relatively broad peak, and its microstructural elements are packed in a relatively disordered fashion. The fats were all processed identically, so therefore it appears that the presence of the initial sharp peaks in

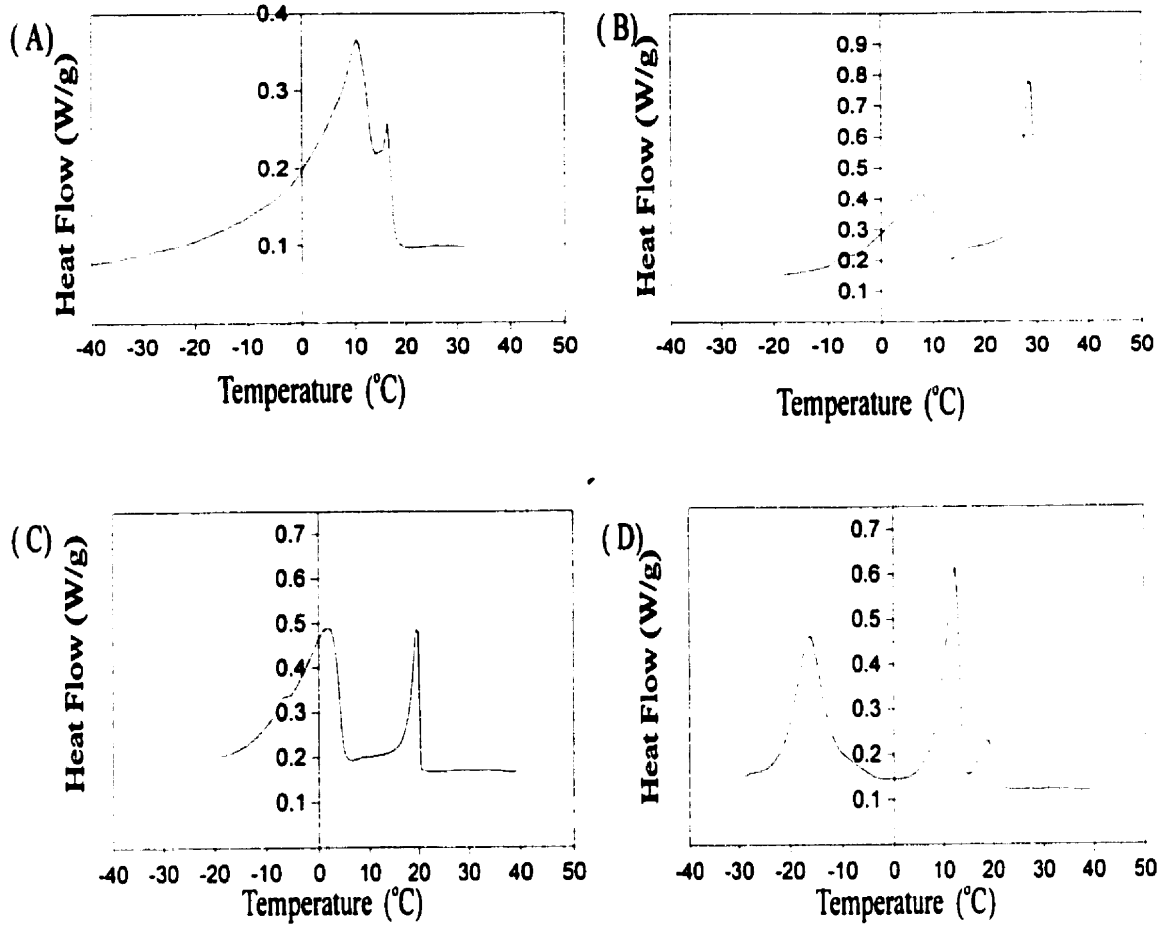

Figure 5.39: DSC profiles of fat samples cooled at 5°C per min. (A)Milkfat, (B)Tallow, (C)Palm Oil, (D)Lard

the heat released vs. temperature DSC plots have an ordering effect on the packing of the microstructural elements.

Figure 5.40 demonstrates that if one decreases the rate of cooling of milkfat, a sharp initial peak appears – this peak is represented as a shoulder in the DSC profiles of the samples which are cooled at 20°C per min (5.40 (A)) and 12°C per min (5.40 (B)). However, in the DSC profiles of the samples cooled at 5°C per min (5.40 (C)) and 1°C per min (5.40 (D)), this peak appears more defined, and represents a greater amount of heat released over a narrow temperature range. Therefore this suggests that if milkfat is cooled slowly, the fat will demonstrate a relatively ordered packing of the microstructural elements compared to a situation where it is cooled quickly. It is uncertain what is causing the peak to appear – but it is most probably due to the composition of the milkfat (it is well-known that milkfat is composed of a number of different melting fractions, e.g. Marangoni and Lencki, 1998). The sharp peak could be due to the highest melting fraction in milkfat crystallising out before any of the other fractions. If the fat is cooled quickly, this event would not be an initial effect, since practically all of the fractions will crystallise out at once. However, if the fat is cooled slowly enough, the highest melting fraction (or the highest melting fraction compounded with an amount of the middle melting fraction) would have the time to crystallise before the crystallising temperature of the other fractions is reached. Additionally, if the highest melting fraction has a narrow melting range (which it does – see Marangoni and Lencki, 1998), then the burst of heat released as it crystallises will be in a narrow temperature range. Almost certainly, this sharp crystallisation peak is due to the high melting fraction of milkfat crystallising out in

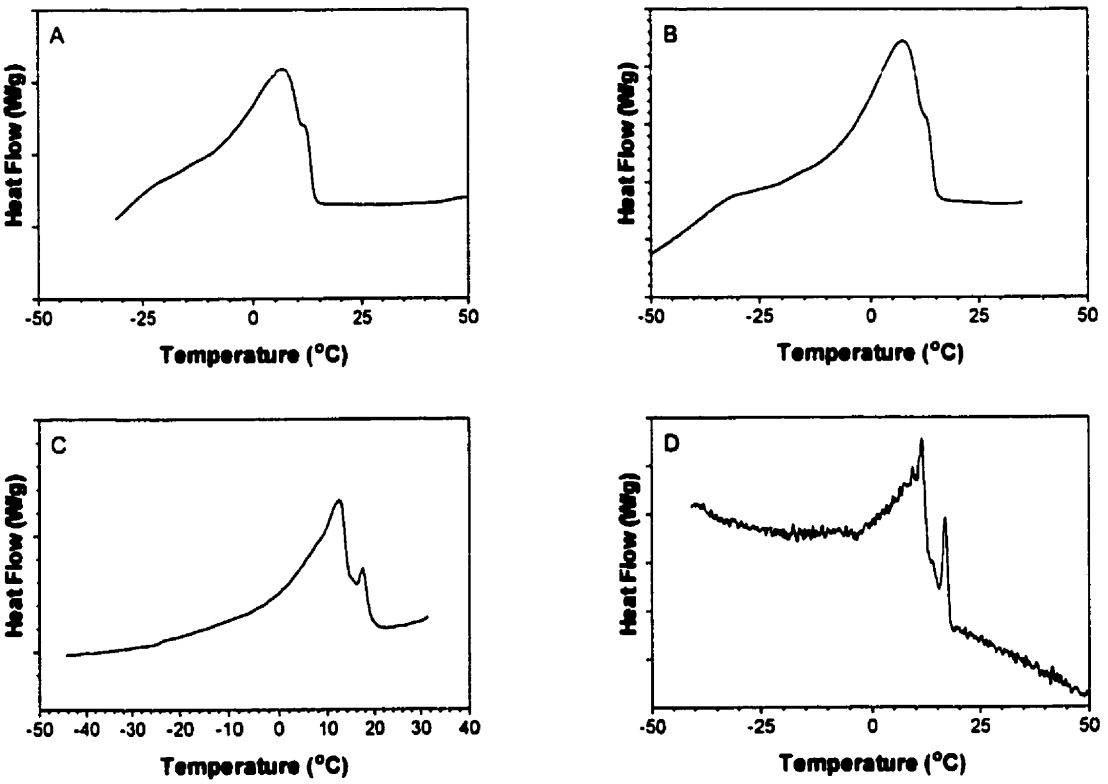

Figure 5.40: Showing DSC profiles of milkfat, with different rates of cooling. (A)20°/min, (B) 12°/min, (C)5°/min, and (D) 1 °/min.

isolation or with a small amount of compounded middle melting fraction. Given this sharp burst of crystallisation, the appearance of microstructural elements of the high melting fraction of milkfat will establish an ordered template upon which the rest of the fractions will grow. This is indeed the case when one examines figure 5.41 – the micrograph of the sample cooled slowly (5.41 (B)) demonstrate a relatively ordered packing of the microstructural elements compared to the sample cooled quickly (5.41 (A)). Additionally, in agreement with the discussion of order and fractal dimension above, the fractal dimension calculated for the samples cooled slowly was 2.65 compared to 2.27 for the samples cooled quickly. As is evidenced by the micrographs shown in figure 5.41, the size of the microstructural elements are different in the two differently prepared samples. This is good indication that the constant γ for these samples are also different, since it has been suggested that this constant depends in part on the nature of the microstructural elements. In fact, the rheological analysis yielded γ values of 2.0 x 10^{-4} MPa and 7.0 x 10^{-2} Mpa, for the slow and fast cooled samples, respectively. This issue will be re-visited in Chapter 6, but it is important to note here that the changes effected in the fractal dimension by changing the processing conditions are not isolated, but in fact are followed as well by changes in the constant γ. The point here is that it is myopic to assume that the elastic constant of the network will change only according to the changes in D due to different processing conditions – chances are that γ will also change.

5.5 Conclusions

It has been shown in this chapter, from a structural basis established by a

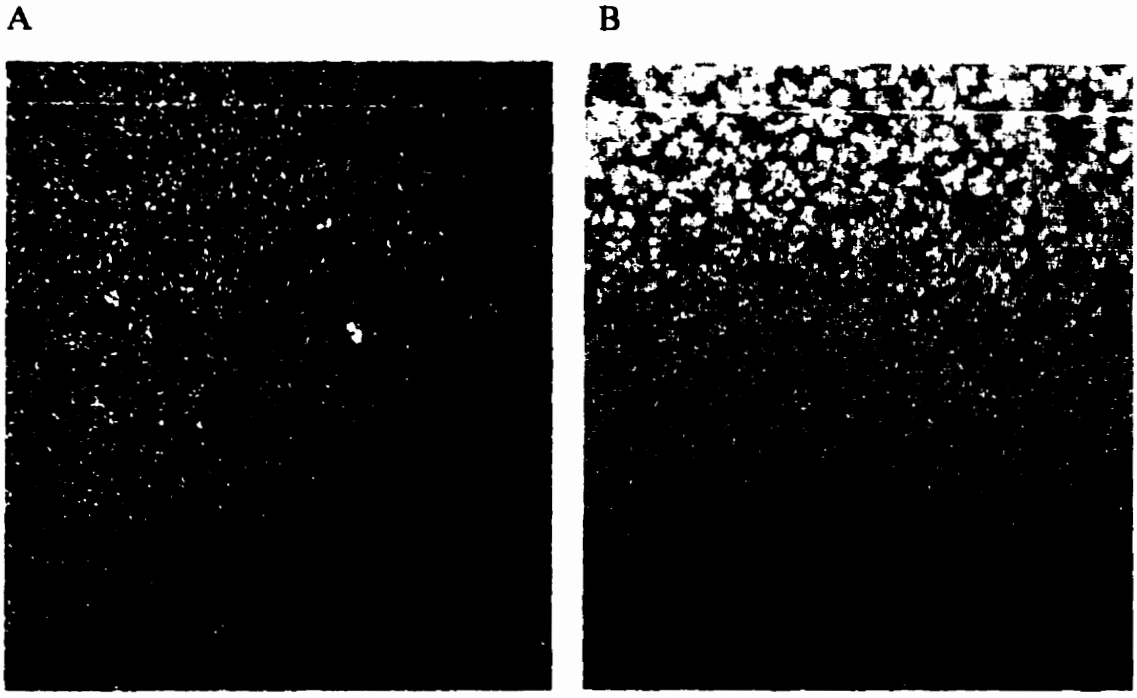

Figure 5.41: (A) Sample of milkfat cooled quickly, (B) Sample of milkfat cooled slowly. Both samples are at 5°C, and the magnification is the same(10X objective lens used to image both samples on the same microscope).

multitude of microscopy techniques, that fat crystal networks crystallised statically are fractal within certain length ranges. Furthermore, it was shown that the weak link theory is applicable to fat crystal networks. The microscopical method developed to calculate fractal dimensions produced values which were in good agreement with those calculated from application of the weak link theory. However, it must also be mentioned that the microscopical method requires the use of a subjective method of thresholding, which brings into question the value of its use in an industrial setting. Additionally, it was discussed above that many fat systems with densely-packed microstructural elements may not be suitable to be analysed by this method. Through the choice of fat systems suitable to be analysed by this method, however, it has been shown that the rheological method of analysis employed by Rousseau and Marangoni (detailed in Chapter 2) is valid for fat networks.

It has been established that a higher degree of order in the packing of the microstructural elements represents a higher fractal dimension. Additionally, it has been shown that processing conditions may be changed in ways that can result in changes in the fractal dimension. It is important to realise that changes in crystallisation behaviour seen with a sample of a particular fat under different processing conditions are not necessarily reproducible with samples of greater bulk. If the temperature trajectory of the crystallisation process can be determined, the relative broadening or narrowing of initial peaks in the temperature-time curve due to changes in processing conditions will produce dis-ordering or ordering effects. The origin of these effects is however not straightforward – factors such as supercooling, rate of transfer of heat from the containing

vessel, ease of nucleation events, formation of different polymorphs, existence of separate fractions, etc., will all play a role.

The structure of the network developed in this chapter has been for fats that were crystallised under static conditions, without any shearing of the fat (as is usually done in industry) and without any heat-removal techniques such as those employing scraped-surface heat exchangers. Additionally, the fats were not crystallised under conditions of severe supercooling. Therefore, the structure that is presented here is not necessarily representative of fat crystal networks crystallised under industrial-like conditions. Some controversy presently exists about whether fats that were crystallised in scraped-surface heat exchangers at high levels of supercooling are indeed fractal. This work can make no claims about the validity of any side of this argument, since none of the fats studied here were crystallised under such conditions. Suffice to say that from brief discussions with other researchers (personal communication with Dr. Pieter Walstra and Dr. William Kloek), it seems unlikely that fats crystallised under such industrial-like conditions are fractal in nature.

Chapter 6

Mechanical Model at Low Deformations: Investigating γ

The quantification of the spatial distribution of microstructural elements within the microstructures in fat crystal networks has been studied in Chapter 5. The weak link theory was applied to the structure of fat crystal networks, producing a relationship of the shear elastic modulus (G') to the solid fat content (Φ_{SFC}) via the mass fractal dimension (D) of the network. From Chapter 5, the elastic modulus of a fat crystal network is related to the solid fat content of the network via the following relationship at high solid fat contents:

$$G' = \gamma \Phi_{SFC}^{\frac{1}{d-D}} \qquad (6.1)$$

where G' is the elastic modulus, Φ_{SFC} is the solid fat content, d is the Euclidean dimension of the network – usually 3 – and D is the fractal dimension of the network, measured at length scales bounded by the average size of the microstructural elements and the size of one microstructure. All of these parameters are well-defined, except for the constant γ, which has been proposed to be dependent on the nature of the microstructural elements, the links between microstructures, the relationship between ξ (size of microstructures), Φ (microstructural element volume fraction), and D, and the proportionality between Φ_{SFC} and Φ. The exact dependence of the constant γ on network properties has not been formulated: it is the motivation of the model outlined in this chapter to formulate a relationship of γ to fundamental characteristics of the fat

network in a manner that would relate γ to structural characteristics of the network. As will be demonstrated, it is not possible to formulate an *exact* relationship for γ, but it is worthwhile to identify some of the parameters that affect its value.

Network models aimed at relating the shear elastic modulus to the particle volume fraction for fat crystal networks are summarized in Chapter 2. One of the reasons previous models of fat crystal networks have failed was that they predicted a linear relationship between the elastic modulus and the solid fat content of the network. As suggested by Eqn. 6.1 and shown by figure 5.33 (Chapter 5), the elastic modulus of the network actually depends on the solid fat content in a power law fashion. This relationship has also been documented by a variety of other researchers in the field (e.g. Nederveen, 1963; Payne, 1964; Papenhuijzen, 1971; 1972; van den Tempel, 1979; Vreeker *et al.*, 1992b; Narine and Marangoni, 1999a; 1999b; 1999c).

The implications for altering the mechanical properties of fat crystal networks (by following changes in structure, which implies changes in γ and/or D) by varying processing conditions will also briefly be discussed in this chapter.

6.1 Theory

The elastic modulus of fat crystal networks are virtually independent of frequency (in LVR) and in the linear viscoelastic region demonstrate a very low value of damping (Nederveen, 1963; Rousseau *et al.* 1996c). An example of the lack of variation of the

elastic modulus with frequency is shown in figure 1 (experimental details are summarized below). This suggests that the viscosity of the liquid (oil) portion of the network plays no essential part in the transmittance of forces; if this was the case, one would expect increases of the loss modulus (at frequencies corresponding to the relaxation time of the network) with increases in frequency (Nederveen, 1963). The fact that fat crystal networks do demonstrate a measurable elastic modulus as well as a yield value suggests that the solid fat particles are the entities responsible for the elastic modulus and therefore these particles must have strong mutual interactions.

6.1.1 Structural Model

As presented in Chapter 5, at the microstructural level, the solid network is an orthodox amorphous solid, whilst the intra-microstructural level is fractal in nature. The arrangement of the microstructures can be imagined as an assembly of chains, each chain consisting of a linear array of microstructures with an average small distance apart. The chains are branched and interlinked to form a three-dimensional network with oil present in the void volume, both within and outside the microstructures. In this way the network is similar to the network as described by van den Tempel (1961). However, van den Tempel did not consider that the particles forming the chains were clusters of smaller particles arranged in a fractal manner; the way the microstructures are clusters with microstructural elements arranged within them in a fractal manner. In a later publication, van den Tempel(1979) did consider that the network is formed via interaction of clusters rather than primary particles, but did not consider the fractal arrangement of the "primary particles" within the clusters. Evidence of the existence of ordered microstructures were

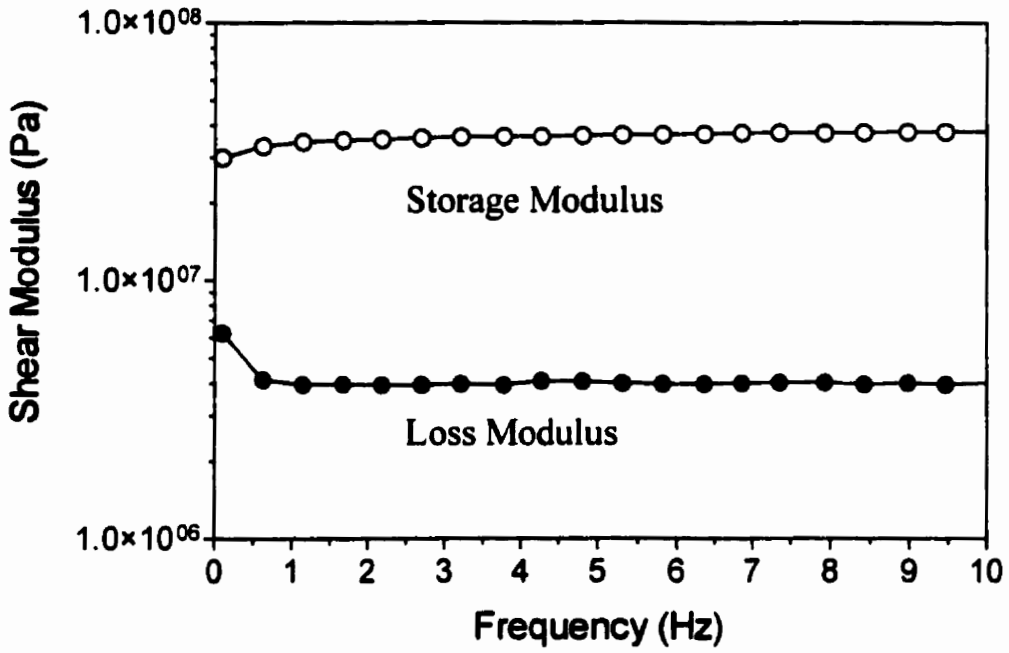

Figure 6.1: Shear elastic modulus, G', and loss modulus, G" plotted against frequency for cocoa butter (solid fat content of sample is 75% and strain level is 0.5%)

presented in Chapter 5, and is also given by Heertje and co-workers (Heertje *et al.* 1987; Juriaanse and Heertje, 1988; Heertje, 1993). The fractal nature of the microstructures was demonstrated in Chapter 5.

The relationship shown by Eqn. (6.1) was formulated by assuming the so called "weak-link theory" in which the elastic constant of the network is dependent on the nature of the links between microstructures, as opposed to the strength of the microstructures themselves. This theory is applicable to fat crystal networks at relatively high percentages of solid content. The weak link theory suggests that when a deforming force is placed on the fat crystal network such that the resulting deformation is within the linear viscoelastic region of the network, the links between the microstructures are stressed, rather than the microstructures themselves.

6.1.2 Fractal network model

In a 1 cm^3 sample containing N_ξ microstructures, with N_σ microstructural elements in each microstructure, the particle volume fraction (microstructural element volume fraction) of the network is given by

$$\Phi = \frac{4}{3}\pi\left(\frac{\sigma}{2}\right)^3 N_\sigma N_\xi \qquad (6.2)$$

where σ is the diameter of a microstructural element assumed to be spherical. This assumption is not a bad assumption for most natural fat systems at high solid fat contents as have been discussed in Chapter 5. However, this is an important assumption of the model being developed, and should be taken into consideration when large deviations

from sphericity are observed. The number of microstructural elements within a microstructure is given by the following equation:

$$N_\sigma \sim \left(\frac{\xi}{\sigma}\right)^D \qquad (6.3)$$

$$\Rightarrow \qquad N_\sigma = c(\xi)^D \qquad (6.4a)$$

where ξ is the diameter of a microstructure and c is a proportionality constant. As explained in Chapter 5, the fractal dimension of a fat crystal network may be calculated by utilizing Eqn. (6.4a) in the following form:

$$N_\sigma = c(R)^D \qquad (6.4b)$$

where $\sigma \le R \le \xi$. Taking logarithms:

$$\log(N_\sigma) = D\log(R) + \log(c) \qquad (6.5).$$

Therefore, a plot of $\log(N_\sigma)$ vs. $\log(R)$ yields $\log(c)$ as the intercept and D as the slope. Therefore, from Eqn. (6.2),

$$\Phi = \frac{4}{3}\pi\left(\frac{\sigma}{2}\right)^3 c(\xi)^D N_\xi \qquad (6.6).$$

The number of microstructures in a sample of volume 1cm^3 may therefore be written as:

$$N_\xi = \frac{6\Phi}{c\pi\sigma^3\xi^D} \qquad (6.7).$$

If the distance between neighboring microstructures in a chain is small compared to ξ, the total length of all the chains present in the 1cm^3 sample is:

$$N_\xi\xi = \frac{6\Phi\xi}{c\pi\sigma^3\xi^D} \qquad (6.8).$$

It can be safely assumed that the total chain length is made up of straight chains oriented in three mutually perpendicular directions in a cubic sample, given the regular manner in which the microstructures have been observed to pack. Therefore, when the network is stressed in a given direction only one third of the total chain length represents the number of chains supporting stress in that direction. In a cube of volume 1 cm^3, a cross-section of area 1cm x 1cm cuts through the following number of 1cm chains:

$$\frac{N_c\xi}{3} = \frac{2\Phi\xi^{1-D}}{c\pi\sigma^3} \qquad (6.9).$$

These are therefore the total length of chains that transmit stress from one part of the sample to the other.

6.1.3 Forces acting within the network

It is assumed that the attractive forces between microstructures consist of van der Waals interactions between microstructural elements that form nearest-neighbors at the interface between two microstructures. Again, this is an important assumption of the model being developed. At this point, the author cannot account for any other forces acting in the network at this level of structure. As explained below, polar forces at this level of structure are relatively negligible. Furthermore, the fat particles are non-polar and the oil is a non-polar medium. However, this assumption must be taken into account when considering "real" systems with significant amounts of water present or significant amounts of polar components present. One can imagine that if the microstructures all are of the same size and shape, there will be some m interactions due to nearest-neighbor interactions between microstructural elements at the edge of two neighboring

microstructures. Therefore, as far as the elastic modulus of the network constitutes a measure of the mechanical strength of the network at small deformations, all of the microstructural elements present do not contribute to the mechanical strength. The relatively few microstructural elements that link the microstructures together are moved with respect to their nearest neighbors in a neighboring microstructure when the network is stressed, whilst the microstructures themselves behave as rigid units. This view of the behavior of the network under a deforming stress is shared by Papenhuijzen (1972). The assumption that van der Waals interactions are the interactions of importance with fat particles is not new (van den Tempel, 1961, Nederveen, 1963; Payne, 1964) and as Nederveen (1963) has stated, it may be calculated that dipolar forces are about a factor of 10^{10} smaller than van der Waals forces, making these negligible enough to ignore.

It is difficult to take into consideration non-spherical shapes in a calculation of van der Waals' forces, although this has been attempted before (Vold, 1951). Therefore, in the following development, the microstructural elements are assumed to be spherical, as explained above, a reasonable assumption. Below, we summarize a development of the calculation of van der Waals interaction between two microstructural elements, developed by Nederveen (1963). The Lennard-Jones potential between two non-polar atoms is formulated as:

$$U = -\lambda r^{-6} + \mu r^{-12} \qquad (6.10a)$$

$$\lambda = 2|U_o|r_o^6 \qquad (6.10b)$$

$$\mu = \frac{\lambda}{2} r_o^6 \qquad (6.10c)$$

where U is the potential energy of two molecules at a distance r. When the two molecules are at their equilibrium distance r_o apart, the potential energy is U_o. In order to calculate the attractive energy between two spheres consisting of a large number of molecules (say, q /m^3), Eqn. 6.10(a) must be integrated over the volumes of both spheres:

$$U = q^2 \int_{v_1} dv_1 \int_{v_2} dv_2 (-\lambda r^{-6} + \mu r^{-12}) \qquad (6.11)$$

where dv_1, dv_2, V_1 and V_2 are volume elements and volumes of the 2 spheres 1 and 2 and r is the distance between dv_1 and dv_2. Hamaker (1937) had before Nederveen carried out the integration of the attractive term. By carrying out the integration for the repulsive term as well, it is possible to calculate the stiffness of a van der Waals bond for small deviations from equilibrium, such as is the case when the network is deformed during measurement of the elastic modulus. Nederveen performed the integration for two spheres with equal radii R separated by a distance d (making the distance between the centers of the two spheres $C = 2R + d$). The steps of the integration are cumbersome and unnecessary to re-state at this point. It is sufficient to say that for $d << R$, Nederveen's integration agreed with an independent check by the authors and yielded:

$$U = \frac{-AR}{12d}\left[1 - \frac{1}{420}\left(\frac{r_o}{d}\right)^6\right] \qquad (6.12)$$

where $A = \pi^2 q^2 \lambda$ is the Hamaker's constant. The attractive force between the two spheres is given by differentiation of Eqn. (6.12) with respect to d:

$$F = \frac{\partial U}{\partial d} = \frac{AR}{12d^2}\left[1 - \frac{1}{60}\left(\frac{r_o}{d}\right)^6\right] \qquad (6.13).$$

Equations (6.12) and (6.13) suggests that there is an equilibrium distance where the potential energy between the two spheres is a minimum and the force between them becomes zero:

$$d_o = \frac{r_o}{\sqrt[6]{60}} \qquad (6.14).$$

If the deformation ε of all volume elements in the two spheres is homogeneous, then d may be written as a function of the radius of the spheres:

$$d = d_o + 2R\varepsilon \qquad (6.15).$$

When Eqns. (6.14) and (6.15) are substituted into Eqn. (6.13):

$$F = \frac{AR^2\varepsilon}{d_o^3}\left(1 - \frac{11R\varepsilon}{d_o}\right) \qquad (6.16).$$

This equation is valid only when $11R\varepsilon / d_o$ is small compared to unity. Therefore, for very small deformations, the force between the two spheres varies linearly with the deformation(ε).

It is expected that as two microstructural elements move apart due to a stress on the network, the resulting gap is filled with the liquid oil present in these networks. Papenhuijzen(1972) has shown that by considering the microstructural elements as spheres and using a corrected Stokes equation:

$$f_h = 3\pi\eta_L Ru\alpha \qquad (6.17)$$

where f_h is the force necessary to move a sphere with diameter R at speed u to a flat plate, n_L is the viscosity of the oil and α is a correction factor which depends on the

distance between the sphere and the plate, the corresponding hydrodynamic force can be expressed as:

$$f_h = \frac{3\pi\eta_L R^2 u}{8d} \qquad (6.18).$$

As reported by Kamphuis and Jongschaap (1985), the elongation rate between the two spheres is assumed to be very small:

$$u << \frac{A}{\eta_L R d} \qquad (6.19),$$

and therefore only the Lennard-Jones potential as described above needs to be taken into account. These authors also suggested that the inertial forces are negligible with respect to the interactive forces (Kamphuis *et al.*, 1984). This is assumed as well in our treatment. Again, it is important to note these assumptions, which simplifies the model considerably. There seems to be plausible reasons why these can be made, as explained above.

Figure 6.2 shows a schematic of two neighboring microstructures. The force between two neighboring microstructural elements is given by Eq. (6.16). If the microstructural elements are assumed identical, the interaction between neighboring microstructural elements can be represented by a spring. Therefore, the forces between microstructures can be represented as m identical springs of spring constant k in parallel. If one assumes that the pairs of microstructural elements are all moved the same distance apart, then the total force can be approximated by;

$$F = \sum_{1}^{m} k_n \Delta x = \sum_{1}^{m} f_n = mf \qquad (6.20)$$

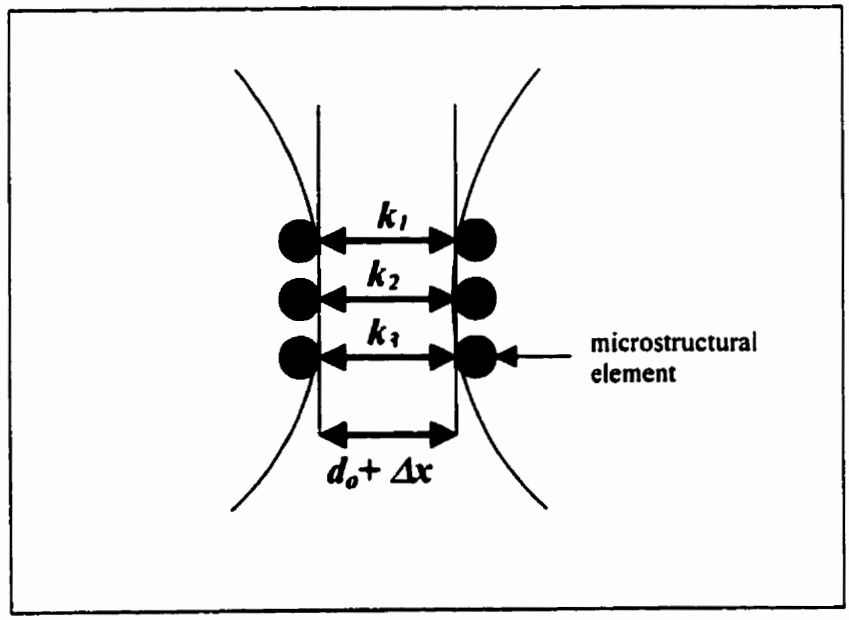

Figure 6.2: Schematic showing forces between two microstructures.

where f is the restoring force of one spring of force constant k extended by a distance of Δx. Therefore, if there are m identical pairs of microstructural elements at the interface between two microstructures, the force between the microstructures is given by:

$$F = m\frac{A\sigma^2\varepsilon}{4d_o^3}\left(1-\frac{11\sigma\varepsilon}{2d_o}\right) \qquad (6.21)$$

where R in Eqn. (6.16) has been replaced by $\sigma/2$ to represent the radius of the microstructural elements.

6.1.4 Elastic modulus

In a sample that is a cube of volume $1cm^3$ which is stressed in one direction, the number of chains carrying the stress is given by Eqn. (6.9). Therefore, the stress s transmitted through a 1cm x 1cm cross-section is given by (van den Tempel, 1961; Nederveen, 1963; Kamphuis and Jongschaap, 1985):

$$s = m\frac{A\sigma^2\varepsilon}{4d_o^3}\frac{2\Phi\xi^{1-D}}{c\pi\sigma^3}\left(1-\frac{11\sigma\varepsilon}{2d_o}\right) = m\varepsilon\frac{A\Phi\xi^{1-D}}{2c\pi\sigma d_o^3}\left(1-\frac{11\sigma\varepsilon}{2d_o}\right) \quad (6.22).$$

The tensile modulus of the network is then given by:

$$E = \frac{s}{\varepsilon} = m\frac{A\Phi\xi^{1-D}}{2c\pi\sigma d_o^3}\left(1-\frac{11\sigma\varepsilon}{2d_o}\right) \qquad (6.23a).$$

When the deformation is small enough that one is in the linear elastic region and the following relationship holds:

$$\frac{11}{2}\frac{\sigma\varepsilon}{d_o} < 0.1 \qquad (6.23b),$$

Eqn. (6.23a) reduces to:

$$E = \frac{s}{\varepsilon} = m\frac{A\Phi\xi^{1-D}}{2c\pi\sigma d_o^3} \qquad (6.24)$$

The storage shear modulus is given by:

$$G' = \frac{E}{3} = m\frac{A\Phi\xi^{1-D}}{6c\pi\sigma d_o^3} = m\frac{A\Phi\xi^{2-D}}{6c\pi\sigma\xi d_o^3} \qquad (6.25).$$

If the fractal dimension within microstructures is D, i.e. the spatial distribution of the microstructural elements within the microstructures is characterized by D, the scaling relationship between the average microstructural size ξ and the solid volume fraction Φ can be found by approximating the solid volume fraction inside the microstructures as the overall solid volume fraction (as was demonstrated in Chapter 2):

$$\xi \sim \Phi^{\frac{1}{D-d}} \qquad (6.26).$$

From Eqn. (6.26),

$$\xi^{2-D} \sim \left[\Phi^{\frac{1}{D-d}}\right]^{2-D} = \Phi^{\frac{2-D}{D-d}} \qquad (6.27).$$

Therefore,

$$\Phi\xi^{2-D} \sim \Phi\Phi^{\frac{2-D}{D-d}} = \Phi^{\frac{d-2}{d-D}} \qquad (6.28).$$

From the above,

$$G' \sim m\frac{A}{6c\pi\sigma\xi d_o^3}\Phi^{\frac{d-2}{d-D}} = m\frac{A}{6c\pi\sigma\xi d_o^3}\Phi^{\frac{1}{d-D}} \qquad (6.29).$$

Recalling from Chapter 5 that Φ and Φ_{SFC} are related:

$$\Phi = \frac{\rho_t}{\rho_{ME}}\Phi_{SFC} \qquad (5.16),$$

(where ρ_t is the density of the entire network, and ρ_{ME} is the density *within* the microstructural elements) then Eqn. 6.29 becomes:

$$G' \sim m\left(\frac{\rho_t}{\rho_{ME}}\right)^{\frac{1}{3-D}} \frac{A}{6c\pi\sigma\xi d_o^3} \Phi_{SFC}^{\frac{1}{3-D}} \quad (6.30)$$

Equation (6.30) therefore reduces to a form equivalent to Eqn. (6.1). Comparing Eqn. (6.1) and Eqn. (6.30):

$$\gamma \sim \frac{mA}{6c\pi\sigma\xi d_o^3}\left(\frac{\rho_t}{\rho_{ME}}\right)^{\frac{1}{3-D}} \quad (6.31).$$

6.1.5 Dimensional Analysis

The relationships represented by Eqns. (6.30) and (6.31) do not have an equal sign, but instead, both represent a scaling relationship. Therefore, the model does not provide an absolute formulation, but instead helps to de-mystify the origins of γ - i.e. identify some of the structural parameters which affect the value of γ.

The scaling nature of the relationship stems from the following relationship:

$$\xi \sim \Phi^{\frac{1}{D-d}} \quad (6.26)$$

now, if we write this equation as:

$$\xi = k\Phi^{\frac{1}{D-d}} \quad (6.32),$$

then k has dimensions of L.

Therefore, if one re-visits Eqns. 6.28 and 6.29:

$$\Phi\xi^{2-d} = k^{2-D}\Phi^{\frac{2-D}{D-d}}\Phi = k^{2-D}\Phi^{\frac{d-2}{d-D}} \qquad (6.33),$$

which implies that:

$$G' = \frac{k^2 k^{-D} mA}{6c\pi\sigma\xi d_o^3}\Phi^{\frac{1}{d-D}} \qquad (6.34).$$

Taking into consideration the relationship of Φ to Φ_{SFC}, Eqn. 6.34 becomes:

$$G' = \frac{k^2 k^{-D} mA}{6c\pi\sigma\xi d_o^3}\left(\frac{\rho_t}{\rho_{ME}}\right)^{\frac{1}{d-D}}\Phi_{SFC}{}^{\frac{1}{d-D}} \qquad (6.35),$$

which implies that:

$$\gamma = \frac{k^2 k^{-D} mA}{6c\pi\sigma\xi d_o^3}\left(\frac{\rho_t}{\rho_{ME}}\right)^{\frac{1}{d-D}} \qquad (6.36).$$

One can express the dimensionalities of the parameters in the system as:

$[c] = L^{-D}$, $[k] = L$, $[\sigma] = L$, $[\xi] = L$, $[d_o] = L$, $[A] = NL$ (N = Newton),

m, π and $\left(\frac{\rho_t}{\rho_{ME}}\right)^{\frac{1}{d-D}}$ are dimensionless quantities. Therefore, the right hand side of equation 6.36 is dimensionally equal to:

$$\frac{L^2 L^{-D} NL}{L^{-D} LLL^3} = \frac{N}{L^2} = Pa \qquad (6.37)$$

The dimension of the constant γ is of course Pa – this shows that Eqn. 6.31 is dimensionally correct. Therefore, could a scaling constant be defined, the subsequent equality would be dimensionally correct. If one has an "approximately proportional to" relationship (like there is in a scaling relationship), dimensional analysis must take into consideration the dimensions of the constant of proportionality.

6.2 Experimental

(a) Rheology

Rheological analysis of all the fat systems was performed as detailed in Chapter 3, using a CarriMed CSL^2 500 Rheometer - TA Instruments (except where stated below). Rheological analysis of cocoa butter was performed at 20°C -- the molds of this sample (prepared according to the experimental details in Chapter 3) were cooled at 5°C for 1 h and then incubated at 20°C for 48 h). After the sample was mounted in the manner described in Chapter 3, frequency sweeps of the sample was carried out at constant strains (0.5%) over a frequency range of 0.1 – 10 Hz. Figure 6.1 shows such a frequency sweep for cocoa butter at 75% solid fat content.

(b) Measuring effective values of σ and ξ.

Non-interesterified lard and chemically interesterified lard were crystallized under identical crystallization conditions and a small amount of fat was

placed on a glass slide. A drop of paraffin oil was then added as a dispersing aid. A cover slip was then firmly pressed on the sample to remove air bubbles and excess liquid. This process breaks the network in such as manner as to allow the imaging of dispersed microstructural elements with a polarized light microscope. This method was used as one way of visualising effective diameters of lard and chemically interesterified lard. Figure 6.3 (a) and (b) respectively shows polarized light microscope images of 70% w/w samples of non-interesterified lard/canola oil and chemically interesterified lard/canola oil, using the above method of imaging. The shear elastic moduli corresponding to these samples are 1.25×10^4 Pa and 3.34×10^5 Pa, respectively. As is evidenced by the sizes of the microstructural elements represented in the pictures, the fat with the smaller microstructural elements (chemically interesterified lard/canola oil) has a larger value of shear elastic modulus.

The diameters of the microstructural elements of the fat systems that can be measured using the *in-situ* polarized light microscope images of fat systems (shown in Chapter 5) are not necessarily an absolute measure of these diameters. However, PLM images of these entities does allow an "effective" diameter to be measured, which may then be used to demonstrate the dependence of G' on these parameters. A PLM image of microstructural elements contains those elements both in focus as well as those elements out of focus. An attempt was made to select those microstructural elements that are obviously in focus to be measured for values of σ. For measurement of the diameter of microstructures (using images shown in Chapter 5), attempts were made to measure only

those elements with an obviously repeating size, i.e. effort was made to ignore those clusters of fat which seemed to be composed of more than one microstructure.

Figure 6.4(a) shows a plot of values of G' vs. $1/\sigma$, where σ is a measure of the effective diameters of microstructural elements for five different fat systems (milkfat, tallow, palm oil, lard – all crystallised at 5°C for 24h, 24h, 24h, and 72h – and cocoa butter, crystallized at 5°C for 1 h and then at 20°C for 48h). The effective diameters were measured from *in-situ* polarized light micrographs of these samples, shown in Chapter 5. Figure 6.4 (b) shows a plot of values of G' vs. $1/c\sigma\xi$ for three of the five different fat systems. Values of the constant γ was calculated from the intercept of the $\ln(G')$ vs. $\ln(\Phi_{SFC})$ for each of the five fat systems mentioned above. Values of G' used in figures 6.4 (a) and 6.4 (b) were calculated using the rheologically determined values of γ, the mass fractal dimension, Eqn. 6.1, and a common value for the solid fat content ($\Phi_{SFC} = 70\%$). A common value for the solid fat content was used in order to effectively normalize the value of G' with respect to solid fat content, thereby allowing a better comparison to other parameters such as σ, c, and ξ.

In an effort to examine the potential of utilizing changes in processing conditions to affect structure, and therefore γ and D, samples of milkfat were cooled rapidly and slowly, and then the structure investigated. The methods of cooling are given in section 5.4.3.2 in Chapter 5. Figure 6.5 (a) show the cooling profile of the samples cooled slowly. The average cooling rate to 5°C is 0.13°C/min. The cooling rate of the rapidly-cooled sample was not measured, but these samples were plunged to 5°C from 40°C,

therefore the rate of cooling for the rapidly-cooled samples were much higher. Figure 6.5 (b) shows the evolution of the solid fat content of the two sets of differently cooled samples (measured in triplicate), with the slowly cooled samples being represented by open circles and the rapidly-cooled samples being represented by solid circles.

In an effort to determine whether the samples cooled differently had different crystal packing, the DSC melt profiles of these samples were determined after incubation at 5°C for 10 days. The DSC used was a Dupont Model 2090 machine, with melting rates of 5°C/min being used with both samples. The samples were put into the machine at 5°C, and the temperature ramped up to 80°C at this rate. Figure 6.6(a) shows the melt profile for the rapidly cooled sample, and figure 6.6 (b) the slowly cooled sample.

Rheological analysis performed on the rapidly cooled and the slowly cooled samples are described in section 5.4.3.2 in Chapter 5. Figure 6.7 (a) shows the compressive storage modulus of the two samples (with the rapidly cooled samples being represented by solid circles and the slowly cooled samples by open circles) plotted against solid fat content. These measurements were made after the samples were incubated at 5°C for 10 days.

Cone penetrometry measurements were also performed on the rapidly and slowly cooled samples. Metal muffin-tin containers were filled with milkfat melted at 80°C. The muffin-tins were filled to a vertical height of 2 cm. A series of muffin-tins containing milkfat were then tempered according to the slow-cooling method, and a

series tempered according to the rapidly-cooled method (see section 5.4.3.2 in Chapter 5). Then, using the method described in Chapter 3 (section 3.3), a cone weighing 40 g with an angle of 50.3° was used to measure penetration depths. Cone penetrometry measurements were made on each set of samples, starting from the time both sets of samples achieved a temperature of 5°C, and continuing for a period of 15 days. Six replicates were made of each measurement. Figure 6.7 (b) shows cone penetrometry measurements (in mm) made on each set of samples (slowly cooled samples represented by open circles, rapidly cooled samples represented by solid circles) plotted against time.

6.3 Discussion

It is important to note that the power law relationship between G' and Φ_{SFC} of Eqn. (6.1) and Eqn. (6.30) is only valid for deformations of the fat network small enough such that Eqn. (6.23b) holds. Additionally, Eqn. (6.30) has been manipulated to represent the same functional form as Eqn. (6.1). As a result, the average diameter of the microstructures in the network ξ appears in the denominator of Eqn. (6.31). However, according to Eqn. (6.26), ξ is related to the solid volume fraction. It is important to realize that Eqns. (6.1), (6.30) and (6.31) are only valid at high solid fat contents. It has been experimentally proven that at high solid fat contents, the constant γ is independent of the solid fat content; plots of $\log_{10} G'$ vs. $\log_{10} \Phi_{SFC}$ of some 14 different fat systems were statistically good straight lines with a measurable intercept corresponding to $\log_{10} \gamma$ (Table 5.2, Chapter 5). This therefore would suggest that ξ as it appears in the denominator of Eqns. (6.30) and (6.31) does not change significantly over the applicable range of solid fat content. Furthermore, the author have observed no measurable change

in the diameter of microstructures of cocoa butter observed in its natural state at 20°C and at dilutions of 5, 10, 15, 20, 25, and 30 percent w/w with canola oil. The canola oil in this case was used purely as a diluent to vary the solid fat content.

The dependence of the hardness of fats on the solid fat content has been studied by a variety of researchers (e.g. Bailey, 1950; Nederveen, 1963; Vreeker *et al.* 1992b; Narine and Marangoni, 1999a; 1999b; 1999c; Haighton, 1976). In all cases hardness depended on the solid fat content in a power law fashion. Given the proportional manner in which hardness is related to the shear elastic modulus, shown in Chapter 3, this power law relationship is supported by Eqn. (6.30). Furthermore, as is demonstrated by figure 5.34 (Chapter 5), a plot of ln G' vs. ln Φ_{SFC} yields a straight line, verifying the power law dependence of G' on Φ_{SFC}. Additionally, as have already been shown in Chapter 5, rheologically calculated values of fractal dimension agree well with fractal dimensions calculated from image analysis. This suggests that both Eqns. (6.1) and (6.30) are correct in their description of fat crystal networks, as far as variation of G' with Φ_{SFC} and D is described by the model.

Particle size has been shown experimentally to be an important parameter in the hardness of fat crystal networks (e.g. Bailey, 1950; Nederveen, 1963; Shama and Sherman, 1970; Haighton, 1976; de Man, 1961; de Man, 1964; Mulder and Walstra, 1974; Foley and Brady, 1984; Kawanari, 1996) but previous network models except for those by van den Tempel (1961; 1979) failed to show a dependence on particle size in the final expression for the shear elastic modulus (e.g. Nederveen, 1963; Payne, 1964;

Papenhuijzen, 1971; 1972; Kamphuis *et al.* 1984; Kamphuis and Jongschaap, 1985). Overwhelming experimental evidence have been submitted by other researchers (de Man, 1961; de Man, 1964; Mulder and Walstra, 1974; Foley and Brady, 1984; Kawanari, 1996) which demonstrate that the hardness of fat crystal networks are inversely proportional to the particle size (microstructural element size). This is also supported by Eqn. 6.30. Equation (6.30) demonstrates a dependence on both the size of the microstructures and the size of the microstructural elements.

As a visual example of the effect a decrease in microstructural element size has on the shear elastic modulus, figure 6.3 shows marked decrease in particle size from the sample of non-interesterified lard/canola oil to the sample of chemically interesterified lard/canola oil. There is a corresponding decrease in the shear elastic modulus as well; the shear elastic modulus increases from 1.25×10^4 Pa to 3.34×10^5 Pa, as would be expected from the decrease in the diameter of the microstructural elements shown dispersed in the images.

As is demonstrated by figure 6.4 (a), a plot of G' vs. $1/\sigma$ yields a proportional relationship, as is predicted by Eqns. (6.30) and (6.31), and as have been shown before by other researchers (de Man, 1961; de Man, 1964; Mulder and Walstra, 1974; Foley and Brady, 1984; Kawanari, 1996). The fit to a straight line yields an r^2 value of 0.68. The fit is significantly improved when G' is plotted versus $1/c\sigma\xi$ as is seen in figure 6.4 (b), the r^2 value here being 0.98. This relationship is again predicted by Eqns. (6.30) and (6.31). The fact that the straight line fit to the plot of G' versus $1/c\sigma\xi$ is better than the

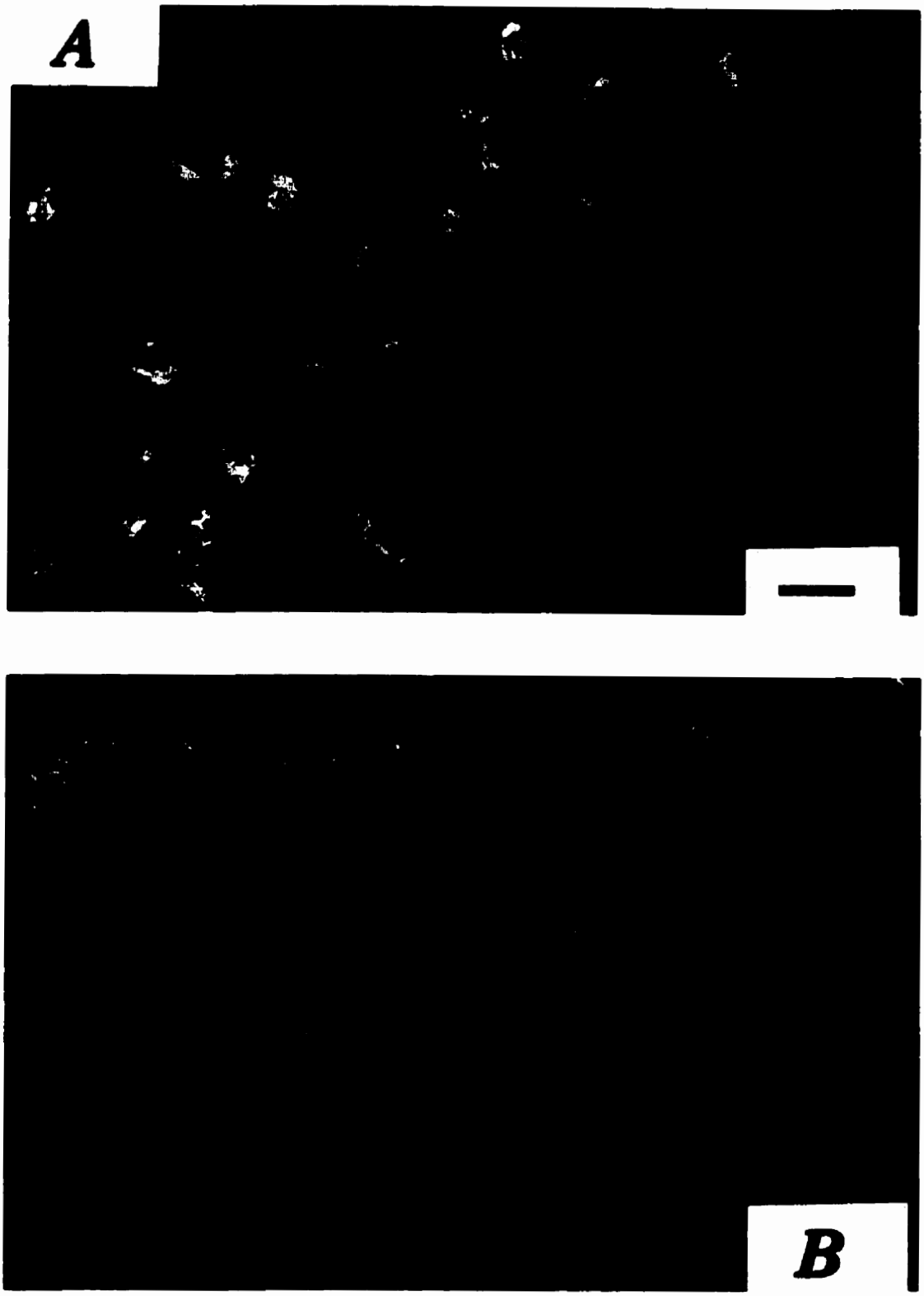

Figure 6.3: Polarised light microscope images of (A) 70% w/w samples of noninteresterified lard/canola oil and (b) chemically interesterified lard /canola oil. These samples were first broken and dispersed in paraffin oil. The horizontal bar represents 6μm.

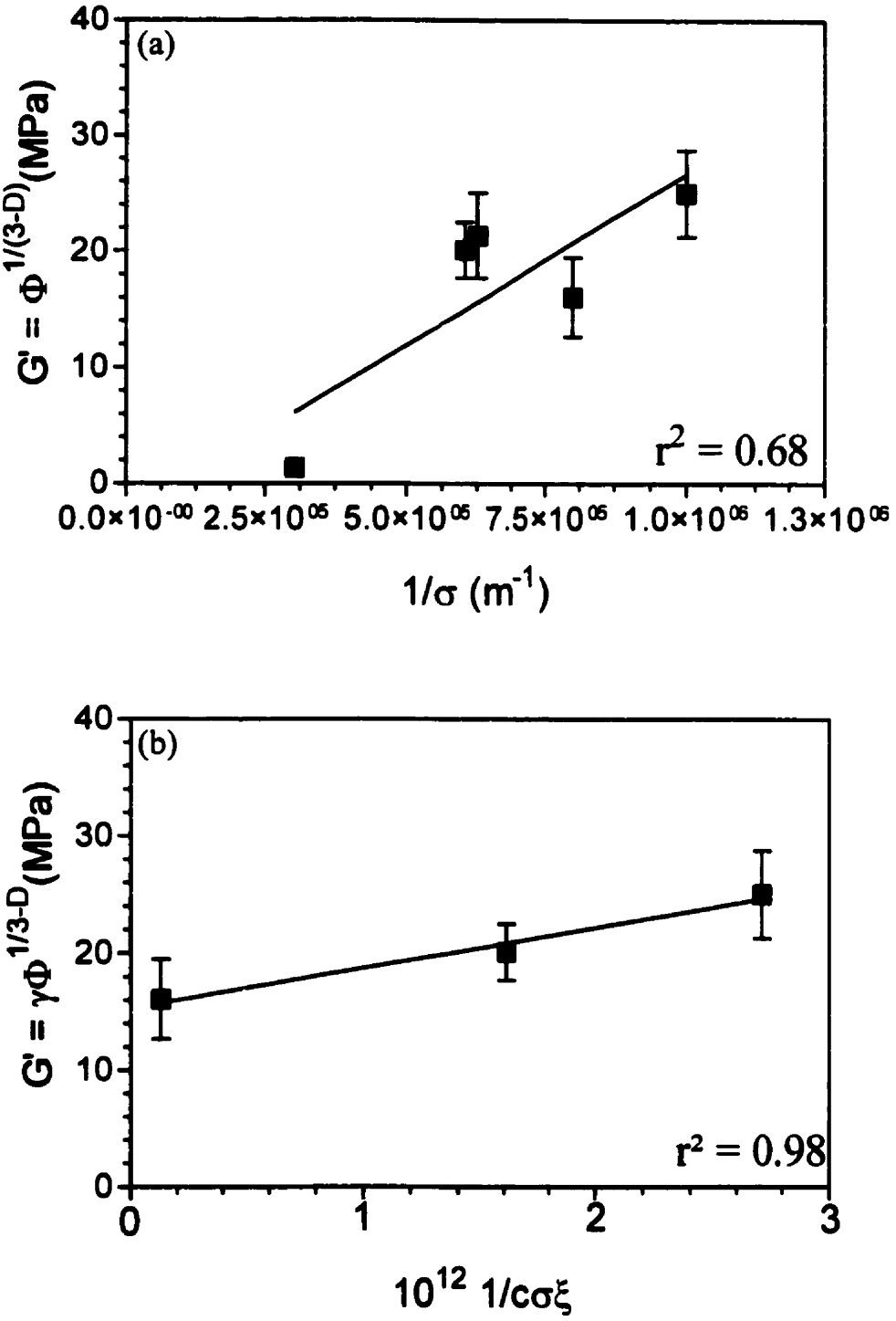

Figure 6.4: (a) Plot of G'vs. $1/\sigma$ for five different fat systems. (b) Plot of values of G'vs. $1/c\sigma\xi$ for three different fat systems. For both (a) and (b), symbols with error bars represent average values of rheological measurements and their standard deviations.

plot of G' vs. $1/\sigma$ is important to note, since it seems that changes in σ are followed by changes in both c and ξ. It is not surprising that these parameters are co-variants, since from Eqns. (6.3) and (6.4a), the parameter c is a measure of how many microstructural elements of a particular diameter σ are contained in a microstructure of a particular diameter ξ for that particular fat with a particular value for the fractal dimension D. Obviously, changes in ξ and σ also affects the value of c. Consequently, a better analysis of the agreement of the model with such parameters as c, σ and ξ is provided by evaluating the effect of these parameter on G' collectively rather than individually. Measurements of m, d_o and A are difficult to perform. The author knows of no method to measure A, and the methods of microscopy discussed in Chapter 5 do not allow for an accurate measurement of m or d_o.

The morphology of the microstructural elements also affects the mechanical strength of the network (e.g. Cornily and leMeste, 1985; Hoerr and Waugh, 1955; Hoerr, 1960). Since the interactions between the microstructural elements in this model were developed for spherical microstructural elements, obviously morphological changes of these elements would vary the form of Eqn. (6.30). Additionally, changes in morphology would probably cause changes in the Hamaker's constant as well. Morphology and size of crystals are affected by the particular polymorphism of the fat crystals formed (Chapman, 1962; Hoerr, 1960). Therefore, it is to be expected that changes in polymorphism may affect the network in a manner not predicted by Eqn. 6.30, even though to a certain extent the Hamaker's constant will be affected by polymorphic changes. However, the Hamaker's constant as its represented in this model is little more

than a fudge-factor – there is no known method of calculating these for fat crystal networks. The triglyceride composition also influences the size and rigidity of the crystals (Bailey, 1950). Therefore, it is important to establish a relationship between Hamaker's constant and triglyceride composition and polymorphism. Certainly, the model would be significantly improved if the crystalline packing and the molecular nature of the fat were represented in an explicit manner, rather than through the rather opaque relationship with the Hamaker's constant. However, at this time, the author can think of no method to begin this process, other than by molecular modelling of the triglyceride molecules into crystalline structures. This is a non-trivial task beyond the scope of this thesis, and the capabilities of the author. However, it is important to identify the areas where the model may be improved.

Figure 6.5 (b) demonstrates that the milkfat samples that were cooled slowly and those that were cooled rapidly had very different solid fat contents. After some initial changes, the solid fat contents of both samples seem to indicate that both samples have achieved some kind of equilibrium solid fat content. As is to be expected, the solid fat content of the rapidly-cooled (solid circles) sample of milkfat is higher. From Eqn. 6.30, this implies that the sample cooled rapidly would have a higher elastic modulus.

Figure 6.6 demonstrates the DSC melting profiles of the differently-cooled samples of milkfat. As is evident from the figure, the rapidly cooled samples (6.6 (A)) had a very similar melt profile compared to the slowly-cooled samples (6.6 (B)). This

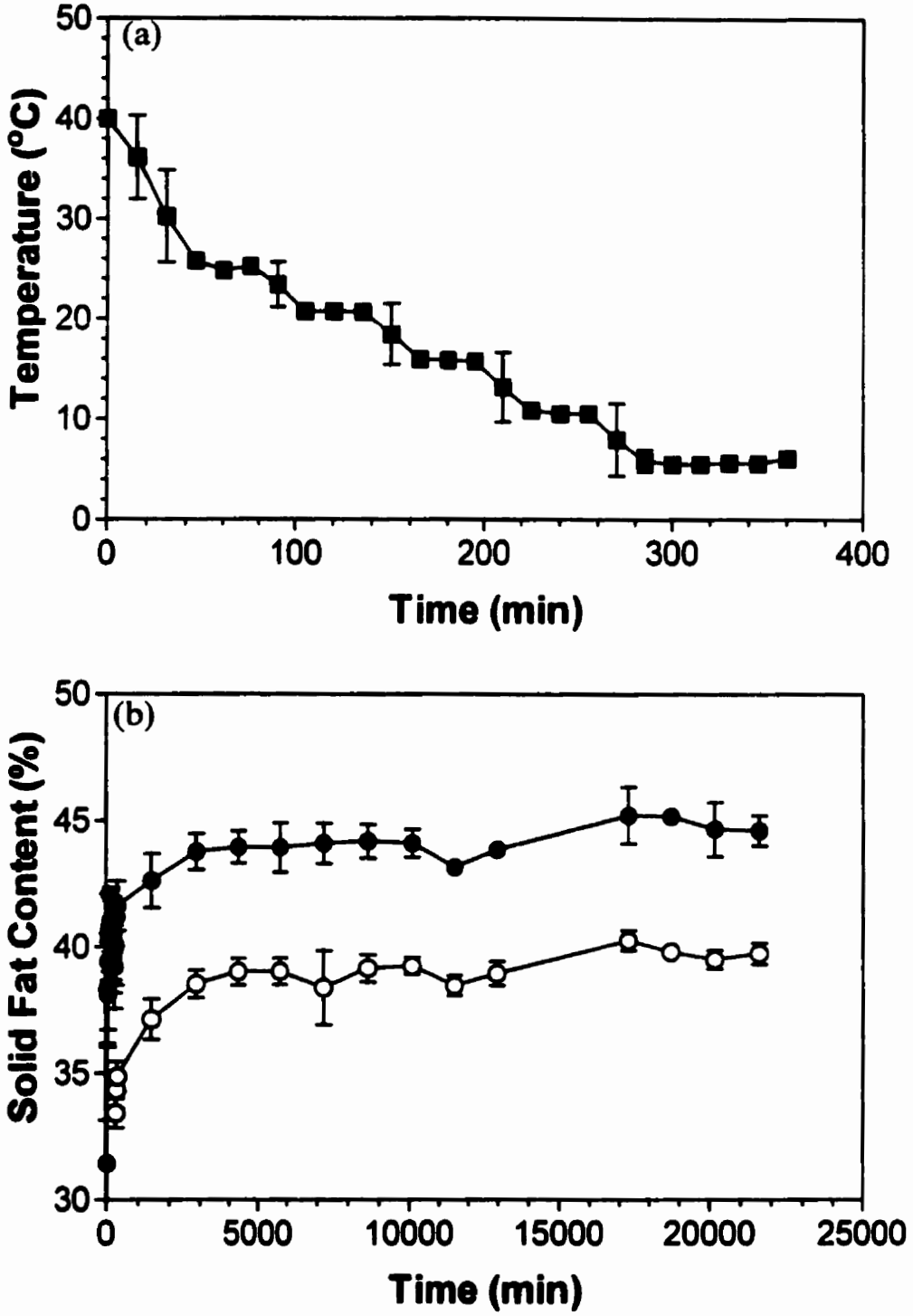

Figure 6.5: (a) Cooling profile of milkfat cooled according to the slow-cooling method. (b) Solid fat content vs. time for the differently-cooled milkfat samples (solid circles - rapidly cooled, open circles - slowly cooled).

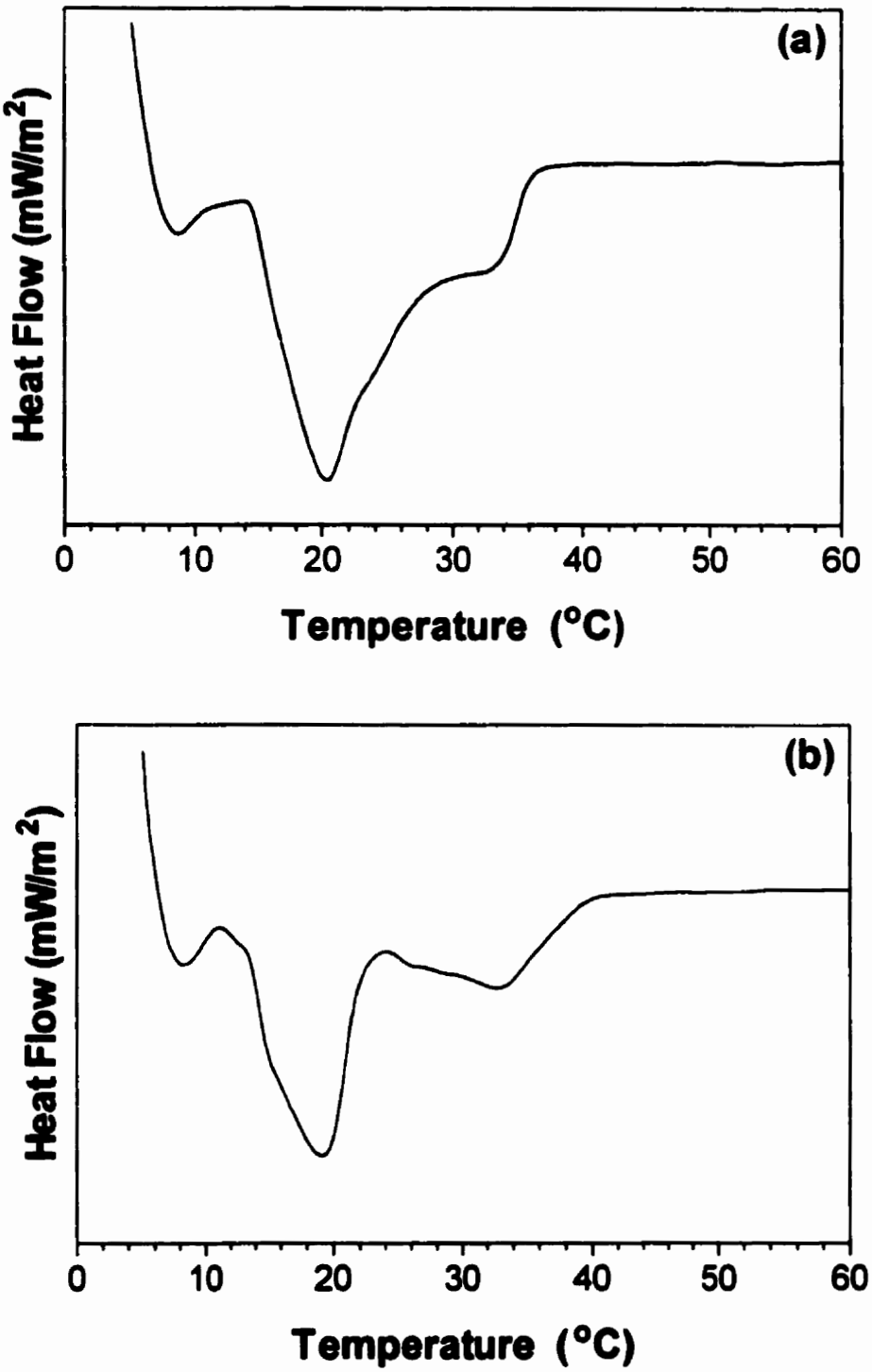

Figure 6.6: Differential scanning calorimeter measurements showing the melt profiles of milkfat (a) Rapidly cooled, (b) slowly cooled.

suggests that the crystalline nature of both samples were the same – i.e. both samples demonstrated the same polymorphic form of milkfat.

Figure 5.41 (Chapter 5) demonstrates that the size of the microstructural elements of the slowly-cooled milkfat samples are much larger than those in the rapidly-cooled samples. From Eqn. 6.31, this result suggests that the value of γ for the slowly-cooled samples should be much lower than those of the rapidly-cooled samples. As was reported in Chapter 5, section 5.4.3.3, rheological analysis yielded γ -values of 2.0×10^{-4} MPa and 7.0×10^{-2} MPa for the slow cooled and rapidly cooled samples, respectively. Therefore, the γ -values of the slow cooled samples are two orders of magnitude lower than those of the rapidly-cooled samples. From Eqn. 6.30, this implies that the sample cooled rapidly would have a higher elastic modulus.

From Chapter 5, section 5.4.3.3, rheological analyses of the differently-cooled samples yielded different fractal dimensions – the slow cooled samples yielded a fractal dimension value of 2.65, whilst the rapidly-cooled samples yielded a D of 2.27. From the discussion in Chapter 5 and from Eqn. 6.30, one would expect from this result that the elastic modulus of the rapidly-cooled samples would be higher.

Therefore, from the foregoing discussion, parameters such as microstructural element size, solid fat content, fractal dimension, and γ all suggest that the elastic modulus of the rapidly-cooled samples will be higher than that of the slowly-cooled samples. Figure 6.7 (a) demonstrates that these predictions were correct, according to

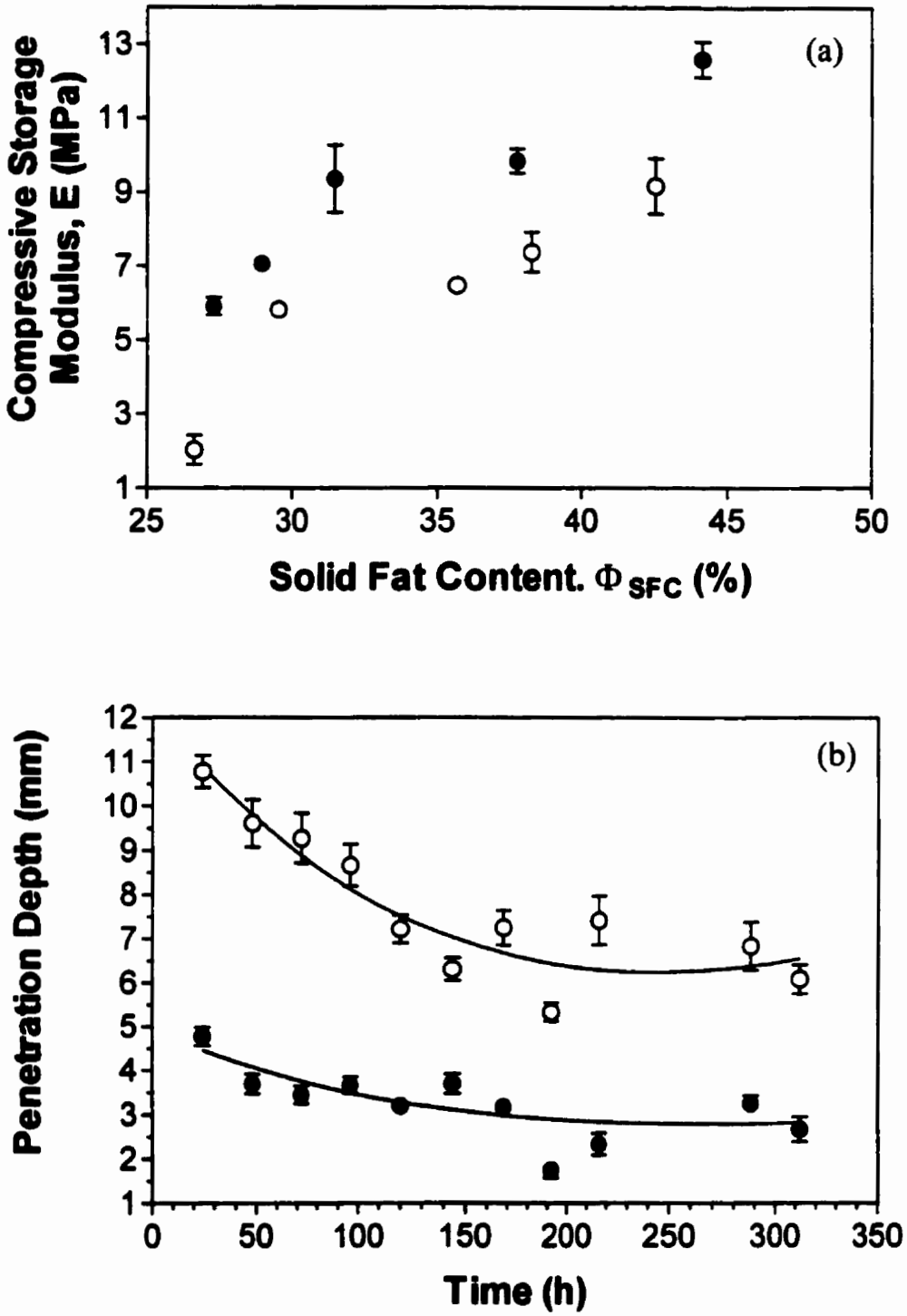

Figure 6.7: (a) Compressive storage modulus vs. solid fat content, for milkfat samples cooled rapidly (solid circles) and slowly (open circles).
(b) Penetration depth vs. time (measured from the point at which both set of samples reached 5°C) for rapidly cooled (solid circles) and slowly cooled (open circles) samples of milkfat.

Eqn. 6.30 and Eqn. 6.31, since at all values of solid fat content, the elastic moduli of the rapidly-cooled samples (solid circles) are higher than those of the corresponding slowly-cooled samples.

According to Chapter 3, the hardness of fats as measured by cone penetrometry are proportional to the elastic moduli, however, the nature of the constant of proportionality of this relationship was not easily defined. However, Figure 6.7 (b) demonstrates that the hardness of the rapidly-cooled samples (solid circles demonstrating lower penetration depths) were consistently higher than the hardness of the slowly-cooled samples (open circles demonstrating higher penetration values). Of interest is also that after approximately 8 days, the hardness of each set of samples had equilibrated to constant values. This suggests that by changing only the processing conditions of the fat, it was possible to produce two sets of fats with a large difference in hardness (60% from figure 6.7 (b)). Furthermore, up until a period of approximately 2 weeks, this difference in hardness was constant.

Therefore, a good case is made by this experiment for the possibilities that exist for producing fats with tailored mechanical properties by varying the way the fat is processed, without changing the chemical composition of the fat. Unfortunately, the way the fats were processed in this experiment is very different form the way fats are crystallized in industry, and therefore it is uncertain what industrial implications are motivated by this study. Additionally, it is important to realise that in this study, *all* of the measurable structural parameters as well as the solid fat content suggested (based on

the model espoused by Eqn. 6.30) that the elastic modulus (and therefore hardness) should be higher for the milkfat cooled rapidly. It is quite conceivable that in some cases, these parameters will be changed through processing in directions which may cause them to promote changes in elastic modulus that are in different directions. Furthermore, although all of the structural parameters examined in this study support the model espoused by Eqns. 6.30 and 6.31, it should be realized that *all* parameters implicated in the model were not measured (because of the difficulty in measuring these) simultaneously. However, in the absence of such measurements, it is reasonable to conclude that all experimental evidence presented in this thesis support the model.

6.4 Conclusion

Whilst Eqn. (6.30) does not provide an absolute formulation for γ in Eqn. (6.1), it does identify key network parameters that are important in determining the shear elastic modulus of fat crystal networks. Furthermore, it agrees well with experimental observations and with Eqn. (6.1), which has been shown in Chapter 5 to be valid for fat crystal networks. The equation provides impetus for the development of phenomenological investigations of relationships between triglyceride composition and polymorphism and values of Hamaker's constants and size of microstructural elements. Insight on the changes in mechanical strength of fat networks whose characteristics such as size of microstructural elements, size of microstructures and distances between microstructures have been altered through processing conditions was also provided.

To certain extents, the model presented in this chapter represents an idealization of the structure of fat crystal networks. It is therefore important that the assumptions highlighted during the development of the model be taken into consideration whenever the model is used. At best, the model provides an indication of the structural influences on the parameter γ, but levels of structure such as the crystalline and molecular structures are not adequately represented.

Chapter 7

Conclusions

The objectives of this study listed in Chapter 2 will now be re-visited, with each objective being discussed with respect to the findings of Chapters 3 to 6.

The elastic modulus was investigated for its suitability as a rheological indicator of hardness, in Chapter 3. It was found that the elastic moduli of some eight different fat systems were directly proportional to the hardness of the fat crystal networks as measured by cone penetrometry. However, the constant of proportionality varied from system to system. Therefore, it was concluded that changes in elastic modulus of a particular fat network would be expected to be followed by corresponding changes in hardness in terms of direction, but not magnitude. The elastic modulus is a rather "indirect" indicator of hardness, since hardness measurements result in the breakage of structures which are not even perturbed during the measurement of elastic moduli.

Cocoa butter and Salatrim®, two confectionary fats, were studied with respect to the phenomenological relationship of the shear elastic modulus(G') to solid fat content(Φ_{SFC}) used by other researchers (detailed in Chapter 2) to study the microstructure of fats (weak link theory). This relationship was formulated for colloidal gels, and is given by:

$$G' = \gamma \Phi_{SFC}^{\frac{1}{3-D}} \qquad (7.1)$$

where D is the fractal dimension of the network and γ was described as being a function of the particles (yet undefined) of the network, and the links between such particles. Both of these fat systems fit well to Eqn. (7.1), and values of D and γ were calculated. However, on observation of these two fat systems at the microstructural level, it was determined that the structural organization at this level of structure was very different for these two fats. It was proposed that the differences in rheological behavior of the fats could be explained by the differences in their microstructure. Furthermore, it was suggested that the structure of Salatrim® was not fractal-like, an observation borne out in Chapter 5, to be discussed below.

Utilizing four different microscopical tools (atomic force microscope, scanning electron microscope, polarised light microscope, and confocal laser scanning microscope), the microstructure of typical fat crystal networks crystallized statically at low levels of supercooling was studied in Chapter 5. At the lower limit of structural organization of the microstructural level, the network is composed of microstructural elements (~1 – 8 μm), which are composed of sintered and intertwined, densely packed

crystallites. The microstructural elements are organized into larger clusters, which pack in a similar manner to form microstructures (~100 – 200 μm). The microstructures themselves pack in a regular, space-filling, orthodox manner to fill the space of the network. It was found that this structure is fractal at a length range bounded by the size of one microstructural element, and the size of one microstructure. The structure of Salatrim® was quite different from this structural organization. A new method was devised to calculate the fractal dimensions of fat crystal networks using polarized light microscope images of the network.

Given the structure of the fat network discussed above, and assuming that at low levels of deformation of the network (such that the linear viscoeleastic range is not exceeded) the links between microstructures are stressed rather than the microstructures themselves, the weak link theory was shown to be applicable to fat crystal networks. Rheological measurements on some five different fat systems analyzed according to the weak link theory (Eqn. 7.1) yielded fractal dimension values which agreed very well with fractal dimension values calculated from polarized light microscope images of the network.

It was found that increasing order of packing of the microstructural elements within the microstructures implied a higher value in the fractal dimension calculated. Furthermore, utilizing Eqn. 7.1, it was shown that the shear elastic modulus of fat crystal networks (given a constant γ value) would decrease with increasing fractal dimension. Additionally, arguments were made which relates the crystallization behavior of a

particular fat to the order of packing of its microstructural elements, and therefore, its fractal dimension. It was argued that if processing conditions can be manipulated in such a manner as to cause an initial burst of crystallization which occurs over a short period of time, the resulting packing of the microstructural elements can be made more ordered. Experimental work on milkfat confirmed that this manipulation of processing conditions can result in the predicted changes.

In order to investigate the origins of the constant γ in Eqn. 7.1, a mechanical model of the fat crystal at low deformations was constructed in Chapter 6. This model is built around a few important assumptions:

a) The liquid oil in the network plays no essential role in the transmittance of forces when the network is stressed.
b) The microstructural elements are assumed to be spherical.
c) The forces of importance in the network are van der Waals forces between microstructural elements.
d) The hydrodynamic forces acting when the network is stressed are negligible compared to the van der Waals forces.
e) Inertial forces are assumed to be negligible.

An expression in agreement with Eqn. 7.1 was constructed from the model:

$$\dot{G} \sim m\left(\frac{\rho_t}{\rho_{ME}}\right)^{\frac{1}{3-D}} \frac{A}{6c\pi\sigma\xi d_o^3} \Phi_{SFC}^{\frac{1}{3-D}} \qquad (7.2)$$

where m is the number of pairs of microstructural elements at the interface between two microstructures, ρ_t is the density of the entire network, ρ_{ME} is the density within the microstructural elements, A is the Hamaker's constant of the network, σ is the size of the microstructural elements, ξ is the size of the microstructures, d_o is the distance between neighbouring microstructures, c is a constant defined during the calculation of fractal dimensions from polarized light microscope images (see Chapter 5), and $G^{'}, \Phi_{SFC}$, and D are as defined earlier. Experimental evidence were presented in Chapter 6 which support well the form of Eqn. 7.2, although methods are not available to measure some of the parameters that appear in the model.

Experiments on milkfat demonstrated that changes in processing conditions can change network characteristics such as microstructural element size. It was shown that the model espoused by Eqn. 7.2 predicts well changes in elastic modulus due to changes in fractal dimension and γ (indicated by changes in microstructural element size).

Now that the objectives have been discussed with respect to the finding described in the various chapters, it is important to discuss briefly the limitations of the implications of the work presented in this thesis. Firstly, the structure of fat networks described here is typical of natural fat systems (systems studied were milkfat, cocoa butter, lard, palm oil and tallow and interesterified versions of some of these) which have been crystallized statically at low levels of supercooling. The author have had conversations with Drs. Richard Hartel, William Kloek, and Pieter Walstra, on the structure of fats crystallized under shear, in scraped surface heat exchangers, at high levels of supercooling. These

researchers are of the opinion that fats crystallized in such an industrial-like fashion do not demonstrate the same levels of structure and fractality as the systems studied in this thesis. This is not surprising, since the fractal structure is very dependent on the heat and mass transfer limited aggregation process which occurs when fats are crystallized relatively slowly (low levels of supercooling). When fats are crystallized under conditions of forced mass transfer and high levels of supercooling, this important aggregation process is bypassed. It is the opinion of the author that systems crystallized under industrial-like conditions may revert over time to demonstrate structure more typical of statically crystallized fats at low levels of supercooling, but this opinion have not been substantiated by any experimental evidence.

The method devised to calculate fractal dimensions from image analysis of polarized light microscope images is highly subjective, and applicable only to fat systems with a reasonably low density of packing of microstructural elements. The theory is eminently sound, but the limitation lies in the nature of the images of the network that are possible from the sources of microscopy available for this purpose. The theory of particle-counting to calculate fractal dimensions is not limited to polarized light microscope images. The industrial application of this method must however be approached with caution, since the networks being analyzed must first be shown to adhere to the strict structural requirements outlined in Chapter 5.

The model outlined in Chapter 6 must be used with the assumptions upon which it was built taken into consideration.

The work detailed in this thesis to relate structure to the elastic properties of the network essentially ignores the role the molecular and crystalline levels of structure play. Although it can be argued that these levels of structure are implicitly involved in the model developed, they are not represented in any transparent, explicit manner. The author would advise that one area of future work would be to improve the model espoused by Eqn. 7.2 to include explicit inclusion of these levels of structure. Furthermore, the nature of the relationship between Hamaker's constant and molecular and crystalline levels of structure should be attempted. In the meantime, other studies in the field, which examines the role of polymorphism and lipid composition in determining elastic properties of the network, should be used in conjunction with the model presented here.

Whilst there are obvious and important limitations to the implications of this work, it also manages to answer some very important questions in the field, and opens up a new area of endeavor to relate structure of fat crystal networks to elastic properties.

REFERENCES

Amey, R. L., and D. Chapman. 1984. "Infrared spectroscopic studies of model and natural biomembranes.," in *Biomembrane structure and function, Topics in molecular and structural biology.*, vol. 4. Edited by D. Chapman, pp. 199-256. Basel: Weinheim.

Applegate, K. R., and J. A. Glomset. 1991a. Effect of acyl chain unsaturation on the packing of model diacylglycerols: a computer modeling study. *J. Lipid Res.* 32:1635 1644.

Applegate, K. R., and J. A. Glomset. 1991b. Effect of acyl chain unsaturation on the packing of model diacylglycerides in simulated monolayers. *J. Lipid Res.* 32:1645-1655.

Arishima, T., N. Sagi, H. Mori, and K. Sato. 1991. Polymorphsim of POS. I. Occurence and polymorphic transformation. *J. Amer. Oil Chem. Soc.* 66:710-715.

Arishima, T., K. Sugimoto, R. Kiwata, H. Mori, and K. Sato. 1996. ^{13}C cross-polarization and magic-angle spinning nuclear magnetic resonance of polymorphic forms of three triacylglycerols. *J. Am. Oil Chem. Soc.* 73:1231-1236.

Arya, A. P. 1990. *Introduction to Classical Mechanics*. Englewood Cliffs, New Jersey: Prentice-Hall.

Aubert, C., and D. S. Cannell. 1986. Restructuring of colloidal silica aggregates. *Phys. Rev. Lett.* 56:738.

Bailey, A. E. 1950. *Melting and Solidification of Fats*. New York: Interscience Publishers.

Berger, K. G., G. G. Jewel, and R. J. M. Pollitt. 1979. "Study of lipid systems.," in *Food Microscopy*. Edited by J. G. Vaughan. New York: Academic Press.

Birker, P. J. W. L., and J. C. G. Blonk. 1993. Alkyl chain packing in a b' triacylglycerol measured by atomic force microscopy. *J. Am. Oil Chem. Soc.* 70:319-321.

Boceik, S. M., S. Ablett, and I. T. Norton. 1985. ^{13}C-NMR study of the crystal polymorphism and internal mobilities of the triglycerides tripalmitin and tristearin. *J. Am. Oil Chem. Soc.* 62:1261-1266.

Bolle, C., C. Cametti, P. Codastefano, and P. Tartaglia. 1987. Kinetics of salt-induced aggregation in polystyrene lattices studied by quasielastic light scattering. *Phys. Rev. A.* 35:837.

Botet, R., R. Jullien, and M. Kolb. 1984. Hierarchical model for irreversible kinetic cluster formation. *J. Phys. A: Math Gen.* 17:L75-L79.

Bremer, L. G. B., B. H. Bijsterbosch, R. Scrijvers, T. v. Vliet, and P. Walstra. 1990. On the fractal nature of the structure of acid casien gels. *Colloid Surf.* 51:159-170.

Bremer, L. G. B., T. van Vliet, and P. Walstra. 1989. Theoretical and experimental study of the fractal nature of the structure of casien gels. *J. Chem. Soc., Faraday Trans.* 85:3359-3372.

Brockerhoff, H. 1965. A stereospecific analysis of triglycerides. *J. Lipid Res.* 6:10-15.

Brooker, B. E. 1990. Low temperature microscopy and X-ray analysis of food systems. *Trends in Food Sci. and Techn.* 1:100-103.

Brown, W. D. 1987. *The structure and Physical Properties of Flocculating Colloids*, University of Cambridge.

Brown, W. D., and R. C. Ball. 1985. Computer simulation of chemically limited aggregation. *J. Phys. A* 18:L517.

Buchheim, W. 1982. Aspects of samples preparation for freeze-fracture/freeze-etch studies of proteins and lipids in food systems. A review. *Food Microstruct.* 1:189-208.

Buscall, R., P.D.A. Mills, J.W. Goodwin, D.W. Lawson. 1988. Scaling behaviour of the rheology of aggregate networks formed from colloidal particles. *J. Chem. Soc., Faraday Trans.* **84**:4249-4260.

Calaghan, P. T., and K. W. Jolly. 1977. The use of ^{13}C spin relaxation to investigate molecular motion in liquid tristearin. *J. Chem. Phys. Lipids* 19:56-73.

Cebula, D., and K. Smith. 1992. Differential scanning calorimetry of confectionary fats; Part II-Effects of blends and minor components. *J. Am. Oil Chem. Soc.* 69(10):992-998.

Chapman, D. 1955. Infra-red spectra and the polymorphism of glycerides. *Nature* 176:216.

Chapman, D. 1960a. Infrared spectroscopic characterization of glycerides. *J. Am. Oil Chem. Soc.* 37:73-77.

Chapman, D. 1960b. Nuclear resonance spectra of the polymorphic forms of glycerides. *J. Chem. Soc.* :436-444.

Chapman, D. 1962. The polymorphism of glycerides. *Chem. Rev.* 62:433-456.

Chapman, D. 1964. Infrared spectroscopy of lipids. *J. Am. Oil Chem. Soc.* 42:353-371.

Chawla, P., J. M. D. Man, and A. K. Singh 1990. Crystal Morphology of Shortenings and Margarines. Food Structure **9**: 329-336.

Chen, M., and B. Russel. 1991. Characteristics of Flocculated Silica Dispersions. *J. Colloid and Interface Sci.* 141:565-577.

Christie, W. W. 1982. *Lipid Analysis - Isolation, Separation, Identification and Structural Analysis of Lipids*, 2nd Edition edition. Oxford: Pergamon Press.

Clarkson, C. E., and T. Malkin. 1934. Alternation in long chain compounds. Part II An X-ray and and trhermal investigation of the triglycerides. *J. Chem. Soc.* :666.

Cornily, G., and M. leMeste. 1985. Flow behavior of lard and its fraction at 15 C. *J. Texture Stud.* 16:383-402.

Courtens, E., J. Pelous, J. Phalippou, R. Vacher, and T. Woignier. 1987. Brillouin-Scattering Measurements of Phonon-Fracton Crossover in Silica Aerogels. *Phys. Rev. Lett.* 58:128-131.

Crownover, R. M. 1995. *Introduction to fractals and chaos.* Boston: Jones and Bartlett.

de Gennes, P. G. 1979. *Scaling Concepts in Polymer Physics*. Ithaca, NY: Cornell University Press.

de Jong, S., and T. C. van Soest. 1978. Crystal structures and the melting points of saturated triglycerides in the b-2 phase. *Acta Crystallogr.* B34:1570-1583.

de Jong, S., T. C. van Soest, and M. A. van Shaick. 1991. Crystal structures and melting points of unsaturated triacylglycerols in the b phase. *J. Am. Oil Chem. Soc.* 68:371-378.

de Man, J. M. 1961. Physical properties of milkfat II. Some factors influencing crystallization. J. Dairy Res. **28**: 117-122.

de Man, J. M. 1962. "Crystal structure and consistency of margarine." *Proc. 1st Intern. Cong. Food Sci. Technol., London, 1962*, pp. 795-806.

de Man, J. M. 1963. Polymorphism in milkfat. *Dairy Science Abstracts* 25:219-221.

de Man, J. M. 1964. Effect of cooling procedures on consistency, crystal structure and solid fat content of milkfat. Dairy Industries **29**: 244-246.

de Man, J. M. 1982. Microscopy in the study o fats and emulsions. *Food Microstruct.* 1:209-222.

de Man, J. M., and A. M. Beers. 1987. Fat crystal networks: structure and rheological properties. *J. Text. Stud.* 18:303-318.

Dimon, P., S. K. Sinha, D. A. Weitz, C. R. Safinya, G. S. Smith, W. A. Varady, and H. M. Lindsay. 1986. Structure of aggregated gold colloids. *Phys. Rev. Lett.* 57:595.

Dixon, B. D., and J. V. Parekh. 1979. Use of the cone penetrometer for testing firmness of butter. *J. Texture Studies* 10:421-434.

Duynhoven, J. v., G.-J. Goudappel, M. C. M. Gribnau, and V. K. S. Shukla. 1999. Solid fat content determination by NMR. *Inform* 10:479-484.

Eads, T. M., A. E. Blaurock, R. G. Bryant, D. J. Roy, and W. R. Croasman. 1992. Molecular motion and transitions in solid tripalmitin measured by deuterium nuclear magnetic resonance. *J. Amer. Oil Chem. Soc.* 74:1213-1220.

Edwards, S. F., and R. B. S. Oakeshott. 1989. The transmission of stress in an aggregate. *Physica D* 38:88-92.

Enden, J. C. v. d., A. J. Haighton, K. v. Putten, L. F. Vermaas, and D. Waddington. 1978. A method for the determination of the solid phase content f fats using pulsed NMR. *Fette Seifen, Anstrichm.* 80:180-186.

Engstrom, L. 1992. Triglyceride systems forming molecular compounds. *J. Fat Sci. Technol.* 94:173-181.

Falconer, K. (1990). *Fractal Geometry*. Chichester, Wiley.

Feng, S., and P. Sen. 1984. Percolation on Elastic Networks: New Exponent and Threshold. *Phys. Rev. Lett.* 52:216.

Feng, S., P. Sen, B. Halperin, and C. Lobb. 1984. Percolation on Two-Dimensional Elastic Networks with Rotationally Invariant Bond Bending Forces. *Physical Review B* 30:5386.

Filer, L. J., S. S. Sidhu, B. F. Daubert, and J. E. Longenecker. 1946. X-ray investigation of glycerides. III. Diffraction analyses of symmetrical monooleyl-disaturated triglycerides. *J. Amer. Oil Chem. Soc.* 68:167-171.

Flint, O. 1984. Applications of light microscopy in food analysis. *Microscope* 32:133-140.

Flint, O. 1991. Microscopy in the development of new food products. *European Microsc. Anal.* 10:21-23.

Foley, J. and J. P. Brady 1984. Temperature-induced effects on crystallization behaviour, solid fat content and the firmness of milk fat. Journal of Dairy Research **51**: 579 - 589.

Forrest, S. R., and J. T.A. Witten. 1979. Long range correlations in smoke-particle aggregates. *J. Phys. A.* 12:L109.

Freeman, N. K. 1968. Applications of infrared absorption spectroscopy in the analysis of lipids. *J. Am. Oil Chem. Soc.* 45:798-809.

Friedlander, S. K. 1977. *Smoke, Dust and Haze.* New York: Wiley.

Gibon, V., F. Durant, and C. Deroanne. 1986. Polymorphism and intersolubility of some palmitic, stearic and oleic triglycerides: PPP, PSP and POP. *J. Am. Oil Chem. Soc.* 63:1047-1055.

Gordon, M. H., and E. A. Rahman. 1991. Effects of minor components on the crystallization of coconut oil. *J. Am. Oil Chem. Soc.* 68(8):577-579.

Goto, M., D. R. Kodali, D. M. Small, K. Honda, K. Kozawa, and T. Uchida. 1992. Single crystal structure of a mixed-chain triacylglycerol: 1,2Dipalmitoyl-2-acetyl-*sn*-glycerol. *Proc. Natl. Acad. Sci. USA* 89:8083-8086.

Grey, F. and J. K. Kjems 1989. Aggregates, Broccoli and Cauliflower. Physica D **38**: 154-159.

Hagemann, J. A. Editor. 1989. *Thermal behavior and polymorphism of acylglycerides. Crystallization and polymorphism of fats and fatty acids*. New York: Marcel Dekker Inc.

Hagemann, J. W., and J. A. Rothfus. 1983. Polymorphism and transformation energetics of standard monoacid tryglycerides from differential scanning calorimetry and theoretical modeling. *J. Am. Oil Chem. Soc.* 60:1123-1131.

Hagemann, J. W., and J. A. Rothfus. 1992. COmputer modeling of packing arrangements and transitions in saturated -*cis*-unsaturated mixed triglycerides. *J. Am. Oil Chem. Soc.* 69:429-437.

Hagiwara, T., H. Kumagai, T. Masunaga, and K. Nakamura. 1997. Analysis of aggregate structure in food protein gels with the concept of fractal. *Biosci. Biotech. Biochem.* 61:1663-1667.

Hagiwara, T., H. Kumagai, and K. Nakamura. 1998. Fractal analysis of aggregates in heat-induced BSA gels. *Fod Hydrocolloids* 12:29-36.

Haighton, A. J. 1959. Measurement of the hardness of margarines and fats with the cone penetrometer. *J. Am. Oil Chem. Soc.* 36:345-348.

Haighton, A. J. 1976. Blending, chilling and tempering of margarines and shortenings. *J. Am. Oil Chem. Soc.* 53:397-399.

Haighton, A. J., L. F. Vermas, and C. den Hollander. 1971. Determination of solid-liquid ratios of fats by wide line NMR. *J. Amer. Oil Chem. Soc.* 48:7-10.

Hamaker, H. C. 1937. The London-van der Waals attraction between spherical particles. Physica [IV] **10**: 1058-1072

Hartel, R. W. 1999. Personal Communication.

Hausdorf, F. 1919. Dimension und Ausseres Mass. *Mathematische Annalen* 79:157-179.

Hayakawa, M., and J. M. d. Man. 1982. Interpretation of cone penetrometer consistency measurements of fats. *J. Texture Stud.* 13:201-210.

Heertje, I. 1993. Microstructural studies in fat research. *Food Structure* 12:77-94.

Heertje, I., M. Leunis, W. J. M. van Zeyl, and E. Berends. 1987a. Product microscopy of fatty products. *Food Microstructure* 6:1-8.

Heertje, I., P. van der Vlist, J. C. G. Blonk, H. A. C. M. Hendrickx, and G. J. Brakenhof. 1987b. Confocal laser scanning microscopy in food research: some observations. *Food Microstruct.* 6:115-120.

Heertje, I., J. van Eendenburg, J. M. Cornelissen, and A. C. Juriaanse. 1988. The effect of processing on some microstructural characteristics of fat spreads. *Food Microstructure* 7:189-193.

Hicklin, J. D., G. G. Jewel, and J. F. Heathcock. 1985. Combining microscopy and physical techniques in the study of cocoa butter polymorphs and vegetable fat blends. *Food Microstructure* 4:241-248.

Hoerr, C. W. 1960. Morphology of fats, oils and shortenings. *J. Am. Oil Chem. Soc.* 37:539-546.

Hoerr, C. W., and D. F. Waugh. 1955. Some physical characteristics of rearranged lard. *J. Am. Oil Chem. Soc.* 32:37-41.

Inoe, S. 1987. *Video Microscopy*. New York: Plenum Press.

Jensen, L. H., and A. J. Mabis. 1966. Refinement of the structure of b-tricaprin. *Acta Crystallogr.* 21:770-781.

Jullien, R., and R. Botet. 1987. *Aggregation and Fractal Aggregates*. Singapore: World Scientific Publishing Co. Pte Ltd.

Jullien, R., M. Kolb, and R. Botet. 1984. "Scaling properties of growth by kinetic clustering of clusters," in *Kinetics of Aggregation and Gelation*. Edited by F. Family and D. P. Landau, pp. 101. Amsterdam: Elsevier.

Kalab, M. 1983. "Electron microscopy of foods.," in *Physical properties of foods*. Edited by M. Peleg and E. B. Bagley, pp. 43-104. Westport, CT: AVI Publishing Co.

Kamphuis, H., R. J. J. Jongschaap, et al. 1984. A transient-network model describing the rheological behaviour of concentrated dispersions. Rheol. Acta **23**: 329-344.

Kamphuis, H., and R. J. J. Jongschaap. 1985. The rheological behaviour of suspensions of fat particles in oil interpreted in terms of a transient-network model. *Colloid Polym. Sci.* 263:1008-1024.

Kantor, Y., and I. Webman. 1984. Elastic Properties of Random Percolating Systems. *Phys. Rev. Lett.* 52:1891-1894.

Kawanari, M. 1996. Butter's characteristics: effect of processing. Inform 7(10): 1104 - 1110.

Kellens, M., W. Meeussen, and H. Reynaers. 1992. Study of the polymorphism and crystallization kinetics of tripalmitin: A microscopic approach. *J. Am. Oil Chem. Soc.* 69:906-911.

Knoester, M., P. D. Bruijne, and M. V. d. Tempel. 1972. The solid-liquid equilibrium of binary mixtures of triglycerides with palmitic and stearic chains. *Chem. Phys. Lipids* 9:309-319.

Kodali, D. R., D. Atkinson, T. G. Redgrave, and D. M. Small. 1987. Structure and polymorphism of 18-carbon fatty acyl triacylglycerols: effect of unsaturation and substitution in the 2-position. *J. Lipid Res.* 28:403-413.

Kolb, M., R. Botet, and R. Julien. 1983. Scaling of kinetically growing clusters. *Physical Review Letters* 51:1123.

Koyano, T., I. Hachiya, and K. Sato. 1990. Fat polymorphism and crystal seeding effects on fat bloom stability of dark chocolate. *Food Structure* 9:231-240.

Lambelet, P., and A. Raemy. 1983. Iso-solid diagrams of fat blends from thermal analysis. *J. Am. Oil Chem. Soc.* 60:845-847.

Landman, W., R. O. Feuge, and N. V. Lovegren. 1960. Melting and dilatometric behavior of 2-oleopalmitostearin and 2-oleodistearin. *J. Am. Oil Chem. Soc.* 37:638-643.

Lands, W. E. M., R. A. Pieringer, P. M. Slakey, and A. Zschoke. 1966. A micro-method for the stereospecific determination of triglyceride structure. *Lipids J.* 1:444-448.

Larsson, K. 1963. The crystal structure of the b-form of triglycerides. *Proc. Chem. Soc.* :87-88.

Larsson, K. 1964. The crystal structure of the b-form of trilaurin. *Ark. Kemi.* 23:1-15.

Larsson, K. 1972. Molecular arrangement in glycerides. *Fette Seifen Anstrichm.* 74:136-143.

Lefebvre, J. 1983. Finished product formulation. *J. Am. Oil Chem. Soc.* 60:295-300.

Leibniz, G. W. 1721. *Principia Philosophiae, More Geometrico Demonstrata.*

Lin, M. Y., H. M. Lindsay, D. A. Weitz, R. C. Ball, R. Klien, and P. Meakin. 1989. Universality in colloid aggregation. *Nature* 339:360-362.

Loncin, M. 1958. Influence des glycerides partiels sur la plasticite des matieres grasses. *Oleagineaux* 13(1):33-37.

Lovegren, N. V., M. S. Gray, and R. O. Feuge. 1971. Properties of 2-oleodipalmitin, 2-elaidodipalmitin and some of their mixtures. *J. Am. Oil Chem. Soc.* 48:116-120.

Lutton, E. S. 1945. *J. Amer. Oil Chem. Soc.* 67:524.

Lutton, E. S., and F. L. Jackson. 1950. The polymorphism of synthetic and natural 2-oleyldipalmitin. *J. Am. Oil. Chem. Soc.* 72:3254-3257.

Lutton, E. S., C. B. Stewart, and A. J. Fehl. 1972. Polymorphism of mixed triglycerides containing odd fatty acids. *J. Am. Oil Chem. Soc.* 49:333-335.

Madison, B. L., and R. C. Hill. 1978. Determination of the solid fat content of commercial fats by pulsed NMR. *J. Amer. Oil Chem. Soc.* 55:328-331.

van Malssen, K., R. Peschar, and H. Schenk. 1996. Real-time X-Ray powder diffraction investigations on cocoa butter. I. Temperature-dependent crystallization behavior. *J. Am. Oil Chem. Soc.* 73:1209-1215.

Mandelbrot, B. B. 1982. *The Fractal Geometry of Nature*. New York: Freeman.

Manning, D. M., and P. S. Dimick. 1985. Crystal morphology of cocoa butter. *Food Microstructure* 4:249-265.

Marangoni, A. G., and R. W. Hartel. 1998. Visualization and structural analysis of fat crystal networks. *Food Technol.* 52:46-52.

Marangoni, A. G., and R. W. Lencki. 1998. Ternary phase behavior of milk fat fractions. *J. Agric. Food Chem.* 46:3879-3884.

Marangoni, A. G., and D. Rousseau. 1996. Is plastic fat rheology governed by the fractal nature of the fat crystal netowrk? *J. Amer. Oil Chem. Soc.* 73:991-993.

Marangoni, A. G., and D. Rousseau. 1998a. The influence of chemical interesterification on physicochemical properties of complex fat systems 1. Melting and crystallization. *J. Am. Oil Chem. Soc.* 75:1265 - 1271.

Marangoni, A. G., and D. Rousseau. 1998b. The influence of chemical interesterification on the physicochemical properties of complex fat systems. 3. Rheology and fractality of the crystal network. *J. Am. Oil Chem. Soc.* 75:1633 - 1636.

Meakin, P. 1983. Formation of fractal clusters and networks by irreversible diffusion-limited aggregation. *Physical Review Letters* 1983:1119.

Meakin, P. 1988. Fractal Aggregates. *Adv. Colloid Interface Sci.* 28:249 - 331.

Medalia, A. I. 1971. *Surf. Colloid Sci.* 4:1.

Mills, B. L., and F. R. v. d. Voort. 1981. Comparison of the direct and indirect wideline NMR methods for determining solid fat contents. *J. Am. Oil Chem. Soc.* 58:776-778.

Minato, A., S. Ueno, K. Smith, Y. Amemiya, and K. Sato. 1997b. Thermodynamic and kinetic study on pahse behavior of binary mixtures of POP and PPO forming molecular compound systems. *J. Phys. Chem. B.* 101:3498-3505.

Minato, A., S. Ueno, J. Yano, K. Smith, H. Seto, Y. Amemiya, and K. Sato. 1997a. Thermal and structural properties of *sn*-1,3-dipalmitoyl-2-oleoylglycerol and *sn*-1,3-dioleoyl-2-palmitoylglycerol binary mixtures examined with synchrotron radiation X-ray diffraction. *J. Am. Oil Chem. Soc.* 74:1213-1220.

Mottram, F. J. 1961. Evaluation of pseudo-plastic materials by cone penetrometers. *Lab. Pract.* 10:767-770.

Mulder, H. 1953. Melting and solidification of milk fat. *Neth. Milk Dairy J.* 7:149-176.

Mulder, H. and P. Walstra 1974. *The Milk fat globule - Emulsion science as applied to milk products and comparable foods.* Wagningen, The Netherlands, Centre for Agricultural Publishing.

Mullins, W. W., and R. F. Sekerka. 1963. Morphological Stability of a Particle Growing by Diffusion or Heat Flow. *J. Appl. Phys.* 34:323.

Narine, S.S., and A. G. Marangoni. 1999a. Fractal nature of fat crystal networks. Phys. Rev. E. 59:1908-1920.

Narine, S.S., and A.G. Marangoni. 1999b. Microscopic and rheological studies of fat crystal networks, *Journal of Crystal Growth* **198/199:**1315-1319.

Narine, S. S., and A. G. Marangoni. 1999c. The difference between cocoa butter and Salatrim lies in the microstructure of the fat crystal network. *J. Am. Oil Chem. Soc.* 76:7-10.

Narine, S. S., and A.G. Marangoni. 1999d. Mechanical and Structural Model of Fractal Networks of Fat Crystals at Small Deformations. *Physical Review E.* **60(6):** 6991-7000.

Narine, S. S., and A.G. Marangoni. 1999e. Factors Influencing the Texture of Plastic Fats, *Inform.* **10(6):** 565-570.

Narine, S. S., and A.G. Marangoni. 1999f. Relating Structure of Fat Crystal Networks to Mechanical Properties: A Review. *Food Research International.* **32:** 227-248.

Narine, S. S., and A.G. Marangoni. In Press. Structure of Fat Crystal Networks: Quantification, Interrelationships, and Prediction of Elastic Properties. *Proceedings of the 3rd International Symposium on Confectionary Science, Pennslyvania State University, Department of Food Science and the PMCA, University Park, PA, U.S.A. (November, 14-16, 1999).*

Nederveen, C. J. 1963. Dynamic Mechanical Behavior of Suspensions of Fat particles in Oil. *Journal of Colloid and Interface Science* 18:276-291.

Niiya, I., T. Maruyama, M. Imamura, M. Okada, and T. Matsumoto. 1973. Effect of emulsifiers on the crystal growth of edible solid fats. Part III. Effect of saturated fatty acid monoglyceride. *Japanese Journal of Food Science and Technology* 20(5):182-189.

Norton, I. T., C. D. Lee-Tuffnel, S. Ablett, and S. M. Bociek. 1985. A calorimetric, NMR and X-ray diffraction study of the melting behavior of tripalmitin and tristearin and their mixing behavior with triolein. *J. Am. Oil Chem. Soc.* 62:1237-1244.

O'Connor, R. T., E. F. DuPre, and R. O. Feuge. 1955. The infrared spectra of mono-, di-, and triglycerides. *J. Am. Oil Chem. Soc.* 33:88-93.

Oyano, T., I. Hachiya, and K. Sato. 1992. Phase behavior of mixed systems of SOS and OSO. *J. Phys. Chem.* 96:10514-10520.

Padley, F. Editor. 1996. *Polymorphism of pure triacylglycerols and natural fats. Advances in Applied Lipid Research*: JAI Press.

Papenhuijzen, J. M. P. 1971. Superimposed steady and oscillatory shear in dispersed systems. Rheol. Acta **10**: 493-502.

Papenhuijzen, J. M. P. 1972. The role of particle interactions in the rheology of dispersed systems. Rheol. Acta **11**: 73-88.

Parker, J. R. 1994. *Practical Computer Vision Using C*. New York, Wiley.

Payne, A. R. 1964. The Elasticity of Carbon Black Networks. *Journal of Colloid Science* 19:744-754.

Rebinder, P. A., and N. A. Semenenko. 1949. Use of the penetrating cone method for the characterization of structural-mechanical properties of visco-plastic material. *Proc. Acad. Sci. (U.S.S.R.)* 64:835-838.

Reddy, S. Y., and J. V. Prabhakar. 1987. Effect of diglycerides o nthe solidification properties of Sal (*Shorea robusta*) Fat. *Fat. Sci. Technol. 89. Jahrgang. Nr.* 10:394-397.

Rojanski, D., D. Huppert, H. D. Bale, X. Dacai, P. W. Schmidt, D. Farin, A. Seri-Levy, and D. Avnir. 1986. Integrated Fractal Analysis of Silica: Adsorption, Electronic Energy Transfer, and Small-Angle X-ray Scattering. *Phys. Rev. Lett.* 56:2505-2508.

Rossel, J. B. 1967. "Phase diagrams of triglyceride systems.," in *Advances in Lipid Research*, vol. 5. Edited by R. Paoletti and D. Kretchevsky, pp. 353-408. New York: Academic Press.

Rousseau, D., K. Forestiere, A. R. Hill, and A. G. Marangoni. 1996a. Restructuring butterfat through blending and chemical interesterification. 1. Melting behavior and triacylglycerol modifications. *J. Am. Oil. Chem. Soc.* 73:963-972.

Rousseau, D., A. R. Hill, and A. G. Marangoni. 1996b. Restructuring butterfat through blending and chemical interesterification. 2. Microstructure and polymorphism. *J. Am. Oil Chem. Soc.* 73:973 - 981.

Rousseau, D., A. R. Hill, and A. G. Marangoni. 1996c. Restructuring butterfat through blending and chemical interesterification. 3. Rheology. *J. Am. Oil. Chem. Soc.* 73:983-989.

Rousseau, D., and A. G. Marangoni. 1998a. Tailoring the textural attributes of butterfat/canola oil blends via *Rhizopus arrhizus* Lipase-catalyzed interesterification. 1. Compositional modifications. *J. Agric. Food Chem.* 46:2368 - 2374.

Rousseau, D., and A. G. Marangoni. 1998b. Tailoring the textural attributes of butterfat/canola oil blends via *Rhizopus arrhizus* Lipase-catalyzed interesterification. 2. Modifications of physical properties. *J. Agric. Food Chem.* 46:2375 - 2381.

Rousseau, D., and A. G. Marangoni. 1999. The effects of interesterification on physical and sensory attributes of betterfat and butterfat-canola oil spreads. *Food Research International* 31:381-388.

Rousseau, D., A. G. Marangoni, and K. R. Jeffrey. 1998. The influence of chemical interesterification on the physicochemical properties of complex fat systems. 2. Morphology and polymorphism. *J. Am. Oil Chem. Soc.* 75:1833 - 1839.

Sambuc, E., Z. Dirik, G. Reymond, and M. Naudet. 1980. Etude de la cristallisation des corps gras plastiques VI. Influence des glycerides et des phosphatides en absence et en presence d'eau A. Cas des monoglycerides stearopalmitiques. *Rev. Franc. Des Corps Gras.* 27(11):505-512.

Sargeant, J. A. 1988. The application of cold stage scanning electron microscopy to food research. *Food Microstruct.* 7:123-135.

Sato, K., T. Arishima, Z. H. Wang, K. Ojima, N. Sagi, and M. Mori. 1989. Polymorphism of POP and SOS. I. Occurence and polymorphic transformation. *J. Amer. Oil Chem. Soc.* 66:664-674.

Schaefer, D. A., J. E. Martin, P. Wiltzius, and D. S. Cannell. 1984. Fractal Geometry of Colloidal Aggregates. *Phys. Rev. Lett.* 52:2371.

Schaefer, D. W., and K. D. Keefer. 1986. Structure of random porous materials: Silica Aerogel. *Phys. Rev. Lett.* 56:2199-2202.

Schroeder, M. 1991. *Fractals, Chaos, Power Laws*. New York: W.H. Freeman and Company.

Shama, F. and P. Sherman 1970. The influence of worksoftening on the viscoelastic properties of butter and margarine. J. Texture Stud. **1**: 196-205.

Shih, W. H., W. Y. Shih, S. I. Kim, J. Lin, and I. A. Aksay. 1990. Scaling behavior of the elastic properties of colloidal gels. *Phys. Rev. A* 42:4772-4779.

Shukla, A., and S. S. H. Rizvi. 1996. Relationship among chemical composition, microstructure and rheological properties of butter. *Milchwissenschaft* 51:144-148.

Siew, W. L., and W. L. Ng. 1996. Effect of diglycerides on the crystallization of palm oleins. *J. Sci. Food Agric.* 71:496-500.

Small, D. M. 1984. Lateral chain packing in lipids and membranes. *J. Lipid Res.* 25:1490-1500.

Small, D. M. 1986. "Glycerides," in *The Physical Chemistry of Lipids, from Alkanes to Phospholipids. Handbook of Lipid Research Series.*, vol. 4. Edited by D. J. Hanahan, pp. 475-522. New York: Plenum Press.

Sonntag, R. C., and W. B. Russel. 1987. Elastic properties of flocculated networks. *J.Colloid Interface Sci.* 116:485-489.

Stading, M., M. Langton, and A. M. Hermansson. 1993. Microstructure and rheological beaviour of particulate b-lactoglobulin gels. *Food Hydrocolloids* 7:195-212.

Stanley, H. E. 1984. *Fractal Concepts in Aggregation and Gelation: An Introduction. Kinetics of Fractal Aggregation.* F. Family and D. P. Landau, Elsevier Science Publishers B.V.: 1 - 4.

Timms, R. E. 1980. The phase behavior and polymorphism of milk fat, milk fat fractions and fully hardened milk fat. *Australian J. of Dairy Technol.* 35:47-52.

Timms, R. E. 1984. Phase Behavior of fats and their mixtures. *Prog. Lipid Res.* 23:1-38.

Uriev, N. B., and I. Y. Ladyzhinsky. 1996. Fractal models in the rheology of colloidal gels. *Colloids and Surfaces A* 108:1-11.

Vacher, R., T. Woignier, J. Pelous, and E. Courtens. 1988. Structure and self-similarity of silica aerogels. *Physical Review B* 37:6500 - 6503.

van Boekel, M. A. J. S. 1981. Estimation of solid-liquid ratios in bulk fats and emulsitons by pulsed magnetic resonance. *J. Amer. Oil Chem. Soc.* 58:768-772.

van den Tempel, M. 1961. Mechanical Properties of Plastic-Disperse Systems at Very Small Deformations. Journal of Colloid and Interface Science **16**: 284-296.

van den Tempel, M. 1968. Surface-active lipids in foods. *S.C.I. Monograph* 32:22-33.

van den Tempel, M. 1979. Rheology of Concentrated Suspensions. *Journal of Colloid and Interface Science* 71:18-20.

van Soest, T. C., S. de Jong, and E. C. Roijers. 1990. Crystal structures and the melting points of saturated triacylglycerols in the b-3 phase. *J. Am. Oil Chem. Soc.* 67:415-423.

Vasic, I., and J. M. d. Man. 1968. "Effect of mechanical treatment on some rheological properties of butter," in *Rheology and Texture of Foodstuffs*, pp. 251-264. London: Soc. Chem. Ind. , Monograph 27.

Vold, M. J. 1951. Van der Waals' Attraction Between Anisotropic Particles, *J. Colloid Sci.* **9**: 451.

Vreeker, R., L. L. Hoekstra, D. C. den Boer, and W. G. M. Agterof. 1992a. Fractal Aggregation of Whey Proteins. *Food Hydrocolloids* 6:423 - 435.

Vreeker, R., L. L. Hoekstra, D. C. den Boer, and W. G. M. Agterof. 1992b. The Fractal nature of fat crystal networks. *Colloids and Surfaces* 65:185-189.

Waddington, D. Editor. 1980. *Some applicatiosn of wide line NMR in the fats and oils industry. Fats and Oils: Chemistry and Technology.* London: Applied Science Publishers.

Weitz, D. A., J. S. Huang, M. Y. Lin, and J. Sung. 1985. Limits of the fractal dimension for irreversible kinetic aggregation of gold colloids. *Phys. Rev. Lett.* 54:1416.

Weitz, D. A., and M. Oliveria. 1984. Fractal Structures formed by kinetic aggregation of aqueous gold colloids. *Phys. Rev. Lett.* 52:1433.

Wille, R. L., and E. S. Lutton. 1966. Polymorphism of cocoa butter. *J. Am. Oil Chem. Soc.* 43:491-496.

Witten, T. A., and L. M. Sander. 1981. Diffusion-Limited Aggregation, a Kinetic Critical Phenomenon. *Phys. Rev. Lett.* 47:1400-1403.

Witten, T. A., and L. M. Sander. 1983. Diffusion-Limited aggregation. *Physical Review B* 27:5686-5697.

Wright, A. M., R. W. Hartel, S. S. Narine, and A. G. Marangoni. Submitted, 1999. The effect of minor components on milkfat crystallizatoin. *J. Am. Oil Chem. Soc.* .

Xu, C., W. Zipfel, J. B. Shear, R. M. Williams, and W. W. Webb. 1996. "Multiphoton fluorescence excitation: New spectral windows for biological nonlinear microscopy." *Proc. Natl. Acad. Sci., USA, 1996*, pp. 10763-10768 93.

Yan, Z. Y., S. D. Huhn, L. P. Klemann, and M. S. Otterburn. 1994. Molecular modeling studies of triacylglycerols. *J. Agric. Food Chem.* 42:447-452.

Yano, J. 1998. Vibrational spectroscopic study on structures and polymorphic transformations of triacylglycerols., Osaka University.

Yano, J., F. Kaneko, M. Kobayashi, D. R. Kodali, D. M. SMall, and K. Sata. 1997a. Structural Analyses of Triacylglycerol Polymorphs with FT_IT Techniques. 2. b'_1-Form and 1,2-Dipalmitoyl-3-myristoyl-*sn*-glycerol. *The Journal of Physical Chemistry B* 101:8120-8128.

Yano, J., F. Kaneko, M. Kobayashi, and K. Sata. 1997b. Structural Analyses of Triacylglycerol Polymorphs with FT_IR Techniques. 1. Assignments of CH_2 Progression Bands of Saturated Monoacid Triacylglycerols. *The Journal of Physical Chemistry B* 101:8112-8119.

Yano, J., and K. Sato. 1999. *Food Research International*.

Yiu, S. H. 1985. A fluorescence microscopic study of cheese. *Food Microstruct.* 4:99-106.